'Roles of cytoskeletal proteins in the predatory life cycle of *Bdellovibrio bacteriovorus*'

Andrew Karl Fenton B.Sc. (Hons)

Thesis submitted to the University of Nottingham for the degree of Doctor of Philosophy

June 2010

Abstract

Bdellovibrio bacteriovorus are small, predatory bacteria that grow within the periplasmic space of a host bacterium. *Bdellovibrio* has a biphasic life-cycle switching from a uni-nucleoid, growth-senescent 'attack-phase' to a novel, multi-nucleoid filamentous 'growth-phase', which elongates and divides, growing saprophytically within the periplasmic space of their prey. Little is known to date about *Bdellovibrio* developmental processes and cell division within this periplasmic niche.

Recent publications have demonstrated that bacterial cytoplasms house highly organised matrices of protein structures, called the bacterial cytoskeleton. The *Bdellovibrio* processes of prey-cell entry, filamentous cell growth and division coordination brings cellular morphological changes and challenges that could be coordinated by cytoskeletal elements. Green Fluorescent protein (GFP)-tagging and gene knock out approaches were used to gain insights into the function of these elements including: an Intermediate filament like protein Ccrp, which has a role in the maintenance of cell morphology; two actin homologues, which appear to function at different points in the predatory cycle, MreB1 and MreB2; and a new type of cytoskeletal element designated 'bactofilin', which may have a role in cell division control.

Recent advances in GFP technologies have led to the development of optimised GFP variants, such as mTFP1 and mCherry. These have been used to reveal previously unseen detail of *Bdellovibrio* development within prey. *Bdellovibrio* do not follow the familiar pattern of bacterial cell division by binary fission, instead divide synchronously at multiple sites along their length, once prey resources are depleted. This yields both odd and even numbers of progeny *Bdellovibrio.*

Acknowledgements

Firstly a huge thank you to my supervisor, Prof. Liz Sockett, thank you for the constant support especially through the starting years of my PhD and for the freedom to 'run out of the door' when I needed to. I am immensely grateful for all of the amazing opportunities you have given me to work with (bacteria/people), on (equipment/things), and in places I would never have expected from the outset of my PhD. Thank you for putting up with my terrible spelling and grammar; I hope I have managed to follow at least some of your writing advice! It's been a real pleasure trying to find out 'how *Bdellovibrio* think' with you and your lab. Thank you!

I would like to thank my PhD second supervisor and my undergraduate 3rd year project supervisor, Dr Thorston Allers. Thank you for teaching me the value of organisation (a skill I now have in abundance) and teaching me a lot about the nature of scientific research.

To the amazing Tammy Kammin, though perhaps you think me unshakable, I could not have done any of the things I have achieved over the last few years without you. Thank you!

I would like to thank my parents (Karl and Kaye) for their unwavering support and encouragement for me to do what I believe in, through my PhD, and always. A big thank you to Ms J Parsons 'my Nana', for her curiosity and constant support. I would also like to thank my brothers Lee and Grant for being a much needed source of fun, especially in the Lego® building department.

To Dale Yates, James Gunn, Sarah Starbuck and Paul Hallam and all those within Sir John Gells Regiment of Foote, within the

Sealed Knott re-enactment society. Thank you for being there as a great source of escapism when I needed it most! We did it! We got regimental status!

Thank you to Carmen Butan and Sriram Subramanian for giving me the opportunity of working with cryo-EM at the NIH and for being such welcoming hosts.

To the members of the C15 lab (in no particular order): Carey, Mike, Laura, Richie, Rob 'T', Tom, Davy, Katy, Marilyn, Rowena, Rob 'A', David, Max, Rashidah and Simon that have made the lab such a great place to work and do science! Thanks for the many good times both in and out of the lab, and for the very helpful scientific discussions, which occasionally happen (usually by accident); a special thank you to Carey Lambert, Katy Evans and Laura Hobley for initially teaching me about the fantastic world of *Bdellovibrio* research. Finally, thanks to the whole lab for some of the completely random words forever etched into my consciousness, due to all of those crosswords at coffee-time and numerous attempts at the 'circle-of-doom', like: Diadem, Umbra, Snoodle and Alan!

To *Bdellovibiro bacteriovorus*, the often overlooked 'smallest' member of our lab; you've been fantastic! I would also like to acknowledge the BBSRC for funding this project.

‘A scientist must also be absolutely like a child. If he sees a thing, he must say that he sees it, whether it was what he thought he was going to see or not. See first, think later, then test. But always see first. Otherwise you will only see what you were expecting. Most scientists forget that.’

Wonko the Sane

(Outside the Asylum)

Taken from the book ‘So long and thanks for all the Fish’

by Douglas Adams

Abbreviations

%	percentage
°C	degrees centigrade
α	alpha
ABC	Adenine-5'-triphosphate binding cassette
Amp	ampicillin
Amp^r	ampicillin resistant
ATP	Adenosine-5'-triphosphate
β	beta
BLAST	Basic Local Alignment Search Tool
bp	single nucleotide base-pair
ca	circa 'approximately'
CFU	colony forming units
δ	delta
Δ	delta denoting gene deletion
Da	Daltons
DAP	diaminopimelic acid.
DAPI	4',6-diamidino-2-phenylindole
DNA	deoxyribonucleic acid
DUF	domain of unknown function
e.g.	'for example'
eGFP	enhanced Green Fluorescent Protein
EM	electron microscopy
FRET	Förster resonance energy transfer
γ	gamma
g	gram
g	unit of gravitational acceleration force equal to 9.8 m/s^2
GFP	Green Fluorescent Protein
GTP	Guanosine-5'-triphosphate
HD	host-dependant
HI	host-independent
i.e.	'that is'
IPTG	Isopropyl β-D-1-thiogalactopyranoside
J	Joule
kb	Kilobase, 1, 000 base pairs
kDa	kilodalton
Kn	Kanamycin
Kn^r	Kanamycin resistant
KO	Knock-out 'gene deletion'
l	litre
M	molar
m	metre
m	milli 10^{-3}

MALDI-TOF	matrix-assisted laser desorption/ionisation-time of flight
Mb	megabase, 1,000,000 base pairs
mCherry	monomeric 'Cherry' Fluorescent protein
µ	micro 10^{-6}
min	minutes
mJ	milliJoule
ml	millilitre
mm	millimetre
mOD	milli optical density
MOI	multiplicity of infection
MS	mass spectrometry
mTFP	monomeric 'teal' fluorescent protein
MW	molecular weight marker
n	nano 10^{-9}
NA	numerical appature
^{o}C	degrees centigrade
OD	optical density
OD_{600}	optical dencity at 600nm
ORF	open reading frame
p	pico 10^{-12}
PCR	Polymerase Chain Reaction
PFAM	protein families database
PFU	plaque forming units
PG	Peptidoglycan
pH	negative $\log_{10}$ of the hydrogen ion concentration
PTA	Phospho-tungstic Acid
RNA	ribonucleic acid
rpm	revolutions per minute
RT-PCR	reverse transcription polymerase chain reaction
s	second
SDS-PAGE	Sodium dodecyl sulphate polyacrylamide gel electrophoresis
TEM	transmission electron microscopy
URA	Uranyl Acetate
UV	Ultra-violet
V	Volts
X^{50}	substance 'X' at a concentration of 50 mg/ml

Table of Contents

List of Figures

List of Tables

CHAPTER ONE

Introduction

1.0 The predatory bacterium *B. bacteriovorus*

Bdellovibrio bacteriovorus are non-pathogenic Gram-negative bacteria that prey upon a wide range of Gram-negative prey. It is hoped that with further study *Bdellovibrio* can be harnessed into a biological tool to control populations of pathogenic Gram-negative bacteria e.g. *Escherichia coli*, *Salmonella* and *Psudomonas* (Jurkevitch et al., 2000, Markelova et al., 2001). The potential applications of *Bdellovibrio* therapy could have wide ranging impacts on plant, animal and human health (Lenz. and Hespell., 1978, Lambina et al., 1981, Fratamico and Whiting, 1995, Jurkevitch et al., 2000, Schwudke et al., 2001).

B. bacteriovorus were first described in 1963 by Stolp and Starr and have become the most extensively studied predatory bacteria (Stolp and Starr, 1963). Beautiful microscopic analysis of the *B. bacteriovorus* strain 109J, carried out between 1960 and 1975, gave initial insights into the basic life-cycle of this organism (Fig. 1.1). Pioneering biochemical work on *B. bacteriovorus* development through the predatory cycle from 1975 to the late 1980s gave mechanistic detail of how these bacteria digest prey and incorporate that material in order to form new *Bdellovibrio*

progeny. A genome-sequenced *B. bacteriovorus* strain HD100 (originally designated strain *Bd*100 in: (Stolp and Starr, 1963)) and modern genetic techniques have led to the re-emergence of the *Bdellovibrio* field in the late 1990s to present (Rendulic et al., 2004, Lambert et al., 2003).

1.1 The *B. bacteriovorus* HD100 genome

Fully sequenced in 2004, the *B. bacteriovorus* strain HD100 has a genome approximately 3.8 Mb in size, which is roughly the same size as that of its prey (Blattner et al., 1997, Rendulic et al., 2004). All the genes required for metabolism and biosynthesis of most amino acids, essential lipids and nucleic acids are also present in the HD100 genome (Rendulic et al., 2004). It has therefore been suggested that the transition to a predatory life style has been recent event, therefore the genome reducing effect that often occurs with parasitic bacteria has not had time to occur. Alternatively, retaining the genes required for biosynthesis gives *B. bacteriovorus* cells the option to grow host-independently (HI) in the wild, this may provide sufficient selective pressure to maintain the biosynthetic genes in the genome, and thus maintain its genome size.

1.2 The *B. bacteriovorus* predatory life-cycle

B. bacteriovorus predation was first described in detail by Starr in 1966 and was historically considered a biphasic growth cycle (Starr and Baigent, 1966). A highly motile and growth-senescent *B. bacteriovorus* 'attack-phase' cell attaches to and enters Gram-negative prey residing within the periplasm (Starr and Baigent, 1966). Once established within this niche the *B. bacteriovorus* cells secrete a series of hydrolytic enzymes to digest the prey (Rendulic et al., 2004). Perhaps the earliest wave of hydrolytic enzymes un-crosslink and partially digest the prey cell wall, this weakens its structure leading to a rounding up the prey cell forming an arrangement known as the bdelloplast (Thomashow and Rittenberg, 1978b, Kessel and Varon, 1973). Monomers of the digested prey are transported into the *B. bacteriovorus* and used for growth in the 'growth-phase'. *B. bacteriovorus* do not grow and divide in the usual bacterial pattern of binary fission, but form an extended vibriod or coiled cell that septates into multiple progeny (Starr and Baigent, 1966). Newly formed *B. bacteriovorus* cells mature by growing new flagella and escape out of the bdelloplast restarting the cycle (Fig. 1.1).

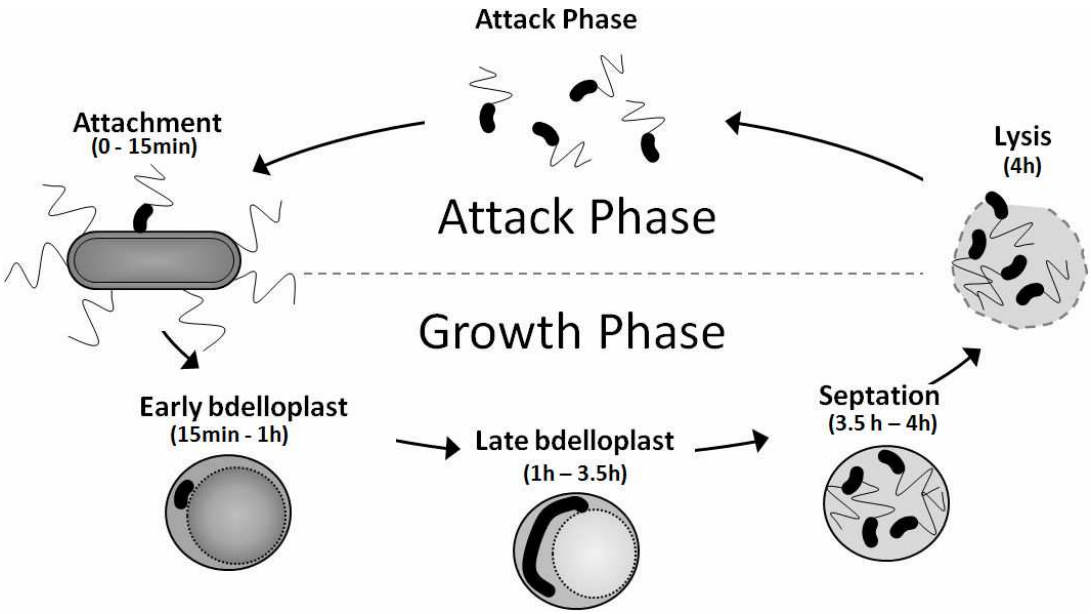

Figure 1.1. Schematic host-dependent predatory cycle for *B. bacteriovorus* on *E. coli* prey. Diagram shows the biphasic growth-cycle of the predatory bacterium *B. bacteriovorus*. Approximate time-points at which each stage of the predatory lifcycle are reached are shown in brackets, these are based on microscopic observations of synchronously infected predatory cultures (see section 2.13.2 and Fig. 3.7).

1.2.1 Attack-phase *B. bacteriovorus* cells

Attack-phase HD100 *B. bacteriovorus* cells are small (1.02μm ± 0.15 X 0.3μm ± 0.02), highly motile cells that can travel up to 160 body lengths a second using a single sheathed polar flagellum (Borgnia et al., 2008, Lambert et al., 2006a). The signals used by *B. bacteriovorus* to find areas of high prey density are still unknown, although oxygen and small biological compounds such as amino acids have been suggested (Straley and Conti, 1974).

Early electron-microscopic (EM) studies provided the initial insights into the cellular structure of *B. bacteriovorus* attack-phase cells (Scherff et al., 1966, Burnham et al., 1968). More recently cryo-electron-microscopic and tomographic techniques have been

used to image unstained *B. bacteriovorus* attack-phase cells in incredible detail (Borgnia et al., 2008) (Fig. 1.2). These techniques have revealed previously unseen detail within *B. bacteriovorus* attack-phase cells; such as the multiple ribosomal complexes and the chemotaxis receptor array (Fig. 1.2).

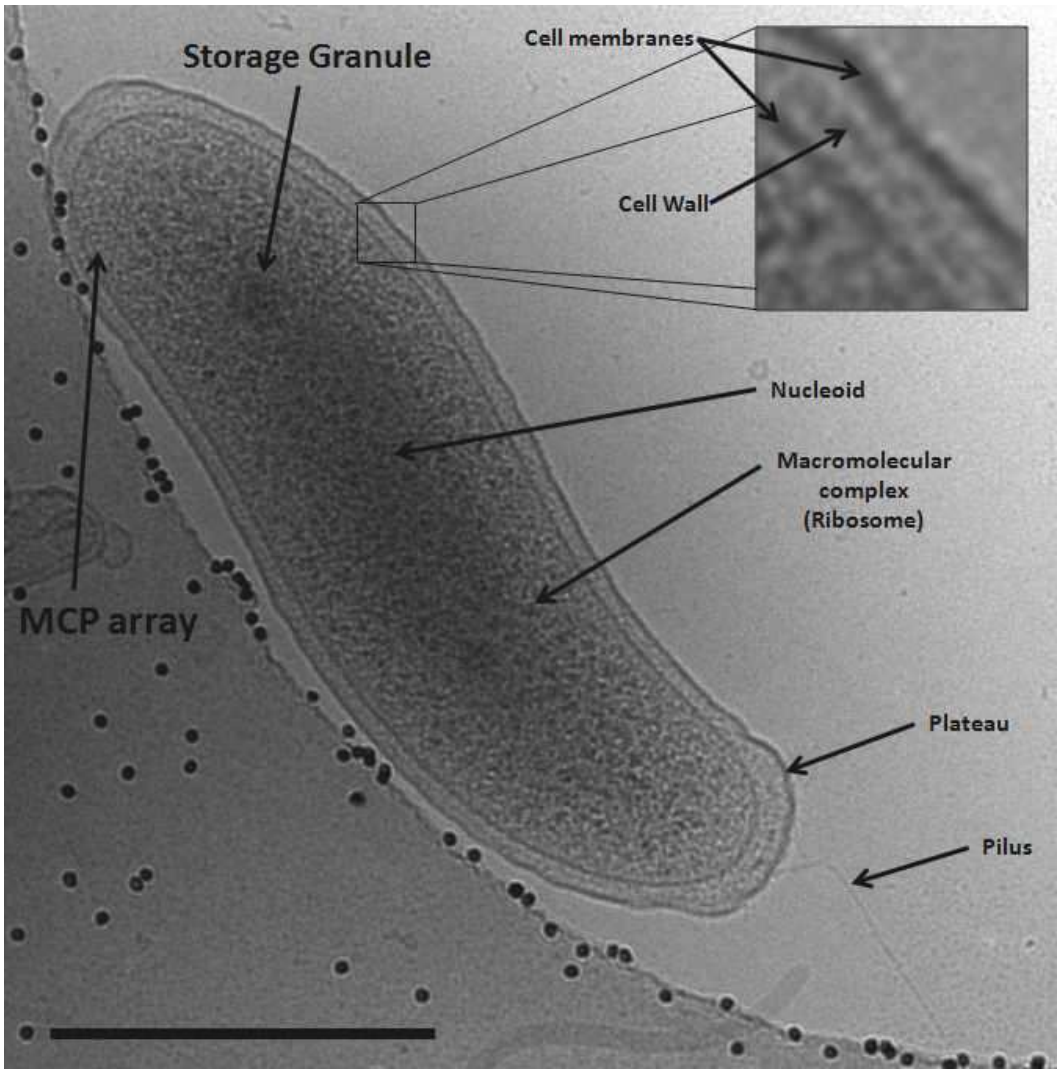

Figure 1.2. *Bdellovibrio bacteriovorus* attack-phase cellular architecture examined by Cryo-Electron Microscopy. Example Cryo-Electron Micrograph a *B. bacteriovorus* attack-phase cell (*Bd1167*::Kn) showing all major cellular architecture (taken at the NIH as a part of this study). The carbon film of the EM grid (which appear as a darker shadowed area) and the 15 nm gold particles (black specs) can be seen surrounding the cells. Image taken jointly with C. Butan under the supervision of S. Subramaniam using methods described in section 2.9.7. Scale bar = 500nm.

1.2.2 *B. bacteriovorus* prey attachment and entry

B. bacteriovorus attack-phase cells reversibly attach to prey at the non-flagellate pole in a short recognition phase (Rendulic et al., 2004). Attack-phase cells will not enter dead prey or prey that have suffered environmental insults; such as plasmolysis (Abram et al., 1974).

B. bacteriovorus prey-cell entry is achieved by dragging and squeezing the attack-phase cell through a small pore made in the prey outer membrane using Type IV pili (Evans et al., 2007). Both TEM and cryo-EM studies have shown that pili are present at the non-flagellate pole of *B. bacteriovorus* attack-phase and HI cells (Evans et al., 2007, Borgnia et al., 2008) (Fig. 1.2). These conclusions have been recently confirmed using different techniques by: (Mahmoud and Koval, 2010). It is still not known precisely what *B. bacteriovorus* pili bind to within the prey, however as a capping structure usually found on Type IV pili encoded by the *pilC1/Y1* gene is absent from the HD100 genome, it is possible that there is no specific binding target (Lambert et al., 2009).

Electron micrographs show *B. bacteriovorus* cells 'squeeze' through a pore made in the prey which is narrower than its width (Fig. 1.3). As the attack-phase cell migrates into the prey the 'squeezing' can be observed at different points running the entire

length of the cell (Fig. 1.3). This technique allows the *B. bacteriovorus* cells to enter through as small a pore as possible, preventing premature prey lysis. The tight seal that this process would create at the site of entry may prevent leakage of prey-periplasmic contents, and maintain prey proton motive force, both of which could be utilised by the invading *B. bacteriovorus* cell. Abram *et al* suggested that attack-phase cells must take on a 'plastic nature' in order to accomplish this 'squeezing' (Abram et al., 1974) (Fig. 1.3).

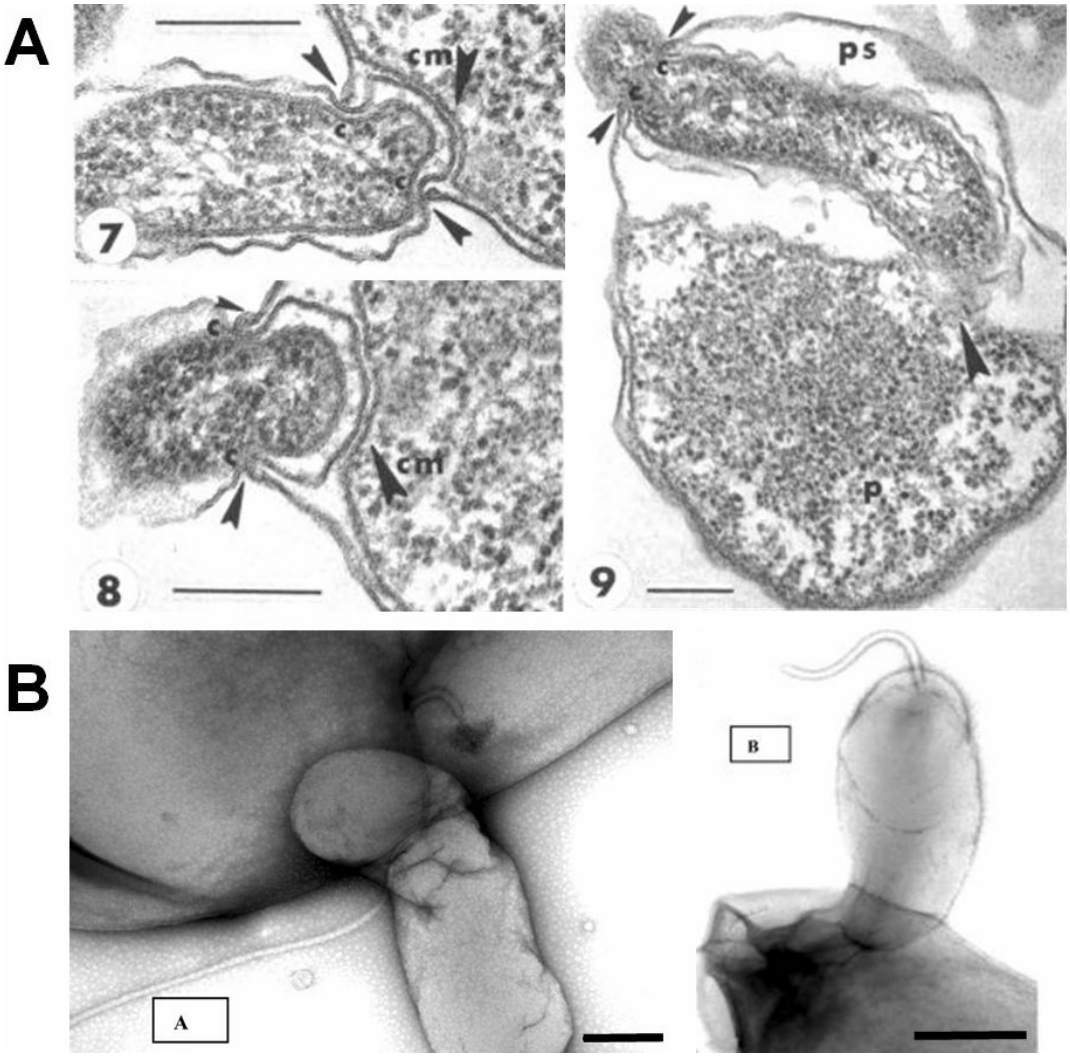

Figure 1.3 *B. bacteriovorus* cells 'squeeze' through a pore made in the prey outer-membrane. (**A**) Electron micrographs showing *B. bacteriovorus* (strain 109J) cells 10-15 min after *E. coli* B prey infection at different stages of prey-entry, running from image 7 to 9. Images show *B. bacteriovorus* cells squeezing through an entry pore smaller that their width (arrows marked 'c'), also *B. bacteriovorus* cells 'flatten out' at the pole of the cell as they are attached to prey internal structures ('cm' arrows). Samples were prepared by OsO_4 fixation, embedded in Epon 812 and sectioned; this gives rise to the visible membrane distortions. Taken from (Abram et al., 1974). (**B**) Transmission electron micrographs of *B. bacteriovorus* (strain HD100) cells invading *E. coli* S17-1 prey, cells stained using 1% URA pH 4.0. Taken from (Evans et al., 2007). All scale bars = 0.2 μm.

1.2.3 The *B. bacteriovorus* growth-phase; bdelloplast formation and establishment

Once prey entry has been achieved the *B. bacteriovorus* cell synthesises and secretes a battery of degradative enzymes that kill and digest the prey. Some of the first enzymes released by the *B. bacteriovorus* cell un-crosslink and solubilise 10-15% of the prey cell wall causing the prey cell to change shape from a rod to a sphere (Thomashow and Rittenberg, 1978b). Digested prey monomers are taken up into the *B. bacteriovorus* cell and growth senescence is relaxed leading to cell elongation. This overall structure of *B. bacteriovorus* cell(s) growing within a dead rounded up prey cell is called a bdelloplast, a name first coined by Kessel and Varon in 1973 (Kessel and Varon, 1973) (Fig. 1.1).

1.2.4 Growth phase – *Bdellovibrio* Septation

Using digested prey components *B. bacteriovorus* elongate into either extended vibriod or coiled 'corksrew' shapes, typically three to five times the length of an attack-phase cell (Starr and Baigent, 1966). EM observations suggested that one pole of the *B. bacteriovorus* cell is fixed to the prey cell wall (presumably by pilli and non-flagellate pole), thus the elongating *B. bacteriovorus* cell would appear to elongate from one pole only (Scherff et al., 1966).

The mature *B. bacteriovorus* growth-phase cell is a single extended multiploid cell immediately before septation. This suggests that unlike many other bacterial species, there is no regulatory coupling between DNA replication and septation in *B. bacteriovorus* (Ruby and Rittenberg, 1983). Septation of *B. bacteriovorus* growth-phase cells in synchronously infected *E. coli* S17-1 predatory cultures takes place between 3 and 4 hours; however what the signal is that causes the cell to septate, or what pattern the filament breaks down remains an unknown; although early EM work suggests that spetation proceeds sequentially along the filament (Scherff et al., 1966). For a more detailed introduction to *B. bacteriovorus* septation see chapter 4 (4.1).

1.2.5 Bdeloplast lysis

Once resources within the bdelloplast are exhausted *B. bacteriovorus* cells secrete lytic enzymes that lyse the remaining prey envelope and allow the newly formed progeny cells to escape (Thomashow and Rittenberg, 1978b). *B. bacteriovorus* progeny swim around within the exhausted bdelloplast prior to lysis; it is not known to what extent this, if at all, contributes to the lysis of the bdelloplast (Fig. 1.1 and supplementary Movie 10).

1.3 *Bdellovibrio* Host-independent growth

Maintenance of *B. bacteriovorus* cultures in the lab involves 'feeding' them Gram-negative prey; usually *E. coli* strain S17-1 in Ca/HEPES buffer (section 2.2.2.2). Under these conditions *B. bacteriovorus* can be considered host-dependent (HD). However, plating many attack-phase cells onto rich media allows the isolation of a few host-indepentent (HI) strains (section 2.2.3). For example Stolp in 1963 described how $5X10^8$ *B. bacteriovorus* attack-phase cells placed on a plate of rich media would yield only a single host-independent colony (Stolp and Starr, 1963). The frequency of 1 HI in approximately $1X10^6$-10^7 *B. bacteriovorus* cells suggests that the generation of HI strains is due to a single mutational event (Cotter and Thomashow, 1992). In the majority of cases HI strains contain a mutation in a specific region of the genome named the host interaction locus, or *hit* locus (Cotter and Thomashow, 1992). Little is known about the function of genes at the *hit* locus; representing the full *Bd108* open reading frame (ORF) and the 3' end of the *Bd109* ORF, and almost nothing is known of the mechanisms of HI growth in strains where the *hit* locus is unmodified (Rendulic et al., 2004).

Growth rates and cell morphologies of *B. bacteriovorus* HI strains are highly variable between isolates. Morphologies vary from small and 'attack-phase like' to very long cells, typically

between 20-50 μm (Shilo and Bruff, 1965) (also see Fig. 5.12C). Spiral shapes and spheroplasts are also often observed in HI cultures (Shilo and Bruff, 1965). HI strains can be re-introduced to prey and effectively 'turned HD' (Shilo and Bruff, 1965); however these strains rarely revert to the wild-type predation rates and often have much more diverse morphologies than parent host-dependent strains (Seidler and Starr, 1969).

A key function of HI strains in *Bdellovibrio* research has been to rescue deletion strains that are non-predatory. An example of this is the *B. bacteriovorus* HD100 *pilA* deletion strain, a strain that is unable to penetrate into the periplasm of prey and thus is non-predatory (Evans et al., 2007). In this case 10 independently generated HI KO lines were tested to confirm the non-predatory phenotype of the *pilA* KO strain was a true phenotype and not the result of HI strains general predation deficiency (Evans et al., 2007).

1.4 The bacterial cytoskeleton

Recent work has shown bacterial cells contain a cellular cytoskeleton analogous to the eukaryotic cytoskeleton, disproving the long standing dogma that the cytoskeleton was a defining feature of the eukaryotic cell (for a detailed review see (Shih and Rothfield, 2006)). A cytoskeleton is a series of internal cellular structures that aid co-ordination of cellular processes and maintenance of proteins at a particular cellular address.

1.4.1 The bacterial actin homologues

Unlike a eukaryotic cell where overall cell morphology is determined solely by the underlying cytoskeleton, bacterial cell shape is principally delimited by the peptidoglycan (PG) cell wall or murein saculus. A detailed review of the biochemistry of the bacterial cell wall and current thinking on how it is carefully enlarged and turned-over without compromising stability see seminal paper by Höltje (Holtje, 1998). The bacterial cell wall can be thought of as a single continuous molecule consisting of glycan strands bridged by short peptides providing strength (Holtje, 1998). The thickness and composition of this structure varies between bacteria, but for a Gram-negative bacteria it can be thought of as between one and three molecules thick (Holtje, 1998). The **P**enicillin-**B**inding-**P**roteins (PBPs) are the enzymes responsible for

carefully making and destroying peptidoglyan, these proteins are present in a tightly controlled complex vital for maintaining cell wall strength as PG is elongated and turned over.

In 2001-03 Jeff Errington's lab provided the evidence which suggested that in *Bacillus subtillis* the positioning of the PBP complex was due to an internal actin homologue that formed an internal helical filament under the inner surface of the cytoplasmic membrane called MreB (Jones et al., 2001, Daniel and Errington, 2003). Inhibiting MreB function using an MreB specific inhibitor A22 results in uncontrolled incorporation of PG into the cell wall generating spherical cells that are non-viable in the long term (Iwai et al., 2002, Iwai et al., 2004) (For more information on A22 and its action see Chapter 5.1.2). Work in other bacteria, such as *Caulobacter crescentus* and *E. coli,* has shown that an MreB filament controls cell shape for most non-spherical bacteria (Kruse et al., 2003, Gitai et al., 2005). In this way the bacterial cytoskeleton indirectly controls cell morphology.

Further work on MreB has shown that it forms a complex with MreC and MreD that penetrates the cytoplasmic membrane and contacts the PBPs (Kruse et al., 2005), in addition RodA as well as the recently discovered RodZ also form part of this 'elongase' complex, Fig. 1.4 (Shih and Rothfield, 2006, Gerdes, 2009,

Bendezu et al., 2009). See chapter 5.1 for a more detailed introduction into the dynamics of the MreB filament.

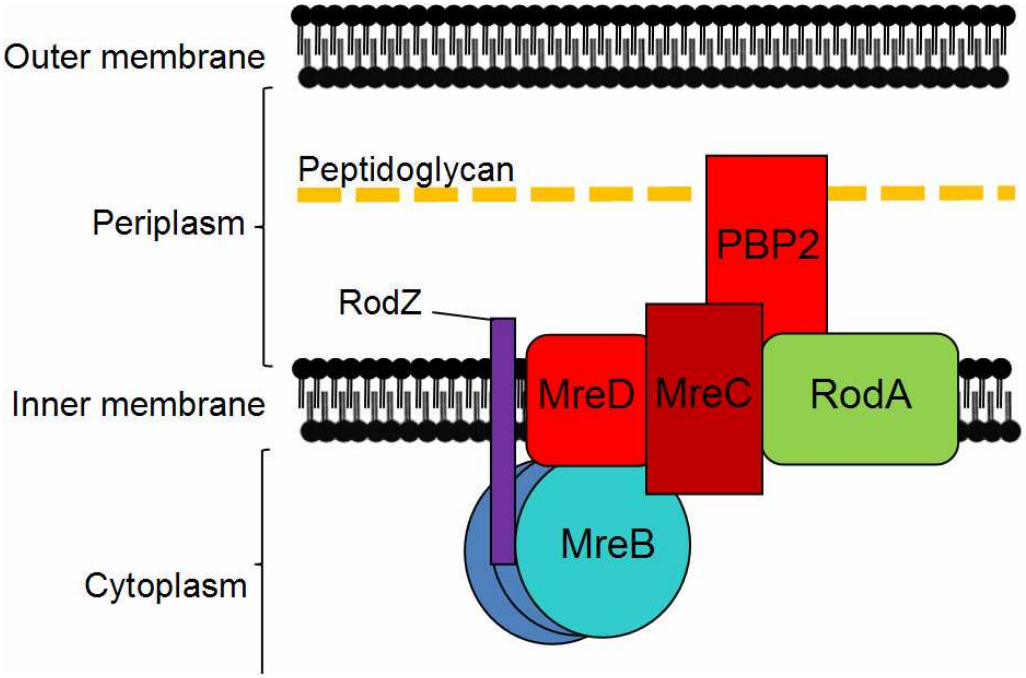

Figure 1.4 The bacterial 'elongase' complex. Schematic representation of the protein complex responsible for coordinating bacterial cell wall elongation. Adapted from (Gerdes, 2009).

Experiments using the MreB specific inhibitor A22 and fluorescently labelled *C. crescentus* chromosomes has shown that the MreB filament plays a role in the initial separation of newly replicated daughter chromosomes (Gitai et al., 2005). This work complemented a similar experiment in *E. coli* where cells were treated with cephalexin, giving elongated polyploid cells, which failed to separate their chromosomes in the presence of both A22

and MreB null mutants (Kruse et al., 2003). Taken together this shows that MreB has wider roles in chromosome segregation.

MreB is not the only actin homologue to be found in bacteria. The FtsA and ParM proteins are both well described members of this protein family (Shaevitz and Gitai, 2010). These proteins have specialised to carry out very different cellular functions; ParM (together with ParR) partitions plasmids to the poles of the dividing bacterial cells ensuring their segregation, whereas FtsA has a role in septation by aiding FtsZ-ring establishment at mid-cell.

The wider family of bacterial actin homologues continues to grow and expand; for example AlfA, a protein distantly related to MreB and ParM, is a recently discovered DNA segregation protein from *Bacillus subtilis* (Popp et al., 2010, Shaevitz and Gitai, 2010). This expansion is due to refined BLAST searches and an appreciation of how actin proteins fold when examining alignments. For a very recent review of the whole family of actin homologues in bacteria see (Shaevitz and Gitai, 2010).

1.4.2 Bacterial intermediate-filament like proteins

Bacterial genomes do not only contain eukaryotic actin homologues, they also contain structural homologues to the family of intermediate filaments, as well as tubulin homologues (discussed in section 1.4.3).

The most studied bacterial intermediate filament like (IF-like) element is the Crescentin (CreS) protein discovered in *Caulobacter crescentus* (Ausmees et al., 2003). The CreS filament gives the *Caulobacter* cell a vibriod shape by physically bending the MreB cytoskeleton on one side from within, leading to a vibriod cell wall and thus the defining 'crescent' cell shape of these bacteria (Cabeen et al., 2009).

IF proteins are thought of as stable filaments in eukaryotic cells providing cell structure, rigidity and adhesion. This is due to the structure of these filaments as these proteins spontaneously oligomerise forming very stable coiled-coiled structures, requiring considerable energy investment to uncoil (Bagchi et al., 2008). A type of IF-like element in *Streptomyces coeilcolor* formed by the FilP protein has been shown to have a similar structural role in bacteria; with cells appearing 'softer' in *filP* deletion strains when probed using atomic force microscopy (Bagchi et al., 2008). See chapter 3.1 for more information on bacterial intermediate-filament like (IF-like) proteins.

1.4.3 Bacterial tubulin homologues - FtsZ

The most studied eukaryotic microtubule (tubulin) homologue in bacteria is the cell division protein FtsZ (Errington et al., 2003). First discovered by complementation studies of mutant *E. coli* strains defective in cell division at non-permissive temperatures, the **F**ilamentous **T**emperature **S**ensitive genes (or *fts* genes) control the process of cell division in bacteria (Goehring and Beckwith, 2005). The first stage in this process is the establishment of an FtsZ polymer just below the cell membrane at midcell forming a ring-like structure, through a series of protein:protein interactions this structure recruits downstream Fts proteins in an hierarchical manner (Goehring and Beckwith, 2005) (Fig. 1.5). These proteins have the peptidoglycan-biosynthetic, DNA translocation/repair and membrane invagination activities required for accurate septation (Errington et al., 2003, Di Lallo et al., 2003). See Chapter 4.2 for a more detailed introduction to bacterial septation machinery.

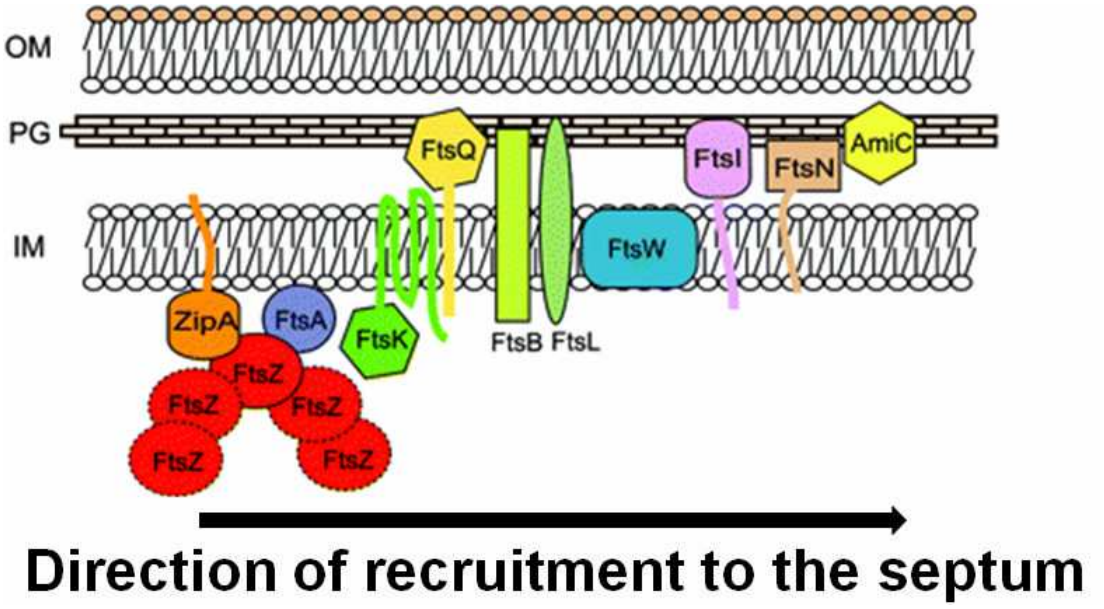

Figure 1.5 Hierarchical recruitment of division proteins to the *E. coli* bacterial septum. The tubulin homologue FtsZ is anchored to the cell membrane by FtsA and ZipA, and the other septation proteins are then added to the complex in an ordered pattern, proceeding from left to right in this figure. This diagram does not accurately represent the details of the protein:protein interactions in this complex. OM = outer-membrane, PG = peptidoglycan, IM = inner-membrane. Adapted from (Shih and Rothfield, 2006).

1.4.4 Bacteria specific cytoskeletal elements – ParA and 'Bactofilin'

In addition to containing homologues of eukaryotic cytoskeletal elements a series of elements have been described which, as yet, are exclusive to prokaryotes.

The ParA family of proteins form long filaments which have been shown to have a role in both plasmid and chromosome segregation (Hiraga, 2000). On binding to a ParB-DNA complex ParA forms filaments which seem to pull plasmids to the poles of *E. coli* cells, ensuring the inheritance of low copy-number plasmids in bacterial populations (Ringgaard et al., 2009).

ParA in *Cyanobacteria* has a role in maintaining the carboxysomes at discrete loci within the cytoplasm along the lengths of the rod-shaped cells. This was demonstrated using a strain carrying a combination of a *parA* knock-out strain and a carboxysome-GFP label, cells of this strain having these carbon-fixing 'organelles' clustered in one large locus (Savage et al., 2010).

The number of cytoskeletal proteins known in bacteria is still growing, a new class of filamentous bacterial proteins has been recently described containing the domain designated DUF583 in the PFAM database (Kuhn et al., 2010). These proteins have been designated 'bactofilins' based on their predicted polymerisation properties (Kuhn et al., 2010). These filaments form stable filament bundles which require no cofactors to polymerise very much like IF elements (Kuhn et al., 2010). Initially discovered in *M. xanthus*, these proteins were also found to localise to the stalk pole in *C. crescentus*, organising the cell-wall biosynthesis, through the localisation of Pbp5 in a cell-cycle dependent manner (Kuhn et al., 2010). In *E. coli* expressing the DUF583 domain-containing gene *SO1662* from *Shewanella oneidensis* the filament localised to the site of cell division (Kuhn et al., 2010). It is still largely unclear what the many functions of these proteins are. See Chapter 4.5 for a more detailed introduction to bacterial septation machinery.

1.5. Challenges to the *Bdellovibrio* cytoskeleton

The *B. bacteriovorus* cell has a series of cell morphological challenges to overcome through its predatory lifestyle that the cytoskeleton may be involved with or influenced by. See Fig. 1.6 for a brief summary of potential cytoskeletal functions.

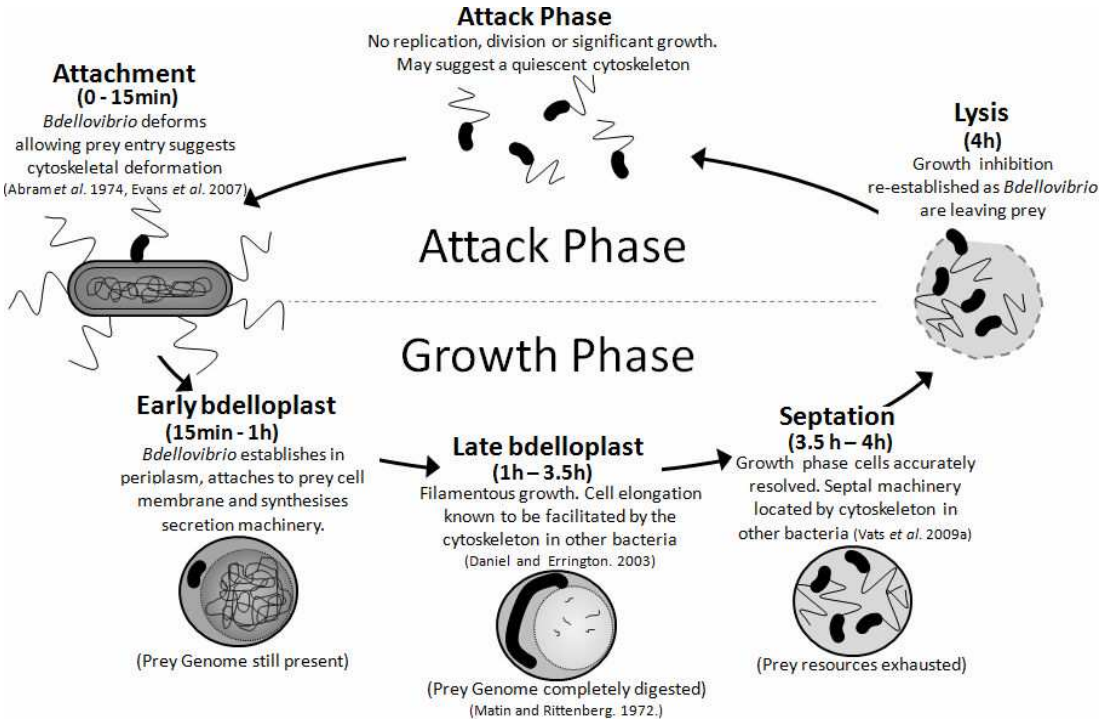

Figure 1.6 Schematic host-dependent predatory cycle for *B. bacteriovorus* on *E. coli* prey, showing the different phases of growth and inferred demands on the *B. bacteriovorus* cell cytoskeleton. References where the roles of the cytoskeleton in cell development have been proven for other bacteria are provided in parentheses. The status of the prey genome is both drawn from an earlier study (Matin and Rittenberg, 1972) and confirmed by work in this study (Fig. 5.5).

The attack-phase *B. bacteriovorus* cell is a growth-senescent cell as it does not significantly change shape or size over extended periods of time. To explain this, cell wall biosynthesis in the attack-phase cell must be inhibited. This could indicate a quiescent

cytoskeleton either delocalised (which is probably not likely) or *in situ* but not turning-over (Fig. 1.6).

Electron micrographs have shown the *B. bacteriovorus* attack-phase cell 'squeezing' through a hole it has made in the outer-membrane of the prey; see Fig. 1.3. This process could involve a 'softening' of the *B. bacteriovorus* cell wall allowing easy deformation; a modification process which would likely be controlled by the underlying cytoskeleton (Fig. 1.6). Alternatively polymers of intermediate filament like proteins could exert an internal pulling of the cell wall to deform the cell at the site of prey entry, as these proteins have been shown to pull against bacterial cellular components in *C. crescentus* and contribute to cell shape stability in *S. coelicolor* (Bagchi et al., 2008, Charbon et al., 2009).

It is also not known how the growth-phase filamentous cell within the bdelloplast is generated and remains resistant to division, despite having multiple potential sites for septation along its length while elongating, until division is initiated prior to bdelloplast lysis (Fig. 1.6). In addition the pattern of filamentous cell division in predatory *Bdellovibrio* is also unknown (see section 4.1.5).

1.6 Aims and objectives of this study

Many of the developmental processes of predatory *B. bacteriovorus* within bdelloplasts are poorly understood. The potential roles of the *B. bacteriovorus* cytoskeleton in these processes (section 1.5, Fig. 1.6) make a tempting target. Therefore, the broad aim of my PhD was:

To identify and investigate the functions of cytoskeletal proteins found in *B. bacteriovorus* strain HD100 in order to gain insight into how *Bdellovibrio* cells develop within the bdelloplast. To achieve this, the specific objectives were:

- Identify and clone bacterial cytoskeletal ORFs in the HD100 genome and investigate their potential roles in *B. bacteriovorus* prey-cell entry and cell morphology. Crescentin was the first target (Chapter 3), a novel bactofilin-like protein Bd3904 became the second (Chapter 4), with MreBs the third (Chapter 5).

- Understand the septation process in *Bdellovibrio*, the first attempt was by trying to GFP-label the tubulin homologue FtsZ in HD100 to better understand the gross patterns of *B. bacteriovorus* cell division (Chapter 4). This was followed by adapting GFP-prey technologies to visualise wild-type *B. bacteriovorus* cells developing within bdelloplasts.

- As some cytoskeletal protein genes were found to be essential for viability a final objective was to develop a technique for GFP tagging specific proteins in *B. bacteriovorus* to investigate both their function and cellular address (methods described in section 2.12, and used in chapters 3, 4 and 5).

1.7 Use of Green Fluorescent Protein (GFP) in cellular biology and challenges when detecting GFP-Protein fusions in *B. bacteriovorus.*

1.7.1 Introduction to the GFP molecule

A large proportion of the work presented in this thesis involves the generation and imaging of both *B. bacteriovorus* and *E. coli* strains carrying the Green Fluorescent Protein(GFP)-like fluorphore mTFP fused to a protein of interest; in order to study the function of the target protein and find its cellular address. This section will provide a brief summary of background information on GFP work in cellular biology and the challenges faced when using this technology in *B. bacteriovorus*.

Recognised for their respective contribution to cellular biology, the award of a Nobel Prize for Chemistry in 2008 was equally awarded to: Osamu Shimomura, for the discovery of the GFP protein from the jelly fish *Aequorea victoria*, Roger Tsien for the insights into the structure and nature of the GFP fluorophore, and to Martin Chalfie for the use of GFP-protein fusions to colour cells and target proteins. Mutational studies and X-Ray crystal structures have revealed that GFP has an 11 stranded beta-sheet barrel-like structure through which is treaded a alpha helix which contains the fluorophore, shown in Fig. 1.7A (Tsien, 1998). The ability of GFP to catalyze the formation of its own fluorophore from the amino-acid

backbone of the central helix (Fig. 1.7B), and show fluorescence activity without the need for co-factors (although it does require oxygen), is the defining feature of this protein which makes it possible to visualise GFP in live unfixed cells. Using this structural data and directed evolution approaches it has been possible to engineer optimised GFP proteins to give a desired spectra, maximal brightness and photostability (Shaner et al., 2004, Ai et al., 2006).

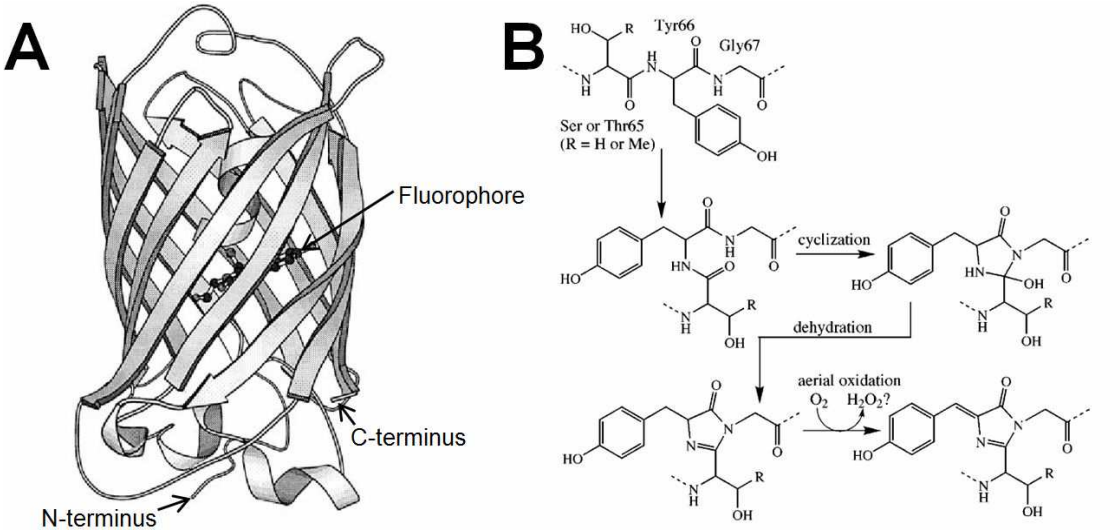

Figure 1.7 The tertiary structure of the GFP molecule (**A**), and the intramolecular biosynthesis of the GFP fluorophore (**B**). Taken from (Tsien, 1998).

1.7.2 Detecting GFP in *B. bacteriovorus*

Work by a previous PhD student, Katy Evans, had shown that an enhanced GFP (eGFP) would fold and function within *B. bacteriovorus* cells (Evans, 2007) (Fig. 1.8). In this work transposon mutagenesis of *B. bacteriovorus* (strain 109J and HD100) was used to randomly introduce a fusion construct

containing the *egfp* ORF into the genome, strains carrying inserts were selected using kanamycin (Evans, 2007). Whilst only a small fraction of isolates showed weak fluorescence activity, presumably as high abundance proteins had been tagged in these case, fewer still had defined sub-cellular foci (Fig. 1.8) (Evans, 2007). This work highlighted the need to select a new brighter GFP fluorophore for use in the tiny *B. bacteriovorus* cells.

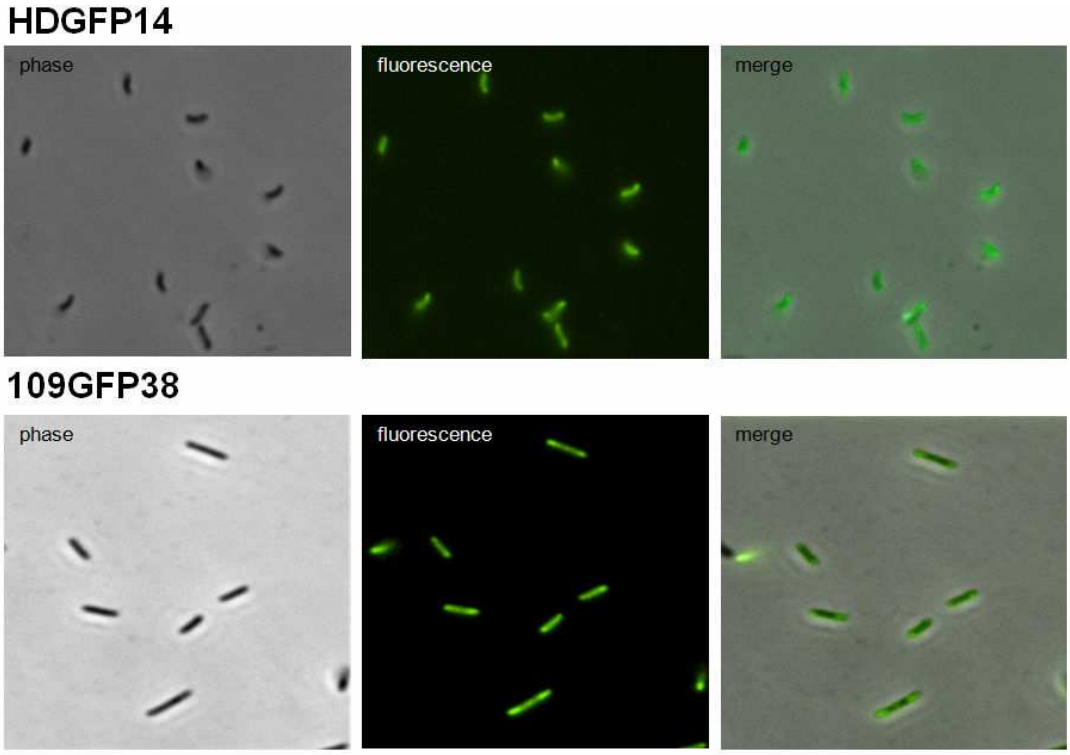

Figure 1.8 Proof-of-principle that GFP can function and be detected in *B. bacteriovorus* attack-phase cells. *B. bacteriovorus* HD100 strain: HDGFP14, and 109J strain: 109GFP26, are shown. All images taken at the same magnification (100x) but digitally zoomed for clarity and to illustrate possible nuclear exclusion or polar localisation of the GFP in the 109GFP38 strain. Stains and images shown here are taken from Katy Evans's thesis: (Evans, 2007).

Auto-fluorescence is also a major problem in cells of rich amino acid content and unfixed membrane structures; like bdelloplasts. Therefore selection of a GFP for use in visualising

developmental events within minuscule *B. bacteriovorus* cells (1 µm X 0.3 µm) (Borgnia et al., 2008), which in turn are within an auto-fluorescent bdelloplast, must produce a strong and clear signal in order to be discriminated from the background.

The overall signal strength of GFP molecules is a trade off between quantum-yield and extinction coefficient (Shaner et al., 2004, Shaner et al., 2005). The extinction coefficient for a given GFP can be thought of as the amount of light energy absorbed (per mole) by the GFP fluorophore, the quantum yield is the proportion of that absorbed energy realised as fluorescence; taken together these provide a rough measure of GFP 'brightness' (Extinction-coefficent X Quantum yield), Table 1.1.

All GFP molecules bleach i.e. fluorescence activity decreases under intense stimulation. Thus detection of a GFP molecule in a live cell is not solely based on its brightness. A GFP fluorophore with high photostability allows for multiple excitations of the same GFP molecule without bleaching; of course if you do this you lose overall image clarity.

Taking all these considerations into account the monomeric teal-fluoresent-protein (TFP) was chosen for tagging *B. bacteriovorus* proteins in this study. The *tfp* gene was first isolated from the *Clavularia* coral and optimised by random mutational methods for monomerisation and fluorophore optimisation,

generating the monomeric derivative mTFP1 (hereafter called mTFP) (Ai et al., 2006). The mTFP molecule has a high brightness and photostability (Table 1.1) without introducing any experimental complications which may result from GFP oligomerisation, as may be the case for the brighter YPet protein (Table 1.1).

Fluorescent Protein	**Max Excitation /Emission (nm)**	**Extinction coefficient (mM^{-1} cm^{-1})**	**Quantum yield**	**Brightness $(mM\ cm)^{-1}$**	**Photo-stability (s)**	**Oligomr -isation**
DsRed-monomer	558/583	35	0.1	3.5	16	Monomer
mCherry	587/610	78	0.22	16	96	Monomer
YPet	517/530	104	0.77	80	49	Weak dimer
eGFP	488/507	56	0.6	34	174	Weak dimer
mTFP1	462/492	64	0.85	54	163	Monomer

Table 1.1 GFP fluorophore data. Adapted from: (Shaner et al., 2004, Shaner et al., 2005, Ai et al., 2006).

The results of my studies using both fluorescent protein technologies and directed mutagenesis are shown in chapter 3 for Crescentin, in chapter 4 for a study on bacterial septation and a novel bactofilin-like protein Bd3904, and in chapter 5 for MreB proteins.

CHAPTER TWO

Materials and Methods

2.1 Strains and Plasmids

Table of bacterial strains used in this study

Strain	Description	Source or reference
E. coli strains		
S17-1	*thi, pro, hsdR*$^-$, *hsdM*$^+$, *rec*A; integrated plasmid RP4-Tc::Mu-Kn::Tn*7*; used as donor for conjugation of plasmids into *B. bacteriovorus*	(Simon et al., 1983)
DH5α	F$^-$ *endA1 hsdR17* ($r_k^-m_k^-$) *supE44 thi-1 recA1 gyrA* (Nal^r) *relA1* Δ(*lacIZYA-argF*) U169 *deoR* (80d*lac*Δ(*lacZ*)M15) ; used as a cloning strain.	(Hanahan, 1983)
S17-1:pZMR100	S17-1 strain containing pZMR100 plasmid to confer Kn^r; Used as Kn^r prey for *B. bacteriovorus* predatory cultures	(Rogers et al., 1986)
S17-1:pCL100	S17-1 strain containing pCL100 plasmid to confer Kn^r and luminescence.	(Lambert et al., 2003)
S17-1:pMAL-p2_mCherry	S17-1 strain containing the pMAL-p2_mCherry plasmid which exports a MalE-mCherry fusion protein into the periplasm.	Dr R. Woods (unpublished)
DH5α:pAKF45	DH5α strain containing pAKF45 plasmid. Strain expresses the HD100 *B. bacteriovorus* gene: *Bd3904*.	This study
DH5α:pAKF52	DH5α strain containing pAKF52 plasmid. Strain expresses the modified HD100 *B. bacteriovorus* gene: *huA-mtfp*.	This study
DH5α:pAKF53	DH5α strain containing pAKF53 plasmid. Strain expresses the modified HD100 *B. bacteriovorus* gene: *Bd3904-mtfp*.	This study
Bdellovibrio bacteriovorus strains		
HD100	Type strain; genome sequenced	(Stolp and Starr, 1963), (Rendulic et al., 2004)
HD100 *ccrp*::Kn^r	HD100 strain with a kanamycin-interrupted *ccrp* gene (*Bd2697*).	This study

Strain	Description	Source or reference
HD100 *Bd1169*::Kn^r	HD100 strain with a kanamycin-interrupted *Bd1169* gene.	This study
HD100 *Bd2345*::Kn^r	HD100 strain with a kanamycin-interrupted '*ABC*' gene (*Bd2345*). Kn^r cassette placed in the equivalent genome position as the *B. bacteriovorus* strain109JK; which has no predatory phenotype. (Lambert et al., 2003)	Dr L. Hobley (unpublished)
HD100 *ccrp-mtfp*	HD100 strain carrying integrated plasmid pAKF42a at the *ccrp* (*Bd2697*) locus	This study
HD100 *Bd1169-mtfp*	HD100 strain carrying integrated plasmid pAKF43a at the *Bd1169* locus	This study
HD100 *huA-mtfp*	HD100 strain carrying integrated plasmid pAKF54 at the *huA (Bd2104*) locus	This study
HD100 *Bd3904-mtfp*	HD100 strain carrying integrated plasmid pAKF58 at the *(Bd3904*) locus	This study
HD100 *mreB1-mtfp*	HD100 strain carrying integrated plasmid pAKF41a at the *mreB1* (*Bd0211*) locus	(Fenton et al., 2010)
HD100 *mreB2-mtfp*	HD100 strain carrying integrated plasmid pAKF40a at the *mreB2* (*Bd1737*) locus	(Fenton et al., 2010)
HD100 *filC1/filC1*::Kn^r	Merodiploid HD100 with both wild-type and kanamycin-interrupted *fliC1*	(Evans et al., 2007)
Bdellovibrio bacteriovorus host-independent strains		
HID2	Host independent derivative of HD100	(Evans et al., 2007)
HID13	Host independent derivative of HD100	(Fenton et al., 2010)
HD100 *mreB1-mtfp* (HI strains 1 – 10)	Ten host independent derivative stains of HD100 *mreB1-mtfp*	This study
HD100 *mreB2-mtfp* (HI strains 1 – 10)	Ten host independent derivative strains of HD100 *mreB2-mtfp*	This study
HD100 *filC1/filC1*::Kn^r (HI strains 1 – 10)	Ten host independent derivative strains of HD100 *filC1/filC1*::Kn^r	This study

Table 2.1 Table of bacterial strains used in this study

Table of plasmids used in this study

Plasmids	Description	Source or reference
pUC19	Amp^r high copy number cloning vector	(Yanisch-Perron et al., 1985)
pGEM7	Amp^r high copy number cloning vector	(Ebright et al., 1992)
pUC4K	High copy number vector used as source of Kn^r cassette in *B. bacteriovorus* kanamycin-interruption knockouts.	(Yanisch-Perron et al., 1985)
pTrc99A	*Ptrc* based Amp^r expression vector from Pharmacia	(Amann et al., 1988)
pSET151	Suicide vector used for conjugation and recombination into the *B. bacteriovorus* genome	(Bierman et al., 1992)
pK18*mobsacB*	Kn^r suicide vector used for conjugation and recombination into *B. bacteriovorus* genome	(Schafer et al., 1994)
pBAD_*mtfp1*	pBAD/His B vector containing the *mtfp1* ORF	(Ai et al., 2006)
pAKF04 remake	Derivative of pTrc99A with insertion of a 722 bp fragment containing the *mtfp* ORF, amplified from the pBAD_*mtfp1* vector using the primers mTFP_F and mTFP_R, and ligated blunt into the the SmaI site downstream of the P*trc* promoter. KpnI site immediately upstream of the *mtfp* ORF used for gene-*mtfp* fusions.	This study
pAKF05	Derivative of pUC19 with insertion of a 2677 bp PCR product containing the HD100 *rodA* gene plus 1 kb of 3' and 5' flanking genomic DNA. PCR amplification of the HD100 genome using the primers RodA_KO_F and RodA_KO_R introduced KasI and XbaI sites used to clone into the MCS of pUC19.	This study
pAKF06	Derivative of pAKF05 containing the inactivated HD100 *rodA* gene with 1Kb 5' and 3' flanking genomic DNA. A Kn^r cartridge from the pUC4K vector was inserted into a unique BamHI site of the *rodA* gene to inactivate it.	This study
pAKF07	Derivative of the mobilisable pSET151 vector containing the kanamycin-interrupted HD100 *rodA* gene with 1 kb 5' and 3' flanking genomic DNA cloned into the MCS using KasI and XbaI sites of pSET151 ligated with a KasI and SpeI fragment of pAKF06	This study
pPW100	Derivative of pUC19 with insertion of a 3009 bp PCR product containing the HD100 *mreB1* gene plus 1 kb of 3' and 5' flanking genomic DNA. PCR amplification of the HD100 genome using the primers mreB2-1 and mreB2-2, introduced KpnI and XbaI sites used for the insertion into the MCS of pUC19.	Mr P. C. Wagstaff
pAKF09	Derivative of pPW100 containing the inactivated HD100 *mreB1* gene with 1 kb 5' and 3' flanking genomic DNA. A blunt Kn^r cartridge from the pUC4K vector digested with HincII was inserted into a unique SnaB1 site of the *mreB1* gene to inactivate it.	This study
pAKF10	Derivative of the mobilisable pSET151 vector containing the kanamycin-interrupted HD100 *mreB1* gene with 1 kb 5' and 3' flanking genomic DNA. A SphI pAKF09 fragment was inserted into the SphI site in the MCS of pSET151.	(Fenton et al., 2010)
pAKF13	Derivative of pGEM7 with insertion of a 3251 bp PCR product containing the HD100 *Bd1167* gene plus 1 kb of 3' and 5' flanking genomic DNA. PCR amplification of the HD100 genome using the primers CreS2_KO2_F and CreS2_KO2_R introduced XbaI sites used to clone into the MCS of pGEM7.	This study

Plasmids	Description	Source or reference
pAKF14	Derivative of pAKF13 containing the inactivated HD100 *Bd1167* gene with 1 kb 5' and 3' flanking genomic DNA. A blunt Kn^r cartridge from the pUC4K vector digested with HincII was inserted into a unique PmlI site of the *Bd1167* gene to inactivate it.	This study
pAKF15	Derivative of the mobilisable pSET151 vector containing the kanamycin-interrupted HD100 *Bd1167* gene with 1 kb 5' and 3' flanking genomic DNA. An XbaI pAKF14 fragment was inserted into the XbaI site in the MCS of pSET151.	This study
pAKF17	Derivative of pGEM7 with insertion of a 2973 bp PCR product containing the HD100 *mreB2* gene plus 1 kb of 3' and 5' flanking genomic DNA. PCR amplification of the HD100 genome using the primers MreB1_KO_F and MreB1_KO_R introduced XbaI sites used to clone into the MCS of pGEM7.	This study
pAKF18	Derivative of pAKF17 containing the inactivated HD100 *mreB2* gene with 1 kb 5' and 3' flanking genomic DNA. A blunt Kn^r cartridge from the pUC4K vector digected with BamHI was inserted into a unique BglII site of the *mreB2* gene to inactivate it.	This study
pAKF19	Derivative of pGEM7 with insertion of a 3129 bp PCR product containing the HD100 *ccrp* gene plus 1 kb of 3' and 5' flanking genomic DNA. PCR amplification of the HD100 genome using the primers CreS1_KO2_F and CreS1_KO2_R introduced XbaI sites used to clone into the MCS of pGEM7.	This study
pAKF20	Derivative of pSET151 containing kanamycin-interrupted HD100 *mreB2* ORF with 1 kb 5' and 3' flanking genomic DNA. An XbaI pAKF18 fragment was inserted into the XbaI site in the MCS of pSET151.	(Fenton et al., 2010)
pAKF21	Derivative of pAKF19 containing the inactivated HD100 *ccrp* gene with 1 kb 5' and 3' flanking genomic DNA. A blunt Kn^r cartridge from the pUC4K vector digected with HincII was inserted blunt into a unique NruI site of the *ccrp* gene to inactivate it.	This study
pAKF22	Derivative of the mobilisable pSET151 vector containing the kanamycin-interrupted HD100 *ccrp* gene with 1 kb 5' and 3' flanking genomic DNA. An XbaI pAKF21 fragment was inserted into the XbaI site in the MCS of pSET151.	This study
pAKF25a	Derivative of pAKF53 with insertion of a 510 bp HD100 *ftsK* ORF fragment 1-1, fused frame with *mtfp*. PCR amplification of the HD100 genome using the primers FtsK_site1_F and FtsK_site1_R, introduced a 5' EcoRI site and a 3' KpnI site used for in frame insertion with the *mtfp* ORF on the pAKF53 vector.	This study
pAKF26a	Derivative of pAKF53 with insertion of a 705 bp HD100 *ftsK* ORF fragment 1-2, fused frame with *mtfp*. PCR amplification of the HD100 genome using the primers FtsK_site1_F and FtsK_site2_R, introduced a 5' EcoRI site and a 3' KpnI site used for in frame insertion with the *mtfp* ORF on the pAKF53 vector.	This study
pAKF27a	Derivative of pAKF53 with insertion of an 888 bp HD100 *ftsK* ORF fragment 1-3, fused frame with *mtfp*. PCR amplification of the HD100 genome using the primers FtsK_site1_F and FtsK_site3_R, introduced a 5' EcoRI site and a 3' KpnI site used for in frame insertion with the *mtfp* ORF on the pAKF53 vector.	This study
pAKF28a	Derivative of pAKF53 with insertion of a 1200 bp HD100 *ftsK* ORF fragment 1-4, fused frame with *mtfp*. PCR amplification of the HD100 genome using the primers FtsK_site1_F and FtsK_site4_R, introduced a 5' EcoRI site and a 3' KpnI site used for in frame insertion with the *mtfp* ORF on the pAKF53 vector.	This study

Plasmids	Description	Source or reference
pAKF29a	Derivative of pAKF53 with insertion of an 1121 bp HD100 *ftsZ* ORF fragment 1-1, fused frame with *mtfp*. PCR amplification of the HD100 genome using the primers FtsZ_site1_F and FtsZ_site1_R, introduced a 5' EcoRI site and a 3' KpnI site used for in frame insertion with the *mtfp* ORF on the pAKF53 vector.	This study
pAKF30a	Derivative of pAKF53 with insertion of a 1541 bp HD100 *ftsZ* ORF fragment 1-2, fused frame with *mtfp*. PCR amplification of the HD100 genome using the primers FtsZ_site1_F and FtsZ_site2_R, introduced a 5' EcoRI site and a 3' KpnI site used for in frame insertion with the *mtfp* ORF on the pAKF53 vector.	This study
pAKF31a	Derivative of the mobilisable pK18*mobsacB* vector containing the *ftsK*(1-1)*mtfp* construct. An EcoRI, BamHI fragment of pAKF25a was inserted into the equivalent sites in the MCS of pK18*mobsacB*.	This study
pAKF32a	Derivative of the mobilisable pK18*mobsacB* vector containing the *ftsK*(1-3)*mtfp* construct. An EcoRI, BamHI fragment of pAKF27a was inserted into the equivalent sites in the MCS of pK18*mobsacB*.	This study
pAKF33a	Derivative of the mobilisable pK18*mobsacB* vector containing the *ftsK*(1-4)*mtfp* construct. An EcoRI, BamHI fragment of pAKF28a was inserted into the equivalent sites in the MCS of pK18*mobsacB*.	This study
pAKF34a	Derivative of the mobilisable pK18*mobsacB* vector containing the *ftsZ*(1-1)*mtfp* construct. An EcoRI, BamHI fragment of pAKF29a was inserted into the equivalent sites in the MCS of pK18*mobsacB*.	This study
pAKF35a	Derivative of the mobilisable pK18*mobsacB* vector containing the *ftsK*(1-2)*mtfp* construct. An EcoRI, BamHI fragment of pAKF29a was inserted into the equivalent sites in the MCS of pK18*mobsacB*.	This study
pAKF36a	Derivative of pAKF53 with insertion of a HD100 *mreB2* 3' ORF fragment lacking the stop codon fused with *mtfp*. PCR amplification of the HD100 genome using the primers MreB1_site1_F and MreB1_site1_R introduced a 5' EcoRI site and a 3' KpnI site used for in frame insertion with the *mtfp* ORF on the pAKF53 vector.	This study
pAKF37a	Derivative of pAKF53 with insertion of a 958 bp HD100 *mreB1* 3' ORF fragment lacking the stop codon fused with *mtfp*. PCR amplification of the HD100 genome using the primers MreB2_site1_F and MreB2_site1_R introduced a 5' EcoRI site and a 3' KpnI site used for in frame insertion with the *mtfp* ORF on the pAKF53 vector.	This study
pAKF38a	Derivative of pAKF53 with insertion of a 937 bp HD100 *ccrp* 3' ORF fragment lacking the stop codon fused with *mtfp*. PCR amplification of the HD100 genome using the primers CreS1_site1_F and CreS1_site1_R introduced a 5' EcoRI site and a 3' KpnI site used for in frame insertion with the *mtfp* ORF on the pAKF53 vector.	This study
pAKF40a	Derivative of pK18*mobsacB* containing a 3' fragment of the HD100 *mreB2* ORF lacking the stop codon fused with *mtfp.* An EcoRI, XbaI fragment of pAKF36a was inserted into the equivalent sites in the MCS of pK18*mobsacB*.	(Fenton et al., 2010)
pAKF41a	Derivative of pK18*mobsacB* containing a 3' fragment of the HD100 *mreB1* ORF lacking the stop codon fused with *mtfp.* An EcoRI, XbaI fragment of pAKF37a was inserted into the equivalent sites in the MCS of pK18*mobsacB*.	(Fenton et al., 2010)
pAKF42a	Derivative of pK18*mobsacB* containing a 3' fragment of the HD100 *ccrp* ORF lacking the stop codon fused with *mtfp.* An EcoRI, BamHI fragment of pAKF38a was inserted into the equivalent sites in the MCS of pK18*mobsacB*.	This study

Plasmids	Description	Source or reference
pAKF45	Derivative of pTrc99A capable of expressing HD100 *Bd3904* ORF. PCR amplification of the HD100 genome using primers Bd3904_pTrc_F and Bd3904_pTrc_R, introduced NcoI and BamHI sites used for insertion immediately downstream of the *Ptrc* promoter in the pTrc99A vector.	This study
pAKF52	Derivative of pAKF04(remake) with a 652 bp insertion containing the full HD100 *huA* ORF lacking the stop codon fused with *mtfp,* and 5' flanking genomic DNA. PCR amplification of the HD100 genome using the primers huA_site1_F and huA_site1_R introduced a 5' EcoRI site and a 3' KpnI site used for in frame insertion with the *mtfp* ORF on the pAKF04remake vector.	This study
pAKF53	pAKF04(remake) cut with XhoI. 3' overhanging ends were PCR filled in and the resulting blunt vector re-ligated. This introduced an additional 4 bp immediately upstream of the KpnI site used for gene-*mtfp* fusions.	This study
pAKF54	Derivative of pK18*mobsacB* containing the full HD100 *huA* ORF lacking the stop codon fused with *mtfp,* and 5' flanking DNA. An EcoRI, BamHI fragment of pAKF52 was inserted into the equivalent sites in the MCS of pK18*mobsacB*.	This study
pAKF56	Derivative of pTrc99A with insertion of a 916 bp fragment containing the *mcherry* ORF, amplified using the primers mCherry_p04_F and mCherry_R, and ligated into the pTrc99A vector using primer incorporated KpnI and BamHI sites. The KpnI site immediately upstream of the *mcherry* ORF is equivalent to that of the pAKF04remake plasmid used for gene-*mtfp* fusions.	This study (Shaner et al., 2004)
pAKF57	Derivative of pAKF04remake with a 658 bp insertion containing the full HD100 *Bd3904* ORF lacking the stop codon fused with *mtfp,* and 5' flanking genomic DNA. PCR amplification of the HD100 genome using the primers Bd3904_site1_F and Bd3904_site1_R introduced a 5' EcoRI site and a 3' KpnI site used in frame insertion with the *mtfp* ORF on the pAKF04remake vector.	This study
pAKF58	Derivative of pK18*mobsacB* containing the full HD100 *Bd3904* ORF lacking the stop codon fused with *mtfp,* and 5' flanking DNA. An EcoRI, BamHI fragment of pAKF57 was inserted into the equivalent sites in the MCS of pK18*mobsacB*.	This study
pAKF69	Derivative of pAKF56 with insertion of the full HD100 *ftsZ* ORF lacking the stop codon fused with *mcherry*. PCR amplification of the HD100 genome using the primers FtsZ_site0_F and FtsZ_site3_F introduced a 5' EcoRI site and a 3' KpnI site used for in frame insertion with the *mcherry* ORF on the pAKF56 vector.	This study
pAKF80	Derivative of the mobilisable pK18*mobsacB* vector containing the *ftsZ*(1-3)*mcherry* construct. An EcoRI, BamHI fragment of pAKF69 was inserted into the equivalent sites in the MCS of pK18*mobsacB*.	This study

Table 2.2 Plasmids used in this study

2.2 Bacterial growth conditions

All chemicals were purchased from Sigma-Aldrich (www.sigmaaldrich.com) unless otherwise stated. All media was prepared in de-ionised-distilled ultrapure water unless specified and was sterilised by autoclaving.

2.2.1 *E. coli* media and growth conditions

E. coli strains were routinely cultured on YT (or occasionally LB) plates and broth. *E. coli* frozen stocks were typically streaked to single colonies on YT plates and incubated at 37^{o}C for over 16 h. Single colonies were picked from YT agar plates, and added to YT broth containing appropriate concentrations of antibiotics (Table 2.3) in suitable sterile containers, and incubated at 37^{o}C with 200 rpm shaking for 16 h. The resulting cultures of stationary-phase *E. coli* cells (typically containing 1X10^{6} - 1X10^{7} cfu/ml) were used as prey for *B. bacteriovorus* predation.

E. coli cells were grown in a similar manner to prepare inocula to produce mid-log-phase cultures for use in conjugative delivery of plasmids, and in preparation for making competent cells.

Frozen stocks of *E. coli* were stored at -80^{o}C and were made by snap freezing a mixture of 700 µl of stationary-phase cultures with 150 µl of 80% glycerol in liquid nitrogen.

YT broth (per litre)

5g	Yeast extract (Difco)
8g	Bacto-tryptone (Difco)
5g	NaCl (Fisher scientific)

Adjusted to pH7.5 using 2M NaOH

Agar plates were made to a final concentration of 10 g/l agar.

2.2.2 *B. bacteriovorus* media and predatory growth conditions

Host-dependant *B. bacteriovorus* strains were grown on YPSC agar overlay plates, consisting of a solid YPSC bottom layer (into which antibiotics were added as appropriate, for concentrations used see Table 2.3) with a of semi-solid YPSC top-agar layer containing both *B. bacteriovorus* and prey. 5 ml of molten YPSC top agar (held at 50^{o}C) was added to 150 µl of stationary phase prey cells, typically *E. coli* S17-1 or the kanamycin resistant S17-1:pZMR100, in a sterile test tube, and immediately poured onto a YPSC bottom plate and left for about 5 min to set. For resurrection of *B. bacteriovorus* strains 50-100 µl of frozen stocks were pipetted onto the pre-poured YPSC overlay plates, resulting in a zone-of-clearing of prey lawns.

For HD *B. bacteriovorus* viable enumerations, 100 µl of predatory cultures were added into the 150 µl of prey immediately prior to YPSC-top mixing and pouring. YPSC overlay plates were incubated in a static 29^{o}C incubator. Confluent lawns of prey cells were visible after 16 h of growth, *B. bacteriovorus* plaques or

zones-of-clearing appeared on the prey lawns between 3 and 10 days after incubation.

Ca/Hepes buffer (per litre)

5.94g	Hepes (Fisher scientific)
0.294g	$CaCl_2.2H_2O$ (Melford)

Adjusted to pH7.8 using 2M NaOH

YPSC broth (per litre)

1.0g	Yeast extract (Difco)
1.0g	Peptone (SLS)
0.5g	Anhydrous sodium acetate (Fisher scientific)
0.25g	$MgSO_4.7H_2O$ (Fisher scientific)

Adjusted to pH7.6 using 2M NaOH

Following autoclaving, sterile $CaCl_2$ (25 g/ml stock) was added to a final concentration of 0.25 g/l

Agar plates were made to a final concentration of 10 g/l agar (YPSC bottom) and 6 g/l (YPSC top).

2.2.2.1 Transferral of *B. bacteriovorus* cells from YPSC overlay plates to liquid predatory cultures.

B. bacteriovorus cells were transferred from cleared regions on YPSC overlay plates to liquid culture by the sterile removal of a small section of the top layer from YPSC overlay plates and transferral of this material into 2 ml predatory cultures (this was usually achieved using a sterile 1000 µl pipette tip). Typically these predatory cultures were set up in 5 ml Bijou tubes containing 2 ml Ca/HEPES buffer (see section 2.2.2 for recipe) and 150 µl stationary-phase *E. coli* prey cells and incubated in a shaking 29^{o}C incubator, at 200 rpm.

2.2.2.2 Maintenance of *B. bacteriovorus* predatory cultures

Visual inspections of the parent *B. bacteriovorus* predatory cultures using phase contrast microscopy revealed the presence of any contaminating Gram-negative bacteria and ensured that the parent culture contained 'pure' attack-phase *B. bacteriovorus* cells (although all *B. bacteriovorus* cultures always contain a small number of surviving prey cells). Fresh *B. bacteriovorus* predatory cultures were set up typically in 250 ml conical flasks containing 50 ml of Ca/HEPES buffer, 3 ml of stationary-phase *E. coli* prey and 1 ml of the parent *B. bacteriovorus* culture from a fresh prey lysate. Scaled down versions of these cultures, containing 10 ml of Ca/HEPES, 600 µl of stationary-phase *E. coli* prey and 200 µl of *B. bacteriovorus* parent cultures were set up in 50 ml universal containers to reduce waste and save space. Mixed cultures were incubated in a 29^{o}C incubator, shaking at 200 rpm, *B. bacteriovorus* predatory cultures set up in this way would clear most of the *E. coli* prey cells within 16-18 h and liberate typically 1x10^{7} *B. bacteriovorus* cells per ml.

Ca/Hepes buffer (per litre)

5.94g	Hepes (Fisher scientific)
0.294g	$CaCl_2.2H_2O$ (Melford)

Adjusted to pH7.8 using 2M NaOH

2.2.3 Isolation of host-independent *B. bacteriovorus* strains

Host-Independent (HI) *B. bacteriovorus* strains were isolated by passing 10 ml of predatory cultures (incubated for 16+ h) sequentially through two 0.45 µm filters, to remove the few remaining *E. coli* prey, then the *B. bacteriovorus* attack-phase cells from the filtrate were harvested in a Sigma 4K15 centrifuge at 5,100 rpm (5,525g) for 20 min. The resultant pellet was re-suspended in 100 µl of PY broth. This enriched cell suspension was spread onto a fresh PY plate (containing antibiotics if appropriate) and incubated upside-down at 29^{o}C. HI *B. bacteriovorus* colonies typically formed within 7-12 days.

PY broth (per litre)

10g	Peptone (SLS)
3g	Yeast extract (Difco)

Adjusted to pH6.8 using 2M NaOH

Agar plates were made to a final concentration of 10 g/l agar.

2.2.3.1 Maintenance of *B. bacteriovorus* host-independent strains

HI strains could be maintained by repeat streaking of colonies onto fresh PY plates. To generate HI cultures, HI colonies were picked into 500 µl of PY broth (plus antibiotics if appropriate), this was incubated at 29°C, shaking at 200 rpm. No conventional quorum sensing system exists in *B. bacteriovorus,* but there is a cryptic requirement for sequential incremental sub-culturing because HI *B. bacteriovorus* cells will not grow if picked into large volumes of PY to begin with (for example 50 ml PY), even if incubated for long periods of time. Visual inspections of resulting HI liquid cultures were used to determine if the culture was 'thick enough' to add additional PY media. Large volumes of HI cultures could only be grown by successive additions of PY broth which double the culture volume each time and further incubation at 29°C, 200 rpm shaking. HI growth rates are highly variable and get faster the longer the HI culture is maintained in liquid media, thus inspection of HI cultures on a two day basis was necessary so that they were not overgrown nor starved of oxygen or nutrients.

PY broth (per litre)

10g	Peptone (SLS)
3g	Yeast extract (Difco)

Adjusted to pH6.8 using 2M NaOH

Agar plates were made to a final concentration of 10 g/l agar.

2.2.3.2 Frozen stocks of *B. bacteriovorus* strains

Frozen stocks of *B. bacteriovorus* HD and HI cultures were stored at -80^{o}C and were made by snap freezing 700 µl of 'pure' attack-phase predatory cultures or thick HI cultures with 150 µl of 80% glycerol in liquid nitrogen.

2.2.4 Antibiotics and media additives

All antibiotics and media additives were purchased from Apollo scientific (www.apolloscientific.co.uk). Concentrations used in the table below apply for *B. bacteriovorus* HI and HD culturing as well as *E. coli* culturing and cloning.

Antibiotic/Additive	Stock concentration	Final concentration	Solvent
Ampicillin (Amp)	50 mg/ml	50 µg/ml	AnalaR water
Kanamycin (Kn)	50 mg/ml	50 µg/ml	AnalaR water
Isopropyl-beta-D-thiogalactopyranoside (IPTG)	200 mg/ml	variable	AnalaR water
5-Bromo-4-chloro-3-indolyl-beta-D-galactoside (XGal)	20 mg/ml	200 µl/mg	Dimethyl-formamide (DMF)

Table 2.3 Antibiotics and Media additives used in this study

2.3 DNA Manipulation Techniques

2.3.1 Small scale plasmid isolations

For routine screening of multiple transformants to determine the most likely clones for further work, a fast and scaled-down version of plasmid isolation by alkaline lysis was used (Birnboim and Doly, 1979). 200 µl of an overnight *E. coli* culture was lysed in 200 µl of freshly made 1% sodium dodecyl sulphate (SDS), 0.2 M NaOH solution, inverted to mix, then neutralised with 200 µl of 3M potassium acetate, at pH5.5. This mix was centrifuged for 15 min at 16,400 g in a microcentrifuge to pellet cell debris and the supernatant removed to a new tube. Addition and mixing of 500 µl 100% isopropanol (at -20^{o}C) caused precipitation of plasmid DNA. Centifugation at 16,400g in a microcentrifuge (held at 4^{o}C) for 15 min generated a crude plasmid pellet, which was further cleaned by washing in 70% ethanol (at -20^{o}C); removal of the supernatant and drying the DNA pellet allowed resuspension in 20µl Tris-EDTA +RNaseA (10mM Tris-HCl, pH8.0, 2 mM EDTA, 10 µg/ml RNase A) and downstream screening by restriction digestion and electrophoresis.

Favoured clones were the re-grown from master plates in YT broth with necessary antibiotics at 37°C for 16 h. Plasmid DNA was prepared using either Qiagen^{TM} Mini-prep or Sigma-Aldrich^{TM} GenElute plasmid miniprep kits, both use the same alkaline lysis

and column purification method of DNA purification. Methods carried out in accordance with manufacturer's instructions, DNA was eluted from the column in the lowest recommended volumes.

2.3.2 Large scale plasmid isolations

For large scale plasmid 'midi preps', alkaline lysis and column DNA purification was carried out using either Sigma-Aldrich™ HP plasmid Midiprep kits according to manufacturer's instructions.

2.3.3 Isolation of bacterial genomic DNA

Total bacterial genomic DNA was isolated using a Sigma-Aldrich GenElute Bacterial Genomic DNA kit, according to manufacturer's instructions for Gram-negative bacteria. 10 ml of 'attack-phase only' predatory *B. bacteriovorus* cultures and 2 ml of HI *B. bacteriovorus* cultures were harvested by centrifugation in a Sigma 4K15 centrifuge at 5,100 rpm (5,525g) for 20 min.

2.3.4 Agarose gel electrophoresis

Agarose gel electrophoresis was carried out using 1x TBE supplemented with 0.1 µg/ml ethidium bromide. Agarose concentrations varied depending on the sizes of DNA fragments being resolved, from between 0.8 and 2.0% (w/v TBE). Gels were run at a constant voltage of 100 V and DNA was visualised under UV light using a BioRad™ gel documentation system and captured using the BioRad™ Quantity One software (version 4.4.0). 5 µl of diluted 1Kb New England Biolabs (NEB) DNA ladder or 10 µl of diluted 100 bp NEB DNA ladder were was used as the molecular weight DNA marker for all gels. DNA samples were loaded in 3 X Orange G loading buffer using the Orange G dye (see recipe below and Appendix 2.1 for a list of marker sizes).

Fragments of DNA required for downstream techniques were excised from agarose gels using a sterile scalpel whilst being visualised using a UVP (UV) transilluminator. The DNA from the agarose gel slice was extracted and purified using either a QIAquick Gel Extraction Kit (Qiagen) or a GenElute Gel Extraction Kit (Sigma-Aldrich). Both were performed according to the instructions provided by the manufacturer and eluted from the columns in the smallest recommended volumes.

Solutions used for Agarose gel electrophoresis

10X TBE

108 g	Tris-HCl
55 g	Boric acid
40 ml	0.5 M EDTA (ethylenediaminetetraacetic acid, pH 8.0)

Made up to 1 l with distilled water

10X loading buffer

25% (w/v)	Ficoll 400
0.4% (w/v)	Orange G dye

Made to volume with distilled water

3X Loading buffer

333 µl	10X Orange G
150 µl	20% (v/v) Glycerol
517 µl	Tris-EDTA (10 mM Tris-HCl, 2 mM EDTA, pH 8.0)

Ready to load DNA markers

20 µl	NEB (1 kb or 100 bp) DNA ladder stock (500 µg/ml)
10 µl	0.5 M EDTA (pH 8.0)
10 µl	AnalaR water
120 µl	10X OrangeG
140 µl	Tris-EDTA (10 mM Tris-HCl, 2 mM EDTA, pH 8.0)
100 µl	20% (v/v) Glyerol

2.3.5 Bacterial DNA cloning

All DNA digestions with restriction endonucleases were carried out using enzymes purchased from New England Biolabs (NEB). Restriction digests were incubated at the recommended temperatures in the recommended buffers for 1-18 hours. Care was taken to never increase the 'enzyme' concentrations of restriction digestions above 10% v/v to avoid 'star activity'. Recommended conditions for digestions containing multiple restriction endonucleases were found using the online NEB double digest finder program (http://www.neb.com/nebecomm/DoubleDigestCalculator.asp).

Dephosphorylation of restriction digested vector DNA molecules was achieved using calf intestinal phophatase (CIP) from NEB as per manufacturer's instructions.

Modification of overhanging 5' or 3' DNA ends following restriction digestion was achieved by incubation of the DNA preparation with the Phusion DNA polymerase at 72^{o}C for 30 min (for reaction recipes see Table 2.4).

Ligations of DNA fragments with compatible ends were carried out in a total volume of 20 µl. Reactions contained T4 DNA Ligase and 10 x T4 ligase buffer (both from NEB), and an approximate 1:3 vector to insert ratio following analysis of the concentration of DNA in each sample by agarose gel

electrophoresis. This reaction was either incubated at 16ºC for 16 h or typically incubated at room temperature for 2 hours.

2.3.6 Competence and transformation of *E. coli* with plasmid DNA

E. coli S17-1 or *E. coli* DH5α cells were made competent in batches which were stored at -80°C in 200 µl aliquots by the following method (Recipes for buffers used se below).

10 ml of YT broth was inoculated with a single colony of the desired *E. coli* strain and grown to stationary-phase for use as a starter culture (section 2.2.1). This was diluted 1/100 in YT broth and grown at 37°C, with shaking at 200 rpm, to an OD_{600} of 0.4 to 0.6. The cells were harvested by centrifugation at 5,525g in a Sigma 4K15 centrifuge (pre-cooled to 4°C) for 5 min, then gently re-suspended in 4°C TFB1 (20 ml/50 ml culture). The cells were incubated in TFB1 on ice for 5 min, and then harvested by centrifugation at 5,525g in a Sigma 4K15 centrifuge (pre-cooled 4°C) for 10 min. The pellet was re-suspended in TFB2 (stored at 4°C) on ice, separated into 200 µl aliquots and snap-frozen in liquid nitrogen before storage at -80°C. Each batch of competent cells was tested by transformation with a control plasmid (such as pUC19) and typically >1000 transformants resulted from transformation with approximately 50 ng of control plasmid DNA.

Prior to transformation, an aliquot of frozen competent *E. coli* cells were thawed on ice and the DNA preparation from a ligation reaction was added to the cells and mixed by gentle pipetting. Following 20 min of incubation on ice, the cells were heat shocked at 42ºC for 2 min before quickly being placed on ice for a further 2 min. 1 ml of YT broth was added to each transformation, and the cells allowed to recover by incubation in a static 37ºC incubator for 1 h. After recovery, the cells were plated out onto appropriate selection plates and incubated at 37ºC overnight. In addition to the DNA from ligations, positive and negative controls using uncut vector DNA and no DNA respectively were also carried out.

Solutions used for *E. coli* competent cell production

TFB1

30 mM	KAc
10 mM	$CaCl_2$
50 mM	$MnCl_2$
100 mM	$RbCl_2$
15% (w/v)	Glycerol

Adjusted to pH 5.8 using 1 M acetic acid. Sterilise by filtration through a 0.22 µm filter, and store at 4^{o}C.

TFB2

10 mM	MOPS (3-(N-morpholino)propanesulfonic acid) or PIPES (1,4-Piperazinediethanesulfonic acid)
75 mM	$CaCl_2$
10 mM	$RbCl_2$
15% (w/v)	Glycerol

Adjusted to pH 6.5 using 1 M KOH. Sterilise by filtration through a 0.22 µm filter, and store at 4^{o}C.

2.4 Conjugation of *B. bacteriovorus* with plasmid DNA

1 ml of stationary-phase donor *E. coli* S17-1 culture containing the desired construct, for gene inactivation or GFP-fusion in *B. bacteriovorus*, was inoculated into 40 ml of fresh YT broth with appropriate selection and grown at 37°C, 200 rpm to an OD_{600} of 0.2-0.4. *B. bacteriovorus* cells were harvested from a 10 ml predatory culture by centrifugation in a Sigma 4K15 centrifuge at 5,525 g for 30 min, and re-suspended in 100 µl Ca/HEPES (see section 2.2.2 for recipe). This mixture was pipetted onto a small piece (approximately 2 cm^2) of autoclaved Hybond^{TM}-N nylon membrane (Amersham) placed on a PY (see section 2.2.3 for recipe). agar plate, to immobilise the *B. bacteriovorus* cells. The 40 ml of donor *E. coli* cells were harvested by centrifugation at 5,525 g in a Sigma 4K15 centrifuge for 5 min, re-suspended in 200 µl of PY and added to the filter. This resulted in approximately $1x10^8$-10^{10} *B. bacteriovorus* and $1x10^7$-10^8 donor *E. coli* cells immobilised on the nylon membrane. The PY conjugation plates were incubated for 16 h at 29°C then the bacterial cells from the Hybond-N filter were re-suspended in 1 ml PY by repeated pipetting. As exconjugant numbers tend to be fairly low, selective overlay plates were then made, to recover the recombinant *B. bacteriovorus* as plaques, with inoculums containing 10 µl, 100 µl, 200 µl and 400 µl of the neat PY broth suspensions, in addition to the 150 µl of *E. coli* prey and 5 ml of molten YPSC-top agar in YPSC overlay plates.

2.5 Amplification of DNA

2.5.1 Polymerase chain reaction (PCR) for specific DNA amplification

PCR DNA amplifications performed during this study were carried out using either the Phusion® High-fidelity DNA polymerase (NEB) or high fidelity Kod HiFi DNA polymerases (Novagen) for cloning work, and the low fidelity *Red hot® Taq* DNA polymerase (ABGene) was used for mutant screening before Southern blotting. Oligonucleotide primers were specifically designed to amplify unique DNA fragments from template DNA, and obtained from Eurofins-MWG-Operon Biotech.

Using a Thermo Hybaid gradient thermal cycler, PCR reaction mixtures were incubated at different temperatures in cycles to allow the denaturing, annealing and extension of the DNA template resulting in the amplification of a specific DNA fragment (Table 2.4). The temperature and length of time in each stage of the cycle was dependent on the DNA polymerase used due to the rate at which elongation of the DNA fragment occurs. Phusion DNA polymerase has an extension time of 30 sec per 1 kb and the KOD and *Taq* DNA polymerases amplify DNA at 1 kb per minute. Incubations and cycling conditions for each DNA polymerase are summarised in Table 2.4. Primers used for PCR amplification in this study are shown in Table 2.5.

A) PCR reaction mixtures

	Phusion	**KOD**	***Taq***
DNA Polymerase	0.25 U (0.25 µl)	0.625 U (0.5 µl)	0.25 U (0.1 µl)
Reaction Buffer (5/10x stock)	1x	1x	1x
dNTPs	200 µM	200 µM	250 µM
MgCl2	(present in reaction buffer)	1 mM	2 mM
Primers	100 pmol	100 pmol	100 pmol
PCR Enhancer System (Invitrogen)	-	5µl	-
Template DNA	20-100 ng as appropriate	20-100 ng as appropriate	20-100 ng as appropriate
AnalaR Water	Made up to 25 µl	Made up to 25 µl	Made up to 25 µl

B) Basic cycling conditions for PCR

Stage	**Temperature**	**Duration**	**# cycles**	**Comment**
1	95°C 98°C	10 min (Taq) 5 min (Kod) 5 min (Phusion)	x1	Initial Denaturation
2	95°C 98°C	1 min (Taq/KOD) 10 s (Phusion)	x30	Denaturation
	50-70°C	1 min (Taq/KOD) 30 s (Phusion)		Annealing
	72°C	1 min/kb (Taq) 30 s/kb (KOD/Phsion)		Elongation
3	72°C	10 min	x1	Finishing step
4	4°C	Hold	x1	Hold

Table 2.4 PCR reaction mixtures and cycling conditions for Phusion, KOD and *Taq* DNA polymerases. (**A**) Final concentrations of PCR reaction components for the three DNA polymerases, (**B**) cycling conditions for the PCR reactions using each polymerase.

Table 2.5 Primers used for DNA amplification

Primer	**Sequence (5'-3')**
Bd3904_pTrc_F	AAAGAACCATGGCAGTAAACCTTTCCCCCGCACTCC
Bd3904_pTrc_R	GCGGATCCATGATAATGTTCGCTGCCTAAGACTTAGGC
Bd3904_site1_F	GAACGAATTCGAAGAAACAGATCGAATTTGCG
Bd3904_site1_R	GTAAGGTACCAGACTTAGGCATGTAGGACG
CreS1_KO2_F	TGCTCTAGACCTTGAAAGATCACTTCAGG
CreS1_KO2_R	GCATCTAGAAGAAACGGTCGACAACATGG
CreS1_site1_F	AGGCGAATTCCGAGCGTGAGTCTGC

Primer	Sequence (5’-3’)
CreS1_site1_R	GTAAGGTACCTTCTTTTTCTTCGGCTTCAAGC
CreS2_KO2_F	TGCTCTAGAAACCATGTTTCAGTATGTCG
CreS2_KO2_R	ACGTCTAGATTCCGATTTCCTTGTTCAGG
FtsK_site1_F	GAACGAATTCCTTAAAAAGTTTCGACAGGACG
FtsK_site1_R	TAAGGTACCTCTGCCAGTTCCTGCAGC
FtsK_site2_R	TAAGGTACCTCTTCCTCTTCTTCAGATGC
FtsK_site3_R	TAAGGTACCGGCATATCCCAGTTTTCAATACG
FtsK_site4_R	TAAGGTACCGTTTCACGCTTTAAGTTCGCGG
FtsZ_site0_F	ATGGAATTCGGAGGATCAAATGTTTGAGTTGG
FtsZ_site1_F	ATGGAATTCTGATCGAATCCGGCATGAACGG
FtsZ_site1_R	GTAAGGTACCGTGATCGGCGGAAGTTCAAC
FtsZ_site2_R	GTAAGGTACCAAGGCAGGAACTTCAAGATTC
FtsZ_site3_R	GTAAGGTACCCTATTCTTTATTCAGATCGAATCC
huA_site1_F	GAACGAATTCACCCTTTTCACTCACAACAACCTTGC
huA_site1_R	GTAAGGTACCGTTAAGGGCGTCTTTTAAGTCTTTGC
mCherry_p04_F	CTCGGTACCTCGAGCATGGTGAGCAAGGGC
mCherry_R2	CGCGGATCCTCATCCGCCAAAACAGCC
MreB1_KO_F	TGCTCTAGACTTTCATACAACTCGGAAGCC
MreB1_KO_R	TGCTCTAGACAACTTTTAAAGCGACAATACC
MreB1_site1_F	CATTGAATTCGGAACAGCTGCAGATCTATACG
MreB1_site1_R	GTAAGGTACCACTTCCAACTGAATTTTATCGAGC
mreB2-2	GCTCTAGAGGACGTTTATGAATCTACCC
mreB2-1	GGGGTACCTTTCATACAACTCGGAAGCC
MreB2_site1_F	CATTGAATTCCGGAATCATCCTTGATGAACC
MreB2_site1_R	GTAAGGTACCTCGACTGTAAGCTGTCTGAGAAGG
mTFP_F	ATGGTGAGCAAGGGCGAGGA
mTFP_R	TTACTTGTACAGCTCGTCCATG
RodA_KO_F	CTTAAAAGGCGCCCACGGTAACATCACGG
RodA_KO_R	CCTCTAGAACAAACACTAGTTCCATGCCG

Table 2.5 primers used for DNA amplification

2.5.2 Purification of PCR products

Purification of PCR reactions were achieved using a Sigma-Aldrich™ GenElute PCR Clean-Up kit and following manufactures instructions. DNA was eluted from the column in the minimum volume of buffer recommended by the manufacturer.

2.6 DNA Sequencing

All DNA sequencing was carried out using the DNA sequencing service provided by Eurofins-MWG-operon. Typically a 15 µl preparation containing 10 ng/µl of template DNA to be sequenced was sent with a 2 pmol/ml solution of the desired primer (see table below). Sequencing results were received by email and analysed using the Bioedit software (version 7.0.9.0) (http://www.mbio.ncsu.edu/BioEdit/bioedit.html).

Table of primers used for sequencing.

Primers used for sequencing plasmids	**Sequence (5'-3')**
M13_uni_(-43)	AGGGTTTTCCCAGTCACGACGTT
M13_rev_(-49)	GAGCGGATAACAATTTCACACAGG
pTrcHis_rev	CTTCTGCGTTCTGATTTAATCTG
pK18_For	ATGTTCAGCAGGAAGCTCGG
pK18_Rev	TTCTCCGGTAAACATTACGG

Primers used for sequencing *B. bacteriovorus* strains	**Sequence (5'-3')**
Kam_1	TGCAATGTAACATCAGAG
Kam_2	CACGAGGCAGACCTCAGC
huA_seq_F	GCGGTCAATTTCATAAGAAAGCACATCG
huA_seq_R	CAAGCTTGCATGCCTGCAGG
mreB2_seq_F	CACGACGTTGTAAAACGACG

Table 2.6 Primers used for sequencing both inserts in plasmid vectors and PCR amplified genome regions of *B. bacteriovorus* strains.

2.7 Southern blot hybridisations

Southern blot hybridisations were carried out to verify the chromosomal insertions for mTFP labelling or gene inactivation in *B. bacteriovorus* HD100 using the NEBlot Phototope Kit (New England Biolabs) according to manufacturer's instructions. Briefly 300-400 ng of genomic DNA was digested with restriction endonucleases for at least 16 h. These preparations were resolved by agarose gel electrophoresis (using both pre-biotinylated markers and 1 kb NEB ladder (New England Biolabs) Appendix 2.1) and transferred to a Hybond^{TM}-N nylon membrane (Amersham) using the capillary transfer method (Southern, 1975). The blotted DNA was UV cross-linked to the dried membrane using a 50 mJ dose from a GS Gene linker UV chamber (Biorad). Cross-linked membranes were then pre-hybridised before the addition of a biotinylated DNA probe, typically for a 'large' gel (15 cm x 10 cm) 100 ng of unlabeled DNA was labelled for 1 h with a Klenow Fragment (3′→5′ exo–) forming approximately 333 ng of biotin-labelled probe. The

chemiluminescent signal detection was carried out using the Phototope-Star Detection Kit (New England Biolabs) according to manufacturer's recommendations, the emitted light was captured by exposing the membrane to X-ray film. For solutions and buffers see below.

Solutions used for Southern blot hybridisations

20X SSC

3 M	NaCl
0.3 M	Sodium citrate

Adjusted to pH 7.0 with NaOH, made to volume with distilled water

Denaturation solution

0.5 M	NaOH
1.5 M	NaCl

Neutralisation solution

1 M	Tris-HCl
1.5 M	NaCl

Adjusted to pH 7.5 with HCl, made to volume with distilled water

100X Denhardt's reagent

2%	Ficoll 400
2%	PVP (Polyvinylpyrrolidone)
2%	BSA (Bovine serum albumin)

Prehybridisation solution

6x	SSC
5x	Denhardt's reagent
0.5%	SDS
100 µg/ml	Denatured salmon sperm DNA

Made to volume with distilled water

Blocking solution

5%	SDS
125 mM	NaCl
25 mM	Sodium phosphate

Adjusted to pH 7.2 with NaOH, made to volume with distilled water

Wash solution I

0.5%	SDS
12.5 mM	NaCl
2.5 mM	Sodium phosphate

Adjusted to pH 7.2

Washing solution II

10 mM	Tris-HCl
10 mM	NaCl
1 mM	$MgCl_2$

Adjusted to pH 9.5

2.8 Protein analysis techniques

2.8.1 Sodium Dodecyl Sulphate Polyacrylamide gel electrophoresis (SDS-PAGE)

SDS-PAGE gels (Laemmli, 1970) were hand poured and prepared using the mini Protean II system (BioRad). Unless otherwise stated, resolving gels were 12.5% acylamide and stacking gels were 7.5% acylamide, for recipes see below. Typically 4-5 µg of whole *B. bacteriovorus* or *E. coli* cell extract protein was run on the small SDS-PAGE gels.

2 x sample buffer was added to a final concentration of 1x and the samples boiled for 5 min (with a brief centrifugation) prior to loading. The samples were the loaded onto SDS-PAGE gels with a suitable molecular weight marker (NEB pre-stained protein ladder, Broad Range (10-230 kDa) (New England Biolabs)) for Coomassie stained gels, see Appendix 2.1 for marker sizes. 1x running buffer was prepared from a 10x stock. Gels were run at a constant 120V until the dye front reached the ottom of the gel.

Staining for non-western blot gels was performed overnight in 0.1% Coomassie blue stain and destained in 30% (v/v) Methanol, 10% (v/v) glacial acetic acid for several hours. Protein gel images were captured using a Canon PowerShot A620 digital camera. Occasionally gels were saved and dried using GelAir Cellophane Support (Biorad).

Solutions used for SDS-PAGE protein gels

Resolving gel (12.5%)

3.75 ml	1.5M Tris-HCl, pH 8.8
0.15 ml	10% (w/v) SDS
4.78 ml	AnalaR water
6.25 ml	30% acrylamide / bis-acrylamide (Severn Biotech)
7.5 µl	TEMED (Tetramethylethylenediamine)
125 µl	Ammonium persulphate (Freshly made in water from solid)

Stacking gel (7.5%)

1.75 ml	0.5 M Tris-HCl, pH 6.8
0.10 ml	10% (w/v) SDS
7.38 ml	AnalaR water
1.25 ml	30% acrylamide / bis-acrylamide (Severn Biotech)
7.5 µl	TEMED (Tetramethylethylenediamine)
75 µl	Ammonium persulphate (Freshly made in water from solid)

10 X SDS-PAGE running buffer

30.5 g	Tris
144.13 g	Glycine
10 g	SDS

Made up to 1 l with distilled water

2 X protein sample buffer

630 µl	0.5M Tris-HCl, pH 6.8
2.0 ml	10% (w/v) SDS
0.5 ml	100% Glycerol
1.77 ml	AnalaR water
100 µl	1% (w/v) bromophenol blue
500 µl	β-mecaptoethanol (add last)

Coomassie blue stain

10% (v/v)	Glacial acetic acid
30% (v/v)	Methanol
0.1% (w/v)	Coomassie brilliant blue (ICI)

Made to volume with distilled water. Destain made using the same recipie above, only without the Coomassie brilliant blue.

2.8.2 Lowry assay protocol to determine protein concentration.

A Lowry assay with Markwell's modification to include solubilising membrane proteins (Markwell et al., 1978) was used to measure protein content of *B. bacteriovorus* predatory cultures to use as an indicator of cell number. The Lowry assay measures protein concentration using Folin's phenol reagent in the presence of copper bound proteins, and is measured by colour change at wavelength 750 nm using a Beckman coulter DU 530 Spectrophotometer (Lowry et al., 1951).

Serial dilutions of protein standard, bovine serum albumin (BSA), were prepared ranging from 10-100 µg/ml. 500 µl sterile distilled water served as a blank, the statistical significance of each standard curve was measured.

500 µl of sample was combined with 1.5 ml solution C (solution C = 100 solution A: 1 solution B). Samples were mixed and incubated in the dark for exactly 20 min. 150 µl of fresh Folin's reagent was diluted 1:1 with sterile distilled water was added to each sample and incubated in the dark for exactly 45 min. Absorption at 750nm wavelength for easy assays were recorded versus the blank. Protein concentration of the sample was calculated using the standard curve.

Solutions used for the Lowry assay

Solution A

2% (w/v)	Na_2CO_3
0.4% (w/v)	NaOH
0.16% (w/v)	$Na_4C_4H_4O_6$ (Sodium tartrate)
1% (w/v)	SDS

Made to volume using distilled water

Solution B

4% (w/v)	$CuSO_4 \bullet 5H_2O$

Made to volume using distilled water

2.8.3 Identification of proteins by MALDI-TOF MS analysis

MALDI-TOF MS analysis was carried out to identify protein from SDS PAGE gel slices by Dr Kevin Bailey of the University of Nottingham Biopolymer Analysis unit. A typical data output can be found in Appendix 4.3.

2.8.4 Matched cell numbers of *E. coli* using OD_{600nm}.

Stationary-phase *E. coli* cell cultures (grown in YT broth) were measured for their optical density at 600 nm in a WPA Biowave CO8000 miniature spectrophotomer and diluted in fresh YT media to match the culture with the lowest OD_{600} reading, typically OD_{600} values were in the 1.5-1.8 range. 1 ml of OD_{600} matched stationary-phase cultures were centrifuged at 16,400 g in a microcentrifuge for 1 min, re-suspended in 100 µl AnalaR water and stored at -20^{o}C. 5 µl of this preparation was typically run on an SDS-PAGE gel.

2.9 Microscopy

2.9.1 Fluorescence microscopy

Fluorescence microscopy of *B. bacteriovorus* and *E. coli* was carried out using 10-16 µl samples which were spotted onto a Borosilicate Super Premium glass microscope slide (VMR) and covered with a 22 X 22 mm glass cover slip, thickness No. 1 (VMR). Cells were occasionally immobilised to aid visualisation using a 1% agarose pad made using appropriate media.

Bacterial cells were visualised using a Nikon Eclipse E600 epifluorescence microscope through a plan fluor 100X objective lens (NA: 1.25) (supplied by Nikon). A mercury USH-102D (USHIO) light source in combination with an appropriate filter block (see Table 2.7) was used for fluorescence imaging. Images were captured using a Hamamatsu Orca ER CCD digital camera (C4742-80) and analyzed using either the IPLab software (version 3.64 from Nikon) or the SimplePCI software (version 5.3.1.081004 from Digital Pixel).

For image enhancement using the IPlab software, fluorescence images were background corrected by using the 3D filter tool and normalised within IPLab.

For image enhancement using the SimplePCI software, images were false coloured (typically green for fluorescence and red for brightfield) and enhanced using either (or both) the 'sharpen' and 'smooth' tools.

Filter Name	Filter Use	Excitation (nm)	Emission (nm)
41043 hcRED1 C110624	mCherry/ FM4-64 fluorescence detection	550-600	610-665
CY GFP C121885	mTFP fluorescence detection	420-454	458-500
DAPI DM400	Hoechst fluorescence detection	340-380	435-485

Table 2.7 Fluorescence filter sets used in this study

2.9.2 Hoechst 33372 DNA straining and detection in *B. bacteriovorus*

Hoechst 33372 DNA stain was used to visualise the genome of both attack-phase *B. bacteriovorus* cells, and *E. coli* genomes present in bdelloplasts. Samples were stained at final Hoechst concentrations of 1 µg/ml, for 2-5 min, at room temperature immediately before imaging. Hoechst fluorescence images were taken using a Nikon E600 epifluorescence microscope, set up as described in section 2.9.2, typical Hoechst fluorescence exposure times were 100 ms. Due to the lack of colour options within IPLab and the Simple PCI software, Hoechst merged images were

achieved by using the duplicate channels tool in Adobe Photoshop (version 5.5); 100% opacity was used in all cases.

2.9.3 FM4-64 membrane straining and detection in *B. bacteriovorus*

FM4-64 membrane strain (Invitrogen) was used to stain *B. bacteriovorus* flagella shealth and cell membranes (Iida et al., 2009). FM4-64 was used to stain *B. bacteriovorus* predatory cultures at a final concentration of 10 µg/ml for 10-15 min on ice. Incubations were carried out in the dark due to FM4-64 very low photo stability. FM4-64 fluorescence was imaged using a Nikon E600 epifluorescence microscope, set up as described in section 2.9.2, typical fluorescence exposure time required to visualise the flagella sheath was 1 s.

2.9.4 Time-lapse epifluorescence microscopy using the prior H101a XY-stage and H122 Z-controller.

Synchronous *B. bacteriovorus* predatory infections were set up as described in section 2.13.4 and immobilised on a glass microscope slide coated with a 1% agarose-Ca/HEPES pad into which two reservoirs had been cut and filled with distilled water; to replace moisture lost from the pad through dehydration.

Immobilised bdelloplasts were visualised using a Nikon Eclipse E600 epifluorescence microscope using a 100X objective lens (NA:1.25), and the hcRED filter block with a fluorescence exposure time 0.1 s. Images were acquired using a Hamamatsu Orca ER CCD camera (C4742-80) and the Simple PCI software (version 5.3.1.081004 from Digital Pixel). A Prior H101A XY-motorised stage (Prior Scientific) allowed precise revisiting of different locations on the slide (minimum step size=0.01 μm), and a frictional Z-axis controller (minimum step size = 2 nm) in conjunction with the Simple PCI software allowed fine auto-focusing on immobilised developing bdelloplasts. Typically 10 fields of view were imaged sequentially every 2.5 min per experiment, as this provided a good trade off between temporal-resolution and mCherry photo-bleaching. Time-stamps embedded in image files were used for all measurements of time. Fluorescence mCherry activity in time-lapse movies is false coloured green and enhanced using either (or both) the 'sharpen' and 'smooth' tools in the Simple PCI software to provide additional clarity.

2.9.6 Transmission electron microscopy (TEM)

Transmission electron microscopy TEM was used for high magnification imaging of bacteria. A 15 µl sample was pipetted onto a Formvar/Carbon 200 Mesh Cu EM grid (Agar Scientific) for up to 5 min before drying by touching the grid with filter paper. Occasionally the sample was washed by pipetting 15 µl of AnalaR water and instantly removing by touching the grid with filter paper. The sample was negatively stained using 15 µl of either 0.5% uranyl acetate (URA) pH 4.0 for 30-45 s, or 1% phosphotungstic acid (pH 7.0) for 30-60 s, the stain was removed using filter paper as before. Grids were examined using a JEOL JEM-100S TEM and images captured using the iTEM software.

2.9.7 Cryo-electron transmission electron microscopy (carried out with Dr C. Butan in Dr S Subramaniam's lab at the NIH)

Cryo**-**TEM was used for ultra high magnification imaging of unstained *B. bacteriovorus* attack-phase cells. Sample preparations were carried out using methods described in reference: (Borgnia et al., 2008). Images were taken on a Technai T12 cryo-transmission-electron-microscope (TEM). 5 µl droplets of cell cultures were applied to holey carbon EM grids (QuantifoilMultiA; Micro Tools GmbH, Germany), previously glow discharged for about 30 seconds

and coated with 15 nm protein A–gold conjugates (BB International, Cardiff, United Kingdom). The grids were manually blotted and quenched in liquid ethane using a manual gravity plunger. Vitrified specimens were then transferred into an FEI Tecnai12 transmission electron microscope (TEM) or a Tecnai Polara TEM (FEI Company, Hillsboro, OR, USA). The images were recorded on a 2x2 k CCD camera, under low-dose conditions at 120 KV (Tecnai 12), or 200 KV (Tecnai Polara). Typical magnifications were in the range 6,000–18,000, and 4-6 µm under-focus values. Whole bdelloplasts cannot yet be examined with this technique as they fail to vitrify in liquid ethane.

2.10 Bioinformatic analysis of DNA and proteins

B. bacteriovorus genome and protein sequences were recovered from the xbase server (http://xbase.bham.ac.uk/). The NCBI database was used for retrieval of other bacterial sequences as required.

2.10.1 Basic Local Alignment Search Tool (BLAST)

BLAST analysis of proteins was carried out using the BLASTP server and the blosum62 matrix at NCBI (www.ncbi.nlm.nih.gov/BLAST/) using the non-redundant protein

sequences (nr) database. BLAST analysis against the *B. bacteriovorus* HD100 genome only was carried out using the Wu-BLAST2.0 program and the blosum62 matrix on the JVCI-VMR server (http://blast.jcvi.org/cmr-blast/).

2.10.2 Multiple alignments of DNA and protein sequences

Multiple protein and DNA level alignments and sequence examination was carried out using the BioEdit Sequence Alignment Editor, Version 7.0.1© Isis Pharmaceuticals Inc. Reference: (Hall, 1999). Multiple alignments were created using ClustalW within BioEdit using the standard settings within the program, an 0% shading threshold for matching bases/amino acids and a Blosum62 alignment matrix (Thompson *et al.*, 1994).

2.11 Method of gene inactivation by kanamycin cassette insertion of genes in *B. bacteriovorus*

Methods of gene interruption in *B. bacteriovorus* by kanamycin cassette insertion are described elsewhere, (Lambert et al., 2003). Briefly, a deletion construct containing a kanamycin-interrupted version of the gene targeted for deletion plus 1 kb of flanking 3' and 5' genomic DNA, is conjugated into *B. bacteriovorus* on a mobilisable suicide plasmid pSET151. Kanamycin resistant exconjugants (containing the genome integrated construct) were screened by *Taq* PCR for a secondary homologus recombination event that removed the wild-type gene and pSET151 plasmid backbone from the genome, leaving only the kanamycin-interrupted copy. Exconjugant strains with only kanamycin interruptions present in the genome were confirmed by diagnostic Southern Blot.

2.12 Method of C-terminal GFP tagging of proteins in *B. bacteriovorus*

For C-terminal GFP tagging of specific *B. bacteriovorus* proteins, an ORF-*gfp* construct was conjugated into *B. bacteriovorus* cells using the suicide plasmid pK18*mobsacB* (section 2.4) and expressed *in cis* from its native promoter.

In each case PCR primers amplified a minimum of a 500 bp region of the targeted ORF, removed the stop codon and added a 3' KpnI site which was used for the C-terminal insertion, in frame with the bright, monomeric GFP ORF (from allelebiotech.com) named *mtfp1*, hereafter called *mtfp*, in the pAKF04 plasmid (Ai et al., 2006).

Insertion of each ORF fragment generated short linker coding regions between the last codon of the ORF fragment and the ATG start codon of the *mtfp* gene; this linker codes for the amino acids VQRSS. ORF-*mtfp* fusion constructs were removed intact typically using EcoRI and BamHI sites and inserted into the suicide plasmid pK18*mobsacB* and conjugated into *B. bacteriovorus* where they recombined as single crossovers restoring the function to the context of the whole gene and its native promoter (Fig. 2.1, section 2.4). Exconjugants were selected by kanamycin resistance due to the vector and confirmed by amplification using primers that bound to the genomic DNA both upstream of cloned ORF fragments and

pK18*mobsacB*, and subsequent DNA sequencing of those PCR products (see Fig. 2.1). That a single insertion of the plasmid in each genome had occurred was verified by Southern blot.

Homologous recombinations between these mTFP-constructs and the *B. bacteriovorus* genome could produce one of two outcomes depending on the designed content of the construct, either a merodiploid strain with both a *mtfp*-tagged and fully functional copy of the gene of interest (Fig. 2.1B) or a strain expressing only the *mtfp*-tagged gene as the original genomic copy is inactivated (Fig. 2.1A).

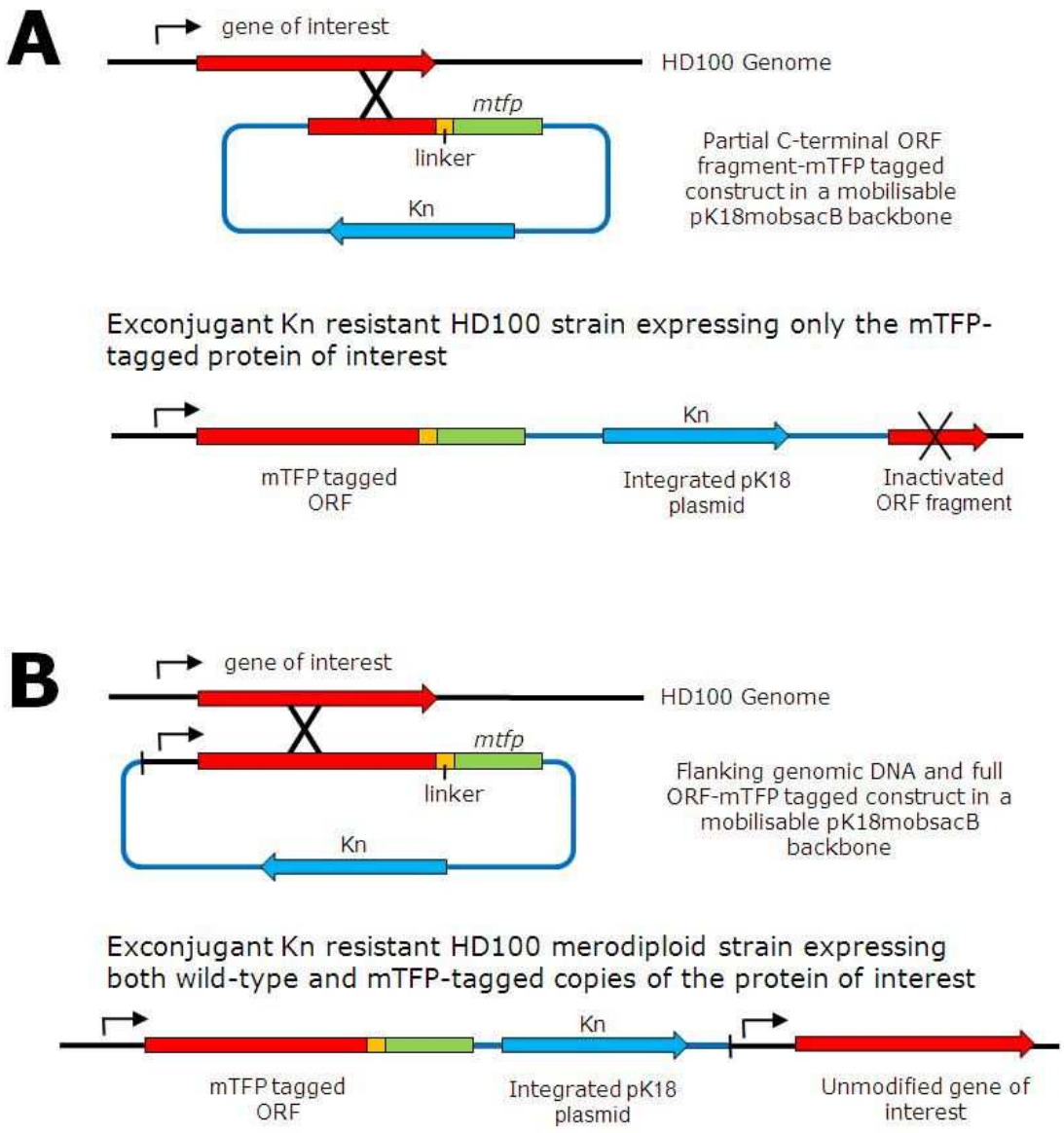

Figure 2.1 Methods of C-terminal mTFP tagging genes of interest in *B. bacteriovorus*. Figure shows the results of homologus recombinations of different constructs into the HD100 genome. (**A**) A construct containing a fragment of the gene of interest ORF in frame with the *mtfp* gene, results in a kanamycin resistant exconjugant strain only capable of expressing the mTFP tagged protein product from the its native promoter. (**B**) A construct containing flanking genomic sequence and the full gene of interest ligated in frame with *mtfp*, results in a kanamycin resistant merodiploid exconjugant strain capable of expressing both wild-type and mTFP tagged protein products each from native promoters. In each case the stop codon of the gene of interest has been removed and ligation in frame with *mtfp* results in a short linker region, that when translated will form a protein linker with the sequence: VPRSS. Kn = kanamycin.

2.13 Methods to ensure synchronous predatory infection of *B. bacteriovorus* on *E. coli* prey

Synchronous *B. bacteriovorus* infections of prey are required to study the developmental processes of this predatory bacterium within bdelloplasts. It has been described previously that for synchronous *B. bacteriovorus* prey infection a predator:prey ratio (or multiplicity of infection (MOI)) must be in excess of 3:1 (Abram et al., 1974, Matin and Rittenberg, 1972). A series of methods described below have been used throughout this study to achieve an MOI of above 3 on different scales for predatory culture. These are derived from the work of Dr Carey Lambert: (Lambert et al., 2006a, Evans et al., 2007, Lambert et al., 2010).

2.13.1 Ultra-large scale synchronous infections for RNA time-course preparation.

To establish synchronicity of large *B. bacteriovorus* infections used for RNA time-course preparations, 50 ml predatory cultures were sub-cultured for 3 days at 24 hour intervals before the resultant *B. bacteriovorus* attack-phase cell culture was used to inoculate a larger 1 l predatory culture, containing 60 ml stationary-phase *E. coli* prey, 50 ml of *B. bacteriovorus* predatory culture and 1 l of Ca/HEPES and incubated for a further 24 h. After microscopic inspection the 1 l *B. bacteriovorus* predatory culture

was centrifuged for at 10K (17,000 g) in a (Sorvall RC-5B PLUS) centrifuge for 30 min, the resulting *B. bacteriovorus* cell pellet was re-suspended 100 ml in fresh Ca/HEPES (pre-incubated to 29^{o}C) and the cells allowed to recover for 3 h in a shaking (200 rpm) 29^{o}C incubator. Simultaneously a 50 ml stationary-phase *E. coli* stationary-phase culture was centrifuged for 10 min at 5,525g in a Sigma 4K15 centrifuge pre-warmed to 29^{o}C, re-suspended in 50 ml Ca/HEPES (pre-incubated to 29^{o}C), back diluted in more Ca/HEPES to an OD_{600} of 1.0, and again allowed to recover for 3 h in a shaking (200 rpm) 29^{o}C incubator.

Synchronous infections were initiated by mixing 50 ml of *B. bacteriovorus* cell preparation, 40 ml of *E. coli* cell preparation to 30 ml of Ca/HEPES (pre-incubated to 29^{o}C). '*E. coli* prey only' and 'attack-phase *B. bacteriovorus* only' controls were set up by diluting the respective preparations to match the final volume of the synchronous predatory-culture. Both *B. bacteriovorus* and *E. coli* were enumerated (see separate methods at 2.2.1 and 2.2.2) and the synchronicity of infection monitored by phase contrast microscopy. RNA preparations of HI *B. bacteriovorus* were made by diluting a starter culture to an OD_{600} of 0.6. For each preparation and time-point 4 ml of culture was removed and added to 1 ml of 5% (v/v) Phenol/ethanol to kill the cells, incubated on ice for a minimum of 45 min, and centrifuged for 10 min at 5,525g in a

Sigma 4K15 centrifuge pre-cooled to 4^{o}C, the supernatant was removed and the pellets stored, for later RNA extraction, at -80^{o}C.

2.13.2 Large scale synchronous *B. bacteriovorus* infections for bdelloplast persistence assays.

To establish synchronicity of large *B. bacteriovorus* infections for bdelloplast persistence assays, 50 ml predatory cultures were sub-cultured for 3 days at 24 hour intervals before the resultant *B. bacteriovorus* cells were used to inoculate a larger 100 ml predatory culture and *B. bacteriovorus* attack-phase cells harvested after 24 h by centrifugation at 5,525g in a Sigma 4K15 centrifuge at 25^{o}C for 20 min, the resulting pellet was re-suspended in 10 ml of fresh Ca/HEPES and *B. bacteriovorus* cells were allowed to recover for 3 h in a shaking (2000 rpm) 29^{o}C incubator. 50 ml of stationary-phase *E. coli* prey culture was centrifuged at 5,525g in a Sigma 4K15 at 25^{o}C for 10 min and the pellet diluted in Ca/HEPES to an OD_{600} of 1.5. The synchronous predatory culture was set up using 4 ml of *B. bacteriovorus* preparation, 3 ml of *E. coli* preparation and 5 ml of fresh Ca/HEPES (pre incubated at 29^{o}C). Typically enumerations revealed that these synchronous cultures contained a *B. bacteriovorus*:*E. coli* MOI in excess 3. This was sufficiently high so that the predatory culture was near synchronous with greater than 95% of *E. coli* prey

cells becoming bdelloplasts at 30 min post *B. bacteriovorus* infection (Abram et al., 1974, Matin and Rittenberg, 1972).

2.13.4 Small scale synchronous *B. bacteriovorus* infections for time-lapse fluorescence microscopy.

Synchronous predatory infections, for time-lapse microscopy, were set-up using methods 'scaled-down' from those described in section 2.13.2. Briefly, 50 ml of fresh predatory *B. bacteriovorus* cultures (sub-cultured at 24 h intervals for three days) were filtered through two 0.45 µm pore-size filters (to remove residual prey and gave pure attack-phase *B. bacteriovorus* typically at 2x 10^7 cells/ml), centrifuged at 5,525g for 20 min in a Sigma 4k15 centrifuge, re-suspended in 10 ml Ca/HEPES, allowed to recover for 30 minutes. Then 500 µl of that resulting *B. bacteriovorus* suspension were added to 500 µl of the fluorescently tagged *E. coli* S17-1:pMAL-p2_mCherry prey and 500 µl Ca/HEPES buffer containing IPTG to give a final concentration of 200 µg/ml. Subsequently infections were incubated in a shaking 29^{o}C incubator for 2-2.5 h. Typically this method led to a predator:prey ratio in excess of 3:1, shown previously to be sufficient for synchronous prey infection (Abram et al., 1974, Matin and Rittenberg, 1972), synchronicity was monitored by light microscopy after 30 min

incubation ensuring that >95% of prey cells had been infected and converted into bdelloplasts.

2.14 Preparation RNA across a *B. bacteriovorus* predatory time-course

Pellets form synchronous RNA time-course predatory cultures, stored at -80^{o}C (see section 2.13.1) were defrosted on ice and the RNA extracted using a Promega SV Total RNA Isolation System, according to manufacturers instructions. 50 µl of RNase free water was used to elute extracted RNA from the column instead of the recommended 100 µl to concentrate preparations. RNA preparations were further DNase treated using an Ambion DNA-free^{TM} kit to remove residual DNA left after RNA extraction using the Promega kit. Complete removal of genomic DNA from RNA samples was assayed by the lack of DNA amplification in *Taq* PCR reactions to amplify small regions of bacterial genomic DNA (typically 100bp).

2.14.1 RNA quality control

RNA quality and concentration was assessed using an Agilent 2100 bioanalyser. In brief this method separates labeled RNA through a capillary gel matrix and is fluorescently detected as it exits the gel. Typically the graphical output shows three major peaks representing the rRNA bands, as these represent the majority of the RNA content of an organism. The width and shape of these bands provides an indication of RNA quality as a degraded sample will typically have broader bands tapered towards the small molecular weight fractions and have an abnormal ratio of the rRNA components. When extracting RNA from early time-points of *B. bacteriovorus* predatory time-courses a certain amount of tolerance was given to assessing sample degradation, as remaining partly-degraded *E. coli* RNA is known to be still present within bdelloplasts at these time-points.

2.14.2 Semi-quantative RTPCR for measuring expression of *B. bacteriovorus* genes through a predatory time-course.

Semi-quantative RNA reactions were carried out using the QIAGEN OneStep RT-PCR kit, according to manufacturer's instructions.

Primers used for *B. bacteriovorus* RNA detection

Primers used *B. bacteriovorus* gene expression analysis	**Sequence (5'-3')**
Bd0042F	AAAGGCTCCATGATCACGTC
Bd0042R	GGATCGATCAGCATTTCCAT
Bd0043_F	CCCAGCAGCTCTATGAAACC
Bd0043_R	CGATCGGAAAGTTGTCAGGT
Bd2460_RTPCR_F	CACCGAAGGGAAAGTCGTAA
Bd2460_RTPCR_R	TCTGTTGCAGATCACGAACC
Bd3904_RTPCR_F	CGGGTTGAGGGAAATCTCTT
Bd3904 _RTPCR_ R	CCTTCGTCGATACGCAGACT
Bd3905_RTPCR_F	GGATCCGAAGAAACAGATCG
Bd3905_RTPCR_R	GCCTCTTCAACTTCCTCGTG
Bd3906_RTPCR_F	TGCGAATAGCTACCATGTGC
Bd3906_RTPCR_R	CCACCAGATCAGGATTAGCC
creS1_RTPCR_F	AACAATCTTCGTAAAGAGC
creS1_RTPCR_R	CAGTTCACTTTCGGATCTA
DapF_F	CCGCTTTATCCAGGAACTGA
DapF_R	TGGATCTTTTGCACCAAGTG
dnaA4F	TTGGATACCTGGCTTGATCC
dnaA4R	AGTACTGGTGAAGGGCGTTG
FtsKF	GTGTGGGAAAACCAACTCGT
FtsKR	ATCGCCAGTGGATCGTATTC
ftsZ_RTPCR_F	TTACCAAGCCGTTCCTGTTC
ftsZ_RTPCR_R	ATTCGGGATCACGATCAGAG
huA_RTPCR_F	CAATCCGAACTGATTCTC
huA_RTPCR_R	GAGCTTCTGGAGAAAGTG
huB_RTPCR_F	GCAGAAGCAATCCTTGAT
huB_RTPCR_R	TAGCTTTAGTGAAAGTACCG

Primers used *B. bacteriovorus* gene expression analysis	**Sequence (5'-3')**
mreB13F	CATGTTGGGACGTACACCTG
mreB13R	AGCATGGACTGGGTGACTTC
mreB23F	AATGTGAAGTCCGCAGAAGG
mreB23R	TCGCAGTAAACGATGTCAGC
mreC_RTPCR_F	TGGATGGTATCGTGCAAAGA
mreC_RTPCR_R	TCCTGAACGTCTTCGGTTCT
mreD_RTPCR_F	TCTTTACCTTGGTCTATGC
mreD_RTPCR_R	AATAGATCAGGTGATAGGC
SSBF	CCAAAGGCCGTCAGGTTTAC
SSBR	GTGGAAGCCACGATTTCAGT

Table 2.8 Primers used for *B. bacteriovorus* RNA detection

2.15 Measuring the rate of *B. bacteriovorus* predatory attachment and entry using a luminescent *E. coli* prey strain.

The luminescence prey assay was used to identify the predatory efficiency of mutant *B. bacteriovorus* strains. Using a 96 well Optiplate (Porvair Sciences Ltd.) and a FLUOstar Optima spectro-photo luminometer supplied by BMG Biotech.

The efficiency of *B. bacteriovorus* predation was tested using *E. coli* prey containing the pCL100 plasmid based upon the assay designed by Lambert and colleagues (Lambert *et al.*, 2003). The pCL100 plasmid contains a full set of lux genes (*luxCDABE*) from *Photohabadus luminescens* and due to the expression of these genes the *E. coli* prey is luminescent. At the outset of the assay, each prey cell emits light, however as *B. bacteriovorus* cells enter and kill the *E. coli* light is no longer emitted from the prey cell.

Dilutions of the *B. bacteriovorus* lysates were added to each well of the plate, the typical dilution series used was 64, 32, 16, 8, 4, 2, 1 and 0 µl. The volume in each well was made up to 64 µl using *B. bacteriovorus* predatory cultures which had been boiled for 5 min and allowed to cool to room temperature. Finally 200 µl of a master-mix containing 25 ml PY broth, 25 ml Ca/HEPES, kanamycin 50 µg/ml and 2 ml of luminescent stationary-phase *E. coli* culture, was added to each well. As soon as the mixture totalling 264 µl was in each well, the completed plate was placed in a BMG FLUOstar machine which was pre-incubated at 29ºC for the first readings to be taken.

Following the completion of the plate, both *B. bacteriovorus* and *E. coli* cultures were enumerated (see separate methods at 2.2.1 and 2.2.2), these counts were required as part of the data analysis.

A complete set of luminescence measurements and optical density at the 600 nm wavelength were taken every 30 min for each well, and the plate was incubated with shaking at 29ºC until the next time point. 49 sets of readings were taken in total corresponding to a 24 h time period. After the last sets of readings were taken, the data was transferred to an Excel spreadsheet for analysis. For each dilution of every *B. bacteriovorus* strain, the time taken for the luminescence of *E. coli* to fall by half of its

highest value was measured using a graph, and the time recorded.

Following the appearance of colonies and plaques of the *E. coli* and *B. bacteriovorus* cells respectively, the number of viable cells in each culture was determined. A second Excel spreadsheet was utilised, where the viable cell counts and the time it took the luminescence to fall by half when in the presence of *B. bacteriovorus* were plotted producing a graph identifying the predatory efficiency of the *B. bacteriovorus* strains.

2.16 Measuring the rate of *B. bacteriovorus* HD development using predatory kill curves.

Rate of *B. bacteriovorus* development within the bdelloplast was measured by a fall in OD_{600} values of a non-synchronous predatory culture over multiple rounds of *B. bacteriovorus* infection. *B. bacteriovorus* attack-phase cells do not give an appreciable absorbance at 600 nm due to their small size, thus OD_{600} values fall over successive rounds of prey lysis.

50 ml of *B. bacteriovorus* predatory culture were filtered through two 0.45 µm filters, to remove any residual prey cells, *B. bacteriovorus* were harvested by centrifugation at 5.1 K (5,525g) for 20 min in an Sigma 4K15 centrifuge and re-suspended in 10 ml Ca/HEPES buffer. Protein concentration of each *B. bacteriovorus* preparation was measured using a Lowry assay (section 2.8.2). *B. bacteriovorus* inocula with matched concentrations of protein were used to inoculate 50 ml predatory cultures containing *E. coli* prey, at matched OD_{600} values of 0.8, plus antibiotics if appropriate. These predatory cultures were incubated at 29^{o}C in a shaking incubator and changes in OD_{600} values were recorded using a Biowave CO8000 miniature spectrophotomer.

2.17 Measuring the rate of *B. bacteriovorus* HI growth.

HI growth rates were recorded as increases in mOD_{600} values of HI cultures over a 72 h period in a 96 well Optiplate (Porvair Sciences Ltd.) incubated and read in a FLUOstar Optima spectro photo luminometer supplied by BMG Biotech. Due to the diverse nature of HI growth patterns and their increase in growth rate with successive PY sub-culturing, care was taken to ensure each HI culture was of equivalent 'age' (section 2.2.3.1).

Duplicate HI cultures were back diluted in fresh PY to a starting OD_{600} of 0.1 using a Biowave CO8000 miniature spectrophotomer. 260 µl of matched OD_{600} HI cultures were loaded into each well of the Optiplate in duplicate, and mOD_{600} recorded every 30 min at 29^{o}C with shaking for 72 h using a FLUOstar Optima spectro photo luminometer. The Optiplate was covered in a Breathe-Easy™ membrane (Sigma-Aldrich) to prevent excessive evaporation.

CHAPTER THREE

The Role of Intermediate Filament-like protein 'Ccrp' in *B. bacteriovorus.*

Structural homologues of Intermediate filaments form a newly discovered family of cytoskeletal proteins in bacteria (Bagchi et al., 2008). This chapter introduces methods, also used in subsequent chapters, to study growth and development of a *B. bacteriovorus* cytoskeletal mutant within prey, and represents the first study of bacterial cytoskeletal elements in a predatory context. It also outlines the cloning techniques used to fluorescently tag specific *B. bacteriovorus* proteins.

3.1 Introduction

3.1.1 Intermediate-filament-like proteins in bacteria

Unlike the actin and tubulin components of the eukaryote cell cytoskeleton, intermediate filaments (IF) such as: nuclear lamins and keratins with oligomerise spontaneously requiring no enzymes or cofactors, forming rigid yet elastic structures when assembled into long fibres (Herrmann and Aebi, 2004). These features of eukaryotic IF are crucial for their role in: cell focal-adhesion attachments and maintaining cell and organelle morphology, by

acting like an internal supporting structure underneath plasma membranes (Herrmann and Aebi, 2004). Work carried out over the last decade has shown that structural homologues of IF in bacteria also contribute to cell architecture; Crescentin (CreS) in *Caulobacter crescentus* establishes and maintains vibroid/coiled cell shape; FilP in *Streptomyces coelicolor* has a role in cell integrity; finally, in *Helicobacter pylori* two IF-like proteins (Ccrp59 and Ccrp1143) have roles in maintaining cell morphology (Ausmees et al., 2003, Bagchi et al., 2008, Waidner et al., 2009). Regulatory proteins that modify, or turnover, IF-like elements in bacteria have not yet been described.

3.1.2 Roles of Intermediate-Filament-like proteins in *B. bacteriovorus*

Intermediate filament-like proteins in bacteria have roles in cell morphology and integrity. The predatory life-cycle of *B. bacteriovorus* places a series of physical and morphological challenges to the cell cytoskeleton, summarised in Fig. 1.6. Electron micrographs show *B. bacteriovorus* attack-phase cells deforming as they enter prey, reducing the pore size required to a minimum (Fig. 1.3). Modifications or Assembly-Disassembly equilibrium changes of IF-like proteins in *B. bacteriovorus* are likely to facilitate the observed 'squeezing' as they are the only

cytoskeletal-element shown to physically fold both bacterial membranes and the cell wall in *C. crescentus*, in addition IF fibres do not shear when forces are applied to them, favouring bending (Cabeen et al., 2009, Herrmann and Aebi, 2004). Taken together these two features show IF-like elements are good candidates for attack-phase cell 'squeezing', and thus could have a role in *B. bacteriovorus* prey cell entry.

The IF-like element CreS in *C. cresentus* has been shown to maintain vibroid cell shape (Ausmees et al., 2003). It has been hypothesised that the hydro-dynamic effects of having a curved cell morphology could be advantageous in cell swarming (Ausmees et al., 2003). In a predatory context, *B. bacteriovorus* cells are also vibroid and this could aid attack-phase cells locate areas of high prey-cell density. However, it may not be possible to measure a predatory advantage of a vibroid cell over a rod-shaped cell over short distances in uniform viscosities, within in a lab setting. Alternatively, IF-like elements could have a role in the coiling of the growth-phase within bdelloplasts (Fig. 1.6), reducing potential developmental complications of growing within this space-limited niche.

In *S. coelicolor* work on the FilP protein has shown that this IF-like protein functions as underlying cell scaffold that contribute directly to cell integrity, until recently thought to be solely a

function of osmotic turgor pressure of the cytoplasmic membrane against the cell-wall (Bagchi et al., 2008). IF-like proteins of *B. bacteriovorus* behaving in this way could be implicated in cell squeezing during prey entry but may also have a wider long-term function in *B. bacteriovorus* attack-phase cell survival in the environment.

3.1.3 Identification of bacterial Intermediate-Filaments

The first IF-like element described in bacteria was the CreS protein discovered in 2003 (Ausmees et al., 2003). Intermediate-filaments have been widely studied in eukaryotic systems (Herrmann and Aebi, 2004), so why did it take so long to discover these proteins in bacteria? The typical structure of eukaryotic IF protein consists of a central structural rod domain which has the potential to form a coiled-coil structure with adjacent monomers, flanked by N-terminal 'head' and C-terminal 'tail' globular domains (Herrmann and Aebi, 2004). The majority of sequence conservation within eukaryotic IF protein lies in the two globular domains allowing identification of homologous proteins by BLAST analysis; whereas the central rod domain has relaxed primary sequence constraints (Herrmann and Aebi, 2004). All bacterial IF-like proteins identified so far share structural homology, but not protein sequence homology, with the central coiled-coil domain of

eukaryotic IF proteins only, and thus were not easily identified until the automation of coiled-coil prediction by software such as COILS in 1991 (Lupas, 1996, Lupas et al., 1991). Fig. 3.1 shows an output file from the COILS program for the CreS protein of *C. crescentus,* as well as a summarised output typically shown in the literature (Ausmees et al., 2003). A multiple protein alignment is shown in Appendix 3.1 to demonstrate the very low protein homology Ccrp elements have with each other (Appendix 3.1).

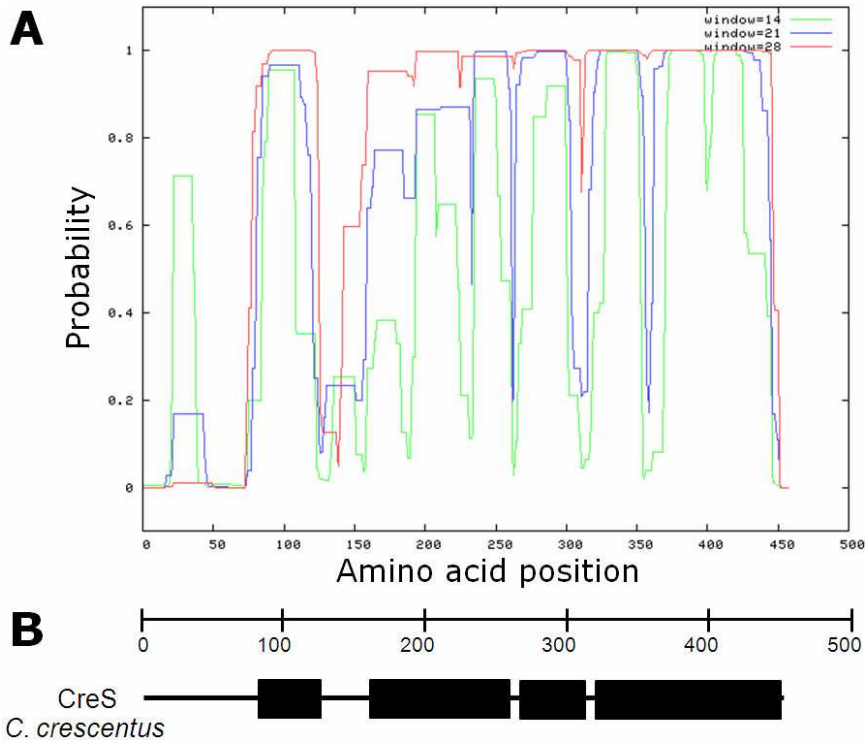

Figure 3.1 Example of a COILS raw output file against a summarised diagram. (**A**) Raw coiled-coil predictions of the CreS protein from *C. crescentus* using the COILS program. (**B**) Summarised 'box' diagram of CreS coiled-coil prediction adapted from (Ausmees et al., 2003). Scale bar represents amino acid positions.

Coiled-coils are amphipathic alpha-helical protein interaction structures. These proteins typically dimerise and form very stable

interactions. The source of this tight interaction is two fold. Firstly the interaction between the hydrophobic surfaces of the amphipathic helixes masking the hydrophobic amino-acid side-chains from the aqueous solution creates a tight bond. Secondly, this oligermisation shifts the register of the two interacting alpha-helixes from the regular 3.6 amino-acid residues per helical turn to 3.5 (Lupas, 1996). The change in register creates an even stronger interaction structure in which individual hydrophobic amino acid side chains, such that found on the Leucine residue, are located within a hydrophobic pocket from the adjacent monomer. The shift in register generates a heptad periodicity in amino acid sequence which can be used for coiled-coil prediction (Lupas, 1996). The COILS protein prediction tool exploits the heptad periodicity using a sliding query window of: 14, 21 or 28 residues, and compares it against a matrix of amino-acid frequencies at each position in the heptad (Fig. 3.1A). The matrix (MTK) was first generated from 16,968 aligned eukaryotic coiled-coil domain protein sequences (Lupas, 1996, Lupas et al., 1991). Since the discovery of the CreS protein in *C. crescentus* multiple bacterial structural IF-like proteins have been identified using the COILS program (Bagchi et al., 2008).

3.2 Bioinformatic identification of Intermediate-Filament-like (Ccrp) proteins in *B. bacteriovorus*

We consulted Christine Jacobs-Wagner, discoverer of crescentin (Ausmees et al., 2003), for advice on finding intermediate-filament-like proteins in *B. bacteriovorus* which were first identified using the coiled-coil prediction program: COILS (http://www.ch.embnet.org/software/COILS_form.html) (Lupas, 1996, Lupas et al., 1991). This search indentified two proteins which were predicted to form coiled-coil containing dimerisation domains in the *B. bacteriovorus* HD100 genome; *Bd2697* and *Bd1167*. Based on the published nomenclature and predicted function of IF-like proteins in bacteria at the time; these genes were named *creS1* (*Bd2697*) and *creS2* (*Bd1167*) (Ausmees et al., 2003). Further analysis of these proteins by COILS predicts that *creS1* has an unusual feature of being devoid of short regions where coiled-coil prediction breaks down so called 'stutter regions' found in IF and IF-like proteins (Herrmann and Aebi, 2004) (Fig.3.2).

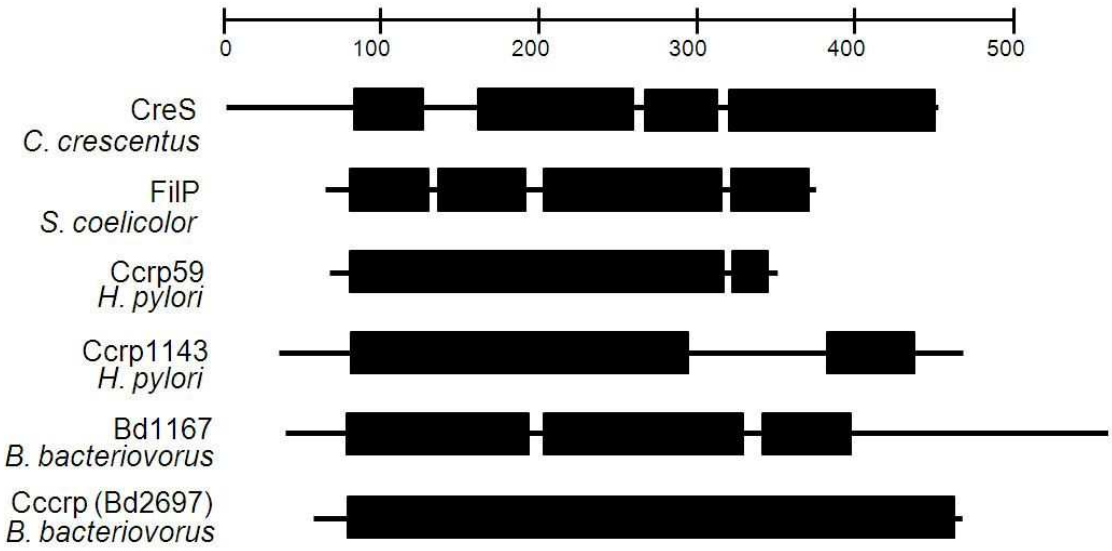

Figure 3.2 Summarised Coiled-coil predictions of *B. bacteriovorus* HD100 proteins compared to known Ccrp proteins using the COILS program. Scale bar represents the amino acid positions along the CreS protein. Subsequent proteins are drawn to scale and aligned to CreS with respect to the first region of coiled-coil prediction. Protein sequences for *H. pylori* strain 26695 used to represent ccrp59 and ccrp1143 COILS predictions. A protein multiple alignment of the same protein sequences shown here can be found in Appendix 3.1.

Prediction of bacterial IF-like proteins cannot be based on COILS prediction alone as other bacterial proteins are known to contain regions which form coiled-coiled structures on dimerisation, such as: SMC and FliC (Melby et al., 1998, Lupas et al., 1991). Recent advances in our understanding of IF-like proteins in bacteria has led to the establishment of the following criteria for their identification: 1, bacterial IF-proteins must have coiled-coil prediction of at least 80 amino-acids in length (this includes short stutter regions); 2, have no other predicted domains; and 3, be located within the cytoplasm (Bagchi et al., 2008, Graumann, 2009). Bacterial proteins fulfilling these criteria are named Ccrps (Coiled Coil Rich Proteins) and not 'IF-like' to better distinguish

them from eukaryotic IF proteins, as these may not be true homologues (Graumann, 2009).

At the time of initial identification both CreS1 and 'CreS2' proteins of *B. bacteriovorus* satisfied these criteria, however advances in secondary structure prediction software has shown the presence of a predicted an OMP-A domain at the C-terminus of the 'CreS2' protein. C-terminally tagged CreS2-mTFP protein expressed in *E. coli* also showed that this protein was also located within the periplasmic space, rather than the cytoplasm of Ccrps (data not shown). Thus *Bd1167* (*creS2*) is not a true Ccrp.

Following the loss of the *Bd1167 ccrp* candidate*,* a recent exhaustive search for *ccrp* genes in *B. bacteriovorus* was carried out using the latest versions of protein domain prediction software, see Appendix 3.2. This analysis revealed that the Bd2967 (previously: CreS1) is the only protein present in the *B. bacteriovorus* genome that is predicted to oligemerize forming colied-coils and thus may be a structural cytoskeletal element, therefore this gene was renamed *ccrp* to better reflect current nomenclature (Graumann, 2009). The Full details of this analysis can be found in Appendix 3.2. In brief candidate genes were initially identified from protein BLAST analysis using the CreS sequence from *C. crescentus* and the two known proteins predicted to form coiled-coils: Bd2697 and Bd1167 as queries against the *B.*

bacteriovorus HD100 genome. As protein BLAST is of limited value when using coiled-coil queries, all hits were analysed regardless of E-value. Coiled-coil prediction using the COILS program and identification of predicted functional domains were carried out using both the ncbi conserved domains database: CCD-37014 and Pfam v24.0 (Marchler-Bauer et al., 2009, Finn et al., 2010). Only two proteins were identified by both Bd2697 and Bd1167 BLAST analyses: Bd1169 and Bd1158, these were also used as queries to further widen the search for Ccrp proteins within the HD100 genome, also shown in Appendix 3.2.

3.3 The role of the *ccrp* gene in *B. bacteriovorus*

3.3.1 The *ccrp* gene of *B. bacteriovorus* is not essential for vibroid cell morphology

In order to study the role of the *ccrp* gene in the *B. bacteriovorus* life cycle, a strain carrying a deletion of *ccrp* by kanamycin cassette insertion and grown host-dependently on kanamycin resistant prey was constructed using methods described previously in Materials and Methods section 2.11. Deletion strains were confirmed by PCR and Southern blotting (see Fig. 3.4), and examined by cryo-electron microscopy to determine whether their vibroid morphology had been altered by the mutation. A Kanamycin control strain *Bd2345*::Kn was selected as a morphological control; this strain has a Kn resistance cassette

placed in the same location as *B. bacteriovorus* 109JK, a strain which has been shown to have no predatorily defective phenotype (Lambert et al., 2003). Surprisingly all cells of the *ccrp*::Kn strain were vibroid in shape, as was the kanamycin resistant *Bd2345*::Kn control (Fig. 3.3).

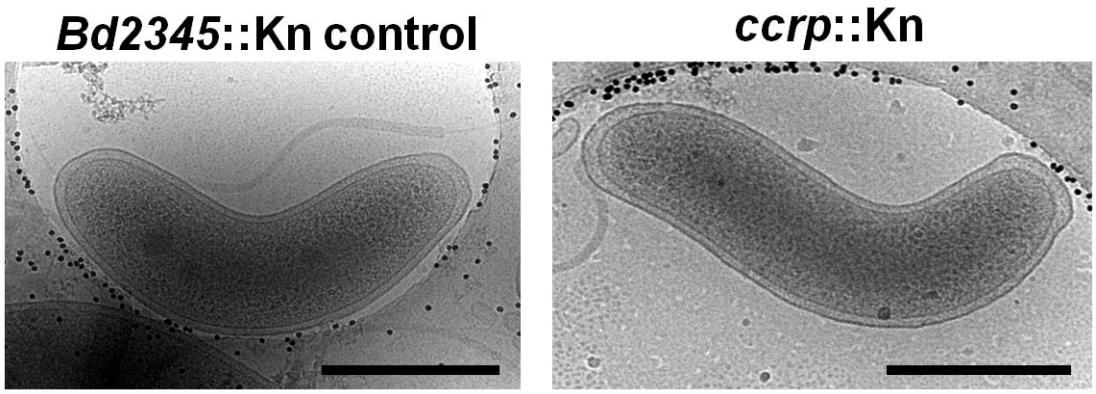

Figure 3.3 Vitrified frozen cells of *B. bacteriovorus ccrp*::Kn and *Bd2345*::Kn visulised by cryo-elecron microscopy. Images show representative examples of cells of both strains showing most of the details described in Fig. 1.2. The carbon film of the EM grid (which appear as a darker shadowed area) and the 15 nm gold particles (black specs) can be seen surrounding the cells. Images taken jointly with C. Butan under the supervision of S. Subramaniam using methods described in section 2.9.7. scale bars = 500nm.

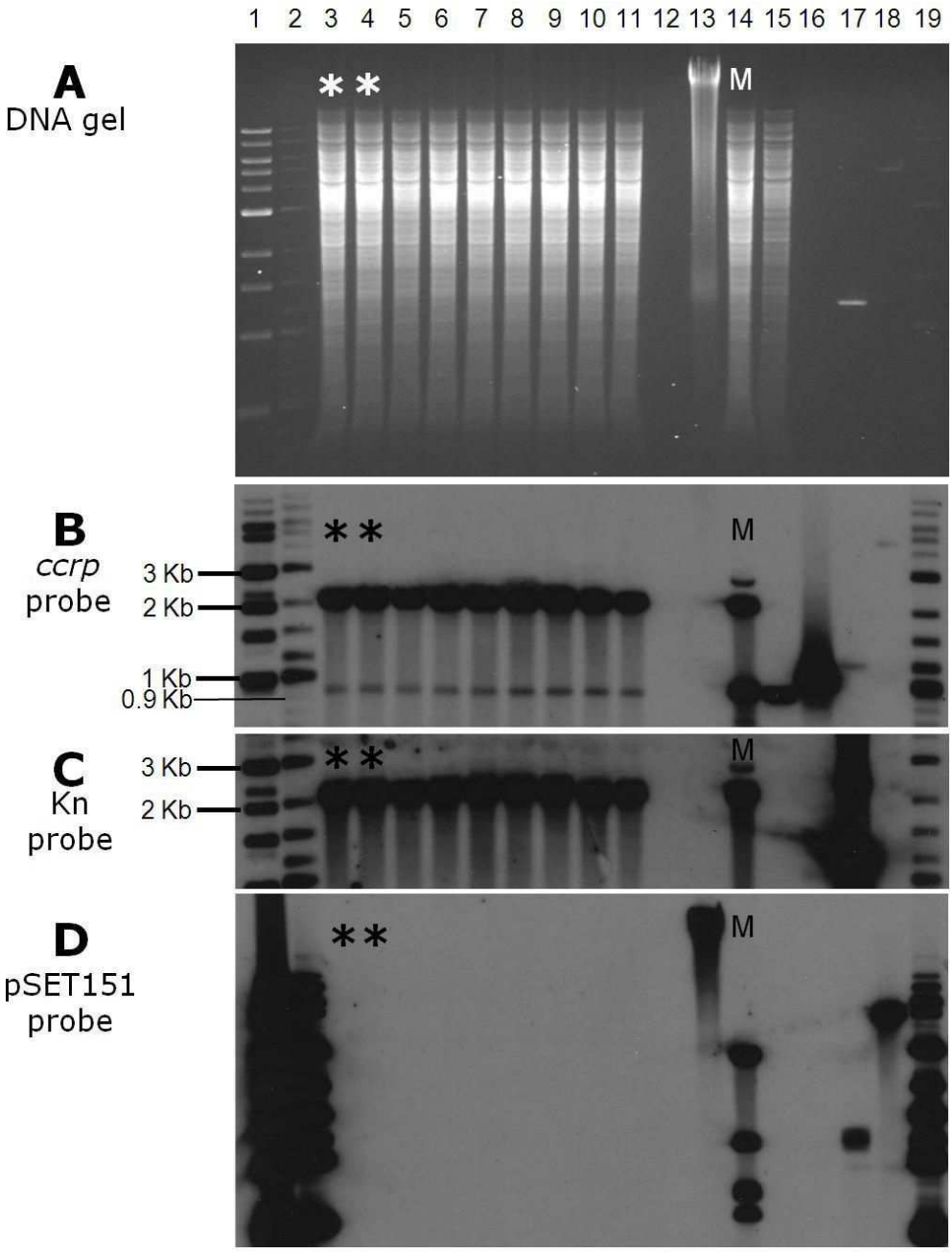

Figure 3.4 Southern blot confirmation of the ccrp::Kn deletion strain. Three identical DNA gels with HincII digested of genomic DNA isolated from pAKF22 exconjugant strains (**A**) were run in triplicate and used for three Southern Blots using probes that bind to: the *ccrp* ORF, kanamycin cassette (Kn) and pSET151 vector backbone (see section 2.7 for methods). Lane order for gel and all blots: 1 = 1Kb NEB ladder, 2 = biotinylated 2-log NEB ladder 3-11 = *ccrp* KO candidates, 12 = gap, 13 = S17-1 control, 14 = ccrp::Kn merodiploid control, 15 = wt HD100, 16 = unlabeled *ccrp* probe, 17 = unlabeled Kn probe, 18 = unlabeled pSET151 probe, 19 = biotinylated 2-log NEB ladder. The 0.9 kb bands in the candidate lanes (3-11) on the ccrp blot are the result of unspecific probe binding (data not shown). DNA in all but the ladder lanes was digested for 16h with HincII. All candidates (lanes 3-11) show the expected gel shift from 1.0 kb to 2.2 Kb on the ccrp blot (**B**), a single 2.2 kb band on the Kn blot (**C**), and no pSET151 bands (**D**). Highlighted (*) candidates were used for phenotyping, lane highlighted with an 'M' contains a known merodiploid control strain.

3.3.2 *B. bacteriovorus* cells of the *ccrp*::Kn strain were physically less robust when visualised under conditions of negative-staining for electron microscopy

A large number of attack-phase cells were visualised for morphological differences by negative staining of whole cells with 0.5% uranyl acetate (URA) pH4.0 for transmission electron microscopy. Interestingly this revealed that in contrast to the usual wild-type smooth vibroid appearance of all the *Bd2345*::Kn control cells, all cells of the *ccrp*::Kn strain had a dented and creased appearance, not seen previously (Fig. 3.5). Negative-staining of *B. bacteriovorus* cells with URA does not cause membrane damage observed with other stains used for electron microscopy (such as PTA), and positively stains the cell wall causing slight cell folding in wild-type and *Bd2345*::Kn control cells (Fig. 3.5), (Abram and Davis, 1970). In contrast to control strains the surfaces of the *ccrp*::Kn strain were severely creased and turned inwards creating deep indentations at both poles in 29% of cells (n=191); a feature not previously observed in *B. bacteriovorus* strains (Fig. 3.5).

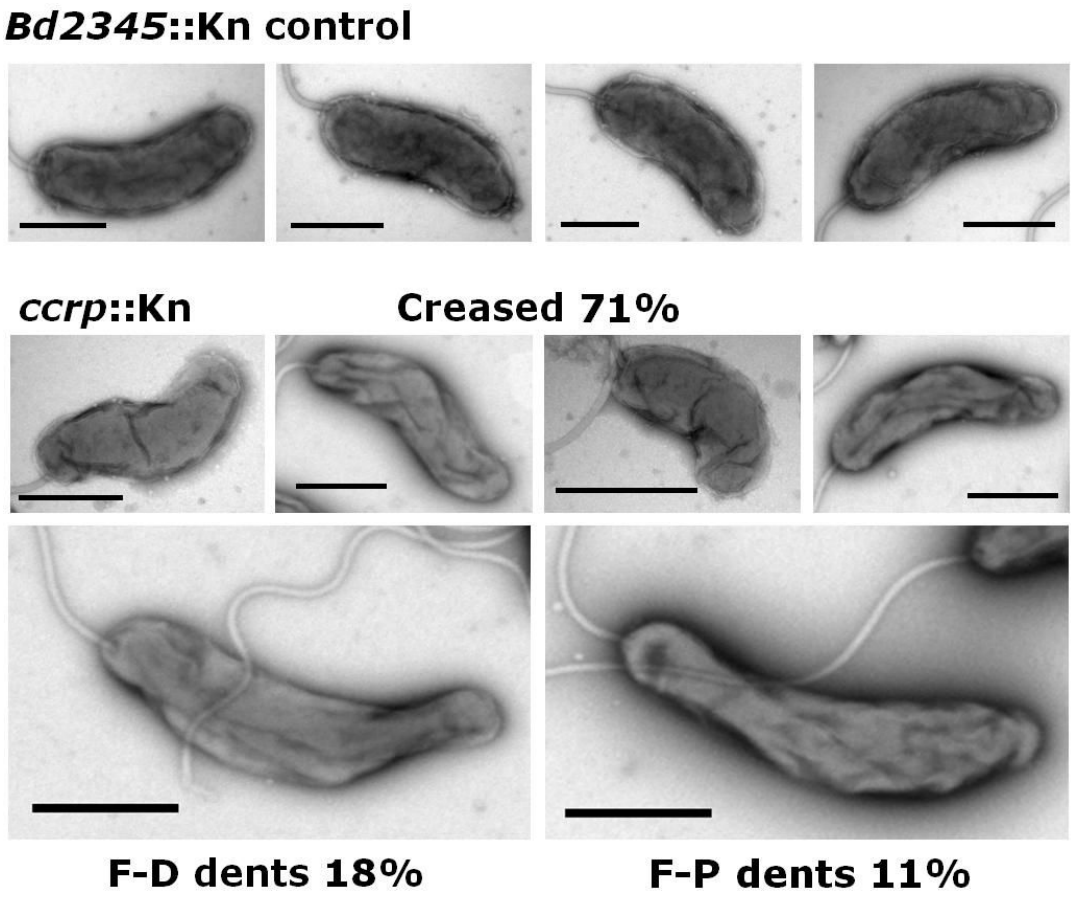

Figure 3.5 *B. bacteriovorus ccrp*::Kn strain shows cellular deformations under the negative-straining conditions for transmission electron microscopy. Representative electron micrographs of *B. bacteriovorus ccrp*::Kn attack-phase cells, showng flagella-proximal dents (F-P), flagella-distal dents (F-D) and 'creased'cell phenotypes; compared to the *Bd2345*::Kn control. Percentages represent the distribution of cells between the three categories; n=191. Cells stained with 0.5%URA pH4.0, scale bars = 500nm.

3.3.3 The predation efficiency of *ccrp*::Kn strain.

The *ccrp*::Kn strain cell deformations visualised under negative-staining conditions appeared to be similar to the squeezed prey-entry forms shown in Fig. 1.3, which suggested that there may be a role of the Ccrp protein in prey entry. Efficiency of prey entry for the *ccrp*::Kn strain was assayed using a prey luminescence assay first used by C. Lambert and co-workers

(Lambert et al., 2003). This assay (described in section 2.15) involves predation of *B. bacteriovorus* on a luminescent *E. coli* prey strain (S17-1:pCL100), and if members of the prey population are killed the luminous signal intensity decreases (Fig. 3.6A). *B. bacteriovorus* cells kill prey rapidly after prey-cell entry, destroying luminescence activity. Thus this assay is a reflection of prey-attachment and entry efficiency for a given strain. Incubation of prey cells with increasing volumes of synchronously grown *B. bacteriovorus* predatory lysates results in a faster decline in luminescence activity after an initial peak; the peak representing the stabilisation of expression in the uninfected prey cells after the initial oxygenic and temperature shock (Lambert et al., 2003) (Fig. 3.6A). Using enumeration data to measure the initial number of *B. bacteriovorus* and *E. coli* per infection, and plotting this as a ratio against the time taken to reduce the luminescence activity to half of its maximum, allows for a comparison of predatory efficiencies between strains; the gradient of the line being a reflection of predatory efficiency (Lambert et al., 2003). Data collected from multiple biologically repeated predation assays against a kanamycin resistant strain control with a wild-type predatory rate (the *filC1*/*fliC1*::Kn merodiploid strain), showed that the *ccrp*::Kn strain did not have a predatory defect (Fig. 3.6B). The *filC1/filC1*::Kn merodiploid control strain was selected as a kanamycin resistant wild-type predatory control in this experiment

over the *Bd2345*::Kn control, as preliminary experiments on the *ccrp*::Kn phenotype and work by others in the lab had shown, by this point, that this strain had a slightly reduced predatory rate (C. Lambert and L. Hobley personal communication).

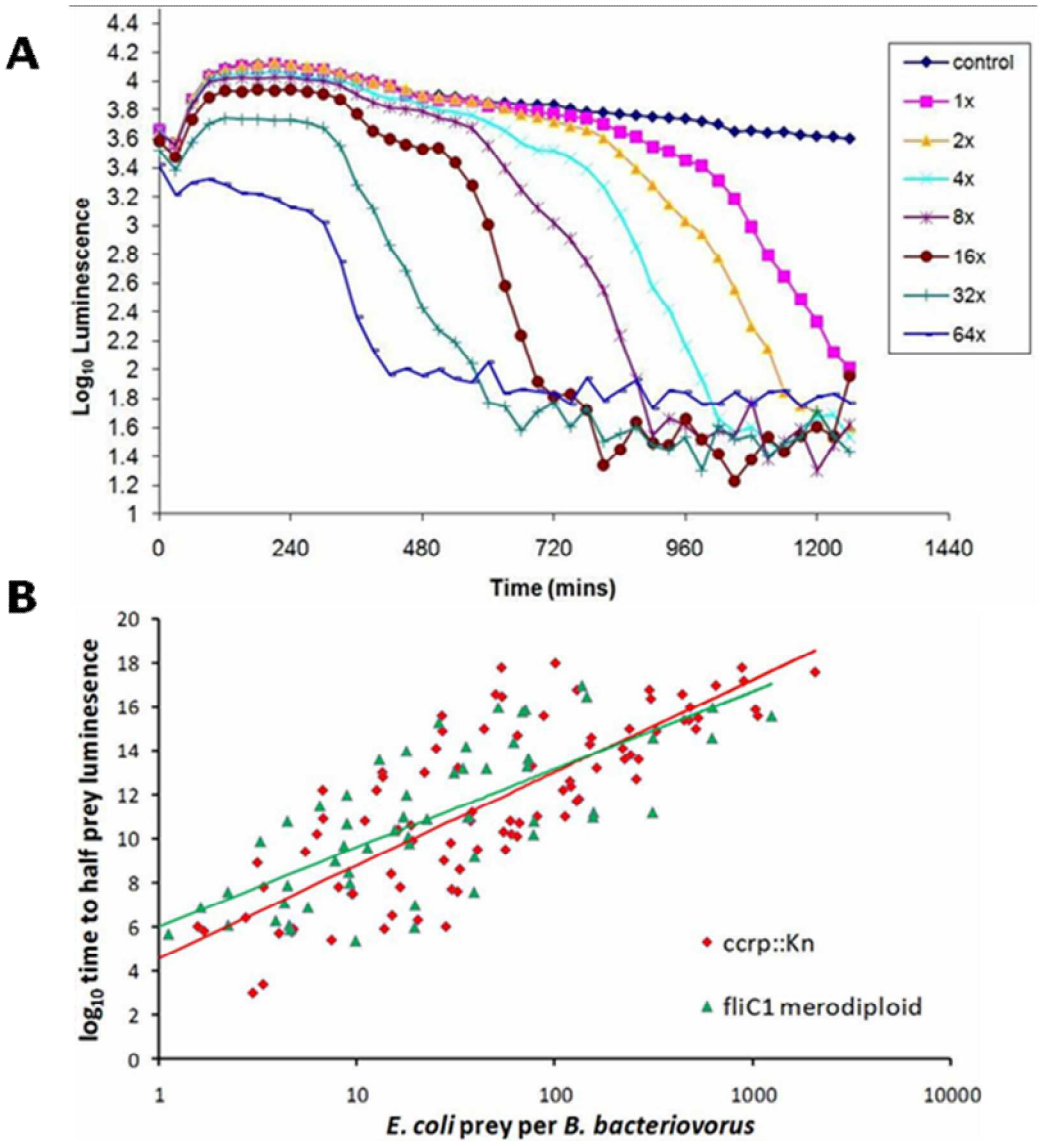

Figure 3.6 The *ccrp*::Kn strain of *B. bacteriovorus* has a wild-type predatory rate. (**A**) Typical *E. coli* S17-1:pCL100 luminescence plot (Log_{10}) with increasing starting concentrations of *B. bacteriovorus ccrp*::Kn cells against time. (**B**) Plot showing Log_{10} of time taken for infections to reach half luminescence against starting ratios of *E. coli*:*B. bacteriovorus* for the *ccrp*::Kn and *fliC1* merodiploid predatory control strains. Each dataset represents 4 biological repeats in the case of the *ccrp*::Kn strain and 2 biological repeats (each with 5 replicates) for the *fliC1* merodiploid strain.

3.3.4 The *ccrp*::Kn strain has no defect in developmental rate or cell morphology within the bdelloplast.

Ccrp proteins have a variety of roles beyond bacterial cell morphological modifiers; both Ccrp59 and Ccrp1143 of *H. pylori* have shown Ccrp proteins can act as MreB-like elements, co-ordinating peptidoglycan biosynthesis (Waidner et al., 2009). To examine the potential role of Ccrp protein in the developmental rate of *B. bacteriovorus* within bdelloplasts, both a bdelloplast-persistence and Prey-killing assays were performed, unlike the luminescent prey assay in section 3.3.3 where infected prey luminescence activity is lost within 20 min of *B. bacteriovorus* entry, these two assays measure prey final lysis of the bdelloplast which occurs after *B. bacteriovorus* cells have matured (see section 2.16). Taken together these assays provide two different results; either altered prey entry and killing rate as measured by the prey-luminesence assay, or altered incubation time of *B. bacteriovorus* within bdelloplasts, measured both directly over a single infection in the case of bdelloplast-persistence assays and indirectly over multiple rounds of infection in prey-killing assays.

A bdelloplast persistence assay involves direct observation of a predatory lysate by light microscopy with a predator:prey ratio or MOI (multiplicity of infection) above 2; sufficient for *B. bacteriovorus* infections to proceed synchronously on *E. coli* prey

(Matin and Rittenberg, 1972, Abram et al., 1974). Under these conditions greater than 95% of prey are infected synchronously and will enter and lyse prey within 4 h. Thus resulting in a return to an almost pure attack-phase *B. bacteriovorus* predatory lysate at between 4.5-5 h, if predation proceeds at a wild-type rate. Representative images captured across the infection cycle are displayed in Fig. 3.7. In addition images of *ccrp*::Kn bdelloplasts show the developing *B. bacteriovorus* cells are vibroid in shape, thus Ccrp is not responsible for vibroid growth-phase cell shape within the bdelloplast (Fig. 3.7, see orange arrows).

Prey-killing assay measuring drops in OD_{600} of a 50 ml predatory lysates over time creates predatory killing curves shown in Fig. 3.8, these differ from luminescent-prey assays as they monitor lysis of bdelloplasts not initial invasion of prey, first published in: (Fenton et al., 2010). Starting OD_{600} values were matched to 0.8 with kanamysin resistant *E. coli* S17-1:pZMR100 prey. Matched protein concentrations of fully-lysed and filtered *B. bacteriovorus* lysates were used to start the infection. Values fall as prey are lysed given that the *B. bacteriovorus* attack-phase cells are too small to register at an OD of 600 nm. The predatory killing curves shown in Fig. 3.8 for *B. bacteriovorus ccrp*::Kn, *Bd1167* '*creS2*'::Kn and *Bd2345*::Kn strains represent two biological repeats (*Bd1167*::Kn KO Southern blot confirmation shown in Appendix 3.3). In conclusion this data showed the *ccrp*::Kn strain

lysed prey at the same rate as the *Bd1167*::Kn strain, suggesting a wild-type predatory development (Fig. 3.8). In addition the Bd2345 'control' strain, known by this point to have a slightly reduced predatory rate, shows a shallower curve suggesting a slower rate of predatory development than both the *ccrp*::Kn and *Bd1167*::Kn strains (Fig. 3.8).

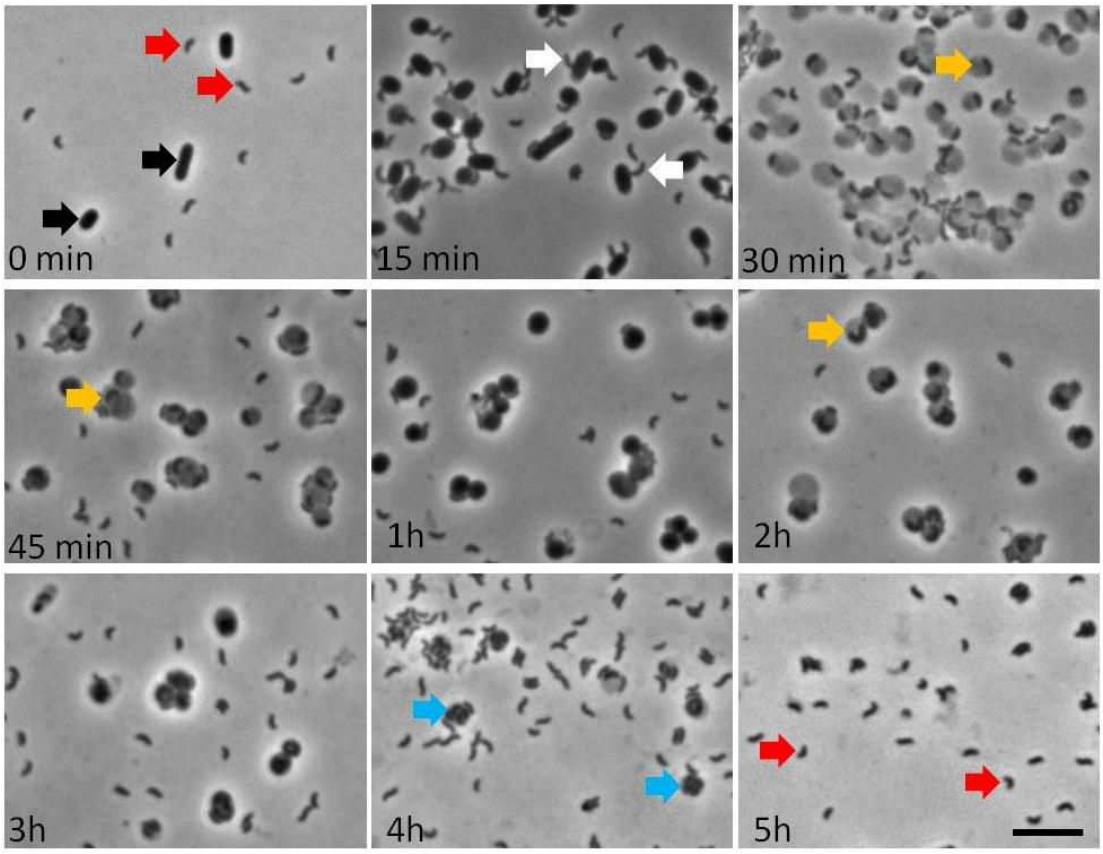

Figure 3.7 The *B. bacteriovorus ccrp*::Kn strain has a wild-type cell morphology and developmental rate within the bdelloplast, measured using a bdelloplast persistence assay. Representative brightfield images representing key time-points of a synchronous *ccrp*::Kn infection. Arrows used to highlight specific cell types; Red: vibroid *ccrp*::Kn attack-phase cells, Black: Uninfected *E. coli* S17-1:pZMR prey, White: Attack-phase cell attachment, Orange: bdelloplsasts containing vibriod growth-phase cells, Blue: Fully septated mature bdelloplasts. Comparison of 15 and 30 min post infection images demonstrate synchronous infection, at 15 min all prey cells show *B. bacteriovorus* attachment, whereas at 30 min all prey are infected. Images of HD100 control infection carried out under the same conditions are not shown. Scale bar=5 μm.

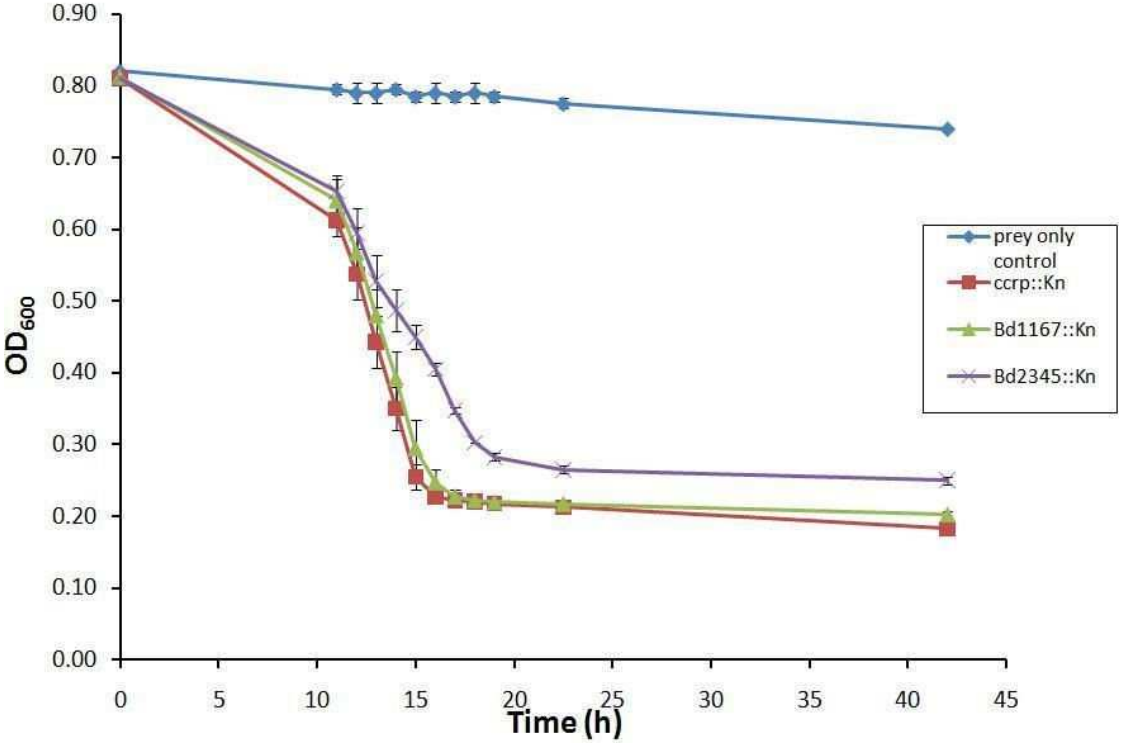

Figure 3.8 The *B. bacteriovorus ccrp*::Kn strain has a wild-type cell morphology and development rate within the bdelloplast, measured using a prey-killing assay. Predatory kill curve of HD100 *ccrp*::Kn, *Bd1167*::Kn and *Bd2345*::Kn strains. Matched OD_{600} values of S17-1:pZMR prey were infected with corrected amounts of *B. bacteriovorus* strains, matched by protein concentration. Data represents two biological repeats, each set up in duplicate. Error bars show standard deviation around the mean.

3.4 Challenges to the *B. bacteriovorus ccrp* deletion strain.

Deformation of *ccrp*::Kn attack-phase cells under conditions of negative staining, shown in Fig. 3.5, raised the possibility of the Ccrp protein contributing directly to cell integrity. To investigate this further, attack-phase *ccrp*::Kn cells were osmotically challenged using 0.1% glycerol in predatory lysates, and motility in conditions of increased resistance was measured using prey-overlay plates in which the concentration of agar in the upper-layer

had been altered. The 0.1% glycerol osmotic challenge, reported previously to cause osmotic shock and shrinking of *E. coli* cells (Alemohammad and Knowles, 1974), showed no appreciable difference in glycerol tolerance between the *ccrp*::Kn and *fliC1* merodiploid control strain. In both cases tolerance was scored as the ability to fully lyse prey cultures observed by microscopy, in addition complications arising from osmotic effects on the prey could not be discounted (data not shown). Motility in assays on *ccrp*::Kn strain on prey overlay plates at differing top-agar concentration again showed no appreciable difference compared to the *fliC1* merodiploid control strain (data not shown).

3.5 A C-terminal Ccrp-mTFP shows location bias in *B. bacteriovorus* attack-phase cells

3.5.1 Construction of a fully functional Ccrp-mTFP fusion protein in *B. bacteriovorus*

In order to study specific protein localisation in *B. bacteriovorus*, a method of targeted mTFP tagging was devised: see Materials and Methods section 2.12. To study Ccrp localisation in *B. bacteriovorus* a fusion construct using a 5' fragment of the *ccrp* ORF was cloned in frame with *mtfp* in the plasmid pAKF04, generating pAKF38a; the ORF fragment if translated would represent 76% of the Ccrp protein. The *ccrp-mtfp* fusion construct

was transferred to the mobilisable pK18*mobsacB* suicide vector (giving pAKF42a) and conjugated into *B. bacteriovorus* (Materials and Method 2.4). Kanamycin resistant exconjugant strains, containing the pAKF42a plasmid recombined into the genome, are only capable of expressing the mTFP tagged fusion protein; as the original copy of *ccrp* on the genome is inactivated by promoter removal and 5' deletion of the 23% of the *ccrp* ORF absent from the pAKF42a construct, shown in Fig. 2.1A. Amplification of the recombined genomic copy of the pAKF42 construct with the surrounding genome, direct sequencing and diagnostic Southern blot of exconjugants confirmed the full *ccrp-mtfp* ORF was free of any point mutations, multiple recombination events had not occurred, and incorporation of the construct was in the expected location (Appendix 3.4 and 3.5).

The HD100 *ccrp-mtfp* strain was visualised by electron microscopy (Fig. 3.9) and did not show the cell deformations observed for the *ccrp* mutant (Fig. 3.5) when exposed to negative staining. This suggests that the Ccrp-mTFP fusion protein was functional, Fig. 3.9.

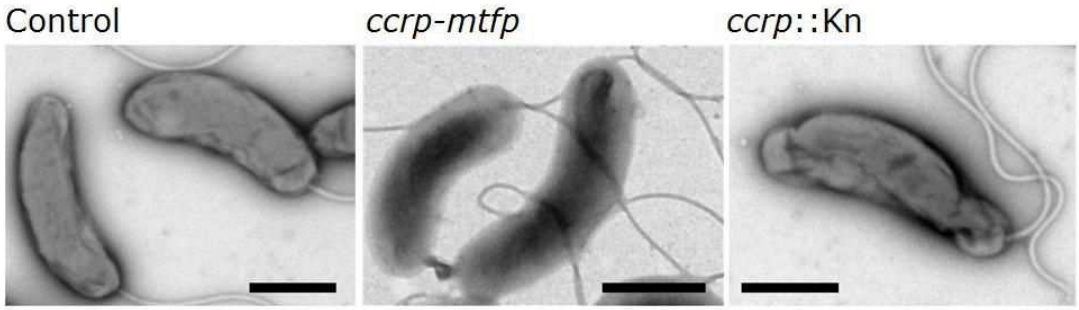

Figure 3.9 Attack-phase *B. bacteriovorus ccrp-mtfp* cells show wild-type cellular morphology under negative staining for transmission electron microscopy. All cells shown here were stained at the same time with 0.5% URA pH4.0, Scale bars = 500 nm.

3.5.2 Ccrp-mTFP fluorescent signal shows bias towards both cell poles of attack-phase *B. bacteriovorus*

The fluorescent Ccrp-mTFP signal in attack-phase *B. bacteriovorus* cells was very faint and generally evenly distributed but showed a bias towards the cell poles (Fig. 3.10). Fluorescent images of attack-phase cells of the non-fluorescent *Bd2345*::Kn strain were captured as auto-fluorescence controls. The faint nature of the Ccrp-mTFP fluorescent signal suggests that this protein is not high in abundance and precluded signal distributions being examined in growth-phase cells; due to the high background fluorescence of bdelloplast structures.

A total of 180 attack-phase cells were scored for Ccrp-mTFP signal distribution, 25% of these had a polar bias (Fig. 3.10). More generally, partitioning of the signal could be observed in cells where a bias to one pole was present (Fig. 3.10c). Using the FM4-64 membrane stain to visualise the sheathed flagellum, and thus

determine cell polarity, showed that single foci could be located to either pole of the attack-phase cell (Fig. 3.10a,b).

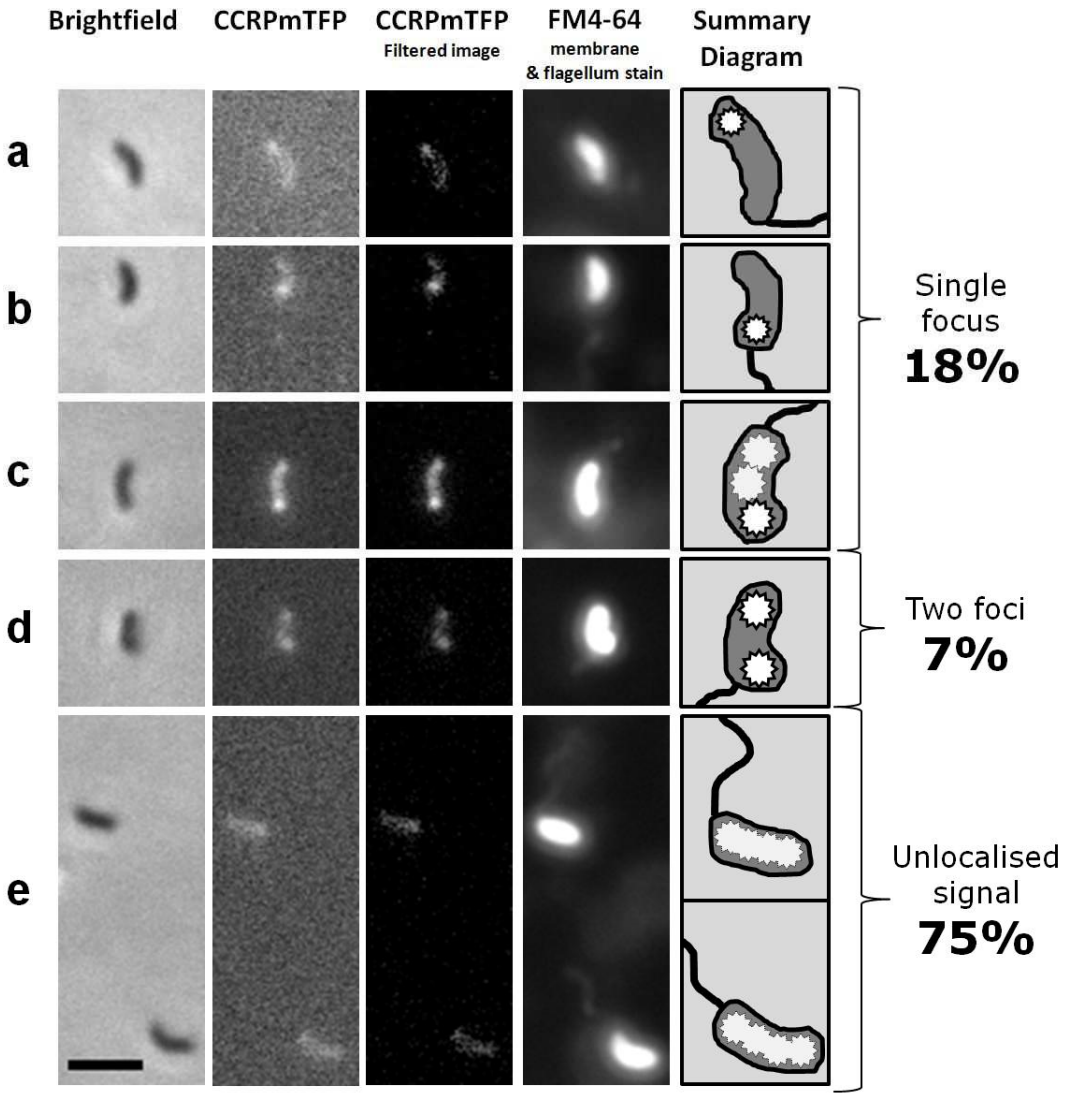

Figure 3.10 Ccrp-mTFP signal shows a distribution bias towards both cell poles of attack-phase *B. bacteriovorus* cells. Ccrp-mTFP fluorescence images provided in raw and corrected formats to better visualise signal distributions, background corrections carried out using the IP-lab software (version 3.64). The fluorescent FM4-64 membrane stain was used to determine cell polarity by its incorporation into the flagella sheath. Summary diagrams are provided for clarity. Ccrp-mTFP signal distributions: single, double and no foci are shown by percentage; n=180. Scale bar = 2 μm.

3.5.3 Ccrp-mTFP fluorescent signal bias is independent of the MreB cytoskeleton

The helical filament of the actin-like protein MreB spatially organises many proteins within the cytoplasm of bacterial cells and helps anchor CreS fibres to the cell poles in *C. crescentus* (Graumann, 2009, Charbon et al., 2009). The location bias of the Ccrp-mTFP protein in *B. bacteriovorus* attack-phase cells in the presence of the MreB specific inhibitor A22 at a final concentration of 10 μg/ml did not significantly alter the Ccrp-mTFP distribution patterns (Fig. 3.11). Work on MreB in *B. bacteriovorus* show A22 concentrations of 10 μg/ml modifies MreB activities in *B. bacteriovorus* without affecting long term viability (Fig. 5.11), in contrast to work carried out on CreS this shows Ccrp-mTFP localisation in *B. bacteriovorus* is independent of the MreB cytoskeleton (Charbon et al., 2009).

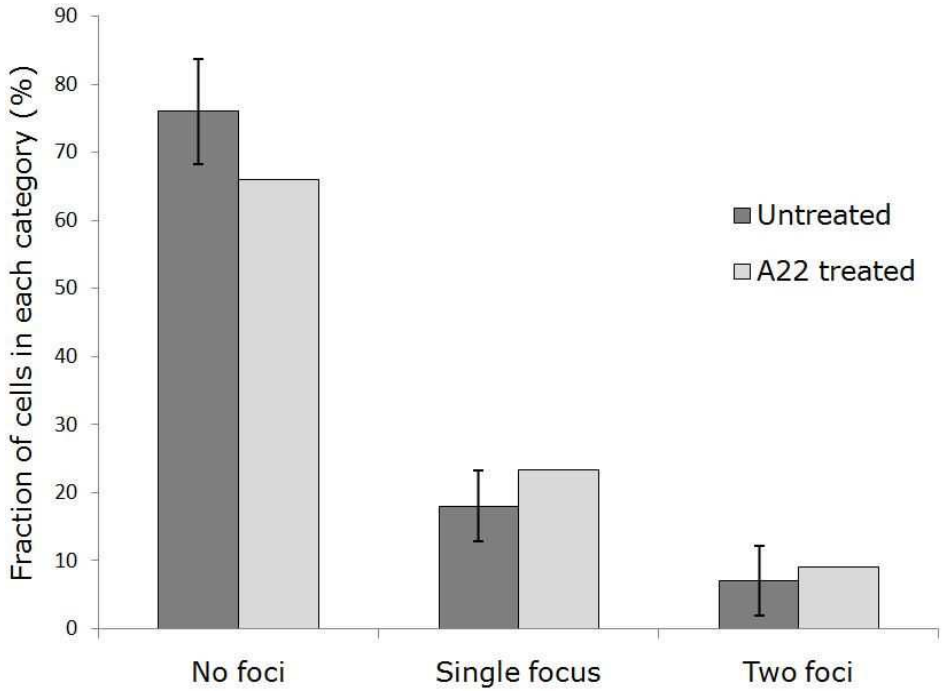

Figure 3.11 The MreB cytoskeletal inhibitor A22 does not significantly affect Ccrp-mTFP signal distribution patterns. Signal distribution patterns of non treated *ccrp*-mTFP cells, error bars represent standard deviation around the mean (n=180) compared to an A22 treated data set (n=77), attack-phase cells were treated for 16h with A22 at a final concentration of 10 μg/ml. Chi square analysis (X^2=4.03, d=2, Q=0.133) confirms that variation in A22 dataset is due to chance: p=0.86.

3.6 Discussion

This chapter showed for the first time that it is possible to C-terminally GFP tag and detect the fluorescence activity of a specific protein in *B. bacteriovorus* (Fig. 3.9 and 3.10). Although the Ccrp-mTFP fluorescent signal was weak, sub-cellular localisation within attack-phase *B. bacteriovorus* cells only 1 μm long was possible; this re-enforces the decision to use the mTFP fluorophore, as a less fluorescent GFP tag would have generated a signal indistinguishable from auto-fluorescence. Although the signal in this case was not strong enough to visualise within the bdelloplast, a protein of higher abundance in the cell may make this possible. Further analysis of Ccrp-mTFP polar bias was possible using the FM4-64 membrane stain that under conditions of long exposure and relatively high image gain can be used to visualise the flagellar sheath (Fig. 3.10).

This chapter also introduced methods of measuring specific events in the *B. bacteriovorus* predatory life-cycle which are applied later in the thesis. Attachment and entry rates can be measured using a prey luminescence assay, and growth-phase cell developmental rates are measured either directly by microscopy or indirectly over multiple rounds of infection through OD_{600} predatory kill curves (Fig. 3.6, 3.7 and 3.8).

Understanding of bacterial Intermediate-filament-like proteins (now called Ccrps) and protein prediction software has advanced during the course of this study, leading to the reclassification of the *Bd1167* 'creS2' gene and the renaming of the *Bd2697* '*creS1*' gene *ccrp*; to better reflect current nomenclature and function (Graumann, 2009). An exhaustive search using a combination of the latest software and the latest published criteria for *ccrp* identification showed *B. bacteriovorus* has only one *ccrp* gene in its genome, *Bd2697 (*Appendix 3.2) (Bagchi et al., 2008).

Both cryo-electron micrographs and brightfield microscope images (Fig. 3.3 and Fig. 3.5) show vibroid *B. bacteriovorus* attack-phase and growth-phase cells within bdelloplasts, suggesting that Ccrp does not maintain vibroid cell shape in *B. Bacteriovorus*. This is in contrast to work on the CreS protein in *C. crescentus* (Ausmees et al., 2003).

A combination of prey-luminescence assays, prey-killing OD_{600} assays, and bdelloplast presistance assays, each designed to examine a different aspect of *B. bacteriovorus* predatory growth all suggested that the *ccrp*::Kn strain possesses a wild-type prey entry and predatory developmental rate (Fig. 3.6, 3.7 and 3.8). Osmotic challenges to mutant *B. bacteriovorus* cells using 0.1% glycerol and indirect motility measurements through media of

differing viscosities showed no appreciable difference of the *ccrp*::Kn strain over a wild-type control (section 3.4.5).

The Ccrp-mTFP fusion protein in attack-phase *B. bacteriovorus* showed a location bias towards both cell poles, at frequencies similar to the cell denting bias observed for the *ccrp* deletion strain under negative-staining for electron microscopy (Fig. 3.5 and 3.10), also cryo-EM studies showed no morphological differences between mutant and control strains (Fig. 3.3), this suggests that the absence of the Ccrp in mutant strains makes them more susceptible to the insults of negative-staining at the cell poles.

It was surprising that a protein which could localise to discrete foci in *B. bacteriovorus* cells, and the absence of which produced large scale denting of the cell surface when visualised by negative staining, did not affect the entry of *B. bacteriovorus* into prey cells (Fig. 3.6). As *B. bacteriovorus* entry to prey was previously shown to be dependent on type IV pili, it is clear that the structures which anchor the pilus retraction machinery at the cell pole do not require this Ccrp protein to be firmly positioned in the cell (Evans, 2007, Mahmoud and Koval, 2010). The question as to whether cytoskeletal proteins or peptidoglycan interactions are key to allowing *B. bacteriovorus* cells to be dragged into prey by pilus retraction remains open.

In conclusion this work suggests that whilst Ccrp in *B. bacteriovorus* does not contribute to the vibroid cell shape, it significantly contributes to cell shape stability by acting as an internal protein scaffold, similar to the FilP protein in *S. coelicolor* (Bagchi et al., 2008), and without it cells are still predatory but may be more prone to osmotic insults from the environment.

CHAPTER FOUR

Investigating the growth and development of *B. bacteriovorus* within bdelloplasts.

4.1 Introduction

Although from microscopic snapshots it was clear that *B. bacteriovorus* enter and round up prey forming bdelloplasts. Early EM studies tended to focus on the initial attachment and prey invasion events. Thus we have not known how exactly a single predatory *B. bacteriovorus* makes use of the finite resources within the bdelloplast to grow, and then manages to coordinate departure of mature progeny at the point at which prey resources are depleted (Scherff et al., 1966, Burnham et al., 1968).

The relatively few early studies that did focus on *B. bacteriovorus* growth were hampered by staining and fixing techniques used for TEM which kill bacterial cells (Abram and Davis, 1970). In the previous chapter (Chapter 3) I used the mTFP fluorescent protein to C-terminally tag and visualise the cellular address of a target protein (Ccrp) within *B. bacteriovorus* attack-phase cells (section 3.5.2, Fig. 3.10). This chapter employs two fluorescent proteins: mTFP and mCherry to investigate *B.*

bacteriovorus developmental processes using direct protein-tagging; and later more indirectly using a fluorescently-labelled prey strain, leading to fluorescent bdelloplasts.

4.1.1 Growth and development of *B. bacteriovorus* within bdelloplasts

Predatory *B. bacteriovorus* elongate into a filamentous growth-phase cell within bdelloplasts using the resources acquired by digestion of the prey (Fig. 1.6) (Lambert et al., 2009). This growth-phase filament divides into multiple progeny contrary to 'normal' bacterial cell division by binary fission (Scherff et al., 1966, Kessel and Shilo, 1976). *B. bacteriovorus* growth-phase cells are multiploid and thus have an increased risk of genome instability by multiple homologous recombination events; therefore there must be significant benefits to this method of growth to increase the overall fitness of *B. bacteriovorus* (discussed further in section 6.1).

To start to understand how *B. bacteriovorus* cells coordinate the processes of DNA replication, chromosome segregation and septation within growth-phase filamentous cells, over arching patterns of growth in live cells must first be identified. To achieve this C-terminal mTFP tags were designed to *B. bacteriovorus* to try and label and observe target proteins involved in the processes of bacterial septation.

4.1.2 The bacterial septation machinery

Septation is the process by which bacteria divide, typically into two. For a Gram-negative bacterium like *B. bacteriovorus* this involves the processes of inner and outer membrane biosynthesis and invagination, combined with peptidoglycan biosynthesis. The first stage in this process involves the bacterial tubulin homologue FtsZ; this protein polymerises specifically at the mid-cell address due to the action of specific control mechanisms (discussed in section 4.1.3). As with eukaryotic tubulins that require microtubule binding protein to function, FtsZ-ring establishment requires the action of multiple stabilising factors *in vivo* including: FtsA, ZipA and ZapA; together these proteins recruit all downstream septal machinery required for cell division in an established hierarchy or pattern: FtsZ→ FtsA/ZipA→ FtsK→ FtsQ→ FtsL/FtsB→ FtsW→ FtsI→ FtsN, shown in Fig. 1.5 (Goehring and Beckwith, 2005). Many other Fts septal proteins (such as FtsY) with non-essential roles in septation have not been shown in Fig. 1.5. Septal proteins either act to recruit further downstream proteins (such as FtsQ) or have specific enzyme functions required for division such as the FtsK protein, required for chromosome cell segregation, and the penicillin-binding-protein FtsI, which aids in lateral cell wall biosynthesis (Goehring and Beckwith, 2005). Together the essential 'Fts' proteins provide a stable protein-protein binding platform and localised enzyme activities to divide the bacterial cell.

4.1.3 Regulation of conventional bacterial septation through FtsZ

Regulation of septation principally hinges on the establishment and stabilisation of the FtsZ-ring at mid-cell (Errington et al., 2003). The MinCDE system is a well studied mechanism for Z-ring control in *E. coli* and works using the FtsZ ring inhibitory complex MinC-MinD; this inhibition is itself inhibited in the presence of MinE specifically at mid-cell (Goehring and Beckwith, 2005). The Gram-positive bacterium *B. subtilis* uses a homologus MinC-MinD system controlled by the DivIVa protein which works by anchoring MinCD to the cell poles leading to the relaxation of FtsZ inhibition at mid-cell (Marston et al., 1998). The often overlooked additional control proteins such as: EzrA and SulA act singularly and bind directly to FtsZ to inhibit Z-ring formation (Goehring and Beckwith, 2005).

The SulA protein is involved in the *E. coli* SOS response and inhibits septation in cells containing condensed genomes at mid-cell, this prevents the genome being guillotined by the closing septa resulting in the loss of viability (Goehring and Beckwith, 2005). As the ratio of *B. bacteriovorus* genome size to cell volume is so high, proteins which inhibit septation by 'nuclear occlusion' may have increased importance in dividing *B. bacteriovorus* growth-phase cells compared to other bacterial species.

4.1.4 Bioinformatic identification of *B. bacteriovorus* septation machinery

Little is known about *B. bacteriovorus* cell division, thus bioinformatic analysis was used to identify the septal genes responsible for this process. This analysis revealed that in general *B. bacteriovorus* HD100 genome has the usual complement of cell septation machinery but is lacking strong homologues of any recognisable control mechanisms, discussed further in section 6.1 (Table 4.1).

Table 4.1

Gene Product Name	Brief description/Notes	*B. bacteriovorus* HD100 Homologue
Proteins known to be important in bacterial septation		
FtsZ	Eukaryotic Tubulin homologue which forms a ring-like structure below the cytoplasmic membrane at the mid-cell point in bacteria. FtsZ-ring formation at mid-cell is the first process in septal protein recruitment and septation. Has a secondary potential role in inner-membrane invagination.	Bd3189
FtsA	Required for FtsZ-ring localization at mid-cell.	Bd3190
ZipA	Required for FtsZ-ring localization at mid-cell. Amino acid sequence too short and diverse for accurate BLAST analysis.	**X**
ZapA	FtsZ-ring assosiated protein. Amino acid sequence too short and diverse for accurate BLAST analysis.	**X**
FtsE	Tighly complexed with FtsX and is essential for division in media containing high salt concentrations in *E. coli*.	Bd0165
FtsX	Tighly complexed with FtsE and is essential for division in media containing high salt concentrations in *E. coli*.	Bd0166
FtsK	Required for physical maintenance of the septum and downstream septal protein recruitment. Responsible for active chromosome partitioning using a RecA like DNA pump. Recognition of DNA 'KOPS' sequences by the C-terminal γ-domain enables genome segregation. Aids recruitment of the XerCD recombination system to the *dif* site.	Bd0041
FtsQ	Required for physical maintenance of the septum and downstream Fts protein recruitment. Forms a sub-complex with FtsB/L	Bd3191
FtsB	Required for physical maintenance of the septum and downstream Fts protein recruitment. Forms a sub-complex with FtsQ/L.	Bd0800
FtsL	Required for physical maintenance of the septum and downstream Fts protein recruitment. Forms a sub-complex with FtsQ/B.	**X**
FtsW	Septal trasmembrane protein. Is a RodA homologue and interacts tightly with FtsI(PBP3) in a similar way to RodA-PBP2.	Bd3198
FtsI	Also named PBP3, is the only specific septal peptidoglycan transpeptidase.	Bd3213
FtsN	Essential Fts gene in *E. coli*, found only among gamma-proteobacteria.	**X**

Gene Product Name	Brief of roles in conventional bacteria /Notes	*B. bacteriovorus* HD100 Homologue
AmiC	Cell wall hydrolase essential for final partitioning.	Bd2699
EnvC	A peptidoglycan amidase required for cell wall remodelling and separation.	Bd0168
Septal machinery control mechanisms		
MinC	Inhibits FtsZ-ring formation in a complex with MinD.	**X**
MinD	Inhibits FtsZ-ring formation in a complex with MinC, forms oscillating helical filamentous structures in *E. coli.*	**X**
MinE	Mid-cell specific membrane binding protein, inhibits MinCD activity and thus allows FtsZ-ring formation at the mid-cell only, forms mid-cell rings independently of septal machinery.	**X**
DivIVA	Carries out the equivalent function of MinE in *B.subtilis,* sequesters MinC-MinD to cell poles thus lowering mid-cell concentration and allowing FtsZ-ring establishment.	Bd0464
MipZ	Controls FtsZ ring localisation in *C. crescentus*. BLAST shows a small amount of homology with the Bd3906-ParA protein in the HD100 genome.	**X**
SulA	Inhibits FtsZ-ring formation if condensed chromosomes are present at mid-cell in *E. coli*, also induced by the SOS response.	**X**
EzrA	Inhibits FtsZ-ring formation by direct binding.	**X**

Table 4.1 Identification of genes involved with septation and FtsZ-ring location control in *B. bacteriovorus* HD100. Table shows BLASTp hits using *E. coli* and *B. subtilis* protein sequences as queries against the translated HD100 genome using Wu-BLAST software v2.0 (http://blast.jcvi.org/cmr-blast/). Initial HD100 hits confirmed using them as queries in an ncbi BLASTp search (http://www.ncbi.nlm.nih.gov/) against the non-redundant protein sequence (nr) database, predicted function of the top hits of these BLAST results were examined. This search was limited to essential (BOLD) and non-essential but well studied proteins septation proteins, genes are arranged in order of recruitment to the septum (Goehring and Beckwith, 2005). Proteins marked with an 'X' showed no significant BLAST hits, with no alignment having an e-value less than 1.

4.1.5 Models of *B. bacteriovorus* growth-phase cell septation

In addition to bioinformatic inventory, this study aimed to understand the basic patterns of *B. bacteriovorus* growth within bdelloplasts in order to understand the underlying mechanisms. EM observations by Burnham *et al* and described the *B. bacteriovorus* growth-phase filament dividing at multiple sites sequentially from one pole to the other (Fig. 4.1), consistent with the predicted division pattern of HI *B. bacteriovorus* strains (Burnham et al., 1970, Scherff et al., 1966). However other patterns of sequential converging and diverging cell-division cannot be ruled out. Conventional logic would argue against the possibility of synchronous septation at multiple sites along the growth-phase cell due to the massive organisational issues and potential DNA damage that such a division pattern may cause.

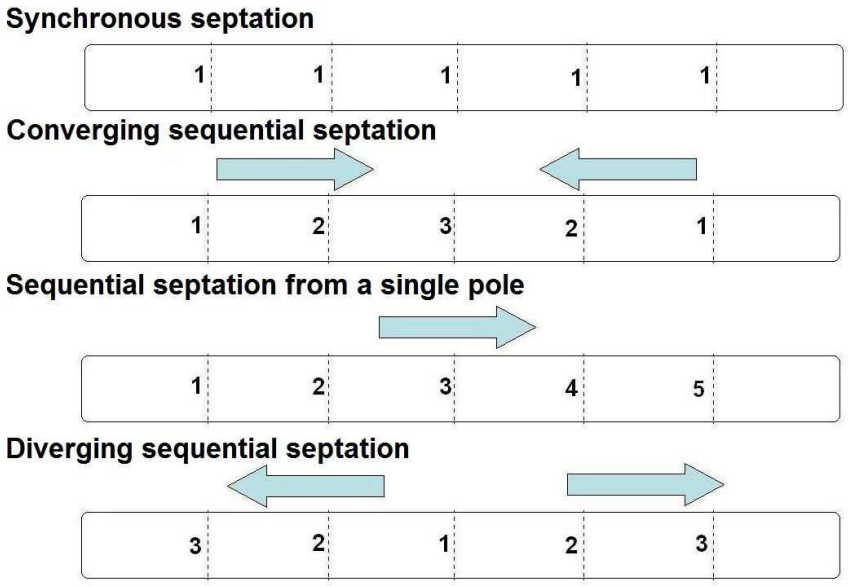

Figure 4.1 Possible models of *B. bacteriovorus* growth-phase cell septation. Figure shows diagrammatic representations of an uncoiled growth-phase *B. bacteriovorus* with multiple potential septation sites (dotted lines), numbers represent the order of septation events along the elongated cell.

4.1.6 Semi-quantitative RT-PCR study of gene expression in *B. bacteriovorus* of genes involved in cell division across a predatory infection cycle.

Multiple RT-PCR analyses of genes involved in cell division and development of *B. bacteriovorus* in synchronously infected prey cells were carried out over the course of this study (Materials and Methods section 2.1.4). Fig. 4.2 shows the expression of key replication and cell division genes over a single predatory time-course. In general expression of these genes show an hierarchical pattern proceeding from DNA initiation (*dnaA*), replication (*ssb*), chromosome condensation(*huA/huB*), septation initiation (*ftsZ*), finally late stage sepation propagation (*ftsK*). This data helped to inform time-points at which fluorescent visualisation of both septal and chromosome condensation mTFP protein tags in order to visualise cells at the highest point of expression. This was necessary as currently there are no inducible promoters available for use in *B. bacteriovorus*.

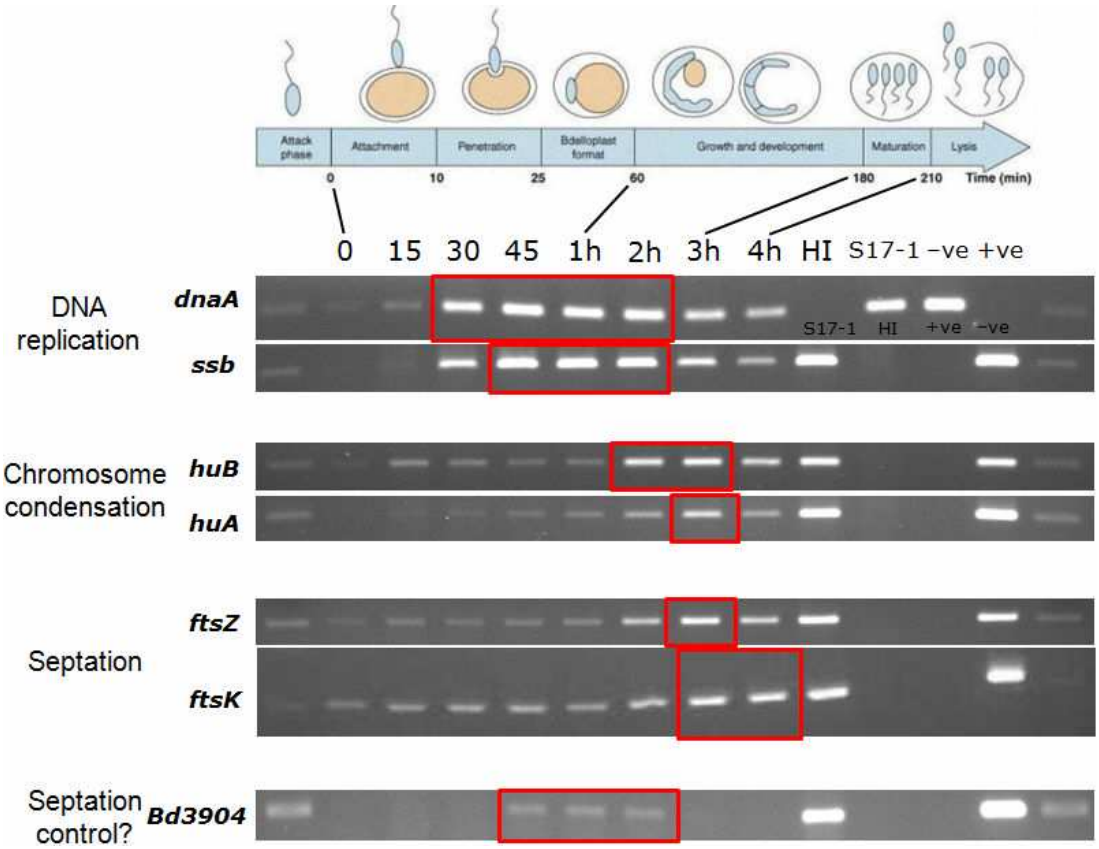

Figure 4.2 Semi-quantitative RT-PCR analysis of genes involved in cell division of *B. bacteriovorus* across the predatory cycle. Lanes are highlighted with red boxes at the point(s) of highest expression. RT-PCR reactions were carried out on RNA extracted at the time points across a synchronous lysate of *B. bacteriovorus* on the *E. coli* strain S17-1. Time points at which the RNA samples were taken are labelled on the figure. The HID13 or HID2 strains were used to assay HI gene expression. *E. coli* S17-1 RNA and no-template reactions provide negative controls, and HD100 genomic DNA was used as a template for a positive control. All lanes are in the same loading with the exception of *dnaA* panel which has had the lanes relabelled where appropriate. Primers for gene detection were designed to amplify an internal region of each gene. The 100 bp marker from the NEB 100 bp ladder is visible in each flanking marker lane. Time-points from the *B. bacteriovorus* predatory life-cycle in illustrated above, adapted from (Lambert et al., 2006b).

4.2 Investigating *B. bacteriovorus* cell division by targeted mTFP protein tagging.

In an attempt to determine growth-phase *B. bacteriovorus* cell division patterns, by visualising septation events within bdelloplasts, two target genes were chosen for C-terminal mTFP tagging; the bacterial tubulin homologue FtsZ and the later stage septal protein FtsK. These were chosen as both proteins contain significant cytoplasmic domains (Fig. 4.4B) and previous work had shown that C-terminal GFP fusions to FtsZ and FtsK are, at least in part, functional in *E. coli* (Osawa and Erickson, 2005, Draper et al., 1998).

The FtsZ protein has been tagged in many bacteria and represents the first logical choice for a septal mTFP tag. However, it was feared that as Z-ring establishment is the first process in septation visulisation of this tag may not have enough temporal resolution to determine the fine filament division patterns.

4.2.1 The FtsZ C-terminal mTFP tag in *B. bacteriovorus*

FtsZ is a well studied protein with four well described domains and a solved crystal structure, reviewed in (Vaughan et al., 2004). FtsZ has two N-terminal globular domains providing the GTP binding and polymerisation activities. Following this a C-terminal domain of variable length with poor homology between species and no fixed structure or function, at the extreme C-terminus is a short conserved peptide sequence which binds FtsA and ZipA (Vaughan et al., 2004), boxed and highlighted in Fig. 4.3.

Work using transposon mutagenesis to insert GFP tags onto the N-terminus of FtsZ in *E. coli*, led to FtsZ truncated proteins which were capable of mid-cell localisation and complementation of FtsZ null strains (Osawa and Erickson, 2005). Taking this data into account three sites were chosen for FtsZ-mTFP insertion in *B. Bacteriovorus* (see numbered positions in Fig. 4.3): 1) before the FtsA/ZipA binding sites after the alanine residue at position 539, 2) within the FtsA/ZipA C-terminal binding site after the Isoleucine residue at amino acid position 399 (the tag best tolerated in *E. coli*) and 3) after the C-terminal Glutamic acid residue.

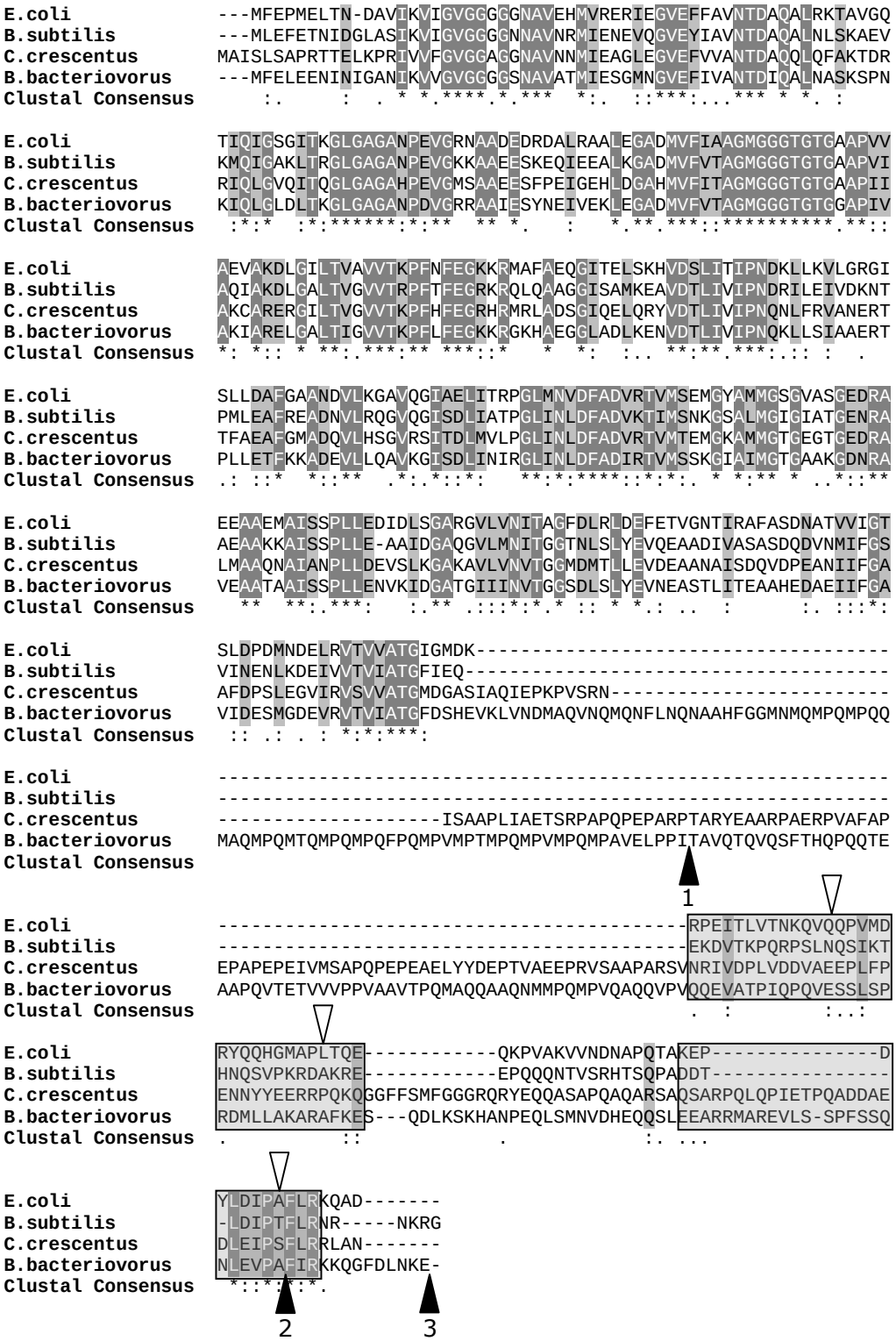

Figure 4.3 Multiple alignment of FtsZ proteins from model bacteria and *B. bacteriovorus* HD100 showing planned mTFP insertion sites. Multiple alignment generated using the online ClustalW2 tool (http://www.ebi.ac.uk/Tools/clustalw2/index.html). Boxed regions highlight regions of protein interaction with FtsA and ZapA. White arrows show location of eGFP and Venus-YFP insertions into *E. coli* FtsZ, where fusions were still capable of mid-cell localisation and complementation of FtsZ null strains (Osawa and Erickson, 2005). Black arrows indicate the three mTFP insertion sites used in *B. bacteriovorus*.

All FtsZ-mTFP tags were cloned in the pAKF04 backbone in frame with mTFP using the method described in section 2.12 and shown in Fig. 2.1. All constructs contained a 5’ deletion of the FtsZ ORF therefore ex-conjugant strains would only express the fusion construct from the native promoter (Fig. 2.1A).

Initial observations of *B. bacteriovorus* FtsZ-mTFP tagged exconjugants (tagged at all sites shown in Fig. 4.3) revealed little/no mTFP fluorescence (data not shown). RT-PCR analysis of FtsZ in wild-type *B. bacteriovorus* HD100 synchronous infections (See Materials and Methods section 2.14.2) revealed expression of *ftsZ* peaks at the three hour time-point (Fig. 4.2). Thus exconjugant strains were screened for fluorescence in synchronous infections at the three hours post infection time-point, however mTFP activity within bdelloplasts still could not be detected (data not shown). Direct genome sequencing and Southern blot analysis showed that the FtsZ-mTFP tagged constructs within exconjugant strains were present (as they could be amplified for sequencing) but were not found in the expected region of the HD100 genome (see Appendix 3.4).

To explore the possibility that the nature of the mTFP protein moiety attached to the FtsZ was causing aberrant protein folding leading to a loss of function, further C-terminal tag constructs at the same three sites shown in Fig. 4.3 were cloned using a

mCherry tag. These again showed no fluorescence activity at any stage in the *B. bacteriovorus* life-cycle (data not shown).

Constructs were created that included the *ftsZ* promoter leading to exconjugant strains capable of expressing both wild-type and tagged FtsZ, see Fig. 2.1B. These strains again showed no fluorescence activity. Expression of FtsZ-mCherry fusion proteins in *E. coli* showed localised fluorescence activity suggesting that this protein was at least partially functional (data not shown).

The approach taken to C-terminally GFP-tag FtsZ in order to visualise patterns of septation events in growth-phase cell filaments failed to produce any stable mTFP or mCherry protein fusions at any of the three sites selected (Fig. 4.3). As stable GFP tags are possible in *B. bacteriovorus*, demonstrated by the Ccrp-mTFP protein in sections 3.5.1-2 and later work in sections 4.3.2 and 5.2.3, this suggests that the C-terminus of FtsZ could have increased importance in cell division. This case is supported by the somewhat longer C-terminal proximal domain of FtsZ in HD100 compared to model organisms (Fig. 4.3).

4.2.2 Cloning FtsK C-terminal mTFP tags in *B. bacteriovorus*

Another choice for septal tagging in *B. bacteriovorus* was FtsK, one of the few septation proteins with a significant cytoplasmic domain (Fig. 4.4B). FtsK has a series of different roles in septation including: downstream septation protein recruitment, chromosome segregation and homologous recombination summarised in Fig. 4.4.

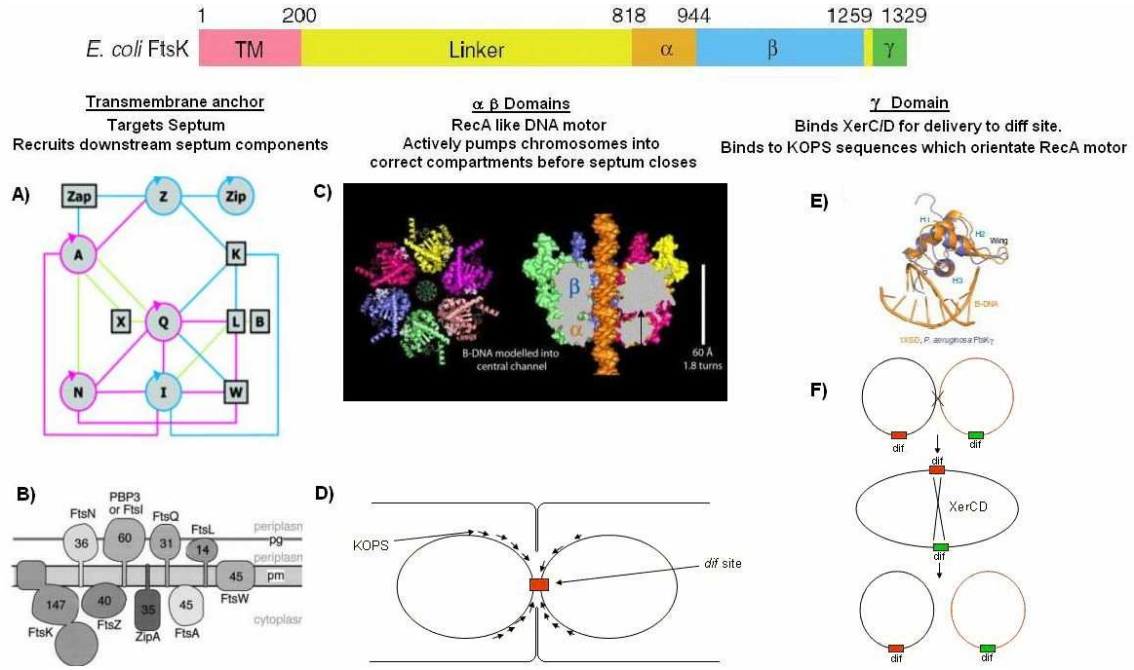

Figure 4.4 The multiple roles of FtsK protein septation. Figure shows domain structure of the trams-membrane (TM), linker, RecA-like motor (α and β) and DNA recognition γ domains in *E. coli* and summarises their three main functions (Massey et al., 2006). (**A**) Yeast 2-hybrid data summary diagram of bacterial septation components, highlighting the role played by the TM domain of FtsK in downstream protein recruitment (Di Lallo et al., 2003). (**B**) Diagram showing the relative size and sub-cellular positions of the septal proteins showing that FtsK has the largest cytoplasmic domain (kDa) (Nanninga, 2001). (**C**) X-ray crystal structure of FtsK RecA-like motor domain, this domain froms a hexamer around a central DNA helix (orange) (Massey et al., 2006). (**D**) using the DNA recognition sequences (KOPS) for orientation the RecA-like motor domain of FtsK actively transports replicated chromosomes to each side of the division septum, KOPS elements point toward the *dif* site (Sivanathan et al., 2006). X-ray crystal structure of FtsK γ-domain showing DNA recognition helixes (Sivanathan et al., 2006). (**E-F**) FtsK γ-domain recruits the site specific recombination proteins XerC-XerD to the dif site causing recombination removing dimeric chromosomes before division, brought about by homologus recombination during replication (Yates et al., 2006).

Protein function assays and X-ray crystal studies have largely focused on FtsK from *Pseudomonas aeruginosa* as the linker region of FtsK in *E. coli* (amino acid positions 200-818, Fig. 4.4) is atypically extended making it hard to purify as it tends to aggregate (Massey et al., 2006). The pair-wise alignment in Fig. 4.5 shows the functional domains of FtsK between *P. aeruginosa* and *B. bacteriovorus* are well conserved between these organisms despite the reality large evolutionary distance separating these species (Fig. 4.5). As only the trans-membrane domain at the N-terminus of FtsK is essential for downstream septation in *E. coli* (Draper et al., 1998) C-terminal mTFP tags were designed and constructed using the method described in section 2.12 (Fig. 2.1), the exact location of mTFP insertions are shown by the black arrows on Fig. 4.5.

In the case of FtsK-mTFP fusions at sites: 1, 3 and 4 exconjugant strains all had slow predatory rates taking 3-5 days to fully clear predatory cultures compared to the normal 16 h and contained persisting bdelloplasts. Significant difficulties were encountered when cloning the FtsK-mTFP fusion construct at site 2 therefore this was discontinued. RT-PCR analysis of *ftsK* in a predatory life cycle showed a peak in expression at three hours (Fig. 4.2). Synchronous predatory cultures were used to try and detect mTFP fluorescence at the three hour time point for any exconjugant strain (see Materials and Methods section 2.13).

Diagnostic Southern blot of FtsK-mTFP strains showed unexpected banding patterns indicating incorrect recombination and in one case complete loss of the *mtfp* ORF (Appendix 3.4).

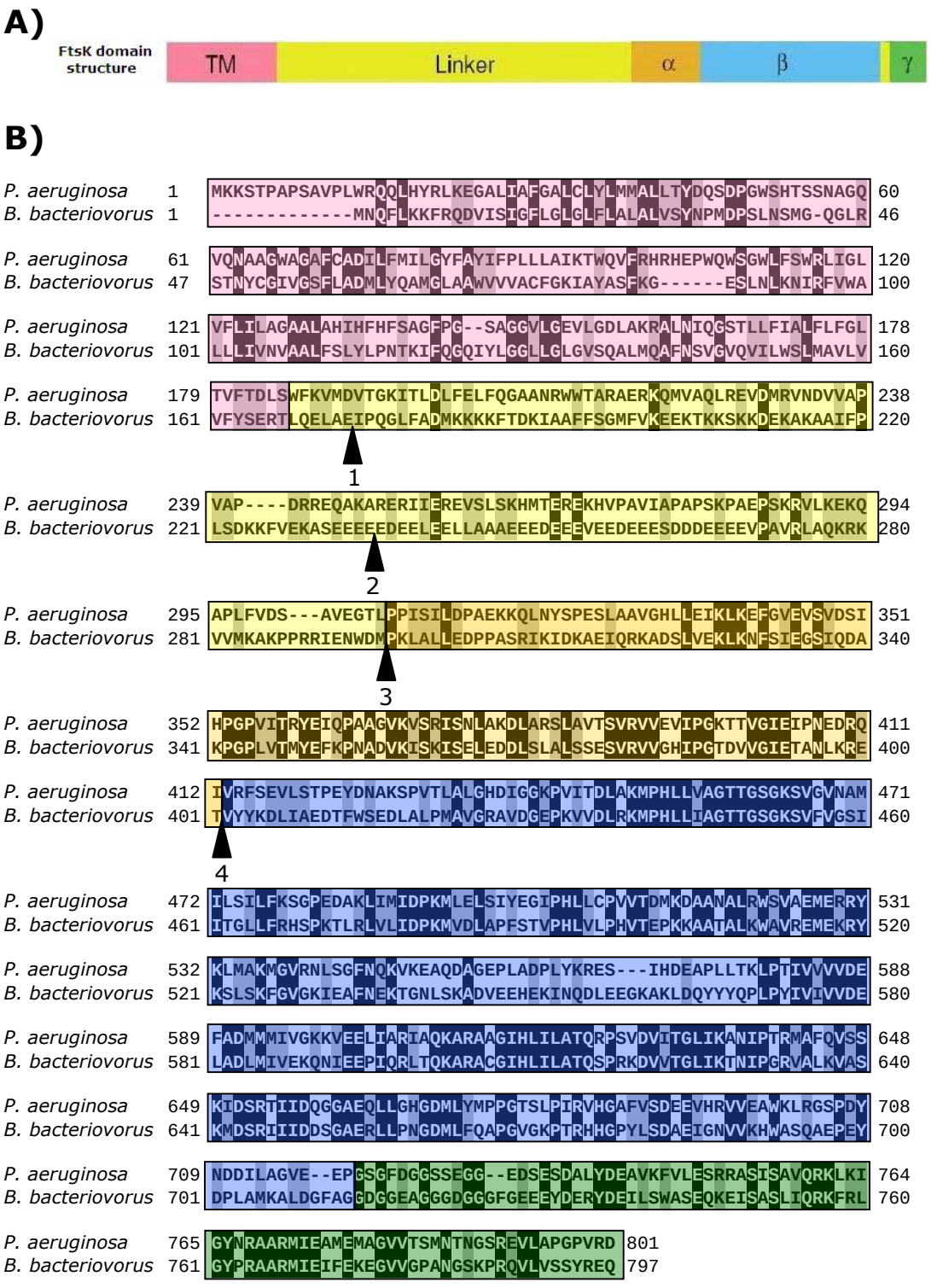

Figure 4.5 Pair wise alignment of FtsK carried out using the ClustalW program (**B**). *E. coli* FtsK sequence used to plot the location of the domain boundaries, though omitted from the alignment due to its long linker region (Massey et al., 2006). Colours of the domains match those on *ftsK* in part (**A**), adapted from (Massey et al., 2006). Black arrows represent mTFP insertion sites chosen for this study.

4.3 Investigating *B. bacteriovorus* cell division using indirect staining and mTFP tagging methods.

Direct septal protein tags in *B. bacteriovorus* had not yielded stable genome inserted constructs therefore this approach could not be used. Two indirect methodologies were therefore devised to try and visualise dividing *B. bacteriovorus* within bdelloplasts:

Chromosome segregation in bacteria occurs largely due to the action of histone-like, DNA condensation proteins. Using a DNA label it should be possible to visualise dividing condensed chromosomes within *B. bacteriovorus* growth-phase cells and thus determine the pattern of septation.

GFP-labelled bdelloplasts arising from wild-type *B. bacteriovorus* invading prey expressing GFP have been used previously to visualise growth-phase cells within bdelloplasts (Lambert et al., 2006a, Evans et al., 2007). Using GFP-labelled prey strains combined with time-lapse microscopy could be facilitate study of growth-phase cell development, however keeping the bdelloplasts in focus over long periods and methods for keeping bdelloplasts viable on microscope slides remained difficult challenges with this approach.

4.3.1 Investigating *B. bacteriovorus* cell division using chromosomal DNA staining.

Fluorescent microscopy using the Hoechst 33372 DNA stain of bdelloplasts gave the first insight into *B. bacteriovorus* developmental processes (see Materials and Methods section 2.9.2). Hoechst staining early in infections gives rise to two fluorescent signals against a dark background: the genome of the growing *B. bacteriovorus* and the genome/plasmids of the prey (Fig. 4.6a, and in much more detail in Fig. 5.5). In later stage bdelloplasts the prey signal is lost presumably due to the action of *B. bacteriovorus* nucleases with the prey cytoplasm (Fig. 4.6b). Examination of Hoechst stained bdelloplasts in synchronous predatory cultures failed to give enough resolution to see separated chromosomes, however occasionally a lobed signal was observed (Fig. 4.6a). This could suggest that the majority of DNA within growth-phase cells is actively transported by a protein, such as FtsK, just before septation. Hoechst staining also provided the first technique for counting progeny *B. bacteriovorus* cells within bdelloplasts by fluorescence microscopy (Fig. 4.6c).

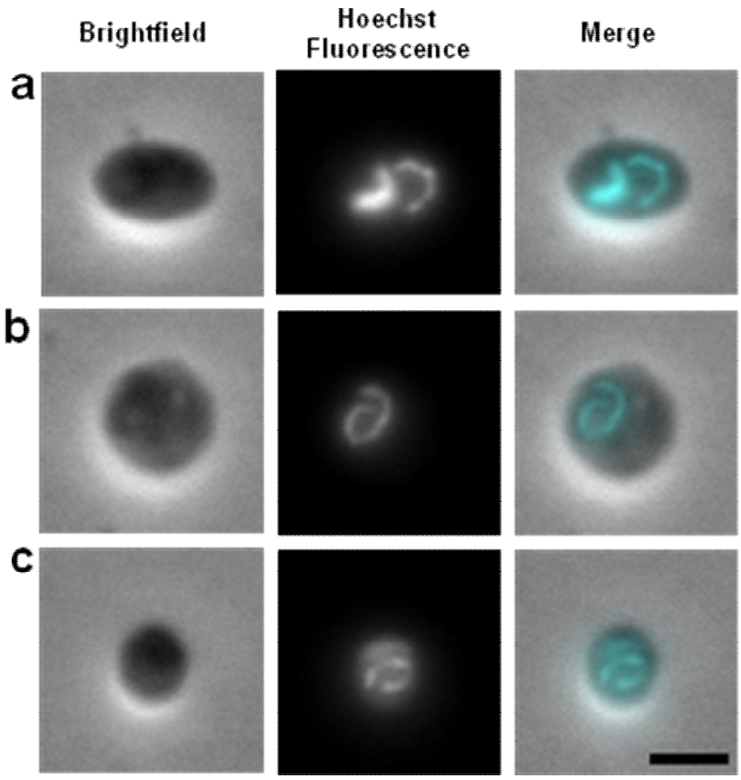

Figure 4.6 Hoechst stained bdelloplasts at all stages of *B. bacteriovorus* development within bdelloplasts. (a) 'early' stage bdelloplasts containing an elongated growth-phase cell and a second prey-cytoplasmic signal; an elongated 'lobed' structure can be seen within the growth-phase *B. bacteriovorus*, perhaps indicating chromosome segregation. (b) 'late' stage unusually large bdelloplast containing a coiled growth-phase *B. bacteriovorus* cell. (c) three septated progeny cells within a bdelloplast. Scale bar = 2 μm.

4.3.2 Investigating *B. bacteriovorus* cell division using a histone-like protein HuA.

Hoechst staining of *B. bacteriovorus* within bdelloplasts did not give enough resolution to visualise separate condensed chromosomes, however GFP tagging of histone-like chromosome binding proteins may provide sharper signals along growth-phase cells. To test this mTFP fusion constructs were generated for the *B. bacteriovorus* histone-like proteins HuA and HuB.

The heterodimeric HU histone-like binding proteins form a single tight focus at the *E. coli* nucleoid within exponentially growing bacterial cells (Fig. 4.7) (Wery et al., 2001). *B. bacteriovorus* homologues were found by BLAST analysis and expression of the two genes that from the HU complex: *huA* (*Bd2104*) and *huB* (*Bd3382*) was measured through a predatory life-cycle (Fig. 4.2). This showed both genes peak in expression at the 3-4h post infection time-point making them a good choice for chromosome visualisation at the point of septation.

C-terminal mTFP tags of the full length HuA and HuB proteins have been shown to be functional in *E. coli* (Wery et al., 2001). *B. bacteriovorus* proteins were tagged in the same way at C-terminal residue 90 for HuA and C-terminal residue 90 for HuB, using the method described in section 2.12 (Fig. 2.1), giving exconjugant strains capable of expressing both wild-type and mTFP-tagged Hu proteins. The HuB-mTFP did not form fusion constructs despite several attempts, which could suggest that this fusion formed heterologous a dominant-negative HU complex in the *E. coli* DH5α strain used for cloning. The *huA-mtfp* construct expressed in *E. coli* showed that this tagged *B. bacteriovorus* protein retained the ability to localise with the *E. coli* nucleoid (Fig. 4.7A). This construct was conjugated into *B. bacteriovorus* and exconjugants

strains were confirmed by direct sequencing and Southern blotting (Appendix 3.4 and 4.1).

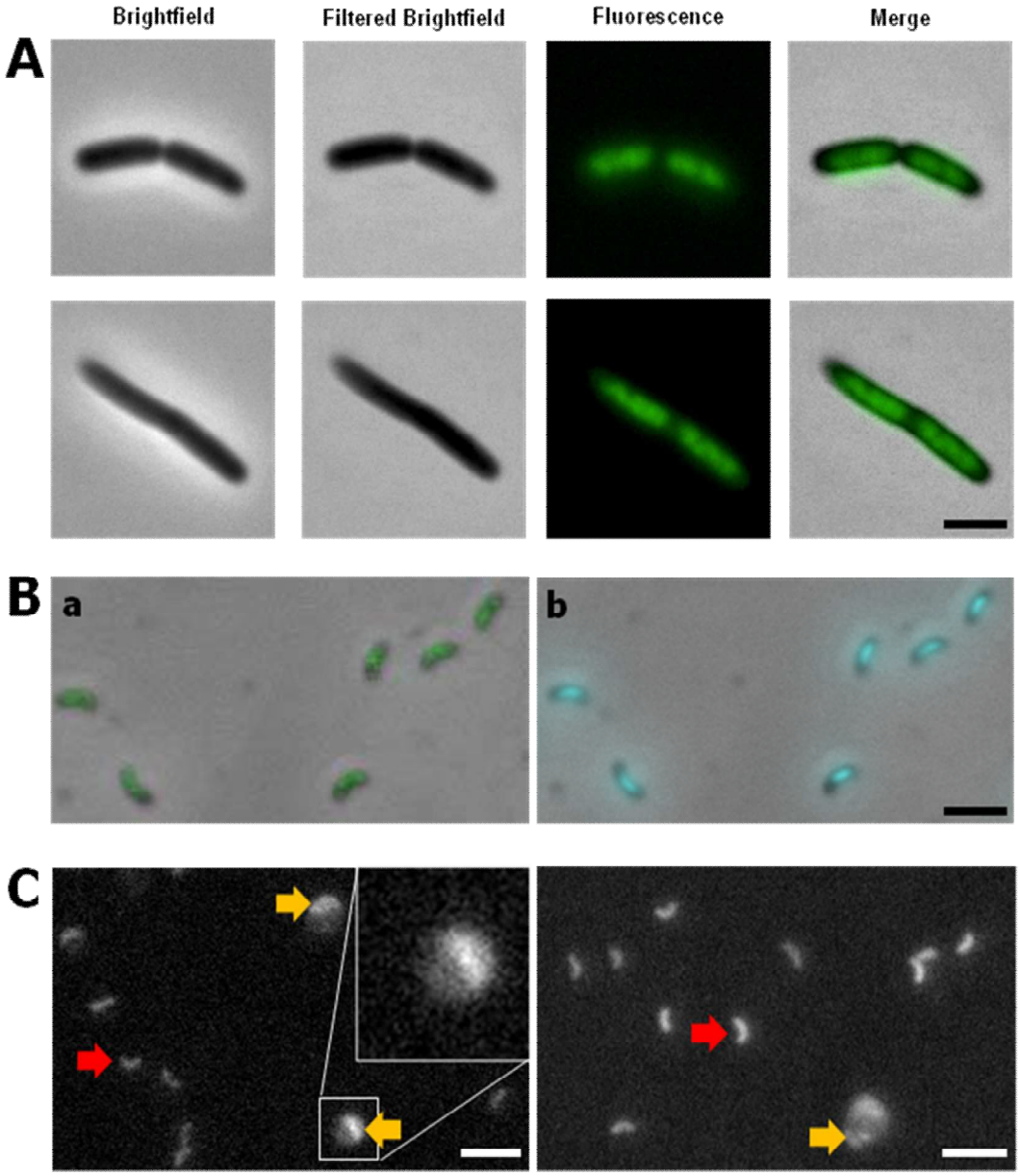

Figure 4.7 The HuA-mTFP fusion protein co-localises with the bacterial nucleoid in both *E. coli* and *B. bacteriovorus*. (**A**) *B. bacteriovorus huA-mtfp* expressed from the pAKF52 plasmid using 200 μM IPTG in exponentially growing *E. coli* DH5α. (**B**) Two merged images of the same attack-phase *B. bacteriovorus huA mtfp* cells, (a) Brightfield- mTFP fluorescence merged image, (b) Brightfield Hoechst DNA stain fluorescence. (**C**) mTFP fluorescent images of HD100 *huA mtfp* strain attack-phase cells (red arrows) and cells within bdelloplasts (yellow arrows). Highlighted bdelloplast in (C) has been enlarged for clarity.
All scale bars = 2 μm.

The *huA-mftp B. bacteriovorus* strain attack-phase cells have a centrally located mTFP signal as expected from the location of the genome in attack-phase cells (see cryo-EM, Fig. 1.2). This signal co-localises with the Hoechst-DNA signal in these cells as expected from a histone-like protein. Due to the relative weakness of the mTFP fluorescent signal longer exposure times are needed for image acquisition, leading to the loss of clarity seen in Fig. 4.7B. Fluorescence activity of the *huA-mtfp* strain within bdelloplasts in a synchronous predatory culture showed the expected pattern of increased brightness at the 3-4h time-point (Fig. 4.2) allowing visualisation of growing growth-phase cells within bdelloplasts (Fig. 4.7C). However, the mTFP signal was not strong enough to show the dividing growth-phase cell in any detail by overcoming the background fluorescence of the bdelloplast (Fig 4.7C, enlarged bdelloplast).

4.4 Investigating *B. bacteriovorus* cell division using indirect prey cell GFP labelling methods.

As predator-fluorescent approaches had failed to yield any usable images for looking at *B. bacteriovorus* development, I turned to prey-labelling. Previous work carried out by Dr Richard Woods on *B. bacteriovorus* growing within prey had shown that growth-phase cells can be visualised in bdelloplasts as a dark-negative against a fluorescent background (unpublished data) Fig. 4.8. As both direct and indirect methods of growth-phase cell labelling had not given strong enough signals to follow *B. bacteriovorus* growth patterns within bdelloplasts, time-lapse microscopic methods were explored.

Using a periplasmically fluorescently-labelled prey strain: *E. coli* S17-1:pMAL-p2_mCherry (R. Woods unpublished), the latest Prior H101A motorised-XY stage and ultra-fine Z-control apparatus, in conjunction with our fluorescent microscope, allowed accurate revisiting and refocusing on bdelloplasts immobilised on Ca/HEPES 1% agarose pads over several hours (see Materials and Methods section 2.9.4). Multiple image captures of bdelloplasts derived from synchronous prey infections generated time-lapse movies used to study *B. bacteriovorus* predatory development (See supplementary Movies 1-10, and stills from those movies in Appendix 4.2A-J). The following sections show the results of these studies of *B.*

bacteriovorus predatory growth and show supporting work carried out by Machi Kanna under the supervision of Shin-Ishi Aizawa at the Prefectural University of Hiroshima, Japan (Fig. 4.9).

4.4.1 *B. bacteriovorus* growth-phase cells divide synchronously forming both odd and even numbers of progeny within bdelloplasts.

Analysis of 146 late-stage fluorescent bdelloplasts containing septated progeny revealed that *B. bacteriovorus* growth-phase cells divide into both odd and even numbers of progeny (Fig. 4.8Aa and examples shown in Fig. 4.8Ab); this observation was also confirmed using EM studies on 77 bdelloplasts which had been formed by non-fluorescent prey (being infected in liquid predatory cultures by *B. bacteriovorus* (Fig. 4.9)). A graph showing the frequency of progeny numbers within bdelloplasts showed no disinclination towards odd numbers of progeny, as these data were normally distributed (Fig. 4.8Aa and Fig. 4.9Aa). The reduced maximal progeny yield in Fig. 4.9 versus Fig. 4.8, correlates with the smaller volume of the prey *E .coli* used (see figure legends for exact sizes); but it must be remembered that in the fluorescent larger prey cells in Fig. 4.9 an unknown, but possibly significant amount of cellular protein was being diverted into mCherry protein synthesis and so was unavailable for *B. bacteriovorus* growth.

In contrast to previous reports based on electron microscopy, and contrary to "normal" bacterial cell division dogma, *B. bacteriovorus* growth-phase cells initiate and complete septation synchronously within prey, even when as many as 8 or 9 progeny are produced (Fig. 4.8B, Appendix 4.2A-C and supplementary Movies 1-3) (Scherff et al., 1966, Burnham et al., 1970). Septation only occurs when the *B. bacteriovorus* has reached its maximal length and initiates synchronously even when high numbers of progeny are formed (Appendix 4.2D, Movie 4). In the time-lapse movies *B. bacteriovorus* appear to be braced against prey internal structures and dramatic shifts in progeny cell orientations are seen at septation, possibly caused as stored tension within the braced growth-phase cell is released during synchronous filament division (subsequent positions in Fig. 4.8B and Movie 5, Appendix 4.2E). These shifts allowed us to accurately measure average septation time (from initiation to division) as 41 min (+/- 4 min 95%CL, n= 47); interestingly this was independent of the number of progeny produced (Fig. 4.11).

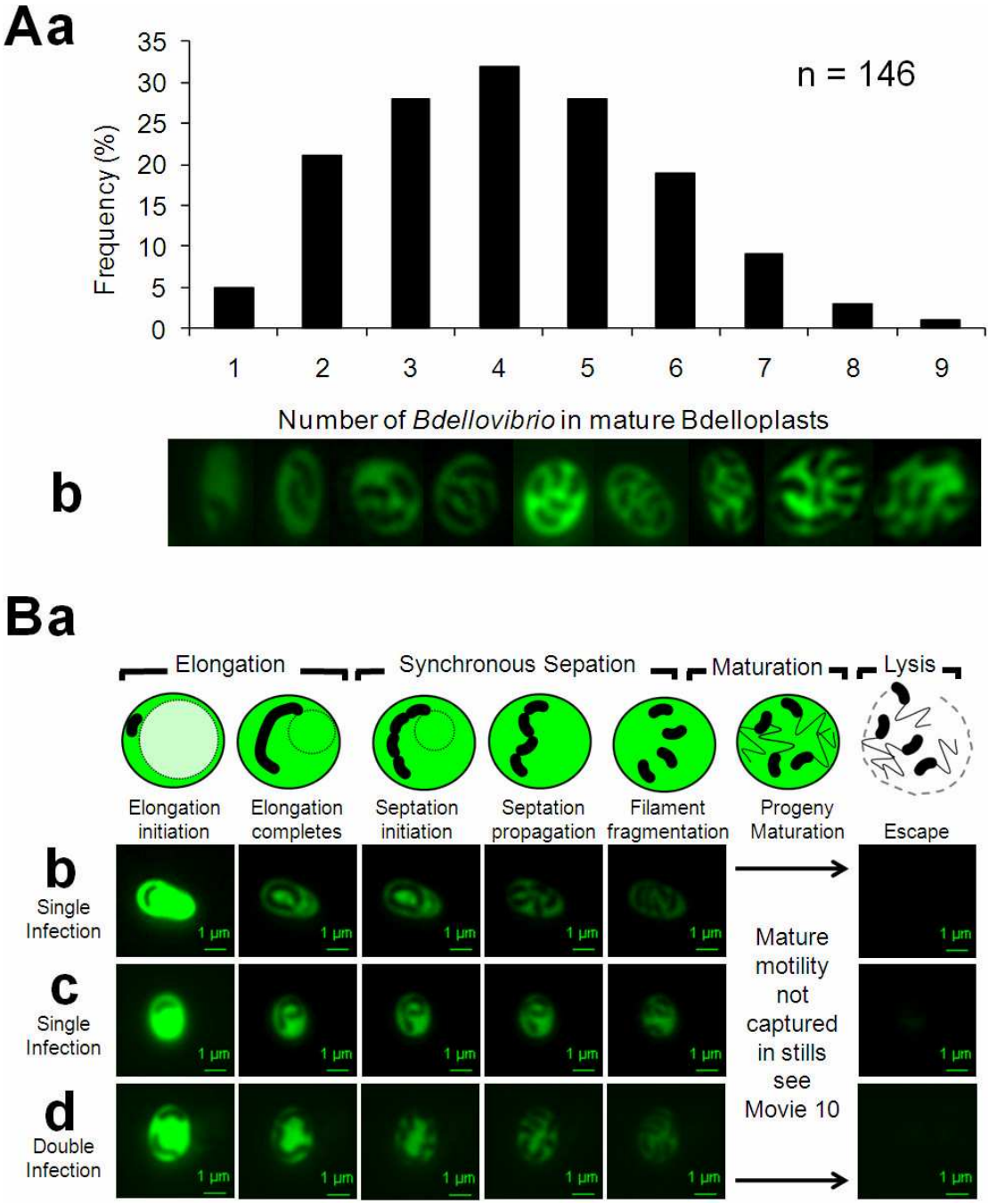

Figure 4.8 *B. bacteriovorus* filamentous growth-phase cells septate synchronously within the bdelloplast forming both odd and even numbers of progeny. (**Aa**) Frequency measurement of numbers of mature *B. bacteriovorus* within 146 *E. coli* S17-1:pMAL-p2_mCherry fluorescent bdelloplasts. Average prey cell length 4.67 µm+/- 1.37 and width 0.97 µm +/-0.09, n=167. (**Ab**) Examples of septated and mature growth-phase *B. bacteriovorus* cells within fluorescently labelled bdelloplasts, images used to illustrate frequency plot above. (**Ba**) Sketch showing key points in *B. bacteriovorus* cell development within a bdelloplast. (**Bb-c**) Selected frames from time-lapse movies showing synchronously dividing growth-phase cells in fluorescent bdelloplasts (**Bd**) Selected frames from time-lapse movies showing two synchronously dividing growth-phase cells forming different numbers of progeny (3 and 4) within a fluorescent bdelloplast. Fluorescence mCherry activity is false coloured green for clarity, scale bars = 1 µm. Full time-lapse movies are provided in supplementary Movies 1 ,2 and 3 and displayed as a spread in Appendix 4.2A-C**.**

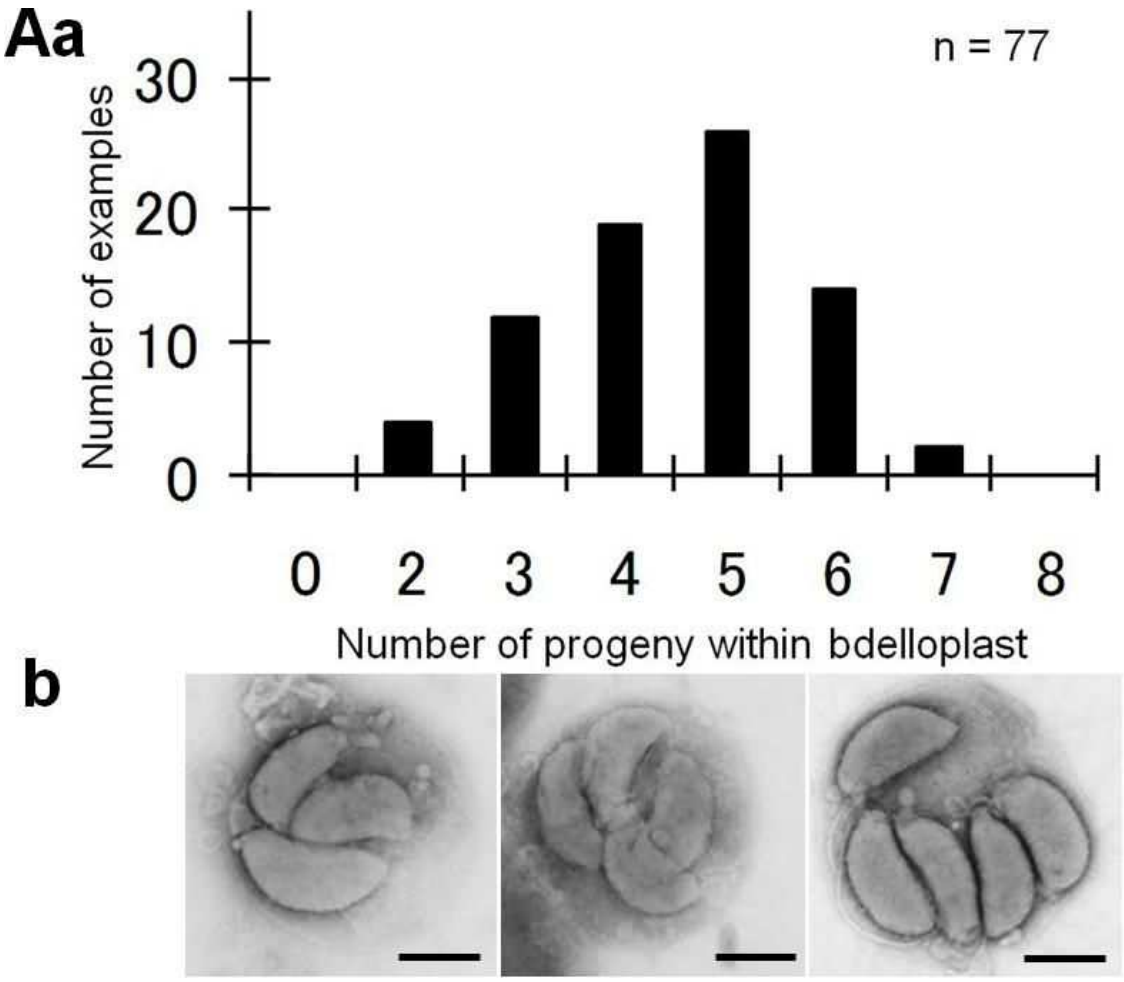

Figure 4.9 *B. bacteriovorus* produce both odd and even numbers of progeny within the bdelloplast, visualised by electron microscopy. (**Aa**) Distribution of progeny number within *E. coli* DFB225 bdelloplasts at 3 hours post infection (n=77). (**Ab**) Examples of septated *B. bacteriovorus* progeny within bdelloplasts at three hours post infection, showing: (left to right) 3, 4 and 5 progeny cells. Cells stained with 2% PTA (pH7.0), scale bars = 500 nm. Average *E. coli* DFB225 average prey cell length in this experiment was 2 μm. This work was carried out by Machi Kanna and shown as supporting data for Fig. 4.9A.

4.4.2 Synchronicity of *B. bacteriovorus* growth-phase cells division is maintained in multiply infected bdelloplasts.

High numbers of *B. bacteriovorus* in predatory cultures can sometimes lead to multiple infections of prey; in these cases invasion of the *B. bacteriovorus* has had to be near simultaneous as the forming of the prey bdelloplast precludes other *B. bacteriovorus* from entry (Thomashow and Rittenberg, 1978a). In double infected bdelloplasts the two growing *B. bacteriovorus* compete for resources, and as I chose to use an *E. coli* prey with diverse cell volumes (Fig. 4.8 legend), double infections sometimes resulted in differing numbers of progeny, derived from two co-infecting *B. bacteriovorus* in a single prey bdelloplast; for example Fig. 4.8Bd shows two co-infecting *B. bacteriovorus* forming three and four progeny in a single bdelloplast. Conventional logic would suggest that the growth-phase cell forming 3 progeny should finish cell division first and lyse the bdelloplast, however synchronicity of septation is maintained between the two different growing *B. bacteriovorus* (Fig. 4.8Bd, Appendix 4.2C and Movie 3). This suggests that there is either a diffusible signal between the two *B. bacteriovorus*, or that they are both reacting simultaneously to the final depletion of (a) key bdelloplast resource(s), beyond the critical level at which another whole progeny *B. bacteriovorus* could have been produced.

4.4.3 *B. bacteriovorus* growth-phase cells appear to elongate from both ends of the growth-phase filamentous cell within bdelloplasts.

Early EM studies had suggested that the pili used for entry were still seen inside prey bdelloplasts; it was proposed that *B. bacteriovorus* cells continued to cling onto the prey cytoplasm (at the site of entry) and thus were predicted to grow unilaterally from the free pole (Scherff et al., 1966). Time-lapse image data shows no evidence of this and both poles of the elongating *B. bacteriovorus* move freely within bdelloplasts (Fig. 4.8Bb-d, Appendix 4.2A-E and Movies 1-5). However, the possibility of free rotation of the unanchored prey cytoplasm within bdelloplasts may also have led to similar observations.

4.4.4 *B. bacteriovorus* cells within bdelloplasts do not always grow and produce another progeny cell.

An unexpected finding of this study (shown in Fig. 4.8) was that a few *B. bacteriovorus* cells entered prey and formed bdelloplasts yet did not elongate or divide (Appendix 4.2F-G and Movie 6-7). The small sizes of these prey bdelloplasts suggest that they may have contained insufficient resources to produce any *B. bacteriovorus* progeny, yet surprisingly these bdelloplasts lysed at wild-type time-points (4-5h), releasing the single original *B.*

bacteriovorus. This suggests that those single *B. bacteriovorus* cells may have gone through the hydrolytic host digestion program, but simply had received insufficient nutrition to allow production of a whole *B. bacteriovorus* genome and thus did not initiate elongation (Appendix 4.2F-G and Movie 6-7).

4.4.5 *B. bacteriovorus* developmental time-points and method of progeny cell bdelloplast escape.

Immature divided *B. bacteriovorus* progeny must develop polar structures such as flagella as *B. bacteriovorus* are seen to be motile as they lyse the bdelloplast (Movie 10); lysis resulting in a loss of prey-derived fluorescence activity (Fig. 4.8B). This specific and rapid loss of bdelloplast fluorescence allowed us to measure the average time taken for *B. bacteriovorus* cells to mature and lyse bdelloplasts, after septation; this mean time to lysis was 26 min (+/- 3 min 95%CL, n=81). In contrast to the similarity in septation times for *B. bacteriovorus* which were independent of filament length and thus progeny number; the 'time to lysis' was inversely proportional to the number of progeny, indicating that the lysing power of multiple progeny in larger bdelloplasts was in some way higher (Fig. 4.10). This also showed that progeny departed bdelloplasts through one (88%) or occasionally two small holes (12%); rather than by catastrophic bdelloplast breakdown

(percentages from n=67 bdelloplasts, Appendix 4.2F-G and Movies 6 and 7).

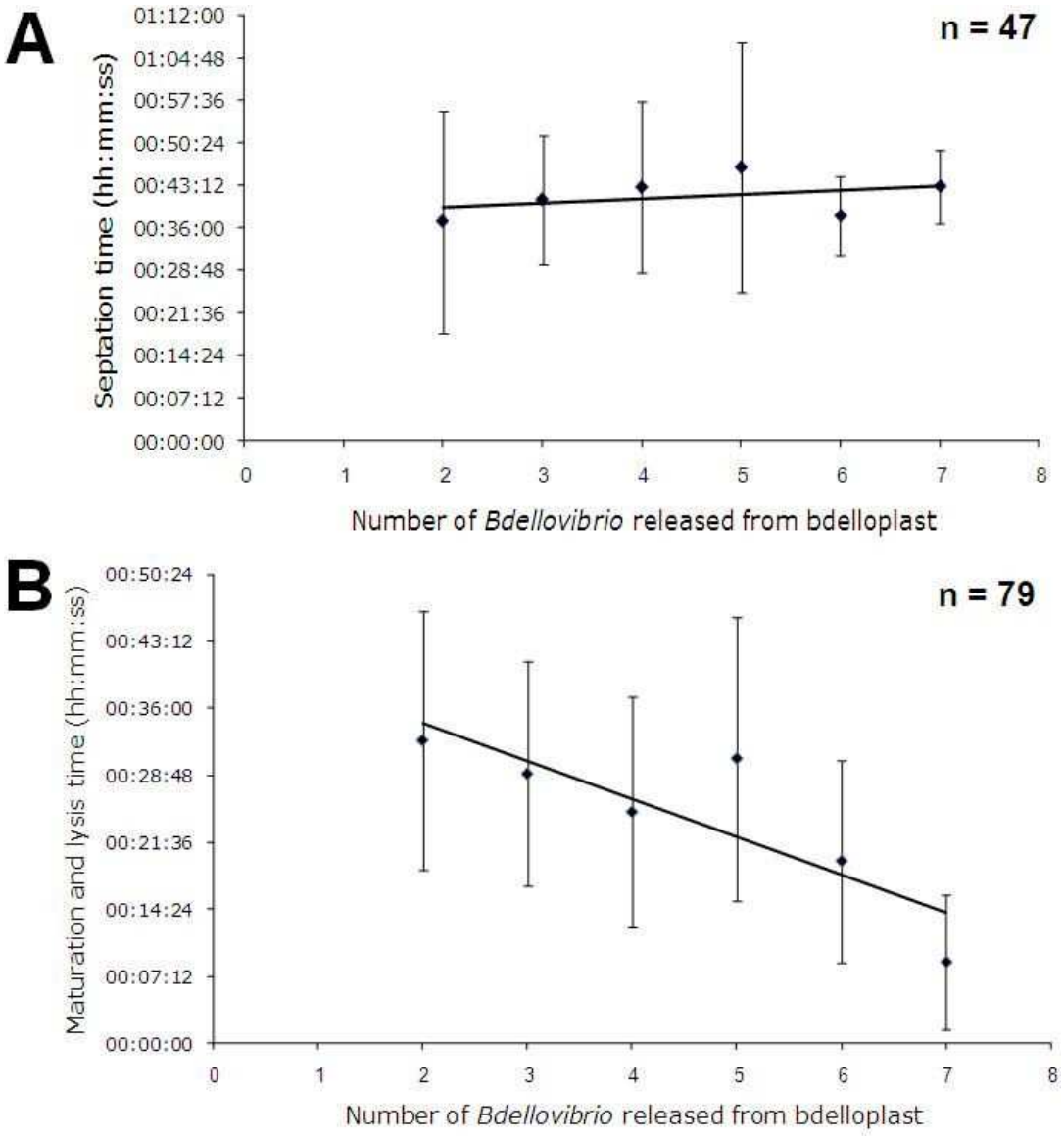

Figure 4.10 (**A**) Rate of septation of the growth-phase *B. bacteriovorus* cell is independent of progeny number (n=47), (**B**) whereas *B. bacteriovorus* maturation and bdelloplast lysis-time decreases as the number of progeny increases (n=79). Time-points were calculated from time-lapse movies using image time-stamp data within the SimplePCI software.

4.5 The role of the Bd3904 protein in *B. bacteriovorus* development within bdelloplasts.

The protein encoded by the *Bd3904* gene in the *B. bacteriovorus* HD100 genome belongs to the recently described 'bactofilin' family of proteins (Kuhn et al., 2010). This gene was initially identified in *B. bacteriovorus* by its high homology to the MXAN_7475 protein of *Myxococcus xanhus,* thought at the time to have a role in cell division and cell morphology (M. Koch, personal communication). Both the genomic context of this gene, being downstream of a DNA partitioning ParAB operon, and preliminary RTPCR data suggested that this protein may have a role in *B. bacteriovorus* synchronous cell division (Fig 4.11). As initial investigations into the function of this protein had yielded a division-inhibitory phenotype in *E. coli* an expedient investigation was carried out to further investigate the function of Bd3904.

The number of cytoskeletal proteins known in bacteria is still growing, a new class of filamentous bacterial proteins has been recently described containing the domain designated DUF583 in the PFAM database (Kuhn et al., 2010). These proteins have been designated 'bactofilins' based on their predicted polymerisation properties (Kuhn et al., 2010). These filament form stable filament bundles which require no cofactors to polymerise very much like IF

elements (Kuhn et al., 2010). Initially discovered in *M. xanthus*, these proteins were also found to localise to the stalk pole in *C. crescentus*, organising the cell-wall biosynthesis, through the localisation of Pbp5 in a cell-cycle dependent manner (Kuhn et al., 2010). In *E. coli* expressing the DUF583 domain-containing gene *SO1662* from *Shewanella oneidensis,* localised to the site of cell division (Kuhn et al., 2010).

The relative position of the *B. bacteriovorus* gene *Bd3904* within the genome, downstream of a *parAB* operon, mirrors the genomic context of the *MXAN_7475* gene in *M. Xanthus* (Fig. 4.11A). RT-PCR analyses of *Bd3904* gene expression across a predatory time-course suggested that the gene product had a role in filamentous growth (Fig. 4.11B). Using primers which bound to the *Bd3904*, *parB* and *parA* ORFs in RT-PCR reactions on purified *B. bacteriovorus* RNA templates confirmed that *Bd3904* forms a co-transcribed operon with the adjacent upstream genes (data not shown) (Fig. 4.11A).

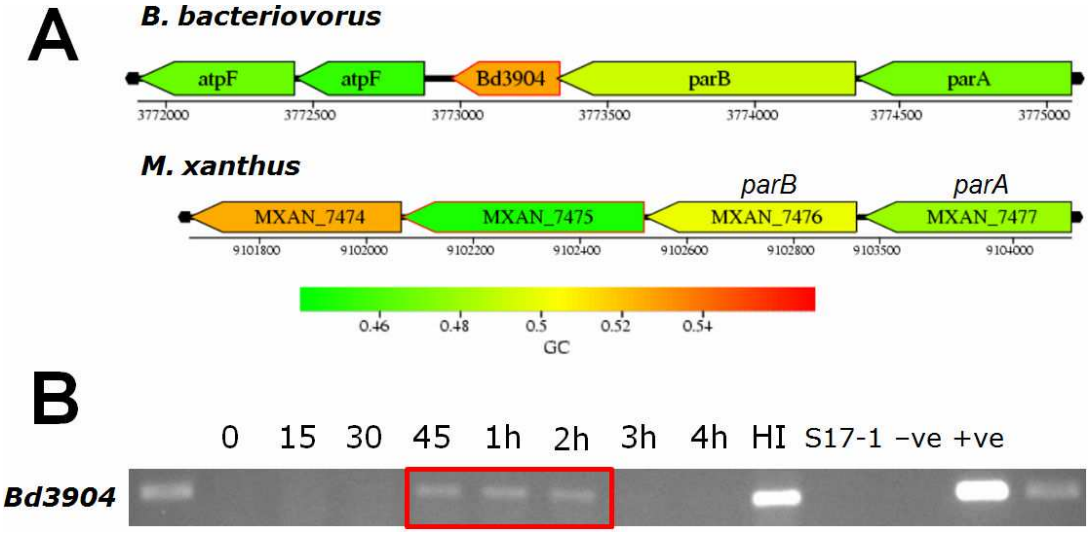

Figure 4.11 Expression profile and genomic context of the 'bactofilin' *Bd3904* in *B. bacteriovorus*. (**A**) Genomic context of the 'bactofilin' *Bd3904* and *MAXAN_7475* in *B. bacteriovorus* and *M. Xanthus* genomes respectively. Graphical displays of the genomes shown here were taken from the online Xbase database (http://xbase.bham.ac.uk/). (**B**) Semi-quantitative RT-PCR analysis of the *Bd3904* gene across the *B. bacteriovorus* predatory cycle, duplicated here from Fig. 4.2 for clarity.

4.5.1 Expression of *Bd3904* in *E. coli* DH5α.

In trans expression of *B. bacteriovorus Bd3904* from plasmid pAKF45 in wild-type *E. coli* DH5α, using the P*trc* promoter of the expression plasmid pTrc99A (of pAKF45), gave an elongated cell phenotype with multiple constrictions along their lengths, where multiple constrictions had occurred these were found clustered together forming a 'beads on a string' pattern (Fig. 4.12Bbii). These constrictions appear to be multiple *E. coli* septation events that have failed to complete the last stages to divide fully. The constrictions in the *E. coli* expressing Bd3904 were 0.38 μm in width (measured using EM data n=11); curiously this is a similar width as that of *B. bacteriovorus* cells (0.3 ± 0.02 μm (n=50) (Borgnia et al., 2008), see Fig. 4.12C.

The severity of the *E. coli:*pAKF45 cell elongation was proportional the concentration of IPTG used to initiate transcription form the P*trc* promoter (data not shown). To confirm that this effect was a direct result of the Bd3904 protein, multiple cultures containing fresh media with containing increasing concentrations of IPTG were inoculated with *E. coli*:pAKF45 and incubated at 37^{o}C for 16 h. 10 ml of crude cellular extracts (matched by OD_{600}) were run on a SDS-PAGE gel, Fig. 4.12A (see Materials and Methods section 2.8). A band of increasing intensity on the protein gels at the expected 12.7 kDa molecular weight (Fig. 4.12A) was analysed by

MALDI-TOF MS by Dr Kevin Bailey of the University of Nottingham Biopolymer Analysis unit, and confirmed to be the Bd3904 protein (Appendix 4.3).

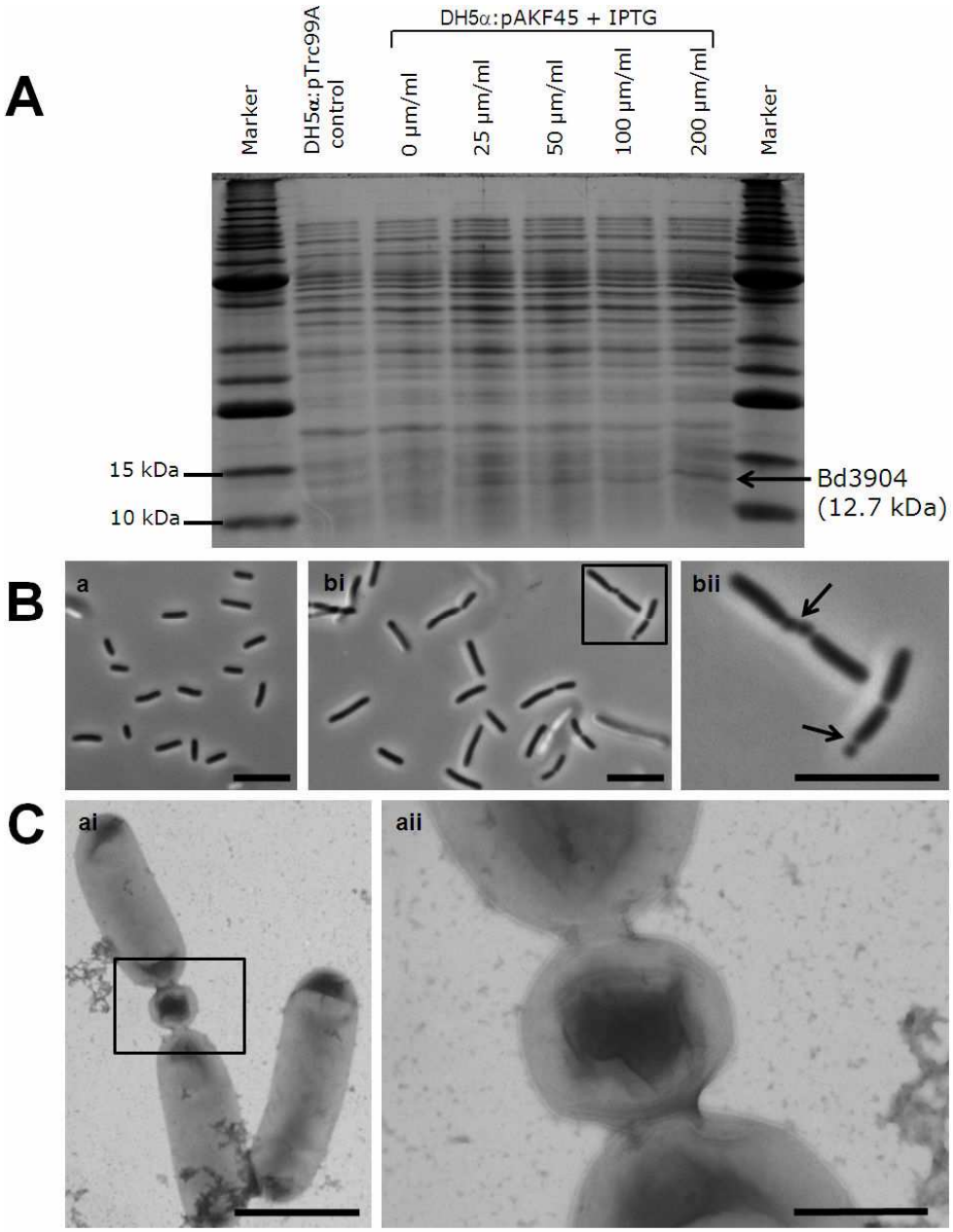

Figure 4.12 Morphological effects of *Bd3904* expression in *E. coli* DH5α. (**A**) SDS-PAGE gel showing the effect of increasing IPTG inducer concentrations on the protein profile of *E. coli* DH5α containing the pAKF45 plasmid expressing the *B. bacteriovorus Bd3904* against a vector only control. 10 µl of NEB pre-stained protein ladder, Broad Range (10-230 kDa) was used in each marker lane. Appropriate size markers have been highlighted. (**B**) *E. coli* DH5α:pAKF45 cells in the absence of inducer (Ba) and in the presence of 40 µm/ml IPTG (Bbi, the boxed region enlarged in Bbii), all scale bars = 5 µm. (**C**) Electron micrograph of a *E. coli* DH5α:pAKF45 cells expressing *Bd3904*, the boxed region in Cai (scale bar = 2 µm) is enlarged in the second panel Caii (scale bar = 500 nm).

In order to investigate the localisation of Bd3904 in the *E. coli* cells a C-terminal mTFP tagged form of Bd3904 was cloned and expressed (using the pAKF53 plasmid) using a final concentration of 40 µg/ml ITPG. The morphological phenotype of this strain was the same as that observed for the untagged Bd3904 suggesting that protein function was not impaired by the mTFP tag. Fluorescence microscopy of this strain revealed that the Bd3904-mTFP fusion protein co-localised with the sites of the cell constriction observed in Fig. 4.12, see Fig. 4.13A.

Induced DH5α *Bd3940-mtfp*-expressing *E. coli* cells show a number of fluorescent signal patterns which seem to form a logical hierarchy. First, shorter cells usually contained a single short focus (Fig. 4.13Aa, blue arrows), although two short foci were observed (Fig. 4.13Aa, purple arrow). Where a single focus had formed in the *E. coli* these were present at either mid-cell or the cell pole (Fig. 4.13Aa, blue arrows). In longer *E. coli* cells where septation is taking place the Bd3904-mTFP protein formed an extended focus that spanned the potential progeny cells (Fig. 4.13Aa, orange arrows). Presumably as these initial septation events fail to complete other septation events occur further along the length of the *E. coli*, leading to the elongated 'beads on a string' morphologies (Fig. 4.13 B).

4.5.2 Investigating the localisation of Bd3904 in dividing HD *B. bacteriovorus* cells.

As the Bd3904-mTFP fusion protein appeared unattenuated in phenotype *in E. coli* by mTFP-tagging; a *Bd3904-mtfp* HD100 strain was constructed to investigate the localisation of Bd3904 in *B. bacteriovorus* (see confirmatory Southern blot and genomic sequencing in Appendix 3.4 and 4.4). The vast majority of the *Bd3904-mtfp* attack-phase cells appeared wild-type in shape and size and none of these showed any mTFP fluorescence (Fig. 4.13 Bab), consistent with the differential expression profile of this gene across the predatory life-cycle, i.e. no detectable product in the attack-phase RT-PCR vs the observed expression at the 45 min-2 h *B. bacteriovorus* growth-phase time-points (Fig. 4.11B). In synchronous predatory infections Bd3904-mTFP fluorescence signals were observed within approximately 10% of bdelloplasts at the 1-2 h post infection time-points, but not at the 3-4 h post infection time-points (Fig. 4.13B); again this was consistent with the *Bd3904* predatory expression profile shown in (Fig. 4.11B).

Fluorescent signals within *Bd3904-mtfp* bdelloplasts appeared to form a single linear focus near the bdelloplast periphery suggesting that this protein forms a filament, or latticed tube, within the growth-phase cell (Fig. 4.13 Bc-d). This was tested

further using the periplasmically labeled mCherry *E. coli* S17-1 prey strain in synchronous *Bd3904-mtfp* infections. Bdelloplasts within which both the prey and growing *B. bacteriovorus* were fluorescently visualised were rare, but revealed that Bd3904-mTFP could form a single focus at the pole of the *B. bacteriovorus* cells and was only located exclusively within the growth-phase cell (Fig. 4.13Bef). The dark shadows observed within these bdelloplasts are likely the result of the prey cytoplasm obscuring or reflecting the mCherry fluorescent signal (Fig. 4.13Bef).

Rare, elongated attack-phase *Bd3904-mtfp* cells that did show fluorescence were observed at a frequency of approximately 1 in every 500 attack-phase cells (Fig. 4.13C). These appeared straighter than wild-type in the region containing the Bd3904-mTFP signal, which did not run the entire length of the cell (Fig. 4.13Ca-c). In the case of the single coiled elongated *Bd3904-mtfp* attack-phase cell, shown in Fig. 4.13Cd, the fluorescence signal was out of register with the coil of the cell, suggesting that the Bd3904 filament is associated with the inner membrane, or is suspended at points from the inner membrane as a filament, but is not present as fully-soluble protein within the cytoplasm (as that latter arrangement may have formed a coil in register), Fig. 4.13Cd (this can also be seen in Fig. 4.13Cc).

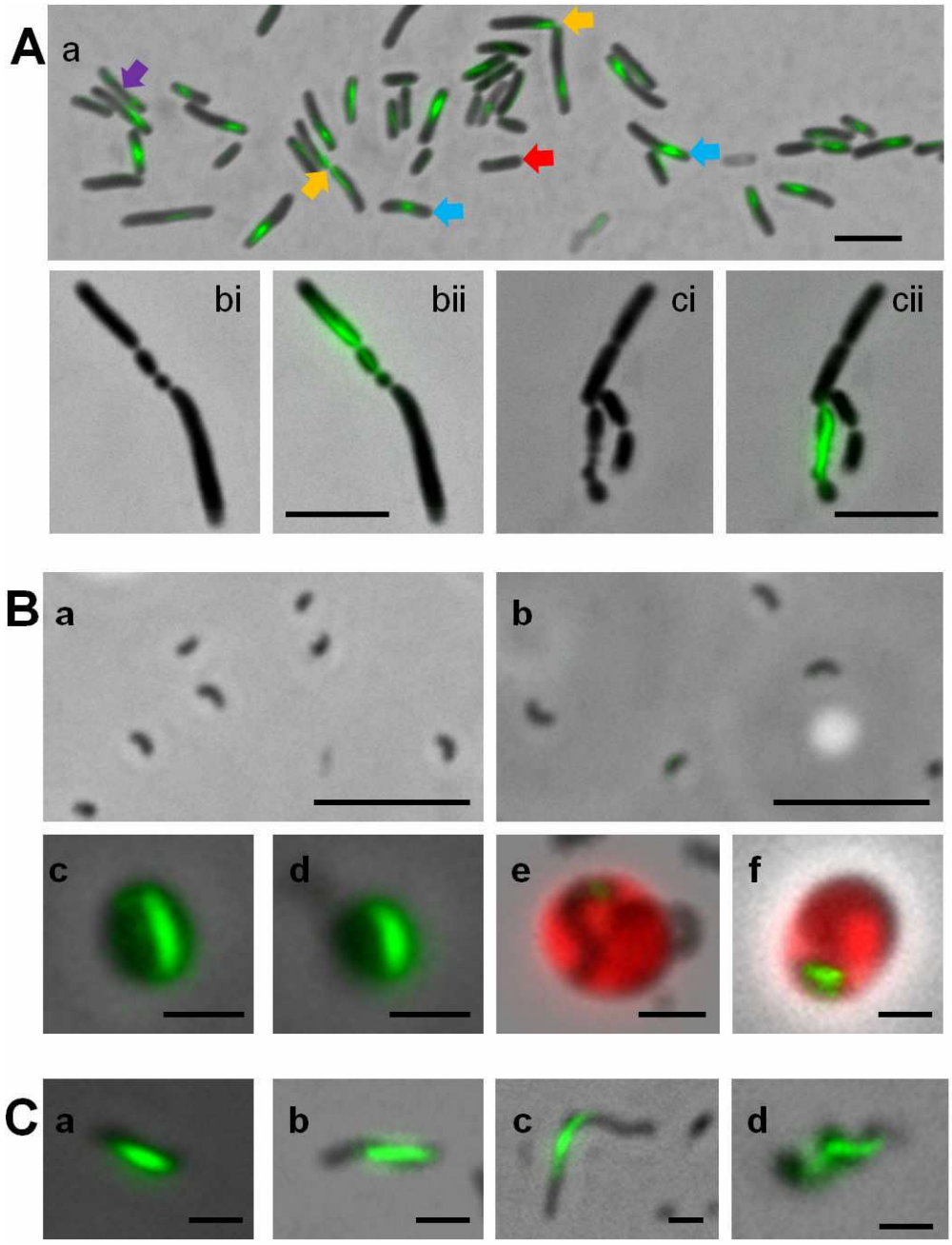

Figure 4.13 Localisation of the Bd3904-mTFP fusion protein in IPTG induced *E. coli* cells and in *B. bacteriovorus Bd3904-mtfp* strain predatory infections. (**A**) Representative merged fluorescent image of *E. coli* DH5α:pAKF53 in the presence of 40 µg/ml IPTG, expressing the Bd3904-mTFP fusion protein. (Aa) Cells showing differing patterns of Bd3904-mTFP fluorescence signal localisation are highlighted: *E. coli* with no fluorescence focus (red arrow), cells with a single focus (blue arrows), cells undergoing septation (orange arrows) and a cell containing two foci (purple arrow), scale bar = 5 µm. (Ab) Brightfield (i) and merged (ii) fluorescence image examples of elongated *E. coli* showing the 'beads on a string' morphology. (**B**) Brightfield and merged fluorescence images of *Bd3904-mtfp* cells from synchronous prey infections. (Ba) attack-phase cells at t =0 and at t = 4h (Bb), scale bars = 5 µm. (Bc-f) Images of bdelloplasts taken at t = 1h (Bc,e) and t = 2h (Bd,f) post infection using both S17-1 (Bcd) and mCherry labelled S17-1 prey (Bef), scale bars = 1 µm. (**C**) Rare elongated *Bd3904-mtfp* attack-phase cells with mTFP fluorescence activity, scale bars = 1 µm.

4.6 Discussion

Time-lapse indirect imaging of developing *B. bacteriovorus* cells within fluorescent bdelloplasts has shown in unprecedented detail how this predatory bacterium grows and divides atypically within another bacterium (summarised in Fig. 4.8Ba). *B. bacteriovorus* growth-phase cells within bdelloplasts grow bi-laterally into elongated cells, and only after reaching maximum length and receiving an unknown signal, divide synchronously into both odd and even numbers of progeny (Fig. 4.8, Fig. 4.9 and Movies 1-5). This contrasts to the classic EM reports suggesting that *B. bacteriovorus* divide sequentially (Burnham et al., 1970, Scherff et al., 1966). Once initiated *B. bacteriovorus* septation takes 41 min, independent of progeny number, and maturation of progeny and final bdelloplast lysis takes on average 26 min depending on progeny number (Fig. 4.10). Synchronicity of septation is maintained in long growth-phase cells and between two *B. bacteriovorus* competing for resources in a single bdelloplast (Movies 6 and 7).

mTFP tagging of septal proteins FtsZ and FtsK in *B. bacteriovorus* failed to form stable signals which would have revealed how the growth-phase cell resolves into multiple progeny. As the method of mTFP tagging of *B. bacteriovorus* proteins has

been shown to form stable tags in all chapters of this thesis, inability of this construct to insert at the expected location in the genome (Appendix 3.4) must be due to a negative effect that the mTFP moiety has on the target protein.

The cell division protein FtsZ has been shown previously to tolerate C-terminal GFP tags (Osawa and Erickson, 2005). *B. bacteriovorus* FtsZ has a larger C-terminal domain compared to other well studied bacterial organisms (Fig. 4.3). Given the unique challenges placed upon *B. bacteriovorus* FtsZ to aid the organisation of synchronous septation along an elongated growth-phase cell (Fig. 4.8B) I speculate that the C-terminus of *B. bacteriovorus* FtsZ may be less able to accommodate GFP tags than other bacteria.

All methods used to C-terminally tag FtsK abolish the chromosome segregative activity of the RecA-like motor domain (Fig. 4.5) which increases the potential for chromosomes to be in the wrong cellular compartment at the time of septation, this is tolerated in other bacterial species due to chromosome condensation at the time of division, making 'guillotining' of the genome by the septa less likely (see Fig. 4.7A for example of condensed chromosomes in dividing *E. coli* cells). Hoechst staining

of *B. bacteriovorus* growth-phase cells in bdelloplasts revealed little evidence of chromosome segregation in advance of cell division (Fig. 4.6a-b). Therefore, FtsK may play a more active role in separating the newly replicated chromosomes in *B. bacteriovorus* growth-phase cells than in other bacteria such as: *E. coli* or *P. aeruginosa.* In addition polar effects, caused by the mTFP tagging method, on the expression of downstream genes in the *B. bacteriovorus* genome: *Bd0042* and *Bd0043* (both genes of unknown function) may also account for this as these genes are present in a conserved operon (data not shown).

The fluorescent *huA-mtfp* HD100 strain did not reveal patterns of *B. bacteriovorus* genome segregation during growth in bdelloplasts due to its relative brightness (Fig. 4.7), yet this strain provided bright mTFP labelled attack-phase cells crucial for optimising the fluorescence microscopy on *B. bacteriovorus*. Due to this strain's evenly highly-expressed fluorescent brightness amongst cells within a tagged population, it is possible to specifically identify huA-tagged cells among other untagged cell types, this could make this strain very valuable tool for *B. bacteriovorus* research in the future.

The *Bd3904* gene lies downstream of a *parAB* operon and was hypothesised to have a role in *B. bacteriovorus* cell division control (Fig. 4.11). The Bd3904 protein is a member of a family of proteins called 'bactofilin' that form stable filaments without cofactors that can bundle together forming lattices of cables *in vitro* (Kuhn et al., 2010). The expression of *Bd3904* is tightly regulated across the predatory cycle and is only expressed between 45 min-2 h post-infection time-points, which temporally matches *B. bacteriovorus* filamentous growth (Fig. 4.2).

Expression of both wild-type *Bd3904* and a *Bd3904-mtfp* fusion in *E. coli* appears to block, septation events at mid-cell and cell poles (Fig. 4.12-4.13). The positioning of the *E. coli* DH5α septation machinery at the poles of the cell despite this strain having a functional MinCDE system suggests that the Bd3904 protein is able to either interfere with these control mechanisms or directly recruit the *E. coli* septal machinery to begin to form abortive septa at the poles (Fig. 4.13Acii), this would also explain why Bd3904-mTFP signals localise to septa in the induced *E. coli*:pAKF53 strain (Fig. 4.13Aa, orange arrows).

Bd3904 filaments appear to inhibit the later stages of *E. coli* septation by either inhibitory interaction with the septation machinery or by physical occlusion of their site of action. Curiously *E. coli* cell septation events stall at an average diameter of 0.38 μm which is similar to the width of a *B. bacteriovorus* cell.

The *Bd3904-mtfp* fusion, expressed from its native promoter in *B. bacteriovorus* cells showed mTFP fluorescence predominantly within bdelloplasts, at time-points consistent with *B. bacteriovorus* filamentous growth (Fig. 4.13 Bcd). A few abnormally long attack-phase *B. bacteriovorus*:Bd3904mTFP cells were seen to have a fluorescent signal. (These made up 0.2% of the observed attack-phase population and fluorescence was not seen in normal vibroid attack-phase cells which were the great majority 99.8%. It is intriguing to speculate that these might be a rare population of attack-phase cells that were 'trying' to complete septation after and exit from a prey bdelloplast. Dogma states that predatory *B. bacteriovorus* do not divide outside prey, but there are reports that if bdelloplasts are prematurely lysed, by accidental environmental insults, that the liberated *B. bacteriovorus* can complete division (Scherff et al., 1966, Ruby and Rittenberg, 1983). Thus the cells observed in Fig. 4.12C may derive from such events and their septation is blocked by Bd3904.

It is worth noting that the 10% of bdelloplasts in which strong *B. bacteriovorus*-Bd3904mTFP fluorescent signals were observed in these experiments, are likely an underrepresentation of the number of *B. bacteriovorus* expressing Bd3904-mTFP due to the limitations of GFP detection within bdelloplasts. Predatory infections using *Bd3904-mtfp* with the periplasmic mCherry S17-1 prey strain confirmed that the Bd3904-mTFP signal is present within the *B. bacteriovorus* growth-phase cells. Proteolytic degradation of the Bd3904-mTFP protein within *B. bacteriovorus* between 2 and 3h post infection would account for the lack of mTFP fluorescence signal in late stage bdelloplasts, this time-point also coincides with the initiation of septation as determined by time-lapse microscopy.

These results suggest that the Bd3904 protein stabilises the growth-phase filamentous cell within the bdelloplast by forming division-inhibitory membrane-associated polymers or tubular lattices. The Bd3904 protein could be controlled temporally by a combination of gene expression, depolymerisation using additional factors (a function lacked by the *E. coli*) and proteolytic breakdown allowing the synchronous septation of *B. bacteriovorus* within bdelloplasts. Future work on the dynamics of the Bd3904 filaments *in vitro* and the generation of a HD100 *Bd3904* KO stain are required to fully support these conclusions.

CHAPTER FIVE

Investigating the roles of two MreB homologues in *B. bacteriovorus* growth.

5.1 Introduction

Chapter 4 showed advancements made in *B. bacteriovorus* cell imaging to establish the elusive patterns of growth within the bdelloplast; however it showed very little about actual gene function. The following chapter focuses on a main bacterial cytoskeletal component MreB, mTFP tagging and gene knock out studies of the two MreB homologues found in *B. bacteriovorus* reveal the different functions of these gene products in *B. bacteriovorus* growth both inside and outside the bdelloplast using a combination of genetic approaches (introduced in Chapter 3) and MreB-inhibitor A22 treatment.

5.1.1 Cell elongation in rod shaped bacteria

The processes of cell elongation in rod shaped bacteria are coordinated by an internal MreB cell cytoskeleton (Jones et al., 2001, Daniel and Errington, 2003). MreB is a eukaryotic actin homologue and has been well studied in *Escherichia coli*, *Bacillus subtilis*, and *Caulobacter crescentus* (Vats et al., 2009b). MreB

monomers polymerise on ATP-binding, forming helical structures *in vivo* that appear to associate with the cytoplasmic side of the bacterial cytoplasmic membrane (Figge et al., 2004, Shih et al., 2003, Jones et al., 2001). Bacterial two-hybrid experiments in *E. coli* suggest that MreB forms a trans-membrane complex with the two proteins MreC and MreD each of which have been shown to form helical structures in *vivo* (Kruse et al., 2005). A complex of MreBCD together with RodA and the newly described RodZ protein influences the shape of the peptidoglycan cell wall, and thus the shape of the cell, by positioning the peptidoglycan biosynthetic machinery so that its action is directionally specific (Daniel and Errington, 2003, Vats et al., 2009a, Kawai et al., 2009). The MreB filament has also been shown to have roles in chromosome segregation, septation and cell polarity (Kruse et al., 2003, Vats et al., 2009a, Gitai et al., 2005, Gitai et al., 2004). Fig. 5.1 shows a diagram I have constructed representing the current thinking on how this complex may form *in vivo*.

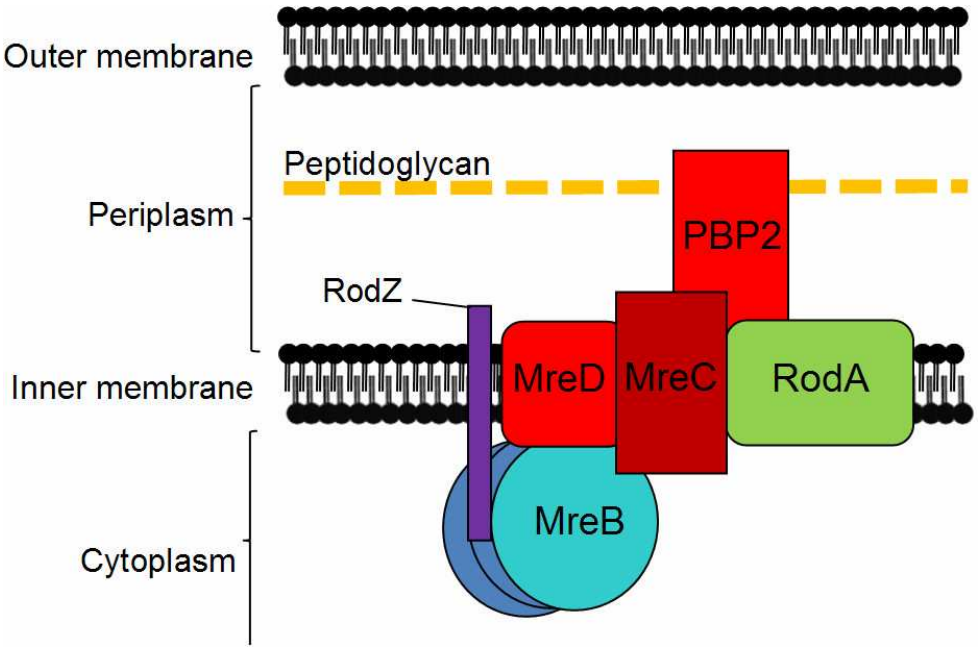

Figure 5.1 The bacterial 'elongase' complex. Schematic representation of the protein complex responsible for coordinating typical Gram-negative bacterial cell wall elongation. Duplicated here from Fig. 1.4 for clarity, adapted from (Gerdes, 2009).

5.1.2 The MreB specific inhibitor A22 caulses a loss of MreB activity resulting in loss of rod shape morphology.

Experimental depletion of the MreB protein levels in *E. coli* and *B. subtilis* were reported to cause cells to take on a spherical morphology with eventual loss of viability as new peptidoglycan was not synthesised evenly along the cell wall (Daniel and Errington, 2003, Varma and Young, 2009). Uneven incorporation of new peptidoglycan in MreB depleted strains is potentially driven by the tubulin homologue FtsZ (Varma and Young, 2009, Bendezu and de Boer, 2008).

A similar phenotype is achieved by addition of the MreB inhibitor A22 (S-(3,4-Dichlorobenzyl)isothiourea) that causes the reversible loss of MreB filament localisation *in vivo* (Gitai et al., 2005, Iwai et al., 2002). A22 was discovered in a chemical library being screened for the ability to generate anucleate mini-cells from *E. coli* (Iwai et al., 2004, Iwai et al., 2002) and has been used extensively by others to examine MreB function in bacteria of many different genera (Gitai Z et al., 2005). Addition of A22 to *E. coli* cells at 3.13 μg/ml leads to the breakdown of MreB filaments, spheroplasting and the generation of minicells (Iwai et al., 2004). In *B. subtilis* A22 at concentrations in excess of 100 μg/ml are required to generate spheroplasts, in *C. crescentus* 6 h incubations of 10 μg/ml are needed before any change to the cell shape can be observed, in this case cells take on a characteristic 'lemon shape' (Iwai et al., 2004, Gitai et al., 2005).

After its initial discovery, isolation and sequencing of A22-resistant mutants of *C. crescentus* showed that this inhibitor bound exclusively to the MreB protein (Gitai Z et al., 2005). Further biochemical evidence from a X-ray crystal structure of purified MreB from *Thermotoga maritima* revealed the A22 resistant mutations identified in *C. crescentus* mapped to the the nucleotide binding pocket of MreB (Gitai et al., 2005, Bean et al., 2009). Thus it was hypothesised that A22 specifically binds the ATP binding sight of MreB and inhibits its polymerisation. *In vitro* light-

scattering assays of *Thermotoga maritima* MreB filamentation showed that A22 acted as a competitive inhibitor of ATP-binding and was able to inhibit the formation of MreB filaments, presumably by sequestering and inactivating MreB monomers preventing their recycling (Bean et al., 2009). This work also demonstrated that, *in vitro*, A22 can have a role in stabilising ADP-bound MreB (Bean et al., 2009). In summary A22 inhibits MreB by acting as a competitive inhibitor of ATP binding preventing MreB polymerisation, which leads to the reversible loss of MreB filaments in bacterial cells.

5.2 Identification of *B. bacteriovorus* genes involved in cell elongation.

Blast analysis using *E. coli* proteins as queries on the B*. bacteriovorus* HD100 genome identified the known components of the cell complex, shown in Table 5.1 below.

Gene Name	Brief description/Notes on gene product	*B. bacteriovorus* HD100 Homologue(s)
mreB	Actin like GTP/ATPase which forms a membrene assosiated helical cytoskeleton under the bacterial cytoplasmic membrane. Forms a ring structure at midcell during cell division in *C. crescentus, E. coli* and *B. subtilis*.	*mreB*(1) *Bd0211* *mreB*(2) *Bd1737*
mreC	Can polymerise into helical filaments independently of MreB. May act like as a bridge between the MreB cytoskeleton and cell wall biosynthetic machinery.	*mreC* *Bd2457*
mreD	Integral membrane protein, may act like a bridge from the MreB cytoskeleton and cell wall machinery in conjunction with MreC.	*mreD* *Bd2459*
rodA	Integral membrane protein required for the coordination of the cell wall biosynthetic protein PBP2. Similar to FtsW in structure.	*rodA* *Bd2461*
pbpA	PBP2 heavy chain gene. Has the transglycosylase activity required to elongate the peptidoglycan cell wall. Similar to FtsI (PBP3) in structure.	*Bd2462*
rodZ	Bd3830 protein alignment shows weak sequence conservation, but has a predicted helix-turn-helix interaction domain known to interact with MreB.	*Bd3830*

Table 5.1 Identification of genes involved with cell elongation in *B. bacteriovorus* HD100*.* Table shows BLASTp hits using *E. coli* protein sequences as queries against the translated HD100 genome using Wu-BLAST software v2.0 (http://blast.jcvi.org/cmr-blast/). Initial HD100 Hits confirmed using them as queries in an ncbi BLASTp search (http://www.ncbi.nlm.nih.gov/) against the non-redundant protein sequence (nr) database, predicted function of the top hits of these BLAST results were examined.

The *B. bacteriovorus* genome contains two genes encoding proteins with high homology to *E. coli* MreB, *Bd0211* encoding MreB1 (45% identity at the protein level), and *Bd1737* encoding MreB2 (58% identity at the protein level). Both of the *mreB* genes in *B. bacteriovorus* are not located upstream of *mreCD*, thus lack an operon organisation that is conserved amongst rod shaped bacteria (Fig. 5.2). Immediately downstream of the *mreCD* genes in the *B. bacteriovorus* genome are a peptidoglycan biosynthetic gene *pbp2* and *rodA* the protein products of which are known to form a complex with MreCD in *E. coli* , see Fig. 5.1 (Kruse et al., 2005). *B. bacteriovorus* belongs to the delta-proteobacteria family of Gram-negative bacteria, and, although the number of *mreB* gene homologues in this family is variable, the gene organisation of *mreC, mreD, pbp2* and *rodA* is conserved.

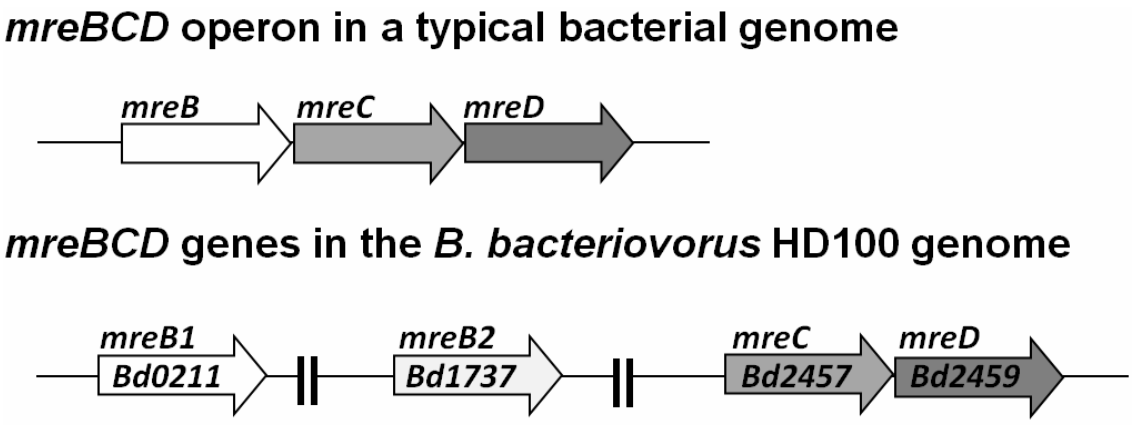

Figure 5.2 Organisation of the *mreBCD* genes*.* Schematic drawing of the *mreBCD* locus in a typical bacterial genome versus that of the *B. bacteriovorus* genome strain HD100.

5.2.1 Inactivation attempts for genes encoding components of the elongation complex in *B. bacteriovorus* in host-dependent and host-independent strains.

Deletion of both *mreB* genes in *B. bacteriovorus* was attempted by kanamycin cartridge insertion by methods described in section 2.11 using both host-dependently grown as well as host-independently grown strains. HI strains were used to attempt to rescue knock-out strains that failed at any point in the HD life cycle (Evans et al., 2007). Deletions of the *mreB* genes were also attempted in *B. bacteriovorus* PY media supplemented with 25 mM $MgCl_2$, known to support growth of *mreB* deletion strains in *B. subtilis* (Formstone and Errington, 2005). Despite these provisions no *mreB* deletion strains were isolated after screening a total of 328 candidates (62HD and 266HI) were screened for a *mreB1* knockout and 572 (136HD and 436HI) for a *mreB2* knockout, which was many fold more than those screened to produce a *pilA* knockout strain in the same *B. bacteriovorus* strain HD100 (Evans et al., 2007, Lambert et al., 2006a). For comparison inactivation of the *ccrp* gene described in section 3.3.1 of this thesis, using the same gene inactivation methods (section 2.11) required 130 of HD candidates to be screened yielding 9 gene inactivation candidates, two of which were confirmed by Southern blot (Fig. 3.4). Similarly for the *Bd1167* gene inactivation 92 HD exconjugants were screened, generating 6 gene inactivation candidates, all of which were confirmed by Southern blot (Appendix 3.3).

Deletion of the *rodA* gene was also attempted in 168 HD and 300 HI strains, using methods described in section 2.11. This technique also failed to recover a *rodA* inactivation strain, suggesting that the RodA protein is also essential to *B. bacteriovorus* cell viability.

5.2.2 *B. bacteriovorus mreB1,2,mreCD* expression patterns

As the *mreB* genes could not be directly disrupted for mutant strains, RT-PCR analyses were carried out on RNA samples taken at intervals from synchronous *B. bacteriovorus* infections to follow the expression of the *mreB1,2,CD* (see Materials and Methods section in 2.14). RT-PCR reactions had the number of amplification steps limited, so as not go to saturation and can therefore be used as a semi quantitative measure of gene expression across a *B. bacteriovorus* infection cycle (Evans et al., 2007, Steyert et al., 2008). Multiple sets of reactions on two independently prepared RNA sample sets are summarised in Fig. 5.3. Despite being located in different regions of the chromosome, expression of both *mreB*, and mre*C* and *D* genes of *B. bacteriovorus* showed an increase in transcription at the 2-3 h post infection stage, with almost undetectable expression at the 0 min attack-phase time-point (Fig. 5.3A). This is consistent with the expectation that *B. bacteriovorus* cell elongation in the growth-phase (Fig. 1.6) involves the MreBCD

proteins as is the case for cell elongation in non predatory bacteria (Fig. 5.1). The *mreB1* gene showed a reproducible (3 repeats, shown in Appendix 5.1) additional peak of expression at 15 min (Fig. 5.3A), around the time of periplasmic invasion, when initial establishment of the growth-phase filamentous cell is occurring (Fig. 1.6). RT-PCR analysis on RNA from both the 2 hr synchronous predatory infection time point and on RNA from HI-grown cells, showed that the *mreCD* genes are co-transcribed on the same mRNA molecule (Fig 5.3B), but that the *pbp2* and *rodA* genes were transcribed separately to each other and to *mreCD* (data not shown).

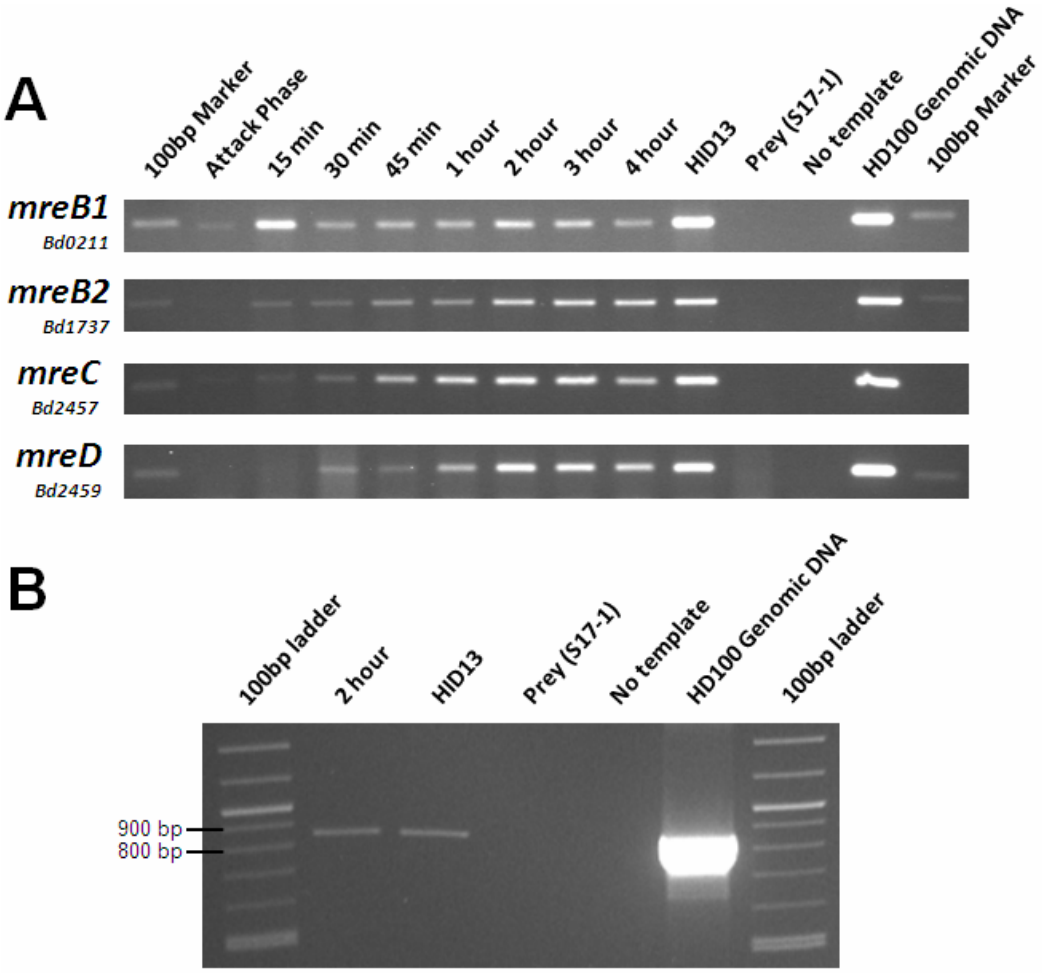

Figure 5.3 Semi-quantitative RT-PCR study of *B. bacteriovorus mreBCD* expression across a predatory infection cycle, and RT-PCR reaction showing that *mreC* and *mreD* are present within an operon. (**A**) RT-PCR reactions were carried out on RNA extracted at the time points across a synchronous lysate of *B. bacteriovorus* on the *E. coli* strain S17-1 (See Materials and Methods section 2.14). Time-points the RNA sample was taken are labelled on the figure. The HID13 strain used to assay HI gene expression. *E. coli* S17-1 RNA and no template reactions provide negative controls and HD100 genomic DNA was used as a template for a positive control. Primers for gene detection were designed to amplify an internal region of each *mreBCD* gene. Only the 100bp marker is visible in each marker lane. (**B**) RT-PCR reaction using the primers mreC_RTPCR_F and mreD_RTPCR_R on both HI (HID13) and HD (prepared at 2h post infection) RNA preparations used as RNA templates, using the HD100 genomic DNA as a positive control. Expected product size = 854 bp.

5.2.3 C-terminal mTFP tagging of each MreB protein in predatory *B. bacteriovorus*.

Previous studies in other bacteria showed that C-terminal GFP tagging altered the turnover dynamics of MreBs, so as I could not inactive the *mreB* genes (section 5.2.1), this method was employed (Jones et al., 2001, Slovak et al., 2005). To determine the involvement of *mreB1* or *mreB2* in the predatory cycle of *B. bacteriovorus* I constructed two *mreB-mtfp* tagged strains in which each MreB protein was individually C-terminally labelled mTFP (see Materials and Methods section 2.12). A 3' fragment of each *mreB* coding regions lacking the stop codon was PCR amplified and cloned in frame with the *mtfp* ORF in pAKF04 and integrated into *B. bacteriovorus* the genome and expressed from its own promoter, a contrast to other studies on MreB in both *E. coli* and *B. subtilis* where GFP-tagged MreB varients are expressed in *trans* (Carballido-Lopez and Errington, 2003, Vats and Rothfield, 2007). These fragments if translated would run from glycine 11 to the C-terminal glutamic acid residue 347 and represent 97% of the MreB1 protein and between glycine 48 to the final valine residue 347 and represent 86% of MreB2. These constructs were transferred to a pK18 backbone generating pAKF41a (*mreB1-mtfp*) and pAKF40a (*mreB2-mtfp*) and integrated into the *B. bacteriovorus* genome giving a strain in which each *mreB-mtfp* fusion was expressed from its native promoter along with a

promoter-less corresponding *mreB* 3'ORF fragment which, if translated, carry the N-terminal deletion (see Fig. 2.1). Each exconjugant strain was verified by sequencing directly specific regions of the genome (Appendix 5.2 and 5.3) and Southern blot (Appendix 3.4).

5.2.4 Developmental defects in both MreB-mTFP tagged strains of predatory *B. bacteriovorus*.

Fluorescence activity within the *mreB1-mtfp* strain was low but detectable, with fluorescent signals being constrained to the growth-phase cell within the bdelloplast, partly consistent with the higher *mreB1* expression at 2-3 h (Fig. 5.3 and 5.6). The *mreB1-mtfp* strain showed a phenotype in which the development of the growth-phase cell, within the bdelloplast, had been compromised instead of proceeding rapidly through the cycle like wild-type *B. bacteriovorus* (Fig 5.5). These *mreB1-mtfp B. bacteriovorus* failed to plaque bacterial lawns (data not shown) and in prey killing experiments in 50 ml cultures the *mreB1-mtfp* strain took between 5-7 times longer than the wild-type strain (which took 24 hours to lyse all the prey cells present and clear the culture) to partially, but never totally clear the prey from the culture, due to the presence of many stable, though abortive bdelloplasts, seen by phase contrast microscopy (Fig. 5.5Bg,h,i).

In contrast the *mreB2-mtfp* strain showed detectable mTFP fluorescence and progressed through the predatory cycle showing no evidence of abortive bdelloplasts, yet had a slightly reduced predatory rate shown also in terms of prey killing efficiency (Fig. 5.4) (section 2.16). As Fig. 5.4 shows the *mreB2-mtfp* strain was effectively predatory but killed *E. coli* at a slightly slower rate compared to the *fliC1* merodiploid kanamycin resistant control strain.

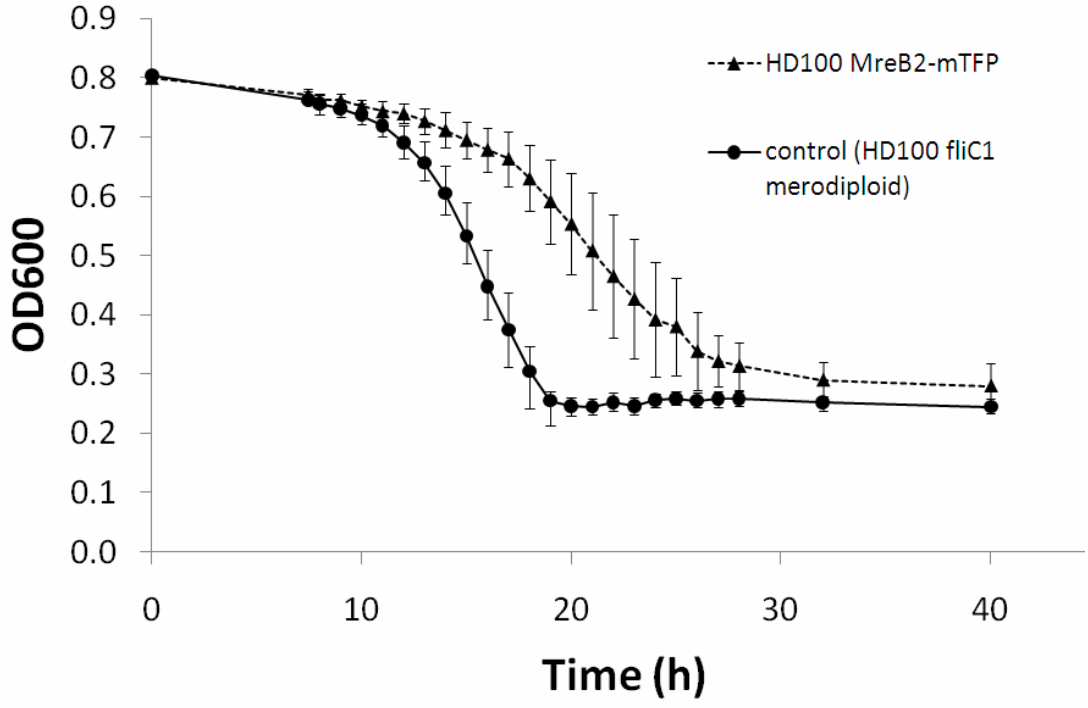

Figure 5.4 Predatory kill curves of HD100 *mreB2-mTFP* versus control. Methods used are described in section 2.16. Matched protein concentrations of *B. bacteriovorus* lysates were used to start 50 ml infections. Values fall as prey are lysed given that *B. bacteriovorus* attack-phase cells do not register at OD_{600}. Points on the graph represent three biological repeats, each experiment set up in duplicate.

5.2.5 Analysis of the HD100 *mreB1-mtfp* strain perturbed development within the bdelloplast.

For analysis of the bdelloplast-stalling phenotype of the *mreB1-mtfp* strain a starting *B. bacteriovorus* 'attack-phase only' inoculum was generated by filtering 5 independent aliquots of 2 ml replicate prey lysates, raised individually from frozen stocks and incubated for five days, through a 0.45 µm filter, to remove all previously stalled bdelloplasts, but allow harvesting of pure attack-phase *mreB1-mtfp B. bacteriovorus*. These attack-phase cells were used in infections with fresh prey, so that the approximate age of bdelloplasts in the resulting prey-lysate could be determined as the time of infection was known. These infections were surveyed microscopically at 24 h intervals and a survey of stalled bdelloplasts taken at day 1 (24 h) are displayed as percentages on Fig. 5.5. For a comparison, stages in a wild-type *B. bacteriovorus* HD100 infection are shown in Fig. 5.5A. As each prey cell was lysed completely by wild-type HD100 within 4 hours, and as no stalled bdelloplast stages were ever seen for wild-type HD100, the images in Fig. 5.5Ac,d,e could not be time-matched to the *mreB1-mtfp* culture, but are shown for morphological and staining comparisons. It was clear that some of the *B. bacteriovorus* cells in the stalled bdelloplasts were sphaeroplasting (Fig. 5.5Bg,h,i and Fig. 5.5Cb,c compared to non sphaeroplasting Fig. 5.6Aa) while others remained as attack-phase sized cells within the bdelloplasts, even

after the prey cytoplasmic material (including DNA which stains bright with Hoechst, shown previously in Fig. 4.6, for Method see section 2.9.2) had been degraded; compare Fig. 5.5Bf to Fig. 5.5Ac the wild-type *B. bacteriovorus* is elongating even while prey DNA remains but in the stalled *mreB1-mtfp* strain the *B. bacteriovorus* is not elongated even though prey DNA is not detected by staining with Hoechst.

To better understand the morphologies and behaviours of *mreB1-mtfp* stalled growth-phase cells in bdelloplasts, Hoechst staining was used to label the *B. bacteriovorus* chromosomes and prey DNA (where still present) within the usually phase-dark, stalled bdelloplasts, and in the minority of the *mreB1-mtfp B. bacteriovorus* that did escape the block and proceed through the predatory cycle (Fig. 5.5Bc,d,e).

Hoechst staining of *B. bacteriovorus* gave a higher fluorescence-intensity than for the *E. coli* prey in the attachment images (Fig. 5.5Ab, Bb) due to the relatively high concentration of DNA, per unit volume within the predator cells, a *B. bacteriovorus* being approximately 1/5 the volume of a *E. coli* yet containing a genome of comparable size (Rendulic et al., 2004). In early bdelloplasts Hoechst staining revealed both the *B. bacteriovorus* and *E. coli* prey chromosomes (Fig. 5.5Ac, Bc). In these bdelloplasts the *B. bacteriovorus* chromosome appeared diffuse

throughout the growth-phase cell where the chromosome of the prey was concentrated within a rounded prey cytoplasm. (Fig. 5.5Ac, Bc). Where the predatory infection continued normally and the prey chromosome was digested in bdelloplasts, produced by wild-type *B. bacteriovorus*, or mutants managing to complete the predatory cycle; Hoechst staining could be used to observe the morphology the *B. bacteriovorus* growth-phase cells within the bdelloplast (Fig. 5.5 Ad Bd) and also be used to observe the fully septated *B. bacteriovorus* progeny within bdelloplasts (Fig. 5.5 Ae, Be).

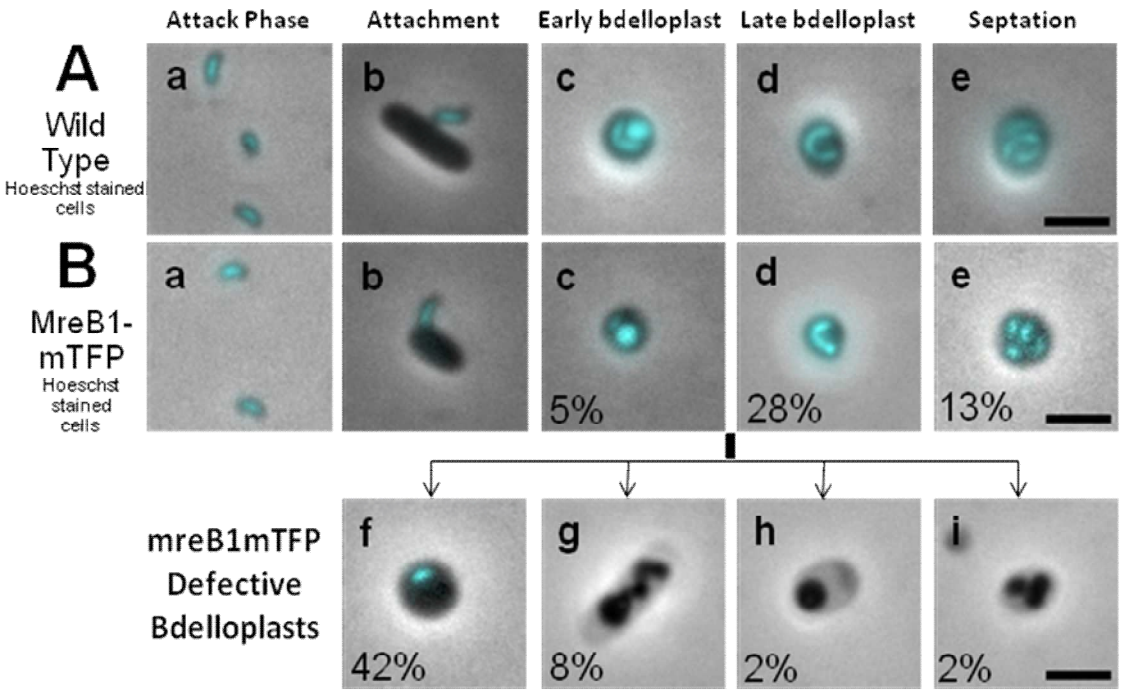

Figure 5.5. Defective bdelloplast development in the HD100 *mreB1-mtfp* strain visualised using the Hoechst DNA stain. (**A**) Merged fluorescent images of a Hoechst-stained wild-type HD100 *B. bacteriovorus* infection. Images show labelled key stages of the *B. bacteriovorus* life cycle (a-e): a) small vibriod attack-phase cells (b) *B. bacteriovorus* prey attachment (c) early stage bdelloplasts where *B. bacteriovorus* and prey DNA are both visible (d) late stage bdelloplasts where the *B. bacteriovorus* has grown to a long filament and the prey DNA and other cytoplasmic contents are digested (e) mature bdelloplasts in which septation of *B. bacteriovorus* has occurred prior to prey-lysis (**B**) Merged fluorescent images of Hoechst-stained HD100 *mreB1-mtfp* strain infection, images taken after 24 h of incubation. (a-e) show *B. bacteriovorus* life cycle stages in common with the wild-type and (f-i) defective bdelloplasts including: (f) stalled bdelloplasts where prey DNA has been degraded yet there is still no growth of *B. bacteriovorus* to form a filament as is seen in wild-type late bdelloplasts, (g) elongated but sphaeroplasting *B. bacteriovorus* that are not producing intact filamentous growth and (h-i) sphaeroplasting *B. bacteriovorus* within bdelloplasts, these are morphologies novel to this *mreB1-mtfp* strain. Percentage values indicate the prevalence of the various morphologies within the 24 h prey-lysate for this strain in which synchrony of infection was breaking down (n= 39).

Strikingly 42% of *mreB1-mtfp* bdelloplasts contained *B. bacteriovorus* that had not yet formed a filamentous growth-phase cell at 24 h of infection (Fig. 5.5Bf) and appeared morphologically similar to wild-type cells in the early stages of development (Fig. 5.5Ac). However the lack of Hoechst stain fluorescence within the prey cytoplasm in these bdelloplasts, compared to true early-stage bdelloplasts (Fig. 5.5Bf, as different to Fig. 5.5Ac, Bc) suggests that prey chromosome digestion had been completed, in those *mreB1-mtfp* derived bdelloplasts, due to the action of *B. bacteriovorus* nucleases (Matin and Rittenberg, 1972). Thus the lack of *B. bacteriovorus* filament-elongation was due to the MreB1-mTFP-tagging, not a lack of growth resources (in the form of prey DNA). The drop in the presence of stalled *mreB1-mtfp*-derived bdelloplasts over time suggests that a fraction of these mutants must eventually find escape and give at least some progeny cells (which could be harvested by filtration after 5 days and used as the *B. bacteriovorus* inoculum for this experiment). Only 28% of *mreB1-mtfp* bdelloplasts had successfully formed an elongated growth-phase filament (Fig. 5.5 Bd) after 24 hours; which should allow attack-phase cells to septate from it and escape the stalled bdelloplast.

For *mreB1-mtfp B. bacteriovorus* within bdelloplasts, 12% (Fig. 5.5Bg,h,i) had failed to develop correctly at 24 hr and the bdelloplasts had become transparent as the prey contents were

completely digested. These *B. bacteriovorus* were either totally spherical (Fig. 5.5Bh), spherical and septated (Fig. 5.5Bi), or at an intermediate phase (Fig. 5.5Bg). These morphologies are similar to those reported for MreB depletion strains in other non-predatory bacteria (Chiu et al., 2008). Spherical *mreB1-mtfp B. bacteriovorus* cells within bdelloplasts persisted in these cultures and fail to lyse prey suggesting that the expression of genes required for prey lysis were not fully activate in these abortive structures. Electron microscopy confirmed that these bdelloplasts contained a spherical *B. bacteriovorus*, see Fig. 5.6Ab-c, which shows a spherical *B. bacteriovorus* within the periplasmic space of an *E. coli* prey cell.

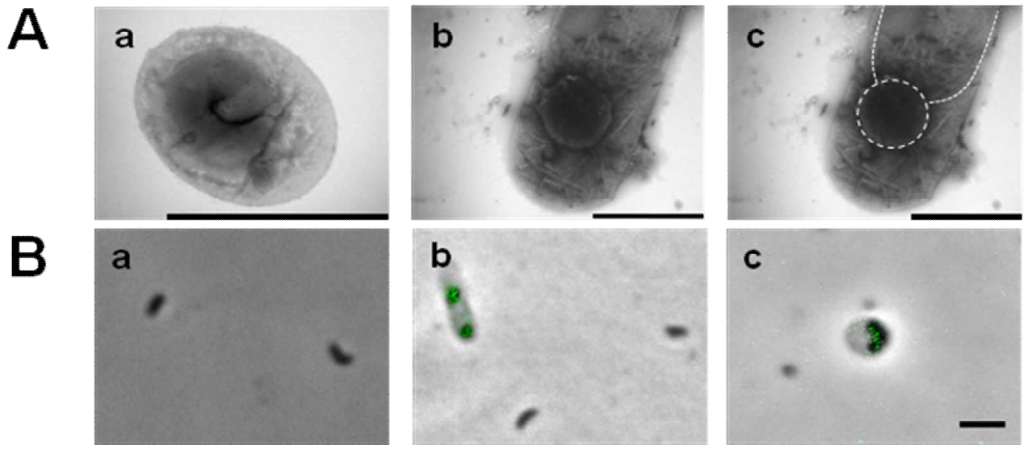

Figure 5.6 Defective bdelloplast development in the HD100 *mreB1-mtfp* strain visualised using fluorescence and electron microscopy. (**A**) Electron micrographs of *mreB1-mtfp* bdelloplasts, (a) a wild-type bdelloplast within which the growth-phase cell has formed correctly (shown in Fig. 5.5 Bd) and an example of the *mreB1-mtfp* strain (shown in Fig5.5 Bf) stalled bdelloplast morphotypes (b) with the spherical *B. bacteriovorus* cell and prey cytoplasmic membrane outlined with a white dotted line in (c). Stain = 0.5% uranyl acetate. (**B**) Merged fluorescence micrographs showing the very low level of mTFP fluorescence in the *mreB1-mtfp* cells and that this is not present in attack-phase cells (a) but is seen in those cells within a bdelloplast (b,c) Scale bars = 2 μm.

Curiously, all attack-phase cells of the *mreB1-mtfp* strain that did complete predation, had wild-type morphology, and all contained a centrally located copy of the genome, revealed by Hoechst staining. (Fig. 5.5Aa compared to Ba) Infections with high prey:*B. bacteriovorus* ratios, using just attack-phase *mreB1-mtfp* cells, filtered out from previous predatory cultures, also containing stalled bdelloplasts, showing that all attack-phase cells of this strain were capable of prey attachment and entry, (Fig. 5.5Bb); but again the same levels of stalled bdelloplasts were produced; thus the main impact of the MreB1-mTFP tagging appeared to take place after prey-entry.

5.2.6 The HD100 *mreB2-mtfp* strain has unusual attack-phase morphologies.

In contrast to the *mreB1-mtfp* strain that had a developmental defect within the bdelloplast (section 5.2.4), the *mreB2-mtfp* strain completed the predatory cycle and lysed prey cells at almost wild-type rates in synchronous predatory cultures with high *B. bacteriovorus*:prey (3:1) ratios (Fig. 5.7). Whereas at low *B. bacteriovorus:*prey ratios (1:6) of predation rates seemed significantly slower than a control strain (Fig. 5.4).

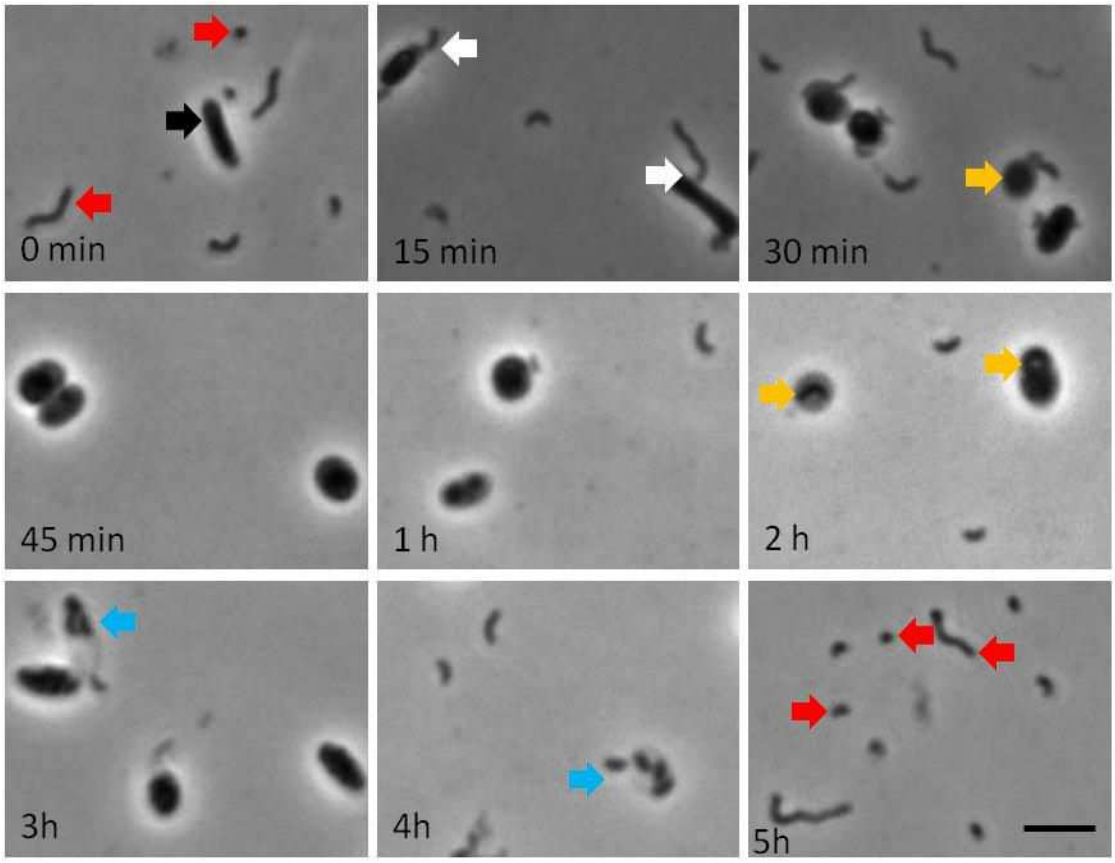

Figure 5.7 The *mreB2-mtfp* strain shows a wild-type developmental rate in a bdelloplast persistence assay. In addition, diverse *mreB2-mtfp* morphotypes are still predatory. Representative brightfield images representing key time-points of a synchronous *mreB2-mtfp* infection. Arrows used to highlight specific cell types; Red: *mreB2-mtfp* attack-phase cells of differing morphotypes (summarised in Fig. 5.8B), Black: Uninfected *E. coli* S17-1:pZMR prey, White: Attack-phase cell attachment, Orange: bdelloplsasts containing growth-phase cells, Blue: Fully septated mature bdelloplasts. Comparison of 15 and 30min post infection images demonstrate synchronous infection, at 15 min all prey cells show *B. bacteriovorus* attachment, whereas at 30 min all prey are infected. Images of HD100 control infection carried out under the same conditions are not shown. Scale bar=5 μm.

The *mreB2-mtfp* strain, probably due to a change in the dynamics of the MreB2 protein caused by the addition of the mTFP, gave fluorescent, attack-phase *B. bacteriovorus* cells with differing morphologies (Fig. 5.8AB). In contrast to the *mreB1-mtfp* strain, which could most readily be visualised by Hoechst staining and fluorescence microscopy, due to faint mTFP fluorescence in the bdelloplast (Fig. 5.5B compared to 5.6B); all cells of the *mreB2-mtfp* stain showed mTFP-fluorescence from pole to pole. TFP activity was detected at all points of the *B. bacteriovorus* cycle from prey attachment to prey-lysis (Fig. 5.8E). The distribution of morphotypes in the *mreB2-mtfp* strain was observed using fluorescence microscopy (Fig. 5.8Ba-d) and scored in five separate experiments summarised in the pie chart (Fig. 5.8D) (n= 718). Observations made using Electron microscopy confirmed this distribution (Fig. 5.8C).

Figure 5.8 Analysis of the attack-phase morphologies of HD100 *mreB2-mtfp* strain. (**A**) Merged brightfield and fluoresent images of (a) HD100 *Bd2345*, non-fluorescent control strain, (b) HD100 *mreB2-mtfp* strain attack-phase cells. (**B**) Attack-phase cell morphologies of the *mreB2-mtfp* strain (a) wild-type, (b) spherical, (c) elongated, (d) branched. (**C**) Representative electron micrograph showing *mreB2-mtfp* attack-phase cells. Cells stained with 0.5% uranyl acetate. (**D**) Pie chart representing a survey of 718 HD100 *mreB2-mTFP* attack-phase cell morphologies. (**E**) Merged brightfield and fluorescent images of MreB2-mTFP strain at the attachment (a), early (b) and late (c) bdelloplast and lysis (d) stages of the HD predatory life cycle. (F) Hoechst stained fluorescent images of *mreB2-mtfp* attack-phase cells. Scale bars = 3 μm.

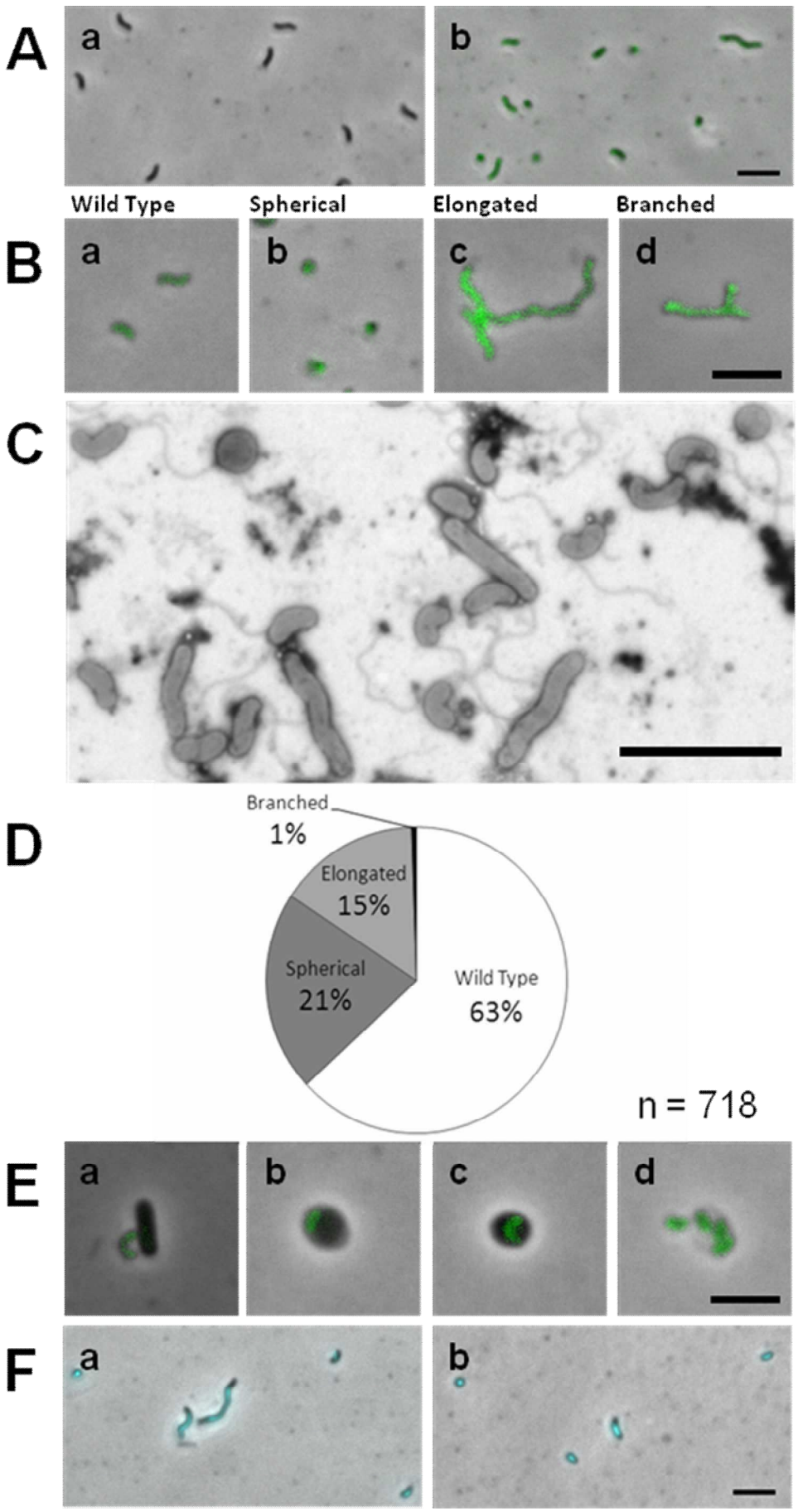
A
a
b
Wild Type
Spherical
Elongated
Branched
B
a
b
c
d
C
D
Branched
1%
Elongated
15%
Spherical
21%
Wild Type
63%
n = 718
E
a
b
c
d
F
a
b

Wild-type *B. bacteriovorus* attack-phase cells are usually very uniform in size and shape, having a length, measured by cryo-electron microscopy, of 1.02 ± 0.15 μm and a width of 0.30 ± 0.02 μm (Borgnia et al., 2008). Whilst the majority of *mreB2-mtfp* attack-phase cells were wild-type in shape (63% Fig. 5.8D) a significant number of cells fell into three additional categories; elongated, spherical and branched (Fig. 5Ba-d). Elongated cells of the *mreB2-mtfp* strain showed significant length variation and were classified as cells that were over double the length of a single wild-type cell (Fig. 5.8Ab,Bc,C). As these cells varied from 2-10 times the length of a wild-type cell and were scored as one cell the score in Fig. 5.8D is an under-representation of the relative biomass of this category. Branched *mreB2-mtfp* cells were in all cases also elongated and only ever branched near one pole (Fig. 5.8 Bd). Cells of the *mreB2-mtfp* spherical morphotype were motile and thus alive; electron microscopy confirmed this and those cells had a single flagellum (Fig. 5.8C). Hoechst staining revealed that all *mreB2-mtfp* cells contained a similar intensity of DNA staining, removing the possibility that the spherical cells of this strain were mini-cells (Fig. 5.8Fb). For *mreB2-mtfp* elongated cells the chromosomal material was never partitioned along the filament but appeared as a single elongated focus always located to the midpoint of the cells (Fig. 5.8Fa-b).

Predatory cultures set up with a low *Bdellovibrio:*prey ratio (1:8) were observed frequently before and after *B. bacteriovorus* prey-entry to determine if any *mreB2-mtfp* cell morphotypes were defective for prey entry. This showed that only the spherical cells were no longer able to enter prey, remaining outside prey cells even after 3 h of incubation. I conclude that, although motile and alive at 3 hours, these spherical *mreB2-mtfp* cells are no longer viable in the longer term, as they cannot enter prey and so replicate via the predatory growth cycle. Surprisingly the *mreB2-mtfp* elongated cells were still able to invade the host periplasm despite their increased size, see Fig. 5.7 15 min panel.

As shown in Fig 5.7 the rate of development of *mreB2-mtfp B. bacteriovorus* within bdelloplasts was found to be wild-type when assayed under conditions of high *B. bacteriovorus*: prey ratios (ca 3:1). In non-synchronous low *B. bacteriovorus*: prey ratios (ca 1:50) the spherical *mreB2-mtfp* cells, which were liberated as some fraction of the attack-phase cells after previous predation; played no part in the infection as they fail to enter the prey (Fig. 5.4). Over successive rounds of infection in non-synchronous cultures the effective removal of the spherical cells as a source of prey infection and lysis reduce the overall predatory efficiency of this culture (Fig. 5.4).

5.2.7 The effects of the MreB inhibitor A22 on wild-type attack-phase *B. bacteriovorus* cells.

The MreB inhibitor A22 (introduced in section 5.1.2) has revealed detail of protein function previously in other bacteria (Gitai et al., 2005, Chiu et al., 2008), causing shape deformations due to loss of directionally-specific peptidoglycan incorporation into the cell wall (Varma and Young, 2009). The addition of A22 at a final concentration 100 µg/ml to wild-type *B. bacteriovorus* attack-phase cells caused no change in shape after 24 h incubation (Fig. 5.9); or even after 48 h; this was an A22 concentration ten times that reported to induce spherical/ lemon shaped cells in *E. coli, and C. crescentus* within 6 hours (Iwai et al., 2004, Gitai et al., 2005). Attack-phase *B. bacteriovorus* cells, incubated at final A22 concentrations of 200 µg/ml for 24 hours, lost motility, formed inclusion bodies, failed to plaque bacterial lawns, but maintained their cell shape (Fig. 5.9) when *E. coli* control cells did show rounding, with A22 at 5 µg/ml. Thus at 200 µg/ml A22 was toxic to the *B. bacteriovorus* but at lower concentrations the wild-type *B. bacteriovorus* attack-phase cells did not respond to A22 by cell shape alteration.

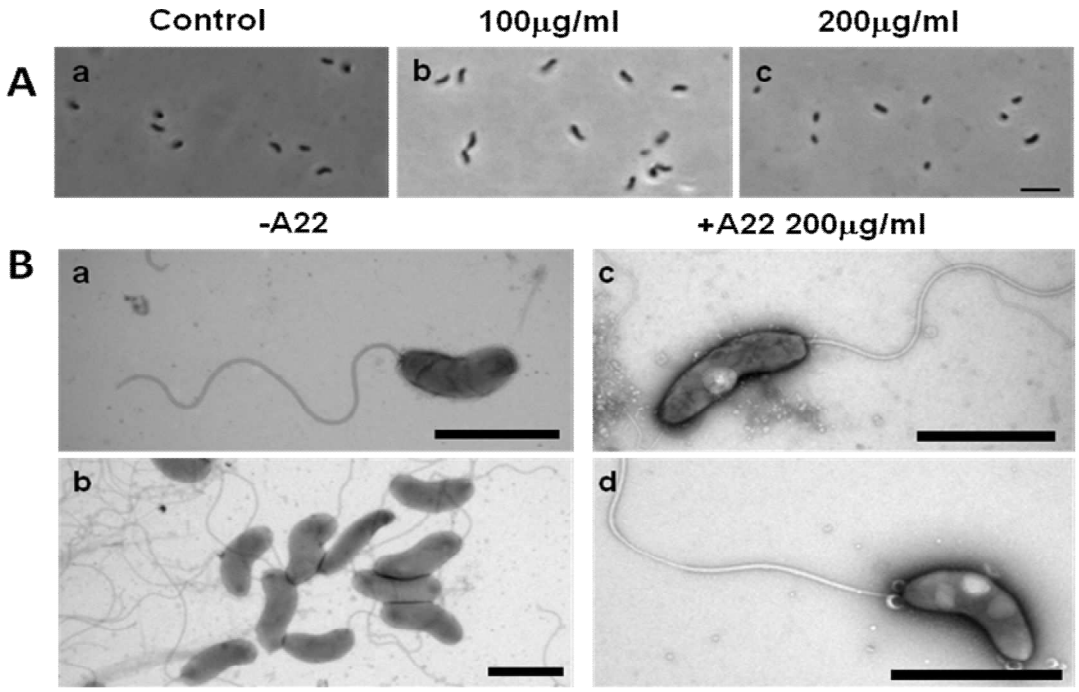

Figure 5.9 Effect of the MreB inhibitor A22 on wild-type *B. bacteriovorus* HD100 attack-phase cells. (**A**) HD100 attack-phase cells after a 24 h incubation of (a) 0 μg/ml A22 (b) 100 μg/ml and (c) 200 μg/ml A22. Scale bar = 3 μm (**B**) Representative electron micrographs of HD100 treated with 200 μg/ml A22 (c-d) versus untreated cells (a-b). Inclusion bodies only ever observed in the A22 treated cells at this concentration. Cells stained with 0.5% uranyl acetate. Scale bars = 1 μm.

5.2.8 The effects of the MreB inhibitor A22 on *mreB1-mtfp* and *mreB2-mtfp* attack-phase cells.

The attack-phase cells of the *mreB2-mtfp* strain gained the capacity to change shape with the addition of non-toxic levels of A22 (Fig. 5.10Aa,b). Overnight incubation of *mreB2-mtfp* attack-phase *B. bacteriovorus* with 100 µg/ml A22 caused statistically significant changes in morphology, compared to control *mreB2-mtfp* cultures of the same age, summarised in Fig. 5.10. mTFP fluorescence of the *mreB2-mtfp* A22 treated cells was maintained throughout (Fig. 5.10). Overnight treatments, at 100 µg/ml A22, reduced ten-fold, but did not abolish, predatory plaque counts on *E. coli* prey for the *mreB2-mtfp* strain compared to when it had no A22 added. Surveys of morphologies of *mreB2-mtfp B. bacteriovorus*, after A22 treatment showed a reduction in the number of elongated cells an increase in the number of spherical *mreB2-mtfp* attack-phase cells (Fig. 5.10C) and a new intermediate form of *B. bacteriovorus* that was mushroom shaped (Fig. 5.10Be-f) and which was not present in controls.

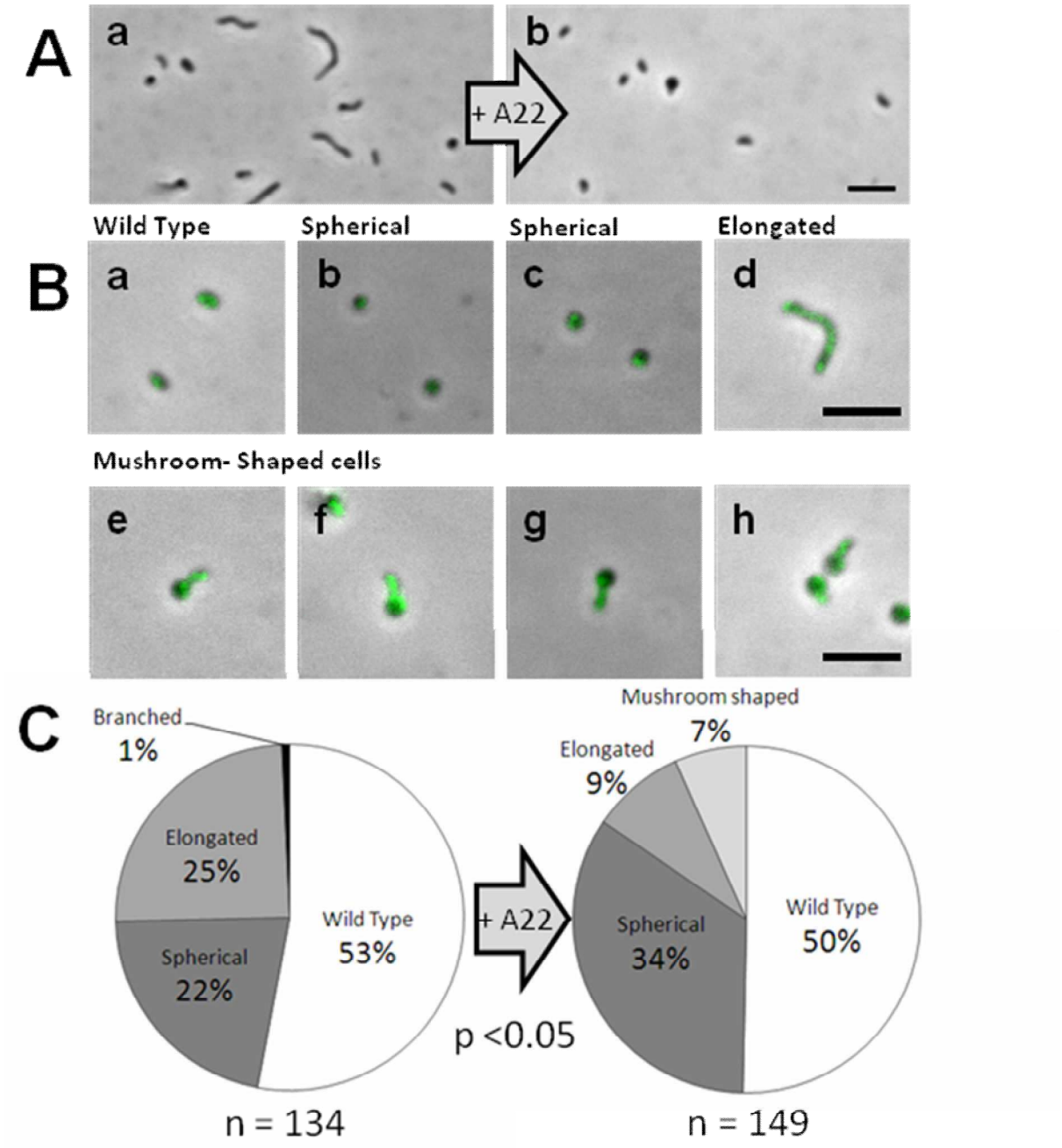

Figure 5.10 Addition of A22 to the *mreB2-mtfp* strain alters attack-phase cell morphology. (**A**) Untreated attack-phase *mreB2-mtfp* cells (a); *mreB2-mtfp* cells treated with a 24 h incubation with 100 µg/ml A22 (b). (**B**) Attack-phase morphologies of the *mreB2-mtfp* A22 treated cells (a) wild-type, (b-c) spherical (d) elongated, (e-h) novel mushroom-shaped cells with fluorescently bright "stalk" shapes indicative of high *mreB2-mtfp* content. (**C**) Pie charts summarising survey of 134 *mreB2-mtfp* untreated attack-phase cells and 149 cells treated with 100 µg/ml A22, both incubated 24 h. Chi squared analysis of morphologies shared between both surveys give a chi squared value of 26.75 giving a P value of <0.05 at 2 degrees of freedom. Scale bars = 3 µm.

Addition of A22 at low concentrations (0.01 µg/ml) seemed to support the predatory growth of, and reduce bdelloplast persistence in, the *mreB1-mtfp* strain, as large numbers of attack-phase *B. bacteriovorus* were seen microscopically, after 24 hours, in predatory infections set up in the presence of that concentration of A22, but not without (data not shown). In these cultures the prey *E. coli* were not morphologically affected by the A22 concentration (data not shown). Additional control prey-killing experiments by the *B. bacteriovorus filC1*merodiploid kanamycin resistant "wild-type" control strain showed that A22 concentrations of 0.01 µg/ml had no effect on predatory growth rate (Fig. 5.11).

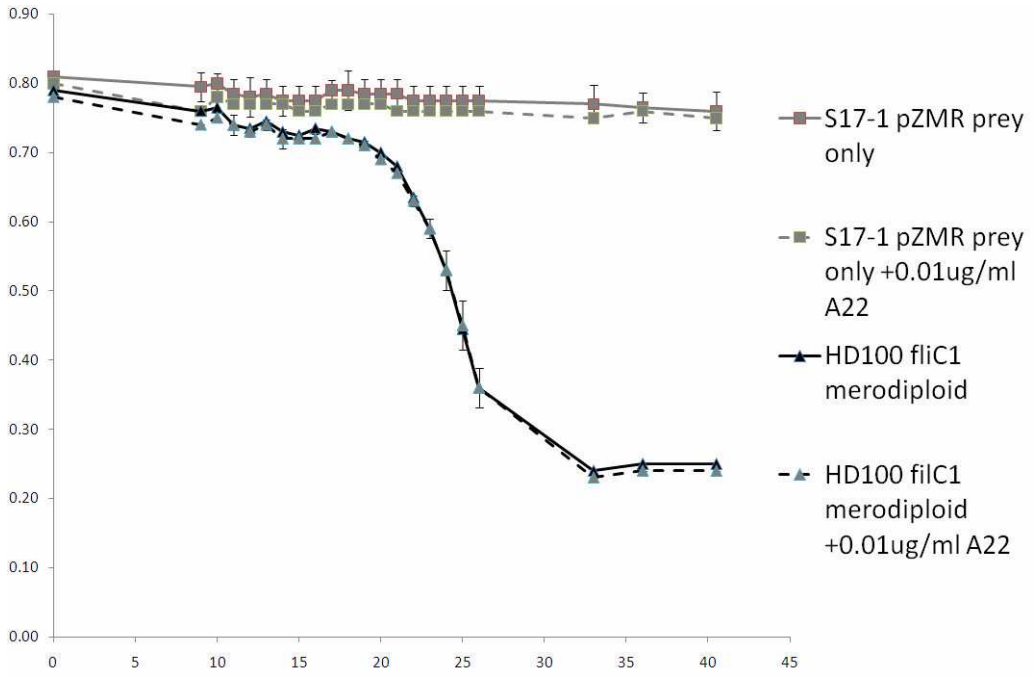

Figure 5.11 Effect of 0.01 µg/ml A22 on the *fliC1* merodiploid, kanamycin resistant, control strain predation rate and stationary phase *E. coli* S17-1 pZMR prey. Predatory cultures/prey only controls, in the presence or absence of 0.01 µg/ml A22, were set up in duplicate containing either stationary phase *E. coli* or a mixture of *E. coli* prey and the *B. bacteriovorus fliC1* merodiploid strain, error bars show standard deviation around the mean, for method see section 2.16.

5.3 Host independent cell morphologies of *mreB1-mtfp* and *mreB2-mtfp* HI strains.

As described previously in section 1.3 HI strains are primarily used in *B. bacteriovorus* investigations to rescue strains that fail to complete any part of the predatory process. That they are studied in their own right is due in part to the high degree of morphological diversity within a single HI culture and variable growth rates. In order to further study *mreB-mtfp* tagged morphologies, ten independently isolated HI candidates were generated for each strain along with ten *fliC1* merodiploid controls, following the precedent set by K. Evans and coworkers (Evans et al., 2007). Evans and coworkers independently isolated ten HI derivatives of a *B. bacteriovorus* mutant to determine common mutational features against a background of HI diversity. Diagnostic Taq PCR reactions confirmed the continued presence of the *mreB-mtfp* constructs (pAKF40a and pAKF41a) for each HI strain, shown in Appendix 5.4.

Very surprisingly all ten *mreB1-mtfp* HI strains were all uniformly small and resembled attack-phase cells. In all cases HI cultures of the *mreB1-mtfp* HI strains contained short attack-phase like cells which never exceeded 3 μm in length (Fig. 5.12), a stark contrast to the expected mixture of morphologies observed in *fliC1* controls (Fig. 5.12). mTFP fluorescence activity remained hard to detect for all *mreB1-mtfp* HI strains; however the background

fluorescence caused by the rich PY media used to support *B. bacteriovorus* HI growth makes fluorescence acquisition more challenging.

All ten *mreB2-mtfp* HI cultures showed a strong tendency to form very large elongated cells, which coil back on themselves forming large networks, only seen in a minority of *filC1* controls (Fig. 5.12). However, unlike the *mreB1-mtfp* strain, the *mreB2-mtfp* HI cultures showed more diverse morphologies, notably the presence of spheroplasts (Fig. 5.12). Currently a method to meaningfully score or count the number of HI cells spheroplasts within HI cultures is unavailable. All *mreB2-mtfp* HI strains showed MreB2-mTFP fluorescence activity (data not shown).

Figure 5.12 Representative images of ten independently generated HI cultures of the *mreB1-mtfp* (A), *mreB2-mtfp* (B) and *fliC1* merodiplod control strains (C). Images taken at the same time and all strains experienced the same growth conditions. Scale bars = 5 μm.

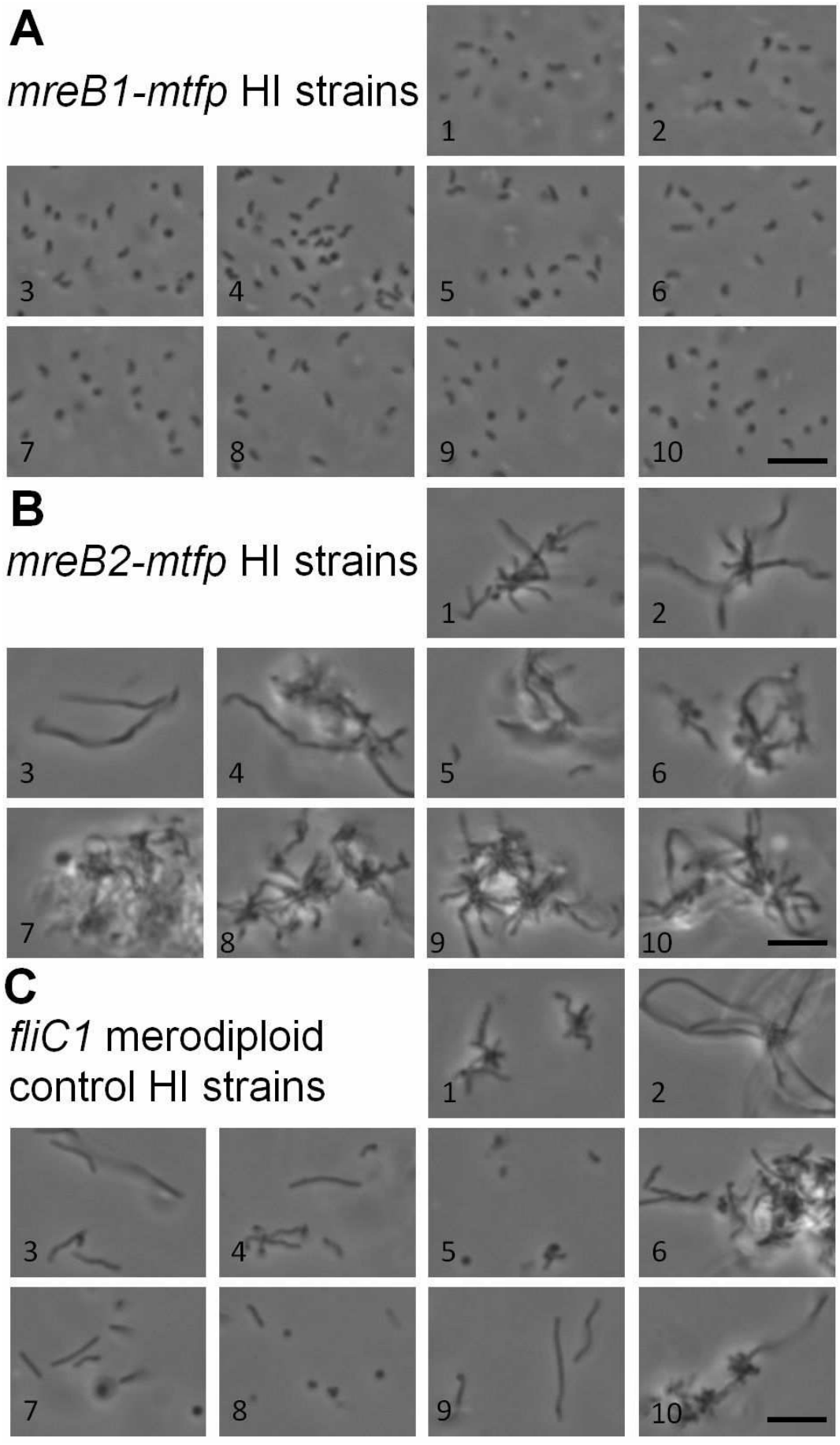
A
mreB1-mtfp HI strains
1
2
3
4
5
6
7
8
9
10
B
mreB2-mtfp HI strains
1
2
3
4
5
6
7
8
9
10
C
fliC1 merodiploid
control HI strains
1
2
3
4
5
6
7
8
9
10

5.3.1 Host independent growth rates of *mreB1-mtfp* and *mreB2-mtfp* HI strains.

As with cellular morphology studies; *B. bacteriovorus* HI growth curves have rarely been conducted due to the high degree of variation of growth rate amongst isolates. A method using OD_{600} readings in a FLUOstar Optima plate reader allows for the detection of growth of *B. bacteriovorus* HI strains over time (Fig. 5.13), see Materials and Methods section 2.17. HI strains gradually lose the ability to re-enter the predatory life-cycle and increase in growth rate as they grow; thus care was taken for each HI culture to ensure that the same growth conditions had been maintained for all strains used in the growth curve shown in Fig. 5.13. Despite the defect in predatory cell growth within bdelloplasts the (smaller) ten HI *mreB1-mtfp* cells showed a significantly faster growth rate over the ten *FliC1* merodiploid control strains (Fig. 5.13). The *mreB2-mtfp* HI strains showed a uniformly slower growth rate than controls never reaching high OD_{600} values, perhaps indicating the detrimental effects of elongated cell growth (Fig. 5.13).

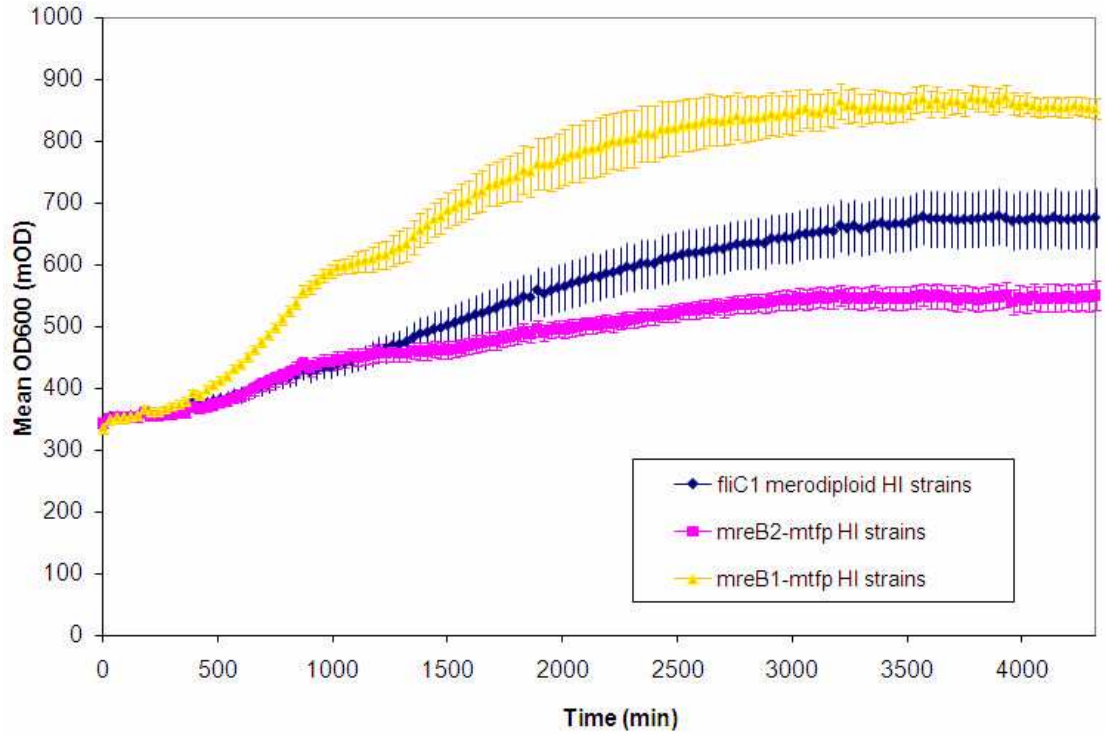

Figure 5.13 Average Host independent growth rates of ten independently isolated *mreB1-mtfp* and *mreB2-mtfp* strains against ten *fliC1* merodiploid controls. Methods used are detailed in section 2.17. Each HI culture was diluted to a starting OD_{600} of 0.1 (using a bench top spectrophotometer). Growth of each HI strain was measured in duplicate over 72 h. Error bars represent 95% confidence levels.

Further growth curves of three independently generated *mreB2-mtfp* HI strains in the presence of 0, 1, 10 and 100 µg/ml A22 were carried out to investigate the A22 growth enhancement effects observed for the *mreB1-mtfp* HD strain (section 5.2.7, Fig. 5.14). The graph in Fig. 5.14 does not show a significant difference in growth rate between the 0 and 1 µg/ml A22 final concentrations; however the average results of HI growth in the presence of 1 µg/ml A22 reached stationary phase faster than the 0 µg/ml control (Fig. 5.14). Cell viability of the three *mreB2-mtfp* growing HI strains was lost in the presence of 100 µg/ml A22 (Fig. 5.14).

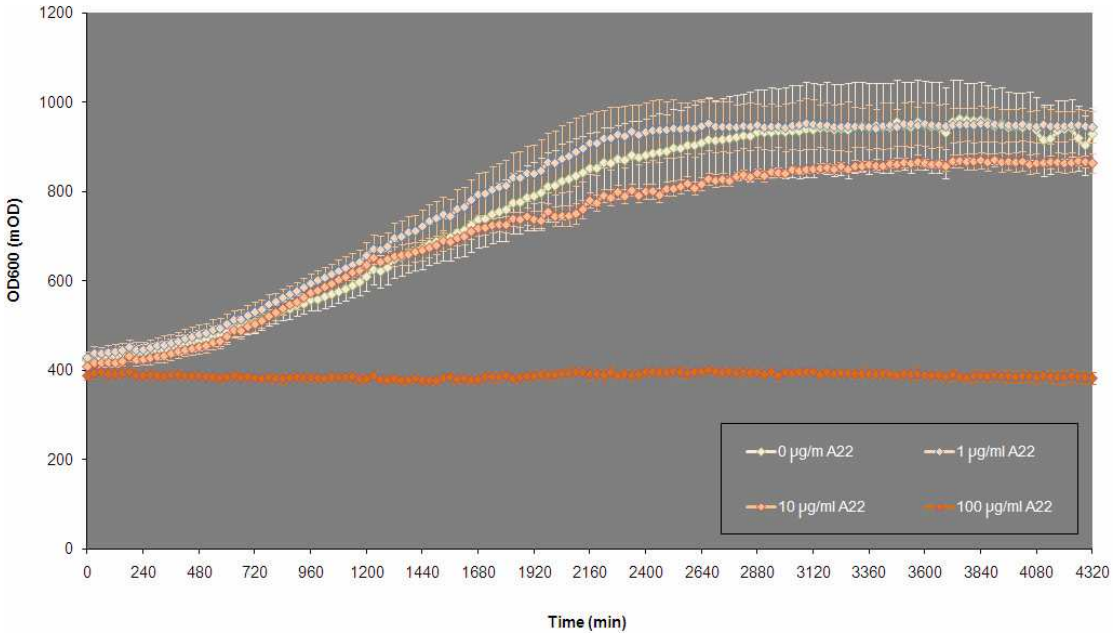

Figure 5.14 Average Host independent growth rates of three independently isolated *mreB1-mtfp* strains in the presence of A22 at varying concentrations. See section 2.17 for Methods. Each HI culture was diluted to a starting OD_{600} of 0.1 (using a bench top spectrophotometer). Growth of each HI strain, under each condition, was measured in duplicate over 72 h. Error bars represent 95% confidence levels.

5.4 Discussion

This work shows that both *mreB* genes of *B. bacteriovorus* were found to be essential for viability and could not be deleted; this is consistent with data for *mreB* from both *E. coli* and *B. subtilis* (Jones et al., 2001, Kruse et al., 2005) (section 5.2.1). Despite their essentiality, the function of the *B. bacteriovorus* MreB proteins in the bdelloplast could be examined using C-terminal mTFP tags (section 5.2.5 and 5.2.6). In each case this fusion gave an *mreB-mtfp* strain with a phenotype very different from wild-type, consistent with work on a *B. subtilis* MreB homologue, Mbl, where C-terminal GFP tagging resulted in a MreB protein with altered dynamics (Jones et al., 2001) (summarised in section 5.2.4).

Wild-type *B. bacteriovorus* treated with the classical MreB-modifying agent A22, which produces shape changes in other bacteria due to MreB filament modifications at concentrations from 3 µg/ml to 100 µg/ml (Iwai et al., 2004), showed that at concentrations approaching 200 µg/ml A22 was toxic to attack-phase *B. bacteriovorus*, as EM studies showed these cells had formed inclusion bodies, but at lower A22 concentrations (those active in shape-changing other bacteria) the wild-type *B. bacteriovorus* attack-phase cell never altered shape upon

incubation with A22, although an *E. coli* control using the same methods did round up at 5 μg/ml (data not shown).

RT-PCR analysis (Fig. 5.3) suggested that the two *mreB* gene products in *B. bacteriovorus* are expressed during developmental stages of the *B. bacteriovorus* growth-phase within the bdelloplast and at undetectable levels in the attack-phase cells (Fig. 5.3A). This is consistent with the expectation that *B. bacteriovorus* cell elongation in the growth-phase (Fig. 1.6) involves MreB proteins. The pattern of increasing expression within the bdelloplast up to a peak at the 2-3 h point is consistent with the increasing size of the growth-phase filamentous cell (Fig. 1.6).

At 3-4 h the *B. bacteriovorus* growth-phase cells are septating, forming progeny and repressing growth giving the slight reduction in *mreB* expression. The expression pattern of both *mreB* genes was similar to that of the *mreCD* operon despite being expressed from different promoters (Fig. 5.3). The *mreB1* gene showed a reproducible additional peak of expression at 15 min (Fig. 5.3A, Appendix 5.1); this could suggest that MreB1 may have a role in invasion and/or early growth-phase cell development. These roles were further investigated using the mTFP-fusion strains.

The *mreB1-mtfp* strain had a major defect in predatory growth with normal development arresting in the early growth-

phase *B. bacteriovorus* inside the bdelloplast (Fig. 5.5Bf). Fluorescence activity within the *mreB1-mtfp* strain was low and detectable fluorescence was constrained to the growth-phase cell, within the bdelloplast, (Fig. 5.6 B, section 5.3). Suggesting MreB1 is not as abundant as MreB2 (which had detectable fluorescence Fig. 5.8, Fig. 5.10) and has a role in filamentous growth establishment.

Growth-phase arrest of the *mreB1-mtfp* strain in the bdelloplast seemed not to be caused by a failure in growth resources, as Hoechst stained stalled bdelloplasts showed no prey-DNA labelling suggesting that the prey chromosome had been digested by *B. bacteriovorus* nucleases. Thus there were at least nucleic acid resources available for *B. bacteriovorus* growth, but the *B. bacteriovorus* were not elongating for other reasons. *B. bacteriovorus* cells, with abortive development within bdelloplasts, failed to lyse prey and the stalled bdelloplasts accumulated within the population (Fig. 5.5 Bg-i). The partial rescue of this phenotype by the addition of low levels of A22, a molecule known to stabilise ADP-bound MreB filaments at sub-inhibitory concentrations in *vitro* using MreB purified from *Thermotoga maritima* (Bean et al., 2009), suggests that possibly the *mreB1-mtfp* strain had a reduced capacity to form filaments within the early bdelloplast, or that its

filaments were less stable than wild-type, and that this impaired early predatory growth. This conclusion is further supported by work on *mreB1-mtfp* HI strain morphology which do not form elongated HI cells (Fig. 5.12). The stabilisation of the *mreB1-mtfp* filaments by A22 in bdelloplasts partly aided rescue and produced more *B. bacteriovorus* attack-phase cells, by the completion of predation (section 5.2.7). This observation in part supported by HI growth assays in the presence of A22, though results were not statistically significant (Fig. 5.14).

Despite their genetic homogeneity a proportion of the *mreB1-mtfp* cells escaped the arrested state, without A22 addition and did continue to the late bdelloplast, filamentous growth-phase septating to give attack-phase cells that were wild-type in shape, contained DNA and were capable of HD growth (Fig. 5.5Ba,Be). These were seen after 24 h of incubation with prey as 14% of the bdelloplast population in Fig. 5.5Be containing sepatated *B. bacteriovorus* that look indistinguishable from wild-type (Fig. 5.5Ae). What genetic events caused these few *mreB1-mtfp* cells to proceed slowly to lyse bdelloplasts at 24 h when so many others arrested (Fig. 5.5 Bf) or sphaeroplasted and died within bdelloplasts (Fig. 5.5Bg-I and Fig. 5.6A) are not known. It must be borne in mind that a wild-type copy of *mreB2* was present in the

mreB1-mtfp strains, but because of the asynchrony of the predatory process for the *mreB1-mtfp* strain, due to the stalling bdelloplasts, it was not possible to meaningfully monitor changes in *mreB2* expression in the *mreB1-mtfp* strains during predation. Alteration of *mreB2* expression in the *mreB1-mtfp* strain by promoter point mutations would be too rare to explain the percentages of *mreB1-mtfp* cells which eventually overcome the developmental stalling in the bdelloplast.

What was very clear was that the low numbers of *mreB1-mtfp* attack-phase cells that completed the predatory cycle, were not revertants to a wild-type (*mreB1*$^{+}$) state. When they were separated by filtration from the stalled bdelloplasts and applied again to a fresh culture of *E. coli* prey, the same bdelloplast stalling effect was produced, with only a few cells making it through to prey lysis, producing attack-phase *B. bacteriovorus* again.

The *mreB2-mtfp* strain gave a phenotypic change that occurred later in *B. bacteriovorus* predatory development in the bdelloplast. This strain had an almost wild-type growth rate within the bdelloplast (Fig. 5.4 and Fig. 5.7), the slightly lowered predation rate being due to a sub-population of non-predatory, spherical cells (Fig. 5.8ABC). However, upon completion of the

predatory cycle, bdelloplast lysis gave *mreB2-mtfp* progeny with altered morphologies, including branched and elongated, in addition to spherical and wild-type vibriod (Fig. 5.8B). I was not able to assess how many of each morphotype was produced from each bdelloplast as the cells are quite constricted within the bdelloplast before release, and the ability to follow growth-phase cell development within bdelloplasts by time-lapse microscopy (described in Chapter 4) was not available at the time. However, it can be presumed that a spherical cell or branched cell was produced along with some attack-phase cells from at least some of the bdelloplasts, rather than pure morphotypes being liberated from single bdelloplasts.

For *mreB2-mtfp* elongated cells the chromosomal material was never partitioned along the filament but appeared as a single elongated focus always located to the midpoint of the cells. (Fig. 5.8 5Fa-b) this is similar to the chromosomal distribution reported in *E. coli* for elongated cells produced by cephalexin treatment expressing MreB with point changes at aspartic acid 165, although this was not mutated in the *mreB1-mtfp* fusion strain (Kruse et al., 2003). I found that, although the spherical cells contained DNA (Fig. 5.8 Fb) and were motile, with a single flagellum (Fig. 5.8 C) they were not able to predatorily enter prey. Thus the spherical cells were a dead end side-product of the predatory cycle of *mreB2-mtfp* cells which also produced the other morphotypes. Interestingly the

elongated morphotypes **did** enter prey. Thus the generation of non-predatory spherical cells effectively reduced the predatory *B. bacteriovorus* yield per bdelloplast of the *mreB2-mtfp* strain and was responsible for the slight reduction in the rate of *E. coli* prey killing, shown in Fig. 5.4.

Interestingly the *mreB1-mtfp* predatory growth inhibition was not evident in HI growth curves using multiple independently generated HI strains. *mreB1-mtfp* strains were all small, with 99% of cell lengths for these stains falling between 1-1.5 μm (the same range as HD attack-phase cells), and grew at a significantly faster rate compared to control strains; whereas the *mreB2-mtfp* HI strain grew slower, a complete reverse of the attack-phase growth defects (Fig. 5.13). The *mreB1-mtfp* HI strains seem to be unable to form long elongated cells often seen in HI cultures (Fig. 5.12C); this inability could be the key to the elevated growth rates of the *mreB1-mtfp* HI strains, as they are not hampered by the gene dosage and genome stability complications arising from having multiple copies of the chromosome within one cell, in contrast to the large *mreB2-mtfp* networks (Fig. 5.12A,B). This was an unexpected role for the *mreB1* gene.

B. bacteriovorus strains with significantly altered attack-phase and HI cell morphologies had not been described before this study. It is worth noting that although cell length and shape were affected in these strains, no significant defect in the widths of viable cells were observed, as is also the case for C-terminally GFP tagged Mbl in *B. subtilis* (Jones et al., 2001). The division-inhibitory properties giving rise to an elongated morphology of the *mreB2-mtfp* HD and HI strains (Fig. 5.8 and Fig. 5.12), are consistent with published observations for GFP tagging of the Mbl filament in *B. subtilis*, but in that bacterium the block in septation involved the change in cell width (Jones et al., 2001).

Interestingly, although the cell shape of wild-type, attack-phase *B. bacteriovorus* was unaffected by A22 addition, shape changes were seen in attack-phase cells of the *mreB2-mtfp* strain, after the addition of A22 at 100 µg/ml; suggesting that possibly this strain was turning-over its cell wall/cytoskeleton in the attack-phase; whereas the wild-type did not seem to do so to the same extent (Fig. 5.9, 5.10).

Incubation with A22 led to loss of elongated cells and a rise in the number of spherical cells, suggesting that like in other model organisms *B. bacteriovorus mreB2-mtfp* cells (but not wild-type)

became spherical on addition of A22 (Fig. 5.9, 5.10). The novel mushroom-shaped morphology, present (Fig. 5.10 Be-h) in a subset of the *mreB2-mtfp* A22-treated population, could represent an intermediate in *mreB2-mtfp* attack-phase cells becoming spherical. As *B. bacteriovorus* attack-phase cells rely on a finite reserve of stored material from the last infection as a nutrition source (and do not take up organic nutrients), there were few resources available to turn over cell wall and allow full conversion of the vibroid-shaped attack-phase cells to spheres. This is likely why adding A22 gave rise to the mushroom shaped cells which are a known intermediate in the process of rod shaped bacteria becoming spherical (Chiu et al., 2008). Fluorescence activity within these A22-treated, mushroom-shaped, *mreB2-mtfp* cells was predominantly in the rod shaped "mushroom stalk" part of the cell and less strongly in the hemi-spherical "cap" shape, suggesting that turnover of the MreB2-mTFP protein at this point, was beginning to cause the shape change from vibroid-shaped to spherical (Fig. 5.10). The fully spherical *mreB2-mtfp* cells produced without A22 did show some fluorescence suggesting that MreB2-mTFP protein remained within them although it was no longer functional in shape determination.

This mushroom-shaped cell production in the *mreB2-mtfp* strain with A22, matches that in *Vibrio parahaemolyticus* cells entering a crisis, where MreB filament-breakdown at the pole of the cell caused that pole to round up ultimately spreading over the whole cell in that case (Chiu et al., 2008). I suggest that the altered dynamics of the MreB2 caused by the mTFP-addition gave a distribution of *B. bacteriovorus* with altered MreB filament states either stabilising the MreB2 filament directly (suggested by the 15% elongated cells, Fig. 5.8D) or increasing MreB2 filament turnover (suggested by the 21% spherical, Fig. 5.8D); the continued presence of MreB2-mTFP giving the cells that capacity to change shape by interaction with MreCD and cell wall synthetic machinery. This would suggest that such additional factors required for MreB2 to direct cell wall biosynthesis were present and active in the *mreB2-mtfp* strain.

This work represents the first investigation into the cytoskeletal activities during predatory *B. bacteriovorus* development yet undertaken and was published in the Journal of Bacteriology (Fenton et al., 2010). This study shows how *mreB* gene duplication and specialisation has facilitated a developmental process that yields septated vibriod attack-phase cells, from an intermediate elongated, filamentously-growing cell; growing within

the confines, and finite nutritional resources, of a dead prey bacterium. It also shows a role for MreB1 cycling in HI growth, suggesting further study of *mreB* genes may yield further insights into the mechanisms which give rise to the diverse HI growth morphologies between isolates.

CHAPTER SIX

Concluding Discussion.

The aim of this project was to establish patterns of intra-periplasmic growth of *B. bacteriovorus* and to investigate any roles that cytoskeletal elements had in that predatory life-style.

This study has successfully described the developmental patterns of *B. bacteriovorus* growth-phase cells within the bdelloplasts using a combination of time-lapse imaging and a fluorescently-labelled prey (section 4.4). I have been able to describe in previously unseen detail how a predatory bacterium grows and divides atypically within another bacterium. Taken together with collaborative work by Machi Kanna and Hoechst DNA staining of bdelloplasts (Fig. 5.5A), this has advanced our understanding of *B. bacteriovorus* predatory development, summarised in Fig. 6.1 and described fully in section 4.5.

My PhD also focused on the activities of three bacterial cytoskeletal elements: Ccrp, Bd3904 and MreB (Chapter 3, 4 and 5 respectively). Both genome knock-out methods and the development of a new technique of mTFP-tagging proteins in *B. bactetriovorus* have given the first insights into the function of these proteins *in vivo* (section 3.6, 4.6 and 5.4).

The *B. bacteriovorus* Ccrp protein contributes to cell shape stability by acting as an internal protein scaffold, similar to the FilP protein in *S. coelicolor* (Bagchi et al., 2008), and does not contribute to the vibroid shape of the *B. bacteriovorus* cells like the Ccrp CreS in *C. crescentus* (Ausmees et al., 2003) (discussed in section 3.6). Further work, beyond the timeline of my project, to measure the cell rigidity directly using AFM (Atomic Force Microscopy) techniques would provide more support to this work in a similar way to that used in (Bagchi et al., 2008). Immuno-precipitation and MALDI-TOF MS analytical methods using the HD100 Ccrp-mCherry tagged stain, using the mCherry antigen as a target, would identify proteins which maintain and modify the underlying Ccrp structure.

On the basis of *E. coli* expression data and *B. bacteriovorus* protein localisation studies, I propose that the 'bactofilin' like protein Bd3904 inhibits synchronous septation within growth-phase cells within bdelloplasts (discussed in section 4.6), until the correct developmental check point is achieved to allow septation. Future work on the dynamics of the Bd3904 filaments *in vitro* and the generation of a HD100 *Bd3904* KO strain (if this is viable) are required to fully support these conclusions.

The two essential *mreB* gene products in *B. bacteriovorus* both function in predatory growth but have major actions in at

different times; the MreB1 protein functions to establish filamentous growth, whereas the MreB2 protein acts later to support filamentous growth and the establishment of growth-inhibition of the attack-phase cell. The 10 *mreB-mTFP* derivative HI strains support these conclusions: the 10 *mreB1-mtfp* HIs are only capable of forming short "attack-phase sized" cells, whereas the *mreB2-mtfp* HI strains from long extended filamentous cell networks (Fig. 5.12). Further work studying the growth rates of *mreB-mtfp* HI strains in the presence of A22 will reveal more about the role of these proteins in the establishment and maintenance of *B. bacteriovorus* cell morphology. Following *mreB-mtfp* HD100 strain development through single infections of fluorescent prey using time-lapse microscopy described in section 4.4 will reveal further insights into MreB function in *B. bacteriovorus* development.

A useful product of my PhD has been the *huA-mtfp* HD100 (and *huA-mcherry* HD100) initially cloned as a chromosomal "paint" as part of the study into *B. bacteriovorus* septation (section 4.3.2). This strain has a strong fluorescent signal which can be used to specifically identify huA-tagged cells among other untagged cell-types, this could make this strain a very valuable tool for *B. bacteriovorus* predatory competition research in the future.

6.1 The growth and development of *B. bacteriovorus* within bdelloplasts.

After a series of false starts and optimisations, time-lapse imaging of fluorescent-prey bdelloplasts revealed many previously unseen details of *B. bacteriovorus* growing within prey (Fig. 6.1, section 4.4). I was able to demonstrate the synchronous septation of *B. bacteriovorus* from single growing filaments, inside bdelloplasts.

Additional EM studies by Machi Kanna (personal communication) revealed that after septation newly formed *B. bacteriovorus* progeny go through a further differentiation phase where cell length increases, yet cell width remains similar, with the newly released cells slightly elongating into the attack-phase form outside prey. This developmental strategy could be advantageous for *B. bacteriovorus* growth within the confines of a bdelloplast before prey-cell lysis. It remains unclear what role *B. bacteriovorus* attack-phase cell organic-molecule scavenging outside of bdelloplasts contributes to this observed elongation and whether cytoskeletal elements play a role.

B. bacteriovorus growth-phase cells must contain multiple copies of the genome before synchronous septation, and thus they risk genome stability by multiple homologous recombination events between newly replicated genomes. Despite these risks to genome

stability the method of filamentous growth must have advantages in both co-ordination of prey digestion and maximising division of prey resources amongst progeny that lead to a net increases in *B. bacteriovorus* fitness.

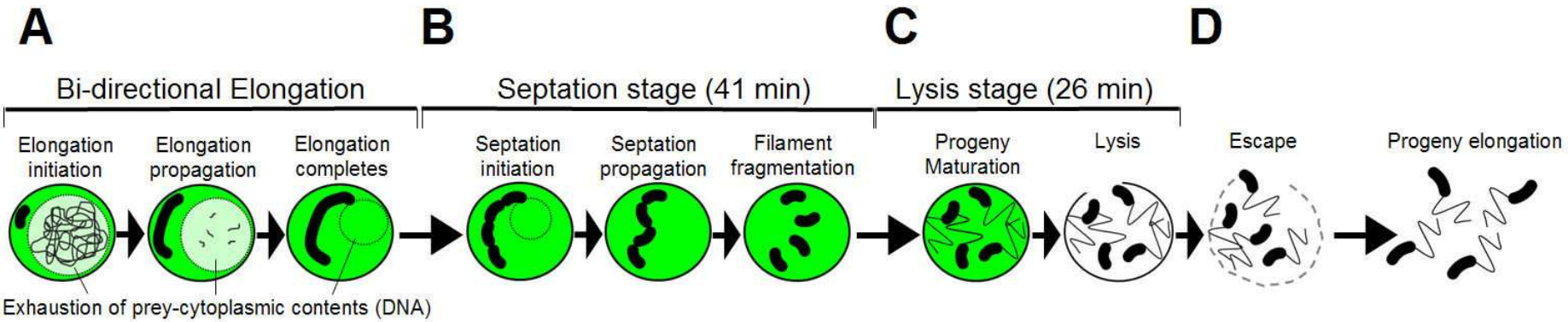

Figure 6.1 Key events through different stages of *B. bacteriovorus* growth within the bdelloplast. Figure shows events which take place after initial attack-phase *B. bacteriovorus* attachment and entry to a 'GFP' green prey, key point in the infection process are highlighted and 4 progeny cells (the average number of cells produced in the time-lapse experiments Fig 4.9A) are produced, these events are visualised in Movies 1-5 and stills from those movies in Appendix 4.2. (**A**) Growing *B. bacteriovorus* cells elongate bi-directionally using the resources gathered from excretion and absorption of prey-cell contents; such as DNA visualised as a loss of Hoeschst-DNA fluorescence activity in Fig 5.5A. Only once growth-phase cells reach their maximum length do they initiate septation, shown in Movies S1-4. (**B**) Septation initiates synchronously along the growth-phase filament forming both odd and even numbers of progeny cells, Fig 4.9A, Movies 1-4. Filament fragmentation often causes dramatic shifts in progeny cell orientations, Movie 5. The whole septation stage takes on average 41 min to complete, and is independent of the number of progeny cells formed, Fig 4.11A (n=47). (**C**) After septation *B. bacteriovorus* mature, developing flagella visualised as *B. bacteriovorus* cell motility within bdelloplasts (Movie 10). *B. bacteriovorus* excrete lytic enzymes which lyse the exhausted bdelloplast (resulting in a loss of GFP activity) in 26 min on average after the completion of septation (n =77), this is inversely proportional to the number of progeny cells produced, Fig 4.11B. (**D**) *B. bacteriovorus* progeny typically exit the bdelloplast out of a single hole (88% n = 67) but can occasionally escape using two holes in the bdelloplast, Movies 8 and 9, section 4.4.5. After escaping the confines of the bdelloplast *B. bacteriovorus* cells elongate into full length mature attack-phase cells,(Machi Kanna personal communication).

B. bacteriovorus must also have unprecedented control over DNA replication to replicate odd numbers of chromosomes from a single template and to maximise use of the quantised material available inside a dead prey bacterium to make the maximum number of progeny. Like other bacteria (such as *E. coli*) *B. bacteriovorus* is predicted to initiate DNA replication using the DnaA protein (see Fig. 4.3 for expression of *dnaA* through a predatory time-course), the concentration of this protein in *E. coli* is finely controlled to initiate DNA replication only once form the origin of replication and then its action is inhibited by a variety of mechanisms, for example sequestering of the *oriC* by the SeqA protein making it unavailable for DnaA binding. *B. bacteriovorus* DnaA must initiate replication multiple times in one cell, thus additional as yet unknown control systems must exist to control this process (Messer, 2002).

Bioinformatic studies on the *B. bacteriovorus* HD100 genome reveal that this bacterium encodes all of the components of regular bacterial septation machinery but no full complement of recognisable control systems i.e. MinCDE system, DivIVA or MipZ (Table 5.1). Although Bd3904 represents a tantalising candidate for septation control (section 4.5-4.6) identifying the mechanisms that

govern how the septal machinery is positioned along the *B. bacteriovorus* filament remains an exciting challenge.

6.2 The development and use of C-terminal mTFP tagging to investigate the function of *B. bacteriovorus* proteins.

The most important methodological advancement in the course of this project was the development of a method to stably C-terminally tag *B. bacteriovorus* target proteins with a GFP moiety (section 2.12). This allowed the study of essential *mreB* gene function in *B. bacteriovorus* by the reduction of wild-type MreB-protein activities (section 5.2 and 5.3) and the sub cellular localisation of Ccrp within attack-phase cells (section 5.3.2).

In retrospect the selection of the mTFP fluorphore used for GFP tagging in this study was a good one, for reasoning see section 1.7. This protein has been specifically engineered to make it fully monomeric; preventing any spurious results introduced by slight GFP-dimerisation effects (Table 1.1). The relatively high brightness and photostability of the mTFP fluorophore still remains in a class of its own amongst the cyan-FPs (Ai et al., 2006). This high brightness has allowed the detection of painfully weak fluorescent signals within *B. bacteriovorus* cells which would have otherwise remained undetected; for example the Ccrp-mTFP activities shown in Fig. 3.10, and the MreB1-mTFP activities shown in Fig. 5.8. However, there is currently no mono- or poly-clonal antibody available for mTFP1 (Alelle biotech personal communication, January 2010). This has slowed further research into the protein

interaction partners of the MreB, Ccrp, HUa and Bd3904 proteins mTFP tagged in this study as immuno-precipitations and subsequent MALDI-TOF MS analyses of partner proteins have not been possible.

The mTFP molecule is however the perfect as a donor fluorphore for the bright yellow fluorescent protein YPet for future FRET (Fluorescence Resonance Energy Transfer) analyses of *B. bacteriovorus* protein-complexes. YPet would be a good choice for mTFP FRET due to its high quantum yield and overlapping emission-absorption septra (see excitation and emission values for mTFP1 and YPet, shown in Table 1.1). This leads me to more suggestions for future work that could build upon my thesis.

6.3 Future work

The Bd3904 protein (section 4.5) could provide part of the solution to the conundrum of *B. bacteriovorus* synchronous cell division, being temporally and spatially positioned to coincide with filamentous growth in *Bdellovibrio*, and having septation inhibitory properties when expressed in *E. coli* (section 4.5 and Fig. 4.3). Further work on the behaviour of this protein within bdelloplasts, monitored by time-lapse microscopy using methods described in section 4.4, and identification of protein interaction partners in *B. bacteriovorus* cells using antibody pull-downs, could provide the best platform from which to understand how growth-phase cells coordinate their unique method of cell-division.

An A22 analogue MP265 has recently been described which has a reduced cyto-toxicity (Takacs et al., 2010). This could be of use in *B. bacteriovorus* cytoskeletal research as clearly the MreB proteins of *B. bacteriovorus* are not as sensitive to A22 as those of other bacteria such as *C. crescentus* and *E. coli*, as much higher concentrations of A22 are needed for any type of morphological or growth-inhibitory effect (section 5.2.8). *B. bacteriovorus* tolerance to A22 is potentially a good thing for future *B. bacteriovorus* therapies, in combination with conventional antibiotics, as A22 represents both a novel and general primary molecule for the development of antibiotics against conventional pathogenic bacteria.

The use of HI strains to probe the function of the *mreB* gene products remains an unexpected and exciting prospect. Further work on the ten HI derivatives of the *mreB1-mtfp* and *mreB2-mtfp* strains against the *fliC1* merodiploid controls support growth and morphological observations of the original HD strains (section 5.2 and 5.3). Measuring the growth-rate of each HI derivative strains in the presence or absence of A22 (or MP265), as shown in Fig. 5.14, could yield additional insight into their respective roles within the bdelloplast.

More generally, time-lapse imaging using the XY-motorized stage and fine Z-controller of growing HI cells on PY Agarose pads would reveal if growth and division of *B. bacteriovorus* HI strains mirrors the synchronous division observed for the HD cells within bdelloplasts (As may be expected when one looks at Fig 2 and Fig 8 in the classic EM papers (Horowitz et al., 1974) and (Burnham et al., 1970) respectively). This would provide a deeper insight into *B. bacteriovorus* HI growth phenotype.

6.4 Conclusion

I set out to discover *B. bacteriovorus* growth-phase cell developmental patterns within bdelloplasts and investigate the roles of cytoskeletal elements within these processes. This has been successful thanks to the advances in GFP-protein and microscopic-imaging technology. The main developmental processes of *B. bacteriovorus* within a bdelloplasts have been accurately described, resulting in a first author manuscript submitted for publication. The study of the functions of the two MreB cytoskeletal proteins at different points in the predatory life-cycle of *B. bacteriovorus* led to a well received publication (Fenton et al., 2010). Work describing the function of the Ccrp cell scaffold in the maintenance of *B. bacteriovorus* cell shape has also led to a small manuscript being submitted for publication. Future work on the sepation inhibitor Bd3904 and further work on the function of the MreB proteins using the HI strains remain as exciting projects for follow-on studies in the immediate future.

There still remains, much more to be done.

References

ABRAM, D., CASTRO E MELO, J. & CHOU, D. (1974) Penetration of Bdellovibrio bacteriovorus into host cells. *J Bacteriol,* 118**,** 663-80.

ABRAM, D. & DAVIS, B. K. (1970) Structural properties and features of parasitic Bdellovibrio bacteriovorus. *J Bacteriol,* 104**,** 948-65.

AI, H. W., HENDERSON, J. N., REMINGTON, S. J. & CAMPBELL, R. E. (2006) Directed evolution of a monomeric, bright and photostable version of Clavularia cyan fluorescent protein: structural characterization and applications in fluorescence imaging. *Biochem J,* 400**,** 531-40.

ALEMOHAMMAD, M. M. & KNOWLES, C. J. (1974) Osmotically induced volume and turbidity changes of Escherichia coli due to salts, sucrose and glycerol, with particular reference to the rapid permeation of glycerol into the cell. *J Gen Microbiol,* 82**,** 125-42.

AMANN, E., OCHS, B. & ABEL, K. J. (1988) Tightly regulated tac promoter vectors useful for the expression of unfused and fused proteins in Escherichia coli. *Gene,* 69**,** 301-15.

AUSMEES, N., KUHN, J. R. & JACOBS-WAGNER, C. (2003) The bacterial cytoskeleton: an intermediate filament-like function in cell shape. *Cell,* 115**,** 705-13.

BAGCHI, S., TOMENIUS, H., BELOVA, L. M. & AUSMEES, N. (2008) Intermediate filament-like proteins in bacteria and a cytoskeletal function in Streptomyces. *Mol Microbiol,* 70**,** 1037-50.

BEAN, G. J., FLICKINGER, S. T., WESTLER, W. M., MCCULLY, M. E., SEPT, D., WEIBEL, D. B. & AMANN, K. J. (2009) A22 disrupts the bacterial actin cytoskeleton by directly binding and inducing a low-affinity state in MreB. *Biochemistry,* 48**,** 4852-7.

BENDEZU, F. O. & DE BOER, P. A. (2008) Conditional lethality, division defects, membrane involution, and endocytosis in mre and mrd shape mutants of Escherichia coli. *J Bacteriol,* 190**,** 1792-811.

BENDEZU, F. O., HALE, C. A., BERNHARDT, T. G. & DE BOER, P. A. (2009) RodZ (YfgA) is required for proper assembly of the MreB actin cytoskeleton and cell shape in E. coli. *Embo J,* 28**,** 193-204.

BIERMAN, M., LOGAN, R., O'BRIEN, K., SENO, E. T., RAO, R. N. & SCHONER, B. E. (1992) Plasmid cloning vectors for the conjugal transfer of DNA from Escherichia coli to Streptomyces spp. *Gene,* 116**,** 43-9.

BIRNBOIM, H. C. & DOLY, J. (1979) A rapid alkaline extraction procedure for screening recombinant plasmid DNA. *Nucleic Acids Res,* 7**,** 1513-23.

BLATTNER, F. R., PLUNKETT, G., 3RD, BLOCH, C. A., PERNA, N. T., BURLAND, V., RILEY, M., COLLADO-VIDES, J., GLASNER, J. D., RODE, C. K., MAYHEW, G. F., GREGOR, J., DAVIS, N. W., KIRKPATRICK, H. A., GOEDEN, M. A., ROSE, D. J., MAU, B. & SHAO, Y. (1997) The complete genome sequence of Escherichia coli K-12. *Science,* 277**,** 1453-62.

BORGNIA, M. J., SUBRAMANIAM, S. & MILNE, J. L. (2008) Three-dimensional imaging of the highly bent architecture of Bdellovibrio bacteriovorus by using cryo-electron tomography. *J Bacteriol,* 190**,** 2588-96.

BURNHAM, J. C., HASHIMOTO, T. & CONTI, S. F. (1968) Electron microscopic observations on the penetration of Bdellovibrio bacteriovorus into gram-negative bacterial hosts. *J Bacteriol,* 96**,** 1366-81.

BURNHAM, J. C., HASHIMOTO, T. & CONTI, S. F. (1970) Ultrastructure and cell division of a facultatively parasitic strain of Bdellovibrio bacteriovorus. *J Bacteriol,* 101**,** 997-1004.

CABEEN, M. T., CHARBON, G., VOLLMER, W., BORN, P., AUSMEES, N., WEIBEL, D. B. & JACOBS-WAGNER, C. (2009) Bacterial cell curvature through mechanical control of cell growth. *EMBO J,* 28**,** 1208-19.

CARBALLIDO-LOPEZ, R. & ERRINGTON, J. (2003) The bacterial cytoskeleton: in vivo dynamics of the actin-like protein Mbl of Bacillus subtilis. *Dev Cell,* 4**,** 19-28.

CHARBON, G., CABEEN, M. T. & JACOBS-WAGNER, C. (2009) Bacterial intermediate filaments: in vivo assembly, organization, and dynamics of crescentin. *Genes Dev,* 23**,** 1131-44.

CHIU, S. W., CHEN, S. Y. & WONG, H. C. (2008) Localization and expression of MreB in Vibrio parahaemolyticus under different stresses. *Appl Environ Microbiol,* 74**,** 7016-22.

COTTER, T. W. & THOMASHOW, M. F. (1992) Identification of a Bdellovibrio bacteriovorus genetic locus, hit, associated with the host-independent phenotype. *J Bacteriol,* 174**,** 6018-24.

DANIEL, R. A. & ERRINGTON, J. (2003) Control of cell morphogenesis in bacteria: two distinct ways to make a rod-shaped cell. *Cell,* 113**,** 767-76.

DI LALLO, G., FAGIOLI, M., BARIONOVI, D., GHELARDINI, P. & PAOLOZZI, L. (2003) Use of a two-hybrid assay to study the assembly of a complex multicomponent protein machinery: bacterial septosome differentiation. *Microbiology,* 149**,** 3353-9.

DRAPER, G. C., MCLENNAN, N., BEGG, K., MASTERS, M. & DONACHIE, W. D. (1998) Only the N-terminal domain of FtsK functions in cell division. *J Bacteriol,* 180**,** 4621-7.

EBRIGHT, R., DONG, Q. & MESSING, J. (1992) Corrected nucleotide sequence of M13mp18 gene III. *Gene,* 114**,** 81-3.

ERRINGTON, J., DANIEL, R. A. & SCHEFFERS, D. J. (2003) Cytokinesis in bacteria. *Microbiol Mol Biol Rev,* 67**,** 52-65, table of contents.

EVANS, K. J. (2007) The Roles of Surface Ultrastructures in the Predatory Life Cycle of *Bdellovibrio bacteriovorus*. Nottingham, University of Nottingham.

EVANS, K. J., LAMBERT, C. & SOCKETT, R. E. (2007) Predation by Bdellovibrio bacteriovorus HD100 requires type IV pili. *J Bacteriol,* 189**,** 4850-9.

FENTON, A. K., LAMBERT, C., WAGSTAFF, P. C. & SOCKETT, R. E. (2010) Manipulating each MreB of Bdellovibrio bacteriovorus gives diverse morphological and predatory phenotypes. *J Bacteriol,* 192**,** 1299-311.

FIGGE, R. M., DIVAKARUNI, A. V. & GOBER, J. W. (2004) MreB, the cell shape-determining bacterial actin homologue, co-ordinates cell wall morphogenesis in Caulobacter crescentus. *Mol Microbiol,* 51**,** 1321-32.

FINN, R. D., MISTRY, J., TATE, J., COGGILL, P., HEGER, A., POLLINGTON, J. E., GAVIN, O. L., GUNASEKARAN, P., CERIC, G., FORSLUND, K., HOLM, L., SONNHAMMER, E. L., EDDY, S. R. & BATEMAN, A. (2010) The Pfam protein families database. *Nucleic Acids Res,* 38**,** D211-22.

FORMSTONE, A. & ERRINGTON, J. (2005) A magnesium-dependent mreB null mutant: implications for the role of mreB in Bacillus subtilis. *Mol Microbiol,* 55**,** 1646-57.

FRATAMICO, P. M. & WHITING, R. C. (1995) Ability of Bdellovibrio bacteriovorus 109J to lyse gram-negative food-borne pathogenic and spoilage bacteria. . *Journal of food Protection,* 58**,** 160-164.

GERDES, K. (2009) RodZ, a new player in bacterial cell morphogenesis. *EMBO J,* 28**,** 171-2.

GITAI, Z., DYE, N. & SHAPIRO, L. (2004) An actin-like gene can determine cell polarity in bacteria. *Proc Natl Acad Sci U S A,* 101**,** 8643-8.

GITAI, Z., DYE, N. A., REISENAUER, A., WACHI, M. & SHAPIRO, L. (2005) MreB actin-mediated segregation of a specific region of a bacterial chromosome. *Cell,* 120**,** 329-41.

GOEHRING, N. W. & BECKWITH, J. (2005) Diverse paths to midcell: assembly of the bacterial cell division machinery. *Curr Biol,* 15**,** R514-26.

GRAUMANN, P. L. (2009) Dynamics of bacterial cytoskeletal elements. *Cell Motil Cytoskeleton,* 66**,** 909-14.

HALL, T. A. (1999) BioEdit: a user-friendly biological sequence alignment editor and analysis program for Windows 95/98/NT. *Nucleic Acids Symposium Series,* 41**,** 95-98.

HANAHAN, D. (1983) Studies on transformation of Escherichia coli with plasmids. *J Mol Biol,* 166**,** 557-80.

HERRMANN, H. & AEBI, U. (2004) Intermediate filaments: molecular structure, assembly mechanism, and integration into functionally distinct intracellular Scaffolds. *Annu Rev Biochem,* 73**,** 749-89.

HIRAGA, S. (2000) Dynamic localization of bacterial and plasmid chromosomes. *Annu Rev Genet,* 34**,** 21-59.

HOLTJE, J. V. (1998) Growth of the stress-bearing and shape-maintaining murein sacculus of Escherichia coli. *Microbiol Mol Biol Rev,* 62**,** 181-203.

HOROWITZ, A. T., KESSEL, M. & SHILO, M. (1974) Growth cycle of predacious Bdellovibrios in a host-free extract system and some properties of the host extract. *J Bacteriol,* 117**,** 270-82.

IIDA, Y., HOBLEY, L., LAMBERT, C., FENTON, A. K., SOCKETT, R. E. & AIZAWA, S. (2009) Roles of multiple flagellins in flagellar formation and flagellar growth post bdelloplast lysis in Bdellovibrio bacteriovorus. *J Mol Biol,* 394**,** 1011-21.

IWAI, N., EBATA, T., NAGURA, H., KITAZUME, T., NAGAI, K. & WACHI, M. (2004) Structure-activity relationship of S-benzylisothiourea derivatives to induce spherical cells in Escherichia coli. *Biosci Biotechnol Biochem,* 68**,** 2265-9.

IWAI, N., NAGAI, K. & WACHI, M. (2002) Novel S-benzylisothiourea compound that induces spherical cells in Escherichia coli probably by acting on a rod-shape-determining protein(s) other than penicillin-binding protein 2. *Biosci Biotechnol Biochem,* 66**,** 2658-62.

JONES, L. J., CARBALLIDO-LOPEZ, R. & ERRINGTON, J. (2001) Control of cell shape in bacteria: helical, actin-like filaments in Bacillus subtilis. *Cell,* 104**,** 913-22.

JURKEVITCH, E., MINZ, D., RAMATI, B. & BAREL, G. (2000) Prey range characterization, ribotyping, and diversity of soil and rhizosphere Bdellovibrio spp. isolated on phytopathogenic bacteria. *Appl Environ Microbiol,* 66**,** 2365-71.

KAWAI, Y., DANIEL, R. A. & ERRINGTON, J. (2009) Regulation of cell wall morphogenesis in Bacillus subtilis by recruitment of PBP1 to the MreB helix. *Mol Microbiol,* 71**,** 1131-44.

KESSEL, M. & SHILO, M. (1976) Relationship of Bdellovibrio elongation and fission to host cell size. *J Bacteriol,* 128**,** 477-80.

KESSEL, M. & VARON, M. (1973) Development of bdellophage VL-1 in parasitic and saprophytic bdellovibrios. *J Virol,* 12**,** 1522-33.

KRUSE, T., BORK-JENSEN, J. & GERDES, K. (2005) The morphogenetic MreBCD proteins of Escherichia coli form an essential membrane-bound complex. *Mol Microbiol,* 55**,** 78-89.

KRUSE, T., MOLLER-JENSEN, J., LOBNER-OLESEN, A. & GERDES, K. (2003) Dysfunctional MreB inhibits chromosome segregation in Escherichia coli. *EMBO J,* 22**,** 5283-92.

KUHN, J., BRIEGEL, A., MORSCHEL, E., KAHNT, J., LESER, K., WICK, S., JENSEN, G. J. & THANBICHLER, M. (2010) Bactofilins, a ubiquitous class of cytoskeletal proteins mediating polar localization of a cell wall synthase in Caulobacter crescentus. *EMBO J,* 29**,** 327-39.

LAEMMLI, U. K. (1970) Cleavage of structural proteins during the assembly of the head of bacteriophage T4. *Nature,* 227**,** 680-5.

LAMBERT, C., CHANG, C. Y., CAPENESS, M. J. & SOCKETT, R. E. (2010) The first bite--profiling the predatosome in the bacterial pathogen Bdellovibrio. *PLoS One,* 5**,** e8599.

LAMBERT, C., EVANS, K. J., TILL, R., HOBLEY, L., CAPENESS, M., RENDULIC, S., SCHUSTER, S. C., AIZAWA, S. & SOCKETT, R. E. (2006a) Characterizing the flagellar filament and the role of motility in bacterial prey-penetration by Bdellovibrio bacteriovorus. *Mol Microbiol,* 60**,** 274-86.

LAMBERT, C., HOBLEY, L., CHANG, C. Y., FENTON, A., CAPENESS, M. & SOCKETT, L. (2009) A predatory patchwork: membrane and surface structures of Bdellovibrio bacteriovorus. *Adv Microb Physiol,* 54**,** 313-61.

LAMBERT, C., MOREHOUSE, K. A., CHANG, C. Y. & SOCKETT, R. E. (2006b) Bdellovibrio: growth and development during the predatory cycle. *Curr Opin Microbiol,* 9**,** 639-44.

LAMBERT, C., SMITH, M. C. & SOCKETT, R. E. (2003) A novel assay to monitor predator-prey interactions for Bdellovibrio bacteriovorus 109 J reveals a role for methyl-accepting chemotaxis proteins in predation. *Environ Microbiol,* 5**,** 127-32.

LAMBINA, V. A., LEDOVA, L. A. & SITUKHINA, N. S. (1981) [Participation of bdellovibrios in sewage self-purification processes]. *Mikrobiologiia,* 50**,** 140-6.

LENZ., R. W. & HESPELL., R. B. (1978) Attempts to Grow Bdellovibrios Micurgically-Injected into Animal Cells. *Arch. Microbiol.*

LOWRY, O. H., ROSEBROUGH, N. J., FARR, A. L. & RANDALL, R. J. (1951) Protein measurement with the Folin phenol reagent. *J Biol Chem,* 193**,** 265-75.

LUPAS, A. (1996) Prediction and analysis of coiled-coil structures. *Methods Enzymol,* 266**,** 513-25.

LUPAS, A., VAN DYKE, M. & STOCK, J. (1991) Predicting coiled coils from protein sequences. *Science,* 252**,** 1162-1164.

MAHMOUD, K. K. & KOVAL, S. F. (2010) Characterization of type IV pili in the life cycle of the predator bacterium Bdellovibrio. *Microbiology,* 156**,** 1040-1051

MARCHLER-BAUER, A., ANDERSON, J. B., CHITSAZ, F., DERBYSHIRE, M. K., DEWEESE-SCOTT, C., FONG, J. H., GEER, L. Y., GEER, R. C., GONZALES, N. R., GWADZ, M., HE, S., HURWITZ, D. I., JACKSON, J. D., KE, Z., LANCZYCKI, C. J., LIEBERT, C. A., LIU, C., LU, F., LU, S., MARCHLER, G. H., MULLOKANDOV, M., SONG, J. S., TASNEEM, A., THANKI, N., YAMASHITA, R. A., ZHANG, D., ZHANG, N. & BRYANT, S. H. (2009) CDD: specific functional annotation with the Conserved Domain Database. *Nucleic Acids Res,* 37**,** D205-10.

MARKELOVA, N., ALEKSEEVA, N. V., ROMANOVA IU, M. & GINTSBURG, A. G. (2001) [Interaction of the vegetative and nonculturable forms of Salmonella typhimurium with bacteria of the genus Bdellovibrio]. *Zh Mikrobiol Epidemiol Immunobiol***,** 16-9.

MARKWELL, M. A., HAAS, S. M., BIEBER, L. L. & TOLBERT, N. E. (1978) A modification of the Lowry procedure to simplify protein determination in membrane and lipoprotein samples. *Anal Biochem,* 87**,** 206-10.

MARSTON, A. L., THOMAIDES, H. B., EDWARDS, D. H., SHARPE, M. E. & ERRINGTON, J. (1998) Polar localization of the MinD protein of Bacillus subtilis and its role in selection of the mid-cell division site. *Genes Dev,* 12**,** 3419-30.

MASSEY, T. H., MERCOGLIANO, C. P., YATES, J., SHERRATT, D. J. & LOWE, J. (2006) Double-stranded DNA translocation: structure and mechanism of hexameric FtsK. *Mol Cell,* 23**,** 457-69.

MATIN, A. & RITTENBERG, S. C. (1972) Kinetics of deoxyribonucleic acid destruction and synthesis during growth of Bdellovibrio bacteriovorus strain 109D on pseudomonas putida and escherichia coli. *J Bacteriol,* 111**,** 664-73.

MELBY, T. E., CIAMPAGLIO, C. N., BRISCOE, G. & ERICKSON, H. P. (1998) The symmetrical structure of structural maintenance of chromosomes (SMC) and MukB proteins: long, antiparallel coiled coils, folded at a flexible hinge. *J Cell Biol,* 142**,** 1595-604.

MESSER, W. (2002) The bacterial replication initiator DnaA. DnaA and oriC, the bacterial mode to initiate DNA replication. *FEMS Microbiol Rev,* 26**,** 355-74.

NANNINGA, N. (2001) Cytokinesis in prokaryotes and eukaryotes: common principles and different solutions. *Microbiol Mol Biol Rev,* 65**,** 319-33 ; third page, table of contents.

OSAWA, M. & ERICKSON, H. P. (2005) Probing the domain structure of FtsZ by random truncation and insertion of GFP. *Microbiology,* 151**,** 4033-43.

POPP, D., NARITA, A., GHOSHDASTIDER, U., MAEDA, K., MAEDA, Y., ODA, T., FUJISAWA, T., ONISHI, H., ITO, K. & ROBINSON, R. C. (2010) Polymeric structures and dynamic properties of the bacterial actin AlfA. *J Mol Biol,* 397**,** 1031-41.

RENDULIC, S., JAGTAP, P., ROSINUS, A., EPPINGER, M., BAAR, C., LANZ, C., KELLER, H., LAMBERT, C., EVANS, K. J., GOESMANN, A., MEYER, F., SOCKETT, R. E. & SCHUSTER, S. C. (2004) A predator unmasked: life cycle of Bdellovibrio bacteriovorus from a genomic perspective. *Science,* 303**,** 689-92.

RINGGAARD, S., VAN ZON, J., HOWARD, M. & GERDES, K. (2009) Movement and equipositioning of plasmids by ParA filament disassembly. *Proc Natl Acad Sci U S A,* 106**,** 19369-74.

ROGERS, M., EKATERINAKI, N., NIMMO, E. & SHERRATT, D. (1986) Analysis of Tn7 transposition. *Mol Gen Genet,* 205**,** 550-6.

RUBY, E. G. & RITTENBERG, S. C. (1983) Differentiation after premature release of intraperiplasmically growing Bdellovibrio bacteriovorous. *J Bacteriol,* 154**,** 32-40.

SAVAGE, D. F., AFONSO, B., CHEN, A. H. & SILVER, P. A. (2010) Spatially ordered dynamics of the bacterial carbon fixation machinery. *Science,* 327**,** 1258-61.

SCHAFER, A., TAUCH, A., JAGER, W., KALINOWSKI, J., THIERBACH, G. & PUHLER, A. (1994) Small mobilizable multi-purpose cloning vectors derived from the Escherichia coli plasmids pK18 and pK19: selection of defined deletions in the chromosome of Corynebacterium glutamicum. *Gene,* 145**,** 69-73.

SCHERFF, R. H., DEVAY, J. E. & CARROLL., T. W. (1966) Ultrastructure of host parasitic relationships involving reproduction of Bdellovibrio bacteriovorus in host bacteria. *Phytopathology,* 56**,** 627-632.

SCHWUDKE, D., STRAUCH, E., KRUEGER, M. & APPEL, B. (2001) Taxonomic studies of predatory bdellovibrios based on 16S rRNA analysis, ribotyping and the hit locus and characterization of isolates from the gut of animals. *Syst Appl Microbiol,* 24**,** 385-94.

SEIDLER, R. J. & STARR, M. P. (1969) Isolation and characterization of host-independent Bdellovibrios. *J Bacteriol,* 100**,** 769-85.

SHAEVITZ, J. W. & GITAI, Z. (2010) The Structure and Function of Bacterial Actin Homologs. *Cold Spring Harb Perspect Biol*.

SHANER, N. C., CAMPBELL, R. E., STEINBACH, P. A., GIEPMANS, B. N., PALMER, A. E. & TSIEN, R. Y. (2004) Improved monomeric red, orange and yellow fluorescent proteins derived from Discosoma sp. red fluorescent protein. *Nat Biotechnol,* 22**,** 1567-72.

SHANER, N. C., STEINBACH, P. A. & TSIEN, R. Y. (2005) A guide to choosing fluorescent proteins. *Nat Methods,* 2**,** 905-9.

SHIH, Y. L., LE, T. & ROTHFIELD, L. (2003) Division site selection in Escherichia coli involves dynamic redistribution of Min proteins within coiled structures that extend between the two cell poles. *Proc Natl Acad Sci U S A,* 100**,** 7865-70.

SHIH, Y. L. & ROTHFIELD, L. (2006) The bacterial cytoskeleton. *Microbiol Mol Biol Rev,* 70**,** 729-54.

SHILO, M. & BRUFF, B. (1965) Lysis of Gram-negative bacteria by host-independent ectoparasitic Bdellovibrio bacteriovorus isolates. *J Gen Microbiol,* 40**,** 317-28.

SIMON, R., PREIFER, U. & PUHLER, A. (1983) A broad host range mobilisation system for *in vivo* genetic engineering: transposon mutagenesis in gram negative bacteria. *Biotechnology,* 9**,** 184-191.

SIVANATHAN, V., ALLEN, M. D., DE BEKKER, C., BAKER, R., ARCISZEWSKA, L. K., FREUND, S. M., BYCROFT, M., LOWE, J. & SHERRATT, D. J. (2006) The FtsK gamma domain directs oriented DNA translocation by interacting with KOPS. *Nat Struct Mol Biol,* 13**,** 965-72.

SLOVAK, P. M., WADHAMS, G. H. & ARMITAGE, J. P. (2005) Localization of MreB in Rhodobacter sphaeroides under conditions causing changes in cell shape and membrane structure. *J Bacteriol,* 187**,** 54-64.

SOUTHERN, E. M. (1975) Detection of specific sequences among DNA fragments separated by gel electrophoresis. *J Mol Biol,* 98**,** 503-17.

STARR, M. P. & BAIGENT, N. L. (1966) Parasitic interaction of Bdellovibrio bacteriovorus with other bacteria. *J Bacteriol,* 91**,** 2006-17.

STEYERT, S. R., MESSING, S. A., AMZEL, L. M., GABELLI, S. B. & PINEIRO, S. A. (2008) Identification of Bdellovibrio bacteriovorus HD100 Bd0714 as a Nudix dGTPase. *J Bacteriol,* 190**,** 8215-9.

STOLP, H. & STARR, M. P. (1963) Bdellovibrio Bacteriovorus Gen. Et Sp. N., a Predatory, Ectoparasitic, and Bacteriolytic Microorganism. *Antonie Van Leeuwenhoek,* 29**,** 217-48.

STRALEY, S. C. & CONTI, S. F. (1974) Chemotaxis in Bdellovibrio bacteriovorus. *J Bacteriol,* 120**,** 549-51.

TAKACS, C. N., POGGIO, S., CHARBON, G., PUCHEAULT, M., VOLLMER, W. & JACOBS-WAGNER, C. (2010) MreB drives de novo rod morphogenesis in Caulobacter crescentus via remodeling of the cell wall. *J Bacteriol,* 192**,** 1671-84.

THOMASHOW, M. F. & RITTENBERG, S. C. (1978a) Intraperiplasmic growth of Bdellovibrio bacteriovorus 109J: attachment of long-chain fatty acids to escherichia coli peptidoglycan. *J Bacteriol,* 135**,** 1015-23.

THOMASHOW, M. F. & RITTENBERG, S. C. (1978b) Intraperiplasmic growth of Bdellovibrio bacteriovorus 109J: solubilization of Escherichia coli peptidoglycan. *J Bacteriol,* 135**,** 998-1007.

THOMPSON, J., HIGGINS, D. & GIBSON, T. (1994) CLUSTALW: improvements to sensitivity of progressive, multiple sequence alignment through sequence weighting, position-specific gap penalties and weight matrix choice. *NAR,* 22**,** 4673-4680.

TSIEN, R. Y. (1998) The green fluorescent protein. *Annu Rev Biochem,* 67**,** 509-44.

VARMA, A. & YOUNG, K. D. (2009) In Escherichia coli, MreB and FtsZ direct the synthesis of lateral cell wall via independent pathways that require PBP 2. *J Bacteriol,* 191**,** 3526-33.

VATS, P. & ROTHFIELD, L. (2007) Duplication and segregation of the actin (MreB) cytoskeleton during the prokaryotic cell cycle. *Proc Natl Acad Sci U S A,* 104**,** 17795-800.

VATS, P., SHIH, Y. L. & ROTHFIELD, L. (2009a) Assembly of the MreB-associated cytoskeletal ring of Escherichia coli. *Mol Microbiol,* 72**,** 170-82.

VATS, P., YU, J. & ROTHFIELD, L. (2009b) The dynamic nature of the bacterial cytoskeleton. *Cell Mol Life Sci,* 66**,** 3353-62.

VAUGHAN, S., WICKSTEAD, B., GULL, K. & ADDINALL, S. G. (2004) Molecular evolution of FtsZ protein sequences encoded within the genomes of archaea, bacteria, and eukaryota. *J Mol Evol,* 58**,** 19-29.

WAIDNER, B., SPECHT, M., DEMPWOLFF, F., HAEBERER, K., SCHAETZLE, S., SPETH, V., KIST, M. & GRAUMANN, P. L. (2009) A novel system of cytoskeletal elements in the human pathogen Helicobacter pylori. *PLoS Pathog,* 5**,** e1000669.

WERY, M., WOLDRINGH, C. L. & ROUVIERE-YANIV, J. (2001) HU-GFP and DAPI co-localize on the Escherichia coli nucleoid. *Biochimie,* 83**,** 193-200.

YANISCH-PERRON, C., VIEIRA, J. & MESSING, J. (1985) Improved M13 phage cloning vectors and host strains: nucleotide sequences of the M13mp18 and pUC19 vectors. *Gene,* 33**,** 103-19.

YATES, J., ZHEKOV, I., BAKER, R., EKLUND, B., SHERRATT, D. J. & ARCISZEWSKA, L. K. (2006) Dissection of a functional interaction between the DNA translocase, FtsK, and the XerD recombinase. *Mol Microbiol,* 59**,** 1754-66.

Appendix 2.1

DNA and protein markers used in this study

1Kb NEB ladder

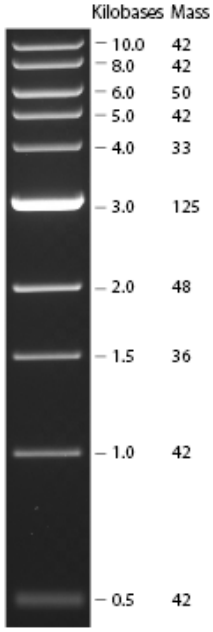

100bp NEB ladder

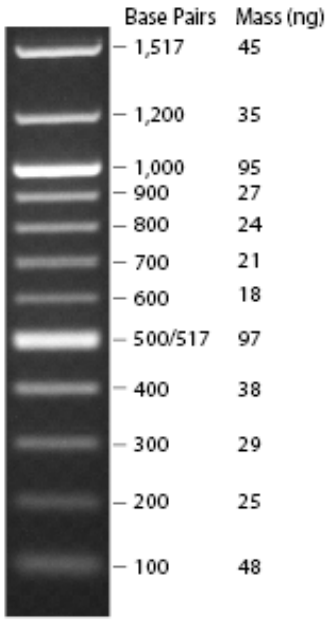

DNA Ladders visualised by ethidium bromide staining on a 1.3% TAE agarose gel. Mass values are for 0.5 µg/lane (Taken from www.neb.com).

Biotinylated NEB 2-Log DNA Ladder

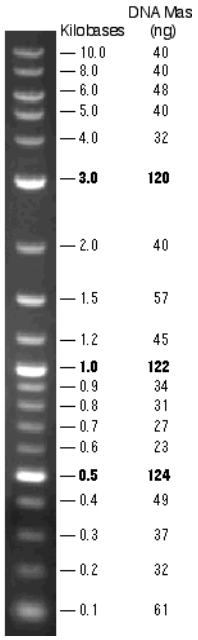

1.0 µg of 2-Log DNA Ladder visualized by ethidium bromide staining on a 1.0% TBE agarose gel (Taken from www.neb.com)

BenchMark Protein Ladder (Invitrogen)

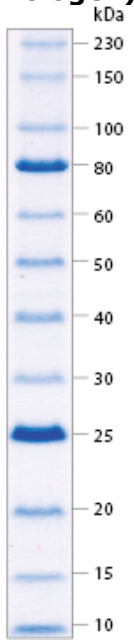

Protein ladder ran on a Invitrogen Novex 10-20% Tris-glycine SDS-PAGE gel. (Taken from www.neb.com)

```
CreS C.crescentus       ---MRLLSKNSRETKNGKPTVLGDEARAEAMQHQIESTQAIGQRYETIHGGLDSIGRVME
FilP S.coelicolor       ---------MSDTSPYG----------FELVRRGYDRAQVDERISKLVSDRDSALARITA
Ccrp1143 H.pylori       ----------MQENQTR----------PFICPKCQEPIDVNEALYKQIE--QENQNKFLA
Ccrp59 H.pylori         --------------MG-----------TFIEKCFGFYQVRKELEARISGLEDENAELFA
Bd1167 B.bacteriovorus  MSFNYQKNKEHSSDSFWTSYSDLFLGLSTIFLLLYVTSSLRTGTDALRGQVENQKLSMKV
Ccrp B.bacteriovorus    --MNHRRRFSMQVKPLG-----------TLLLAALMTGTMPLAAYAQVDSSQIEAEEATA
Clustal Consensus

CreS C.crescentus       HLKAIEPLIAEIRGPVSQEFEARRAEHAELIAVRANLDQAQRQIALIQAEEREVSARLAA
FilP S.coelicolor       LEKRIEELHLETQN-----------------AQAQVNDAEPSYAGLGARVEKILRLAEE
Ccrp1143 H.pylori       QQKEFEKEVNEKRAQYLS-------------YFKNLEQKEETLKEREKEQQAKFDEAVK
Ccrp59 H.pylori         ENEKLALGTSELKD------------------------ANNQLRQKNDKLFTTKENLTQ
Bd1167 B.bacteriovorus  EELENQLKMYENVKN-------------EYLASQAPKDEVQEYEELMDKLTLLQEDAKT
Ccrp B.bacteriovorus    DAEAAKAEANEAKKR----------------AEEDRKRRDKIRAESQSAINKARSLEND
Clustal Consensus                 *

CreS C.crescentus       AETALGESDARRQTQDAALEDNALEIDRLRNALLQSDLKVSSLDASLRDATARIEHLVQD
FilP S.coelicolor       EAKDLREEARRAAEQHRELAESSAQQVRNDAESYAAERKAKAEDEGVR----IVEKAKGD
Ccrp1143 H.pylori       QASALALQDERAKIIEEARKNAFLEQQKGLELLQKELDEKSKQVQELHQKEAEIERLKRE
Ccrp59 H.pylori         EKTELTEKNKVLTTEKGNLDNQLNASQKQVQALEQSQQVLENEKVELTNKITDLSKEKEN
Bd1167 B.bacteriovorus  EKERLIQEARENGEKVKALNKYQQMVRNVLNANKMAKSKLINRDDLIKEQDVEIETQETE
Ccrp B.bacteriovorus    AKKEQADSERESAKLKAETNEHDRAKTAAEKEQASAQARIKAAQEKTQKAIQIRDEAQAK
Clustal Consensus             .           .                                    .    .

CreS C.crescentus       VEGLRVQAQDIDARRGDAEAALARANQDNALLGEEAATLKKR----VDQAGLDLARLSRI
FilP S.coelicolor       ASQLRSEAQKDAQSKRDEADALFEETR-------------------------AKAAQA
Ccrp1143 H.pylori       NNEAESRLKAENEKKLNEKLDLEREKIEKALHEKNELKFKQQ------EEQLEMLRNELK
Ccrp59 H.pylori         LTKANTELKTENDKLNHQVIALTKEQD------------------------------
Bd1167 B.bacteriovorus  IADLNKDIQNKKQLIAQGEQKIAVTQAQLQKRLTELRVAYKNNKLSKQLFEQKMAQARAE
Ccrp B.bacteriovorus    RKQAESKADELRDQAKDQEKQANSATEAGLAATKEAEAAKNE----TLKAEQNLSKAKLL
Clustal Consensus           .   .       .

CreS C.crescentus       ETDLEAQLAAERARVQAVENALAAHQADSGRTIRGLESQVEANRAEISALQ-----TRLE
FilP S.coelicolor       AADFETNLAKRRE---QSERDLASRQAKAEKRLAEIEHRAEQLRLEAEKLR-----TDAE
Ccrp1143 H.pylori       NAQRKAELSSQQFQGEVQELAIEEFLRQKFPLDCIEEIKKGQRGGDCIQVVHT---REFQ
Ccrp59 H.pylori         -------------------SLKQERAQLQDAHGFLEELCANLEKDNQHLT-----DKLK
Bd1167 B.bacteriovorus  GNQKVAQLNQVNAQYQMQLNQANVQLGQVQGELSKTQGLLAQKEDEATHLAGALSRTKAE
Ccrp B.bacteriovorus    TQKAVAEAKAREAKAKQEIARAEADRARAEAEMSRLKAQDEQAKAMIEKVE-----DELK
Clustal Consensus                                         :           :        :

CreS C.crescentus       TATGRADKLEEMNGQISARLADSSAQQKAVERRA-GDLNVALERALDRIRALEEEADGLR
FilP S.coelicolor       RRAR--QTVETAQRQSEDIVADANAKADRIRSES-ERELAALTNRRDSINAQLTNVREML
Ccrp1143 H.pylori       NCGKIYYESKRTKEFQKAWVEKLKSDMREIGADVGVIVSEALPKEMERMGLFEGVWVCSF
Ccrp59 H.pylori         KLESAQKNLENSNDQLLQAIENIAEEKTELEREI-ARLKSLEATDKSELDLQNCRFKSAI
Bd1167 B.bacteriovorus  AGAKIAGLQQGFAEEKAALAAGFGKEKAKLQGAL-SDTQGQLAKARAEIEARKSVAGEIQ
Ccrp B.bacteriovorus    AAVDASKKAKEEAESERKKVAETKSQEEKLKQQA-AKARQELEGNRNNLRKEQATANLEI
Clustal Consensus               :               .   :                 :

CreS C.crescentus       QRHAGVDTARATAIER--------------ADQLAKSAVAQEKALKRAEERAQQLRARL
FilP S.coelicolor       ASLTGAAVAAAPSVE---------------DESVSRGVPAQQSR--------------
Ccrp1143 H.pylori       EEFKGLSAVLREGVIQVS------------LAKKSQENKGDKVNLLYHYLTSSEFSMQV
Ccrp59 H.pylori         EDLKRQNRKLEEENIA--------------LKERAYGLKEQPSKQPKP-----------
Bd1167 B.bacteriovorus  KGFAKAGIKADIDMQTGDVVLDFGQAYFDSDSDRLKHEMKGVLEKAMPIYSRSLFGNPKV
Ccrp B.bacteriovorus    ARSKKAIAEYESEVAR--------------SESELKRLTEETEKAKKERE---KLESRL
Clustal Consensus

CreS C.crescentus       DAMQEAQDQVRRDHEAKIAELQATIERLTSEAALAEGALEAARRDRSRLQMALLGASDGD
FilP S.coelicolor       ------------------------------------------------------------
Ccrp1143 H.pylori       NVIIEGFEQLRADLESEKRAMARIWKSREKQIDKVFEGTINMYGSIKGIAGNAIGQVKAL
Ccrp59 H.pylori         ------------------------------------------------------------
Bd1167 B.bacteriovorus  SDKISAVEIIGFASPTYQGRFVDPHSSKPADKAALKYNMDLSYRRANSIFSYMLDEGNMR
Ccrp B.bacteriovorus    DSAKNEAEEIRIKVATAKANFEAEESRLEAVKIRLDAGLKPKKKK--------------
Clustal Consensus

CreS C.crescentus       VAASA---------------------------------------------------
FilP S.coelicolor       ------------------------------------------------------------
Ccrp1143 H.pylori       ELGYDGEDLED---------------------------------------------
Ccrp59 H.pylori         ------------------------------------------------------------
Bd1167 B.bacteriovorus  FEHQRELLALMKVSGRSFLEVMKVQNRNVATAAEFCKQNDCKKAQRVIIRFNMDPKK
Ccrp B.bacteriovorus    ------------------------------------------------------------
Clustal Consensus
```

Appendix 3.1 Multiple protein alignment of *B. bacteriovorus* Ccrp and Bd1167against experimentally described Ccrp proteins from other bacterial species. Sequences were aligned using the online clustalW alignment program.

Appendix 3.2

A) Query: CreS *C. Crescentus*

B. bacteriovorus HD100 gene number	E-value	Predicted domains/Comments	Does this gene qualify as a *ccrp*?
Bd1169	2.6e-08	Predicted FHA domain	No
Bd2697	1.5e-07	No predicted domains, good coiled-coil prediction	Yes
Bd1158	8.0e-05	*smc* gene (known to contain coiled-coil regions)	No
Bd3341	0.0018	Predicted TarH super family and MA domain	No
Bd0121	0.0030	Predicted TarH super family and MA domain	No
Bd0544	0.0035	Predicted SMC_prok_B domain	No
Bd1340	0.0045	Predicted TarH domain	No
Bd2687	0.0047	Coiled-coil prediction less than 80 amino-acids	No
Bd0417	0.0058	No predicted coiled-coils	No

B) Query: Bd2697 Ccrp 'creS1' *B. bacteriovorus*

B. bacteriovorus HD100 gene number	E-value	Predicted domains/Comments	Does this gene qualify as a *ccrp*?
Bd3062	0.00019	*MAEBL* homologue	No
Bd1188	0.0022	Predicted ATP- synthase _B super family, KH-I super family and HDc super family domains	No
Bd3020	0.14	*motB* gene (known to contain coiled-coil regions)	No
Bd1169	0.19	Predicted FHA domain	No
Bd1907	0.21	No predicted coiled-coils	No
Bd3849	0.30	*rplU* gene	No
Bd1158	0.50	*smc* gene (known to contain coiled-coil regions)	No
Bd3903	0.52	*parA* gene (known to contain coiled-coil regions)	No
Bd3498	0.54	Coiled-coil prediction less than 80 amino-acids	No
Bd1646	0.57	No predicted coiled-coils	No

C) Query: Bd1167 'creS2' *B. bacteriovorus*

B. bacteriovorus HD100 gene number	E-value	Predicted domains/Comments	Does this gene qualify as a *ccrp*?
Bd2697	2.7e-09	No predicted domains, good coiled-coil prediction	Yes
Bd3284	8.5e-06	Predicted SMC domain	No
Bd1169	1.8e-05	Predicted FHA domain	No
Bd2100	0.00038	Predicted PRK00409 recombination and DNA strand exchange inhibitor protein domain	No
Bd1340	0.00059	Predicted TarH domain	No
Bd1473	0.0021	Predicted SMC_prok_B domain	No
Bd1158	0.0055	*smc* gene (known to contain coiled-coil regions)	No
Bd2110	0.016	*smc* gene (known to contain coiled-coil regions)	No
Bd1494	0.019	*ompH* gene	No

D) Query: Bd1169 *B. Bacteriovorus*

B. bacteriovorus HD100 gene number	E-value	Predicted domains/Comments	Does this gene qualify as a *ccrp*?
Bd2697	8.6e-12	No predicted domains, good coiled-coil prediction	Yes
Bd2616	9.1e-08	Predicted ompA domain	No
Bd1268	1.4e-06	Predicted ACD_sHsps-like domain	No
Bd3284	3.2e-06	Predicted SMC domain	No
Bd0161	4.6e-06	Predicted SMC_prok_A and B domain	No
Bd1158	6.6e-06	*smc* gene (known to contain coiled-coil regions)	No
Bd1167	1.8e-05	Predicted OmpA domain	No
Bd0544	5.9e-05	Predicted SMC_prok_B domain	No
Bd2100	8.9e-05	Predicted PRK00409 recombination and DNA strand exchange inhibitor protein domain	No

E) Query: Bd1158 *B. bacteriovorus*

B. bacteriovorus HD100 gene number	E-value	Predicted domains/Comments	Does this gene qualify as a *ccrp*?
Bd2697	1.2e-06	No predicted domains, good coiled-coil prediction	Yes
Bd2946	0.00034	Predicted TIGR03545 and 'IF' domains	No
Bd2110	0.00059	*smc* gene (known to contain coiled-coil regions)	No
Bd3173	0.0017	*recN* gene	No
Bd3192	0.0032	*mcp* gene (known to contain coiled-coil regions)	No
Bd0739	0.0041	Predicted SMC_prok_B domain	No
Bd1169	0.0044	Predicted FHA domain	No
Bd1188	0.0089	Predicted ATP-synthase_B super family, KH-I super family and HDc super family domains	No
Bd3284	0.013	Predicted SMC domain	No

Appendix 3.2. Exhaustive search of *B. bacteriovorus* HD100 genome for genes encoding Coiled-coil-repeat-proteins (Ccrp). *B. bacteriovorus* genes qualified as *ccrps* if they had a coiled-coil prediction over 80 amino-acids long and did not contain any predicted functional domains, this criteria was set out by (Bagchi et al., 2008). Tables display analyses of all non-self BLASTp hits (regardless of e-value) using query protein sequences against the translated HD100 genome using Wu-BLAST v2.0 (http://blast.jcvi.org/cmr-blast/). COILS prediction carried out using the COILS program: (http://www.ch.embnet.org/software/COILS_form.html). Predicted protein domains were identified using the ncbi conserved domains database: CCD-37014 (http://www.ncbi.nlm.nih.gov/Structure/cdd/wrpsb.cgi) and Pfam v24.0 (http://pfam.sanger.ac.uk/).

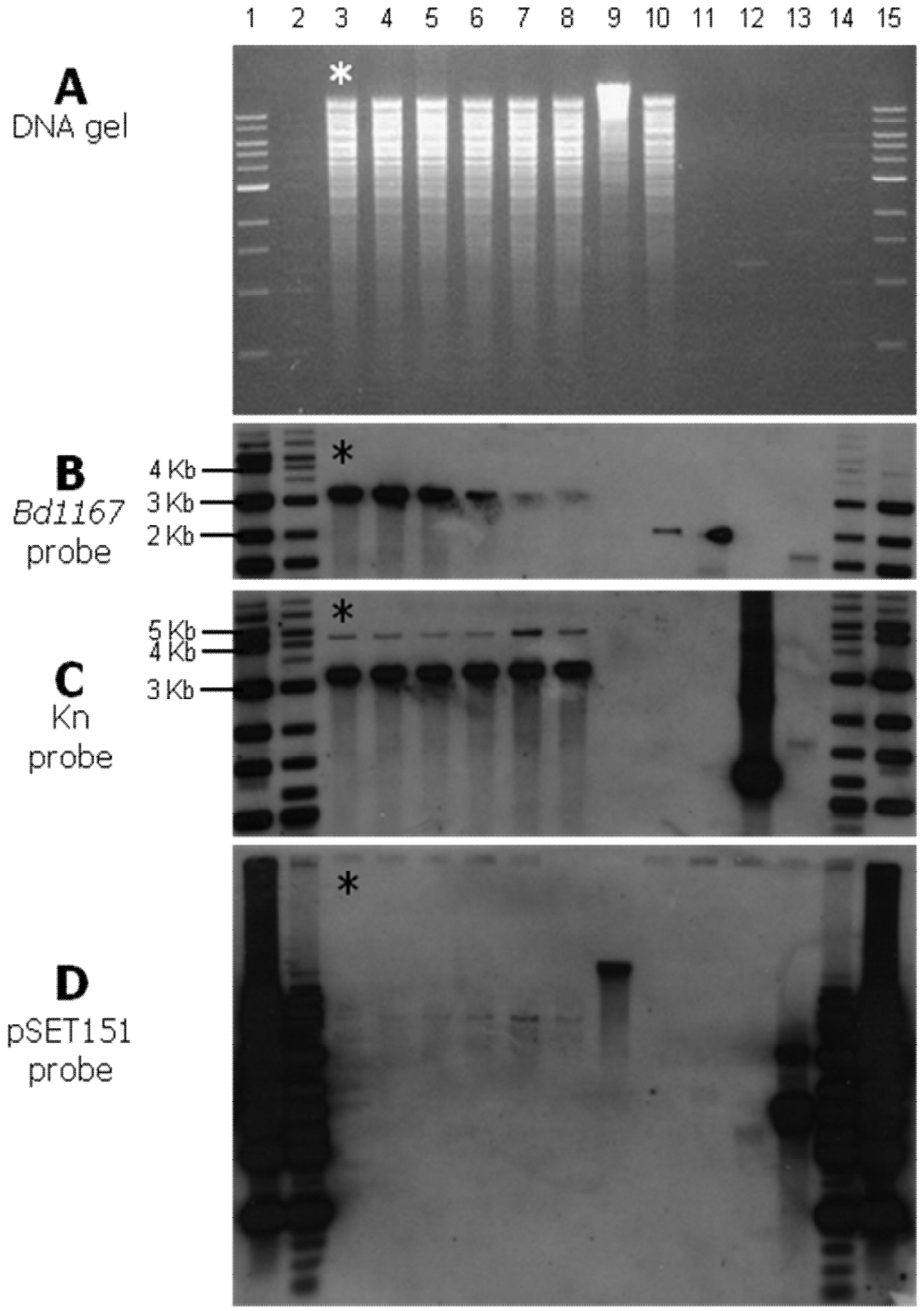

Appendix 3.3 Southern blot confirmation of the *Bd1167*::Kn deletion strain. Three identical DNA gels with BamHI digested of genomic DNA isolated from pAKF15 exconjugant strains (**A**) were run in triplicate and used for three Southern Blots using probes that bind to: the *Bd1167* ORF, kanamycin cassette (Kn) and pSET151 backbone (see section 2.7 for methods). Lane order for gel and all blots: 1 = 1kb NEB ladder, 2 = biotinylated 2-log NEB ladder 3-8 = *Bd1167* KO candidates, 9 S17-1 control, 10 = wt HD100, 11 = unlabeled *Bd1167* probe, 12 = unlabeled Kn probe, 13 = unlabeled pSET151 probe, 14 = biotinylated 2-log NEB ladder, 15 = 1kb NEB ladder. Inhibited DNA transfer on the *Bd1167* blot has limited signal intensity in lanes 5-11, the 4.5 kb bands in the candidate lanes (3-8) on the Kn blot are the result of incomplete genomic DNA digestion, faint non-specific bands are also visible on the pSET151 blot. All candidates (lanes 3-8) show the expected gel shift from 2.1 kb to 3.4 kb on the *Bd1167* blot (**B**), a 3.4 kb band on the Kn blot (**C**), and no pSET151 bands (D). The highlighted candidate (*) was used for phenotyping.

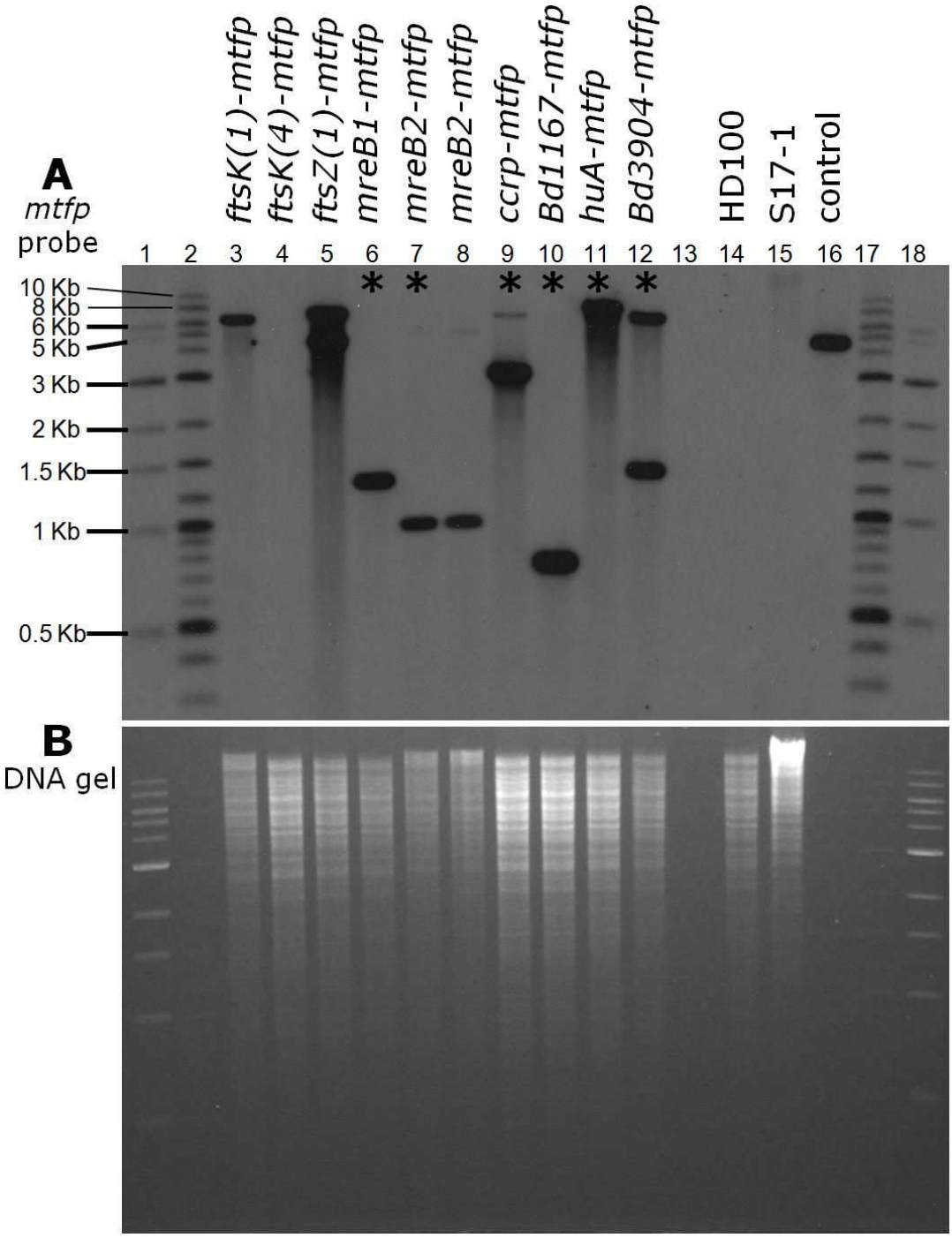

Appendix 3.4 Diagnostic Southern blot showing all mTFP fusion strains used in this study. (**A**) Southern blot using a probe that binds to the genome integrated *mtfp* ORF, DNA in all but the ladder lanes were digested with BamHI. Exconjugant strains highlighted with an (*) show the expected mTFP banding pattern and used for further study. (**B**)Corresponding DNA gel used for Southern blot. Lane order and for both gel/blot and *mtfp* expected band(s) size: 1= 1kb NEB ladder, 2= biotinylated 2-log NEB ladder, 3= HD100 *ftsK1-1mtfp* 3.5 kb band, 4 = HD100 *ftsK1-4mtfp* 4.2 kb band, 5= HD100 *ftsZ1-1mtfp* 2.8 kb band, 6= HD100 *mreB1-mtfp* 1.3 kb band, 7-8= HD100 *mreB2-mtfp* exconjugants 1 and 2 0.9 kb band, 9= HD100 *ccrp-mtfp* 3.1 kb band, 10 = HD100 *Bd1167-mtfp* 0.75 kb band, 11= HD100 *huA-mtfp* 9.4 kb band, 12 = HD100 *Bd3904-mtfp* 1.4 kb and 7.8 kb bands, 13= Blank, 14= wtHD100, 15= S17-1 pZMR100, 16= linear pAKF04 plasmid, 17= biotinylated 2-log NEB ladder, 18 = 1kb NEB ladder.

Appendix 3.5

A

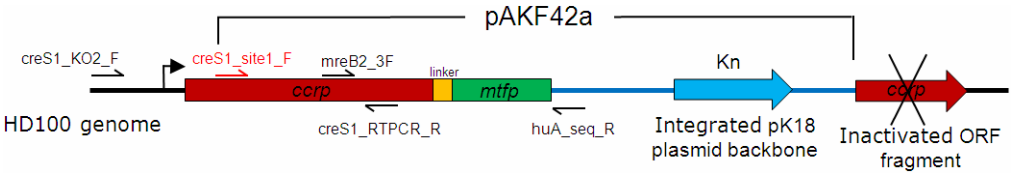

B

```
pAKF42a in HD100   GGCTCCTTGAAAGATCACTTCAGGCACAGTTGTGGTTCAACGCTGACTGGTTCAGGCAGG
creS1_KO2_F        ------------------------------TGGGTTCACGCTGACTGGTTCAGGCAGG
creS1_RTPCR_R      ------------------------------------------------------------
creS1_site1_F      ------------------------------------------------------------
huA_seq_R          ------------------------------------------------------------

pAKF42a in HD100   GCCGGGATGTCTGCTTCGGTAATTGGAGTGAGCTCGTCAGCATCGGTAAAATCAGTGGCA
creS1_KO2_F        GCCGGGATGTCTGCTTCGGTAATTGGAGTGAGCTCGTCAGCATCGGTAAAATCAGTGGCA
creS1_RTPCR_R      ------------------------------------------------------------
creS1_site1_F      ------------------------------------------------------------
huA_seq_R          ------------------------------------------------------------

pAKF42a in HD100   CGAGTCTCCGCCGTAGAACCGTCACCGCCCGCGTTGGCAACGTACAGGGTGTTGTTCTGA
creS1_KO2_F        CGAGTCTCCGCCGTAGAACCGTCACCGCCCGCGTTGGCAACGTACAGGGTGTTGTTCTGA
creS1_RTPCR_R      ------------------------------------------------------------
creS1_site1_F      ------------------------------------------------------------
huA_seq_R          ------------------------------------------------------------

pAKF42a in HD100   ATTTTAAAGGTGGAATAGAATTCCGTGCAACTTAGGAAGGACATGAATTCCTGAGTCAGC
creS1_KO2_F        ATTTTAAAGGTGGAATAGAATTCCGTGCAACTTAGGAAGGACATGAATTCCTGAGTCAGC
creS1_RTPCR_R      ------------------------------------------------------------
creS1_site1_F      ------------------------------------------------------------
huA_seq_R          ------------------------------------------------------------

pAKF42a in HD100   GGGCTTTCTGTAACTACAGTGCCAAGAGTGAAAGTGCCGTTGGTTGGGCCATTGGCTGAA
creS1_KO2_F        GGGCTTTCTGTAACTACAGTGCCAAGAGTGAAAGTGCCGTTGGTTGGGCCATTGGCTGAA
creS1_RTPCR_R      ------------------------------------------------------------
creS1_site1_F      ------------------------------------------------------------
huA_seq_R          ------------------------------------------------------------

pAKF42a in HD100   ATAGGTTCACCAGAGCAGGTGGTGCCATCGAACTTGTAAGTGGTTTTTGTCAGAGTGCCG
creS1_KO2_F        ATAGGTTCACCAGAGCAGGTGGTGCCATCGAACTTGTAAGTGGTTTTTGTCAGAGTGCCG
creS1_RTPCR_R      ------------------------------------------------------------
creS1_site1_F      ------------------------------------------------------------
huA_seq_R          ------------------------------------------------------------

pAKF42a in HD100   TCGTCAGCGAAATGCAGGATGGCGTAATCGCTATAACCACTGCGGCCATTGTCGATGATG
creS1_KO2_F        TCGTCAGCGAAATGCAGGATGGCGTAATCGCTATAACCACTGCGGCCATTGTCGATGATG
creS1_RTPCR_R      ------------------------------------------------------------
creS1_site1_F      ------------------------------------------------------------
huA_seq_R          ------------------------------------------------------------

pAKF42a in HD100   CATTCACCTTTCCAATATCCCGTCAGTTCAGGCTCGGTGGTGGAGCCGGGATTGGAACTG
creS1_KO2_F        CATTCACCTTTCCAATATCCCGTCAGTTCAGGCTCGGTGGTGGAGCCGGGATTGGAACTG
creS1_RTPCR_R      ------------------------------------------------------------
creS1_site1_F      ------------------------------------------------------------
huA_seq_R          ------------------------------------------------------------

pAKF42a in HD100   CTGTTAGAGCACGCCACTGCTGTCAGAAGAGAAGCTGCGATCACGATGTTCAAACTCATT
creS1_KO2_F        CTGTTAGAGCACGCCACTGCTGTCAGAAGAGAAGCTGCGATCACGATGTTCAAACTCATT
creS1_RTPCR_R      ------------------------------------------------------------
creS1_site1_F      ------------------------------------------------------------
huA_seq_R          ------------------------------------------------------------

pAKF42a in HD100   TTTAGGTGTTTCACTCTTGTCCTTTCAAACCGTTCTTGGTTTTCTTTGTTTACAGTGGGG
creS1_KO2_F        TTTAGGTGTTTCACTCTTGTCCTTTCAAACCGTTCTTGGTTTTCTTTGTTTACAGTGGGG
creS1_RTPCR_R      ------------------------------------------------------------
creS1_site1_F      ------------------------------------------------------------
huA_seq_R          ------------------------------------------------------------
```

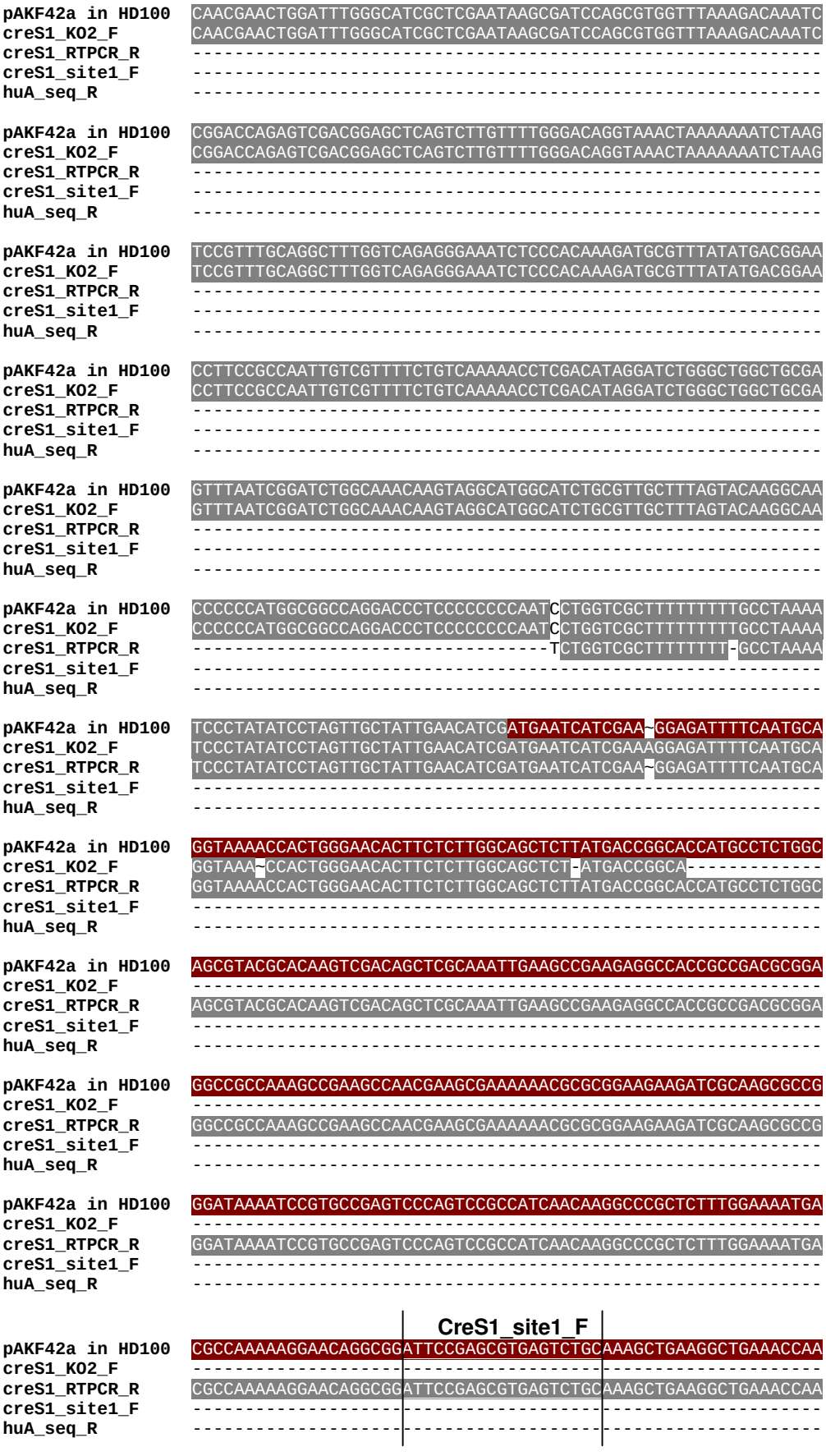
pAKF42a in HD100
creS1_KO2_F
creS1_RTPCR_R
creS1_site1_F
huA_seq_R
CreS1_site1_F

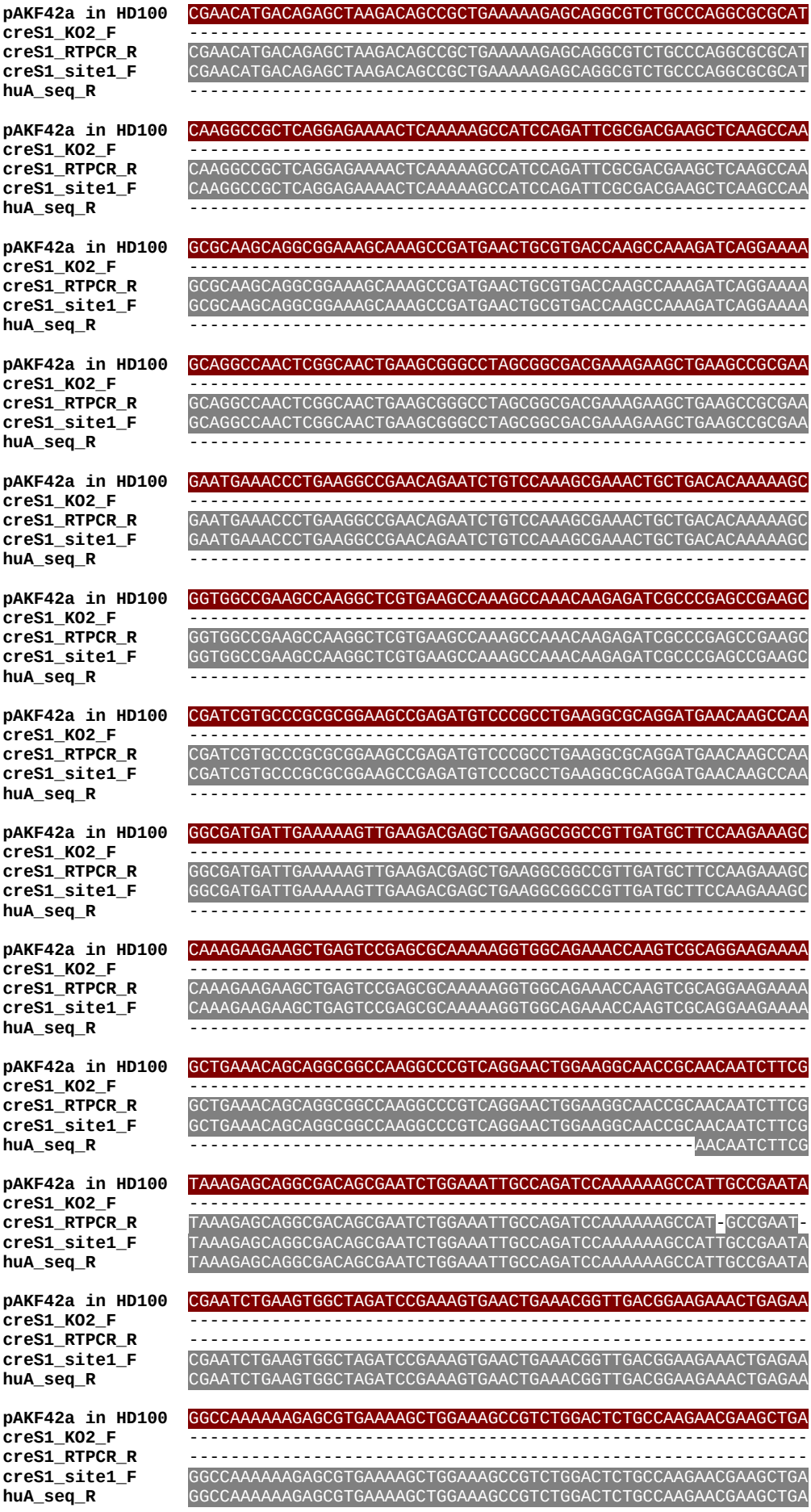
pAKF42a in HD100 CGAACATGACAGAGCTAAGACAGCCGCTGAAAAAGAGCAGGCGTCTGCCCAGGCGCGCAT
creS1_KO2_F ----------
creS1_RTPCR_R CGAACATGACAGAGCTAAGACAGCCGCTGAAAAAGAGCAGGCGTCTGCCCAGGCGCGCAT
creS1_site1_F CGAACATGACAGAGCTAAGACAGCCGCTGAAAAAGAGCAGGCGTCTGCCCAGGCGCGCAT
huA_seq_R ----------
pAKF42a in HD100 CAAGGCCGCTCAGGAGAAAACTCAAAAAGCCATCCAGATTCGCGACGAAGCTCAAGCCAA
creS1_KO2_F ----------
creS1_RTPCR_R CAAGGCCGCTCAGGAGAAAACTCAAAAAGCCATCCAGATTCGCGACGAAGCTCAAGCCAA
creS1_site1_F CAAGGCCGCTCAGGAGAAAACTCAAAAAGCCATCCAGATTCGCGACGAAGCTCAAGCCAA
huA_seq_R ----------
pAKF42a in HD100 GCGCAAGCAGGCGGAAAGCAAAGCCGATGAACTGCGTGACCAAGCCAAAGATCAGGAAAA
creS1_KO2_F ----------
creS1_RTPCR_R GCGCAAGCAGGCGGAAAGCAAAGCCGATGAACTGCGTGACCAAGCCAAAGATCAGGAAAA
creS1_site1_F GCGCAAGCAGGCGGAAAGCAAAGCCGATGAACTGCGTGACCAAGCCAAAGATCAGGAAAA
huA_seq_R ----------
pAKF42a in HD100 GCAGGCCAACTCGGCAACTGAAGCGGGCCTAGCGGCGACGAAAGAAGCTGAAGCCGCGAA
creS1_KO2_F ----------
creS1_RTPCR_R GCAGGCCAACTCGGCAACTGAAGCGGGCCTAGCGGCGACGAAAGAAGCTGAAGCCGCGAA
creS1_site1_F GCAGGCCAACTCGGCAACTGAAGCGGGCCTAGCGGCGACGAAAGAAGCTGAAGCCGCGAA
huA_seq_R ----------
pAKF42a in HD100 GAATGAAACCCTGAAGGCCGAACAGAATCTGTCCAAAGCGAAACTGCTGACACAAAAAGC
creS1_KO2_F ----------
creS1_RTPCR_R GAATGAAACCCTGAAGGCCGAACAGAATCTGTCCAAAGCGAAACTGCTGACACAAAAAGC
creS1_site1_F GAATGAAACCCTGAAGGCCGAACAGAATCTGTCCAAAGCGAAACTGCTGACACAAAAAGC
huA_seq_R ----------
pAKF42a in HD100 GGTGGCCGAAGCCAAGGCTCGTGAAGCCAAAGCCAAACAAGAGATCGCCCGAGCCGAAGC
creS1_KO2_F ----------
creS1_RTPCR_R GGTGGCCGAAGCCAAGGCTCGTGAAGCCAAAGCCAAACAAGAGATCGCCCGAGCCGAAGC
creS1_site1_F GGTGGCCGAAGCCAAGGCTCGTGAAGCCAAAGCCAAACAAGAGATCGCCCGAGCCGAAGC
huA_seq_R ----------
pAKF42a in HD100 CGATCGTGCCCGCGCGGAAGCCGAGATGTCCCGCCTGAAGGCGCAGGATGAACAAGCCAA
creS1_KO2_F ----------
creS1_RTPCR_R CGATCGTGCCCGCGCGGAAGCCGAGATGTCCCGCCTGAAGGCGCAGGATGAACAAGCCAA
creS1_site1_F CGATCGTGCCCGCGCGGAAGCCGAGATGTCCCGCCTGAAGGCGCAGGATGAACAAGCCAA
huA_seq_R ----------
pAKF42a in HD100 GGCGATGATTGAAAAAGTTGAAGACGAGCTGAAGGCGGCCGTTGATGCTTCCAAGAAAGC
creS1_KO2_F ----------
creS1_RTPCR_R GGCGATGATTGAAAAAGTTGAAGACGAGCTGAAGGCGGCCGTTGATGCTTCCAAGAAAGC
creS1_site1_F GGCGATGATTGAAAAAGTTGAAGACGAGCTGAAGGCGGCCGTTGATGCTTCCAAGAAAGC
huA_seq_R ----------
pAKF42a in HD100 CAAAGAAGAAGCTGAGTCCGAGCGCAAAAAGGTGGCAGAAACCAAGTCGCAGGAAGAAAA
creS1_KO2_F ----------
creS1_RTPCR_R CAAAGAAGAAGCTGAGTCCGAGCGCAAAAAGGTGGCAGAAACCAAGTCGCAGGAAGAAAA
creS1_site1_F CAAAGAAGAAGCTGAGTCCGAGCGCAAAAAGGTGGCAGAAACCAAGTCGCAGGAAGAAAA
huA_seq_R ----------
pAKF42a in HD100 GCTGAAACAGCAGGCGGCCAAGGCCCGTCAGGAACTGGAAGGCAACCGCAACAATCTTCG
creS1_KO2_F ----------
creS1_RTPCR_R GCTGAAACAGCAGGCGGCCAAGGCCCGTCAGGAACTGGAAGGCAACCGCAACAATCTTCG
creS1_site1_F GCTGAAACAGCAGGCGGCCAAGGCCCGTCAGGAACTGGAAGGCAACCGCAACAATCTTCG
huA_seq_R ----------AACAATCTTCG
pAKF42a in HD100 TAAAGAGCAGGCGACAGCGAATCTGGAAATTGCCAGATCCAAAAAAGCCATTGCCGAATA
creS1_KO2_F ----------
creS1_RTPCR_R TAAAGAGCAGGCGACAGCGAATCTGGAAATTGCCAGATCCAAAAAAGCCAT-GCCGAAT-
creS1_site1_F TAAAGAGCAGGCGACAGCGAATCTGGAAATTGCCAGATCCAAAAAAGCCATTGCCGAATA
huA_seq_R TAAAGAGCAGGCGACAGCGAATCTGGAAATTGCCAGATCCAAAAAAGCCATTGCCGAATA
pAKF42a in HD100 CGAATCTGAAGTGGCTAGATCCGAAAGTGAACTGAAACGGTTGACGGAAGAAACTGAGAA
creS1_KO2_F ----------
creS1_RTPCR_R ----------
creS1_site1_F CGAATCTGAAGTGGCTAGATCCGAAAGTGAACTGAAACGGTTGACGGAAGAAACTGAGAA
huA_seq_R CGAATCTGAAGTGGCTAGATCCGAAAGTGAACTGAAACGGTTGACGGAAGAAACTGAGAA
pAKF42a in HD100 GGCCAAAAAAGAGCGTGAAAAGCTGGAAAGCCGTCTGGACTCTGCCAAGAACGAAGCTGA
creS1_KO2_F ----------
creS1_RTPCR_R ----------
creS1_site1_F GGCCAAAAAAGAGCGTGAAAAGCTGGAAAGCCGTCTGGACTCTGCCAAGAACGAAGCTGA
huA_seq_R GGCCAAAAAAGAGCGTGAAAAGCTGGAAAGCCGTCTGGACTCTGCCAAGAACGAAGCTGA

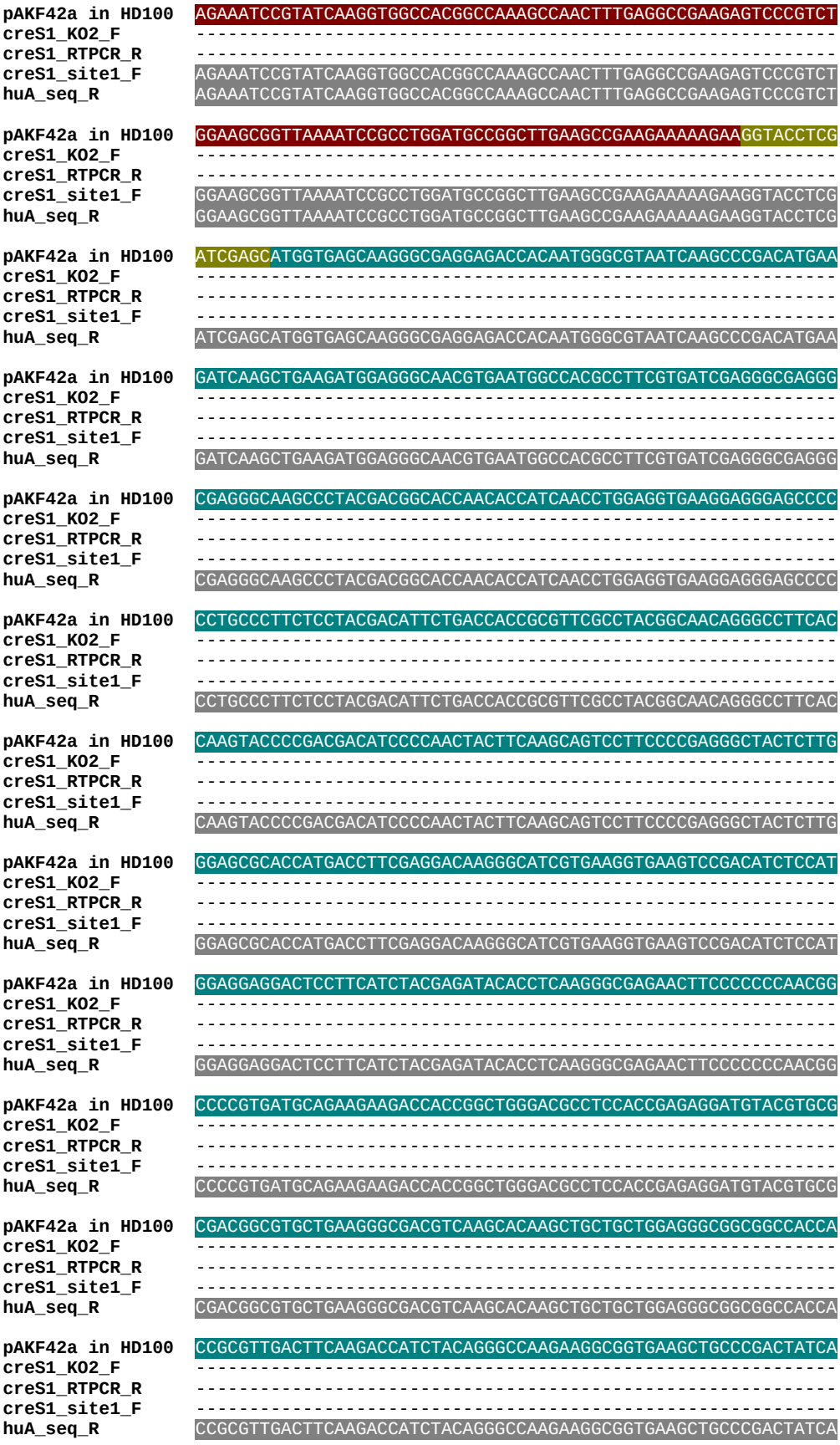
pAKF42a in HD100 AGAAATCCGTATCAAGGTGGCCACGGCCAAAGCCAACTTTGAGGCCGAAGAGTCCCGTCT
creS1_KO2_F ----------
creS1_RTPCR_R ----------
creS1_site1_F AGAAATCCGTATCAAGGTGGCCACGGCCAAAGCCAACTTTGAGGCCGAAGAGTCCCGTCT
huA_seq_R AGAAATCCGTATCAAGGTGGCCACGGCCAAAGCCAACTTTGAGGCCGAAGAGTCCCGTCT
pAKF42a in HD100 GGAAGCGGTTAAAATCCGCCTGGATGCCGGCTTGAAGCCGAAGAAAAAGAAGGTACCTCG
creS1_KO2_F ----------
creS1_RTPCR_R ----------
creS1_site1_F GGAAGCGGTTAAAATCCGCCTGGATGCCGGCTTGAAGCCGAAGAAAAAGAAGGTACCTCG
huA_seq_R GGAAGCGGTTAAAATCCGCCTGGATGCCGGCTTGAAGCCGAAGAAAAAGAAGGTACCTCG
pAKF42a in HD100 ATCGAGCATGGTGAGCAAGGGCGAGGAGACCACAATGGGCGTAATCAAGCCCGACATGAA
creS1_KO2_F ----------
creS1_RTPCR_R ----------
creS1_site1_F ----------
huA_seq_R ATCGAGCATGGTGAGCAAGGGCGAGGAGACCACAATGGGCGTAATCAAGCCCGACATGAA
pAKF42a in HD100 GATCAAGCTGAAGATGGAGGGCAACGTGAATGGCCACGCCTTCGTGATCGAGGGCGAGGG
creS1_KO2_F ----------
creS1_RTPCR_R ----------
creS1_site1_F ----------
huA_seq_R GATCAAGCTGAAGATGGAGGGCAACGTGAATGGCCACGCCTTCGTGATCGAGGGCGAGGG
pAKF42a in HD100 CGAGGGCAAGCCCTACGACGGCACCAACACCATCAACCTGGAGGTGAAGGAGGGAGCCCC
creS1_KO2_F ----------
creS1_RTPCR_R ----------
creS1_site1_F ----------
huA_seq_R CGAGGGCAAGCCCTACGACGGCACCAACACCATCAACCTGGAGGTGAAGGAGGGAGCCCC
pAKF42a in HD100 CCTGCCCTTCTCCTACGACATTCTGACCACCGCGTTCGCCTACGGCAACAGGGCCTTCAC
creS1_KO2_F ----------
creS1_RTPCR_R ----------
creS1_site1_F ----------
huA_seq_R CCTGCCCTTCTCCTACGACATTCTGACCACCGCGTTCGCCTACGGCAACAGGGCCTTCAC
pAKF42a in HD100 CAAGTACCCCGACGACATCCCCAACTACTTCAAGCAGTCCTTCCCCGAGGGCTACTCTTG
creS1_KO2_F ----------
creS1_RTPCR_R ----------
creS1_site1_F ----------
huA_seq_R CAAGTACCCCGACGACATCCCCAACTACTTCAAGCAGTCCTTCCCCGAGGGCTACTCTTG
pAKF42a in HD100 GGAGCGCACCATGACCTTCGAGGACAAGGGCATCGTGAAGGTGAAGTCCGACATCTCCAT
creS1_KO2_F ----------
creS1_RTPCR_R ----------
creS1_site1_F ----------
huA_seq_R GGAGCGCACCATGACCTTCGAGGACAAGGGCATCGTGAAGGTGAAGTCCGACATCTCCAT
pAKF42a in HD100 GGAGGAGGACTCCTTCATCTACGAGATACACCTCAAGGGCGAGAACTTCCCCCCCAACGG
creS1_KO2_F ----------
creS1_RTPCR_R ----------
creS1_site1_F ----------
huA_seq_R GGAGGAGGACTCCTTCATCTACGAGATACACCTCAAGGGCGAGAACTTCCCCCCCAACGG
pAKF42a in HD100 CCCCGTGATGCAGAAGAAGACCACCGGCTGGGACGCCTCCACCGAGAGGATGTACGTGCG
creS1_KO2_F ----------
creS1_RTPCR_R ----------
creS1_site1_F ----------
huA_seq_R CCCCGTGATGCAGAAGAAGACCACCGGCTGGGACGCCTCCACCGAGAGGATGTACGTGCG
pAKF42a in HD100 CGACGGCGTGCTGAAGGGCGACGTCAAGCACAAGCTGCTGCTGGAGGGCGGCGGCCACCA
creS1_KO2_F ----------
creS1_RTPCR_R ----------
creS1_site1_F ----------
huA_seq_R CGACGGCGTGCTGAAGGGCGACGTCAAGCACAAGCTGCTGCTGGAGGGCGGCGGCCACCA
pAKF42a in HD100 CCGCGTTGACTTCAAGACCATCTACAGGGCCAAGAAGGCGGTGAAGCTGCCCGACTATCA
creS1_KO2_F ----------
creS1_RTPCR_R ----------
creS1_site1_F ----------
huA_seq_R CCGCGTTGACTTCAAGACCATCTACAGGGCCAAGAAGGCGGTGAAGCTGCCCGACTATCA

Appendix 3.5 Confirmatory sequencing data for the *ccrp-mtfp* HD100 strain. This strain contains the pAKF42a integrated plasmid which has a pK18 backbone used to confer kanamycin (Kn) resistance to exconjugants (For general recombination diagram see Fig 2.1A). Direct sequencing confirms the *ccrp-mtfp* full ORF sequence and verifies the genomic context of the integrated pAKF42a plasmid using primers that bind outside of the construct (which begins at the highlighted CreS1_site1_F primer binding site). All sequencing reactions were conducted directly on genome amplified PCR products using the primers: creS1_KO2_F and huA_seq_R. (**A**) Diagrammatic representation of the expected pAKF40a HD100 excongugant genome and all primers used for both amplification and direct sequencing, CreS1_site1_F primer is highlighted in red. (**B**) Multiply aligned sequencing data *ccrp*, *linker* and *mtfp* regions are highlighted in the same colours as (A), primers used for each reaction are shown. CreS1_site1_F primer binding site is highlighted and underlined.

Appendix 4.1

A

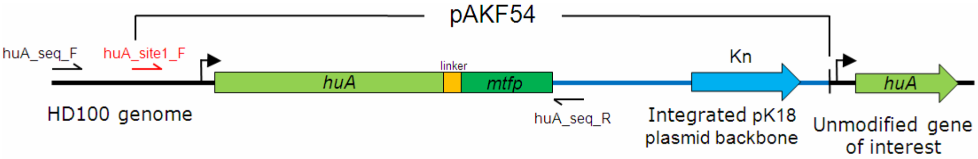

B

```
                                                         huA_site1_F
pAKF54 in HD100  GCGGTCAATTTCATAAGAAAGCACATCGGCTTCTTTGATCAGACCCTTTTCACTCACAAC
huA_seq_F        ---------------------------------------------------CCTCACAAC
huA_seq_R        ------------------------------------------------------------

pAKF54 in HD100  AACCTTGCCCTCGGTATCACGGAACTCCGTTAGCGTCTGCAACCCATCGGTCTGGGGGGC
huA_seq_F        AACCTTGCCCTCGGTATCACGGAACTCCGTTAGCGTCTGCAACCCATCGGTCTGGGGGGC
huA_seq_R        ------------------------------------------------------------

pAKF54 in HD100  AAGATCCACATTCAGAGTAAAAAGAGTTTTTTGGCGATTTGATTTCAAATCATACAGAGT
huA_seq_F        AAGATCCACATTCAGAGTAAAAAGAGTTTTTTGGCGATTTGATTTCAAATCATACAGAGT
huA_seq_R        ------------------------------------------------------------

pAKF54 in HD100  TGCGGAAGAATACGTTTGCGCAAATCCAAAAACCGGAAACAAAAGTGCAAGAACGAATAC
huA_seq_F        TGCGGAAGAATACGTTTGCGCAAATCCAAAAACCGGAAACAAAAGTGCAAGAACGAATAC
huA_seq_R        ------------------------------------------------------------

pAKF54 in HD100  CATAAAACCCCCGATCGAAAGTCCATAGTACCCAATAGATAAGAAAATAAAAAGCATGAC
huA_seq_F        CATAAAACCCCCGATCGAAAGTCCATAGTACCCAATAGATAAGAAAATAAAAAGCATGAC
huA_seq_R        ------------------------------------------------------------

pAKF54 in HD100  ACTTAACAGCCATTATTTTCTGCAATACATCCTGGACCGAAAAATTTCATTTAACTTGAC
huA_seq_F        ACTTAACAGCCATTATTTTCTGCAATACATCCTGGACCGAAAAATTTCATTTAACTTGAC
huA_seq_R        ------------------------------------------------------------

pAKF54 in HD100  CATCCCGACCATGAAAATTAGGGTAAGTTCCTTCGGGATGAGGATTGAAAAGCTATGAAT
huA_seq_F        CATCCCGACCATGAAAATTAGGGTAAGTTCCTTCGGGATGAGGATTGAAAAGCTATGAAT
huA_seq_R        -------------------------AGTTCCTTCGGGATGAGGATTGAAAAGCTATGAAT

pAKF54 in HD100  AAAGCCCAATTGGTGGAACTGGTCGCAGAAAAAAACAAAGACAACCAAAAGTCAATCCGAA
huA_seq_F        AAAGCCCAATTGGTGGAACTGGTCGCAGAAAAAAACAAAGACAACCAAAAGTCAATCCGAA
huA_seq_R        AAAGCCCAATTGGTGGAACTGGTCGCAGAAAAAAACAAAGACAACCAAAAGTCAATCCGAA

pAKF54 in HD100  CTGATTCTCGACGCCACTCTGGAAGCCATTCAGGAAGCTCTCAAAGACGGTGATGAGGTC
huA_seq_F        CTGATTCTCGACGCCACTCTGGAAGCCATTCAGGAAGCTCTCAAAGACGGTGATGAGGTC
huA_seq_R        CTGATTCTCGACGCCACTCTGGAAGCCATTCAGGAAGCTCTCAAAGACGGTGATGAGGTC

pAKF54 in HD100  AAACTGGTTGGCTTTGGCACTTTCTCCAGAAGCTCCCGCAAAGCCCGCCAGGGACGCAAT
huA_seq_F        AAACTGGTTGGCTTTGGCACTTTCTCCAGAAGCTCCCGCAAAGCCCGCCAGGGACGCAAT
huA_seq_R        AAACTGGTTGGCTTTGGCACTTTCTCCAGAAGCTCCCGCAAAGCCCGCCAGGGACGCAAT

pAKF54 in HD100  CCCAAAACAGGCGAAACGGTCAAAATTCCCAGCGCCTACATCCCCAAGTTCAAACCGGGC
huA_seq_F        CCCAAAACAGGCGAAACGGTCAAAATTCCCAGCGCCTACATCCCCAAGTTCAAACCGGGC
huA_seq_R        CCCAAAACAGGCGAAACGGTCAAAATTCCCAGCGCCTACATCCCCAAGTTCAAACCGGGC

pAKF54 in HD100  AAAGACTTAAAAGACGCCCTTAACGGTACCTCGAGCATGGTGAGCAAGGGCGAGGAGACC
huA_seq_F        AAAGACTTAAAAGACGCCCTTAACGGTACCTCGAGCATGGTGAGCAAGGGCGAGGAGACC
huA_seq_R        AAAGACTTAAAAGACGCCCTTAACGGTACCTCGAGCATGGTGAGCAAGGGCGAGGAGACC

pAKF54 in HD100  ACAATGGGCGTAATCAAGCCCGACATGAAGATCAAGCTGAAGATGGAGGGCAACGTGAAT
huA_seq_F        ACAATGGGCGTAATCAAGCCCGACATGAAGATCAAGCTGAAGATGGAGGGCAACGTGAAT
huA_seq_R        ACAATGGGCGTAATCAAGCCCGACATGAAGATCAAGCTGAAGATGGAGGGCAACGTGAAT

pAKF54 in HD100  GGCCACGCCTTCGTGATCGAGGGCGAGGGCGAGGGCAAGCCCTACGACGGCACCAACACC
huA_seq_F        GGCCACGCCTTCGTGATCGAGGGCGAGGGCGAGGGCAAGCCCTACGACGGCACCAACACC
huA_seq_R        GGCCACGCCTTCGTGATCGAGGGCGAGGGCGAGGGCAAGCCCTACGACGGCACCAACACC

pAKF54 in HD100  ATCAACCTGGAGGTGAAGGAGGGAGCCCCCCTGCCCTTCTCCTACGACATTCTGACCACC
huA_seq_F        ATCAACCTGGAGGTGAAGGAGGGAGCCCCCCTGCCCTTCTCCTACGACATTCTGACCACC
huA_seq_R        ATCAACCTGGAGGTGAAGGAGGGAGCCCCCCTGCCCTTCTCCTACGACATTCTGACCACC
```

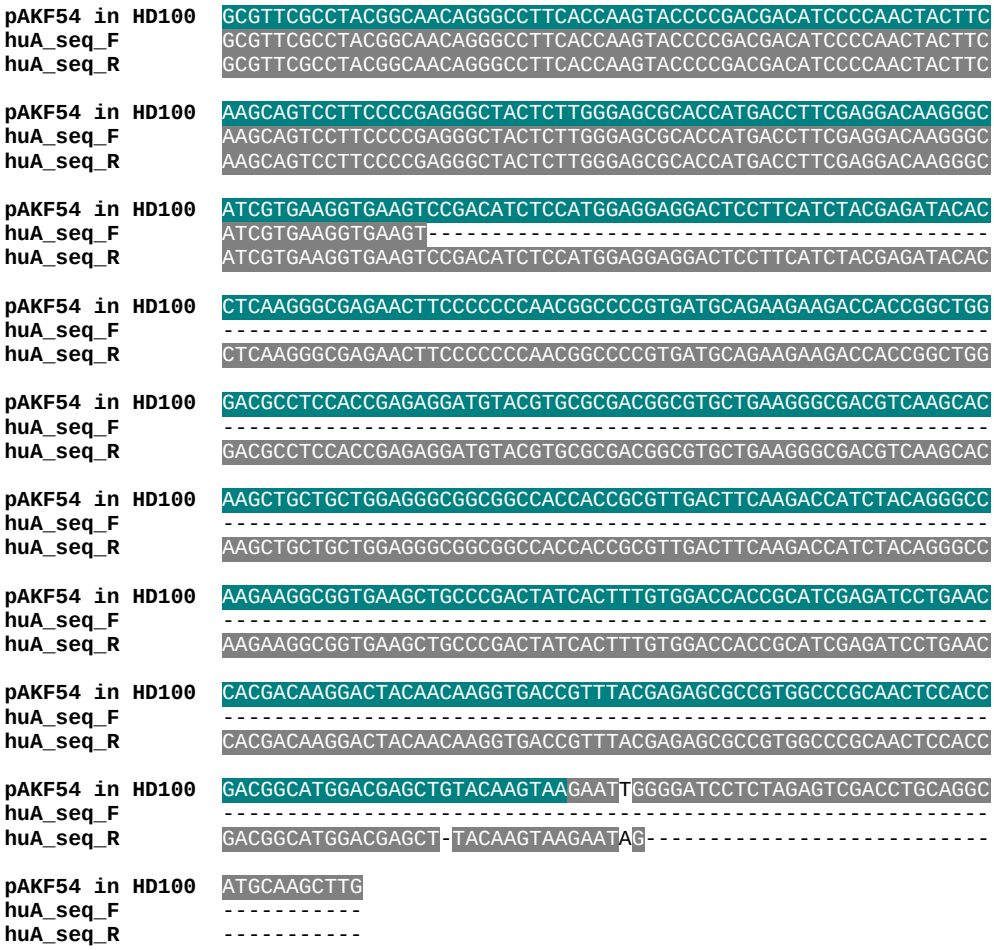

Appendix 4.1 Confirmatory sequencing data for the *huA-mtfp* HD100 strain. This strain contains the pAKF54 integrated plasmid which has a pK18 backbone used to confer kanamycin (Kn) resistance to exconjugants (For general recombination diagram see Fig 2.1B). Direct sequencing confirms the *huA-mtfp* full ORF sequence and verifies the genomic context of the integrated pAKF54 plasmid using primers that bind outside of the construct (which begins at the highlighted huA_site1_F primer binding site). All sequencing reactions were conducted directly on genome amplified PCR products using the primers: huA_seq_F and huA_seq_R. (**A**) Diagrammatic representation of the expected pAKF54 HD100 excongugant genome and all primers used for both amplification and direct sequencing, huA_site1_F primer is highlighted in red. (**B**) Multiply aligned sequencing data *huA*, *linker* and *mtfp* regions are highlighted in the same colours as (A), primers used for each reaction are shown. huA_site1_F primer binding site is highlighted and underlined.

Appendix 4.2 Montage of Images taken from supplementary Movies 1 - 10.

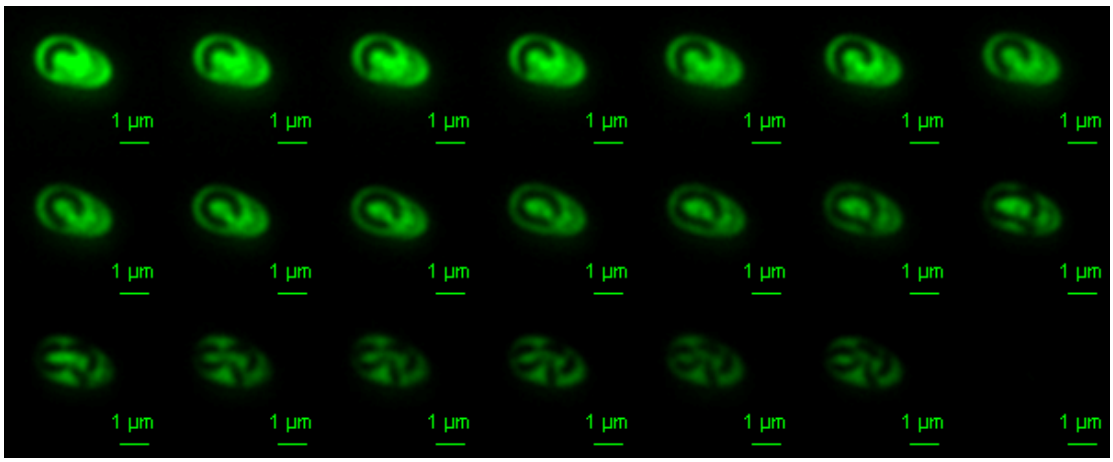

Appendix 4.2A *B. bacteriovorus* growth-phase cells septate synchronously in bdelloplasts **(also shown as supplementary Movie 1)**. Montage of images displaying every third frame of time-lapse Movie 1, showing a bdelloplast of an infected fluorescent prey cell with a dark growing *B. bacteriovorus* cell within; this cell elongates from both poles until it reaches its maximum length and septates synchronously into 5 progeny, which lyse the bdelloplast resulting in the loss of fluorescence activity. Contrast shifts within the bdelloplast are likely due to shifts in the prey cytoplasmic membrane. Images were captured every 2.5 min, thus each frame represents 7.5 min, scale bar = 1 µm.

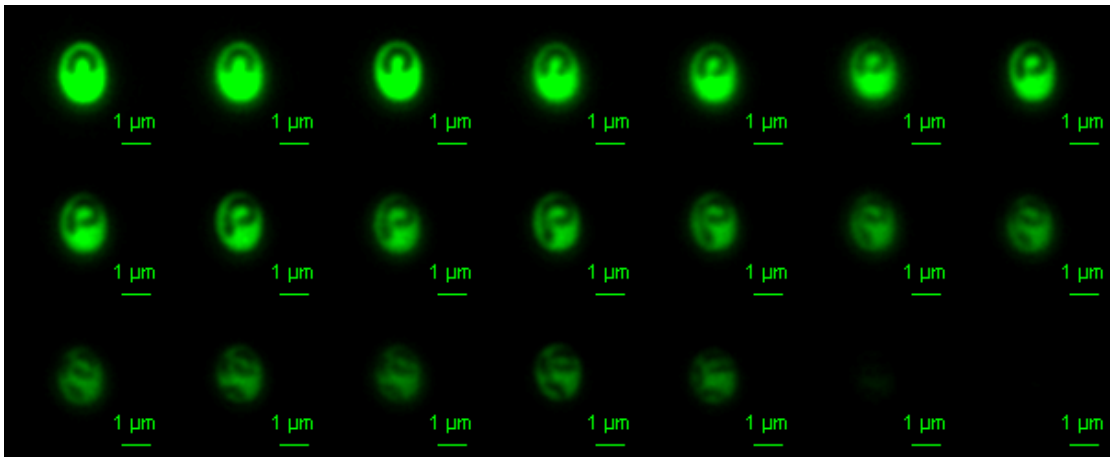

Appendix 4.2B *B. bacteriovorus* growth-phase cells septate synchronously in bdelloplasts **(also shown as supplementary Movie 2).** Montage of images displaying every third frame of time-lapse Movie 2, showing a bdelloplast of an infected fluorescent prey cell with a dark growing *B. bacteriovorus* cell within; this cell elongates from both poles, until it reaches its maximum length and septates synchronously into 4 progeny, which lyse the bdelloplast resulting in the loss of fluorescence activity. The growing *B. bacteriovorus* cell coils back on itself resulting in polar growth in the latter stages of elongation. Images were captured every 2.5 min, thus each frame represents 7.5 min, scale bar = 1 µm.

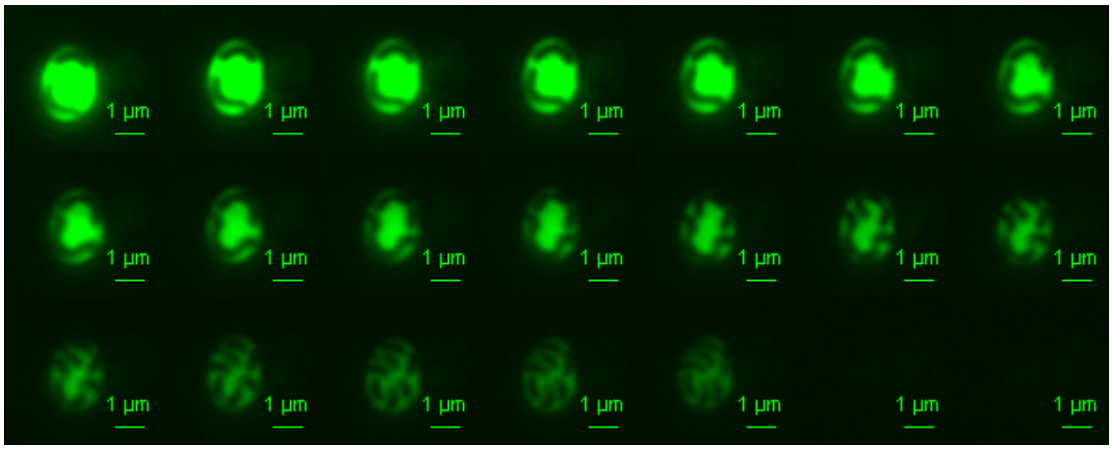

Appendix 4.2C Two separate *B. bacteriovorus* growth-phase cells synchronously septate in doubly infected bdelloplasts **(also shown as supplementary Movie 3).** Montage of images displaying every third frame of time-lapse Movie 3, showing a bdelloplast of an infected fluorescent prey cell with two separate dark growing *B. bacteriovorus* cells within; these cells elongate from both poles, until they reach their maximum length and septate synchronously into a total of 7 progeny (4 from the lower and 3 from the upper cell), which lyse the bdelloplast resulting in the loss of fluorescence activity. Growing cells seem to favour the bdelloplast periphery, presumably due to an unseen obstacle (for example the prey cell cytoplasm) in the centre; this inhibition seems to be released in the final stages of septation. Images were captured every 2.5 min, thus each frame represents 7.5 min, scale bar = 1 µm.

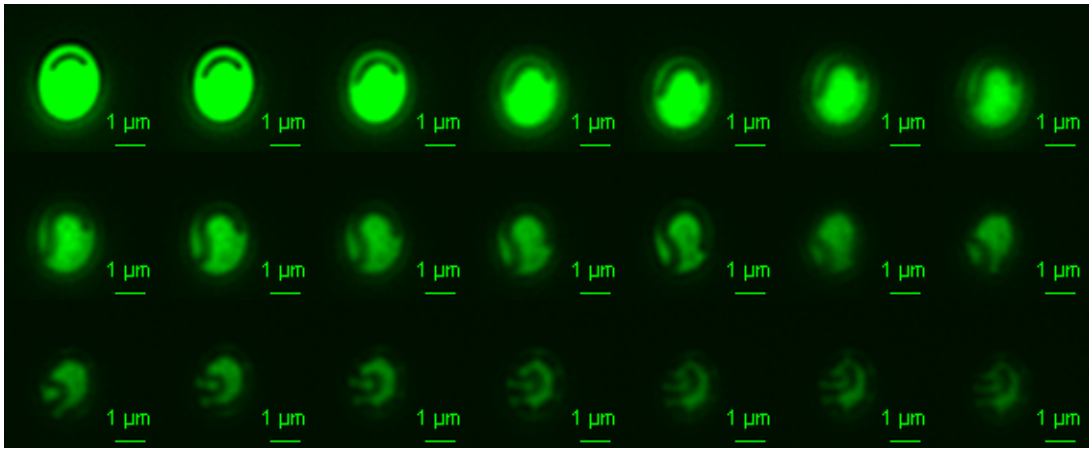

Appendix 4.2D Long *B. bacteriovorus* growth-phase cells initiate septation synchronously in bdelloplasts **(also shown as supplementary Movie 4).** Montage of images displaying every third frame of time-lapse Movie 4, showing a bdelloplast of an infected fluorescent prey cell with a dark growing *Bdellovibrio* cell within; this cell elongates from both poles until it reaches its maximum length and initiates septation synchronously along an extended filament which will ultimately generate 8 progeny. Right hand pole of the elongating *B. bacteriovorus* cell seems to get caught on an unseen obstacle, which is released in the later stages of growth. Contrast shifts within the bdelloplast are likely due to shifts in the prey cytoplasmic membrane. Growing cells seem to favour the bdelloplast periphery, presumably due to an unseen obstacle (for example the prey cell cytoplasm) in the centre; this inhibition seems to be released in the final stages of cell elongation. Images were captured every 2.5 min, thus each frame represents 7.5 min, scale bar = 1 µm.

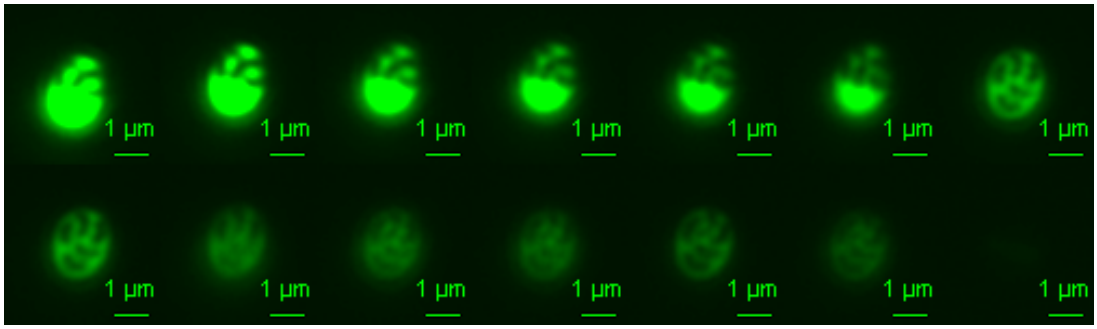

Appendix 4.2E Stored tension within a *B. bacteriovorus* growth-phase filament leads to dramatic re-orientation of progeny cells after synchronous septation **(also shown as supplementary Movie 5)**. Montage of images displaying every third frame of time-lapse Movie 5, showing a bdelloplast of an infected fluorescent prey cell with a dark elongated and coiled *B. bacteriovorus* cell within; this growth-phase cell septates leading to a dramatic shift in orientation of the 5 progeny cells, only possible if septation was synchronous. Progeny cells lyse the bdelloplast resulting in the loss of fluorescence activity. Images were captured every 2.5 min, thus each frame represents 7.5 min, scale bar = 1 µm.

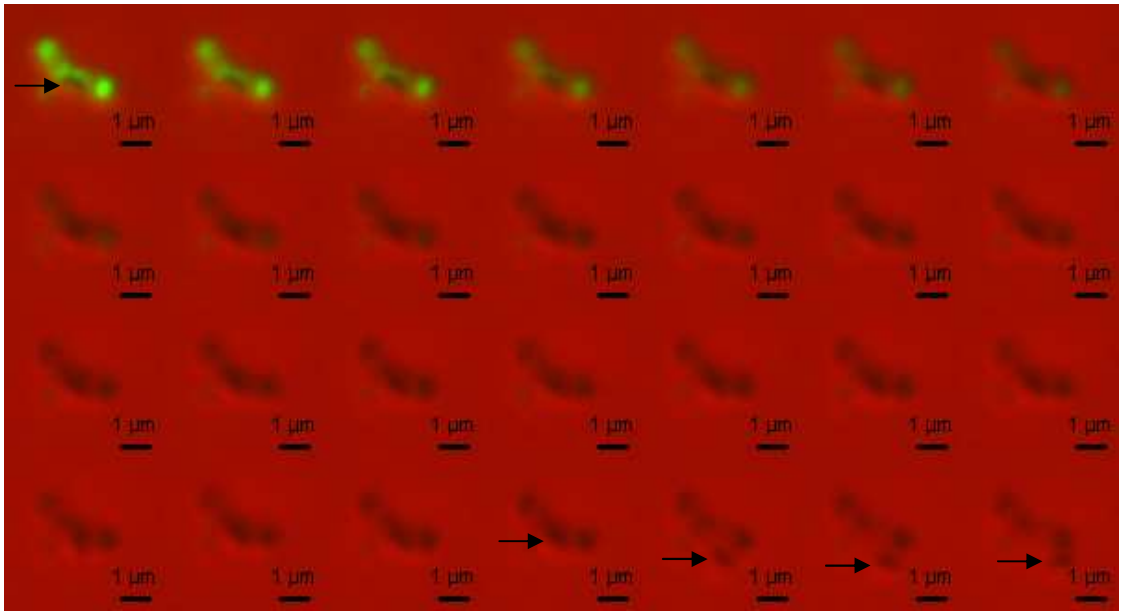

Appendix 4.2F *B. bacteriovorus* enter prey cells and do not always elongate and divide forming new progeny cells **(also shown as supplementary Movie 6)**. Montage of images displaying every third frame of time-lapse Movie 6, and shows overlaid brightfield (red) and fluorescence (green) images, revealing a single dark *B. bacteriovorus* cell in an atypical unrounded bdelloplast of a fluorescent prey cell. Fluorescence activity of this bdelloplast is patchy and bleaches quickly suggesting a lack of resources within the initial prey cell. *Bdellovibrio* cell does not elongate and persists in the bdelloplast eventually lysing and escaping (arrow). Images were captured every 2.5 min, thus each frame represents 7.5 min, scale bar = 1 µm.

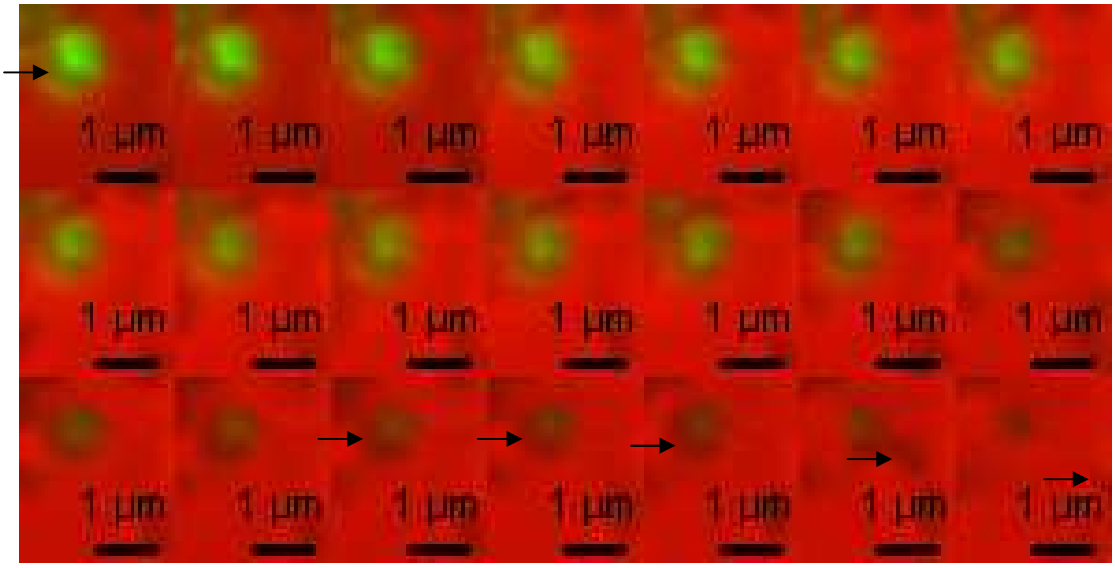

Appendix 4.2G *B. bacteriovorus* enter prey cells and do not always elongate and divide forming new progeny cells **(also shown as supplementary Movie 7)**. Montage of images displaying every frame of time-lapse Movie 7, and shows overlaid brightfield (red) and fluorescence (green) images, revealing a single dark *B. bacteriovorus* cell in a small fluorescent bdelloplast. *B. bacteriovorus* cell does not elongate and persists in the bdelloplast eventually lysing (leading to a loss of fluorescence activity) and the single cell escapes (arrow). Images were captured every 2.5 min, scale bar = 1 µm.

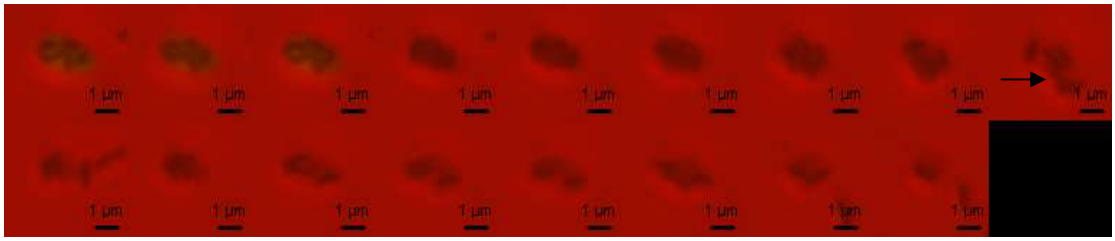

Appendix 4.2H Mature *B. bacteriovorus* progeny escape the bdelloplast through a single hole **(also shown as supplementary Movie 8)**. Montage of images displaying every third frame of time-lapse Movie 8, and shows overlaid brightfield (red) and fluorescence (green) images, showing a bdelloplast of an infected fluorescent prey cell with a dark growing *B. bacteriovorus* cell within, and is the same bdelloplast shown in Movie 1. The growing *B. bacteriovorus* cell septates synchronously into 5 progeny, which lyse the bdelloplast resulting in loss of fluorescence activity; progeny cells are then seen leaving the now exhausted prey cell through a hole in the bottom of the bdelloplast (arrow). This pattern was seen in 88% of observed bdelloplasts (n=67). Images were captured every 2.5 min, thus each frame represents 7.5 min, scale bar = 1 µm.

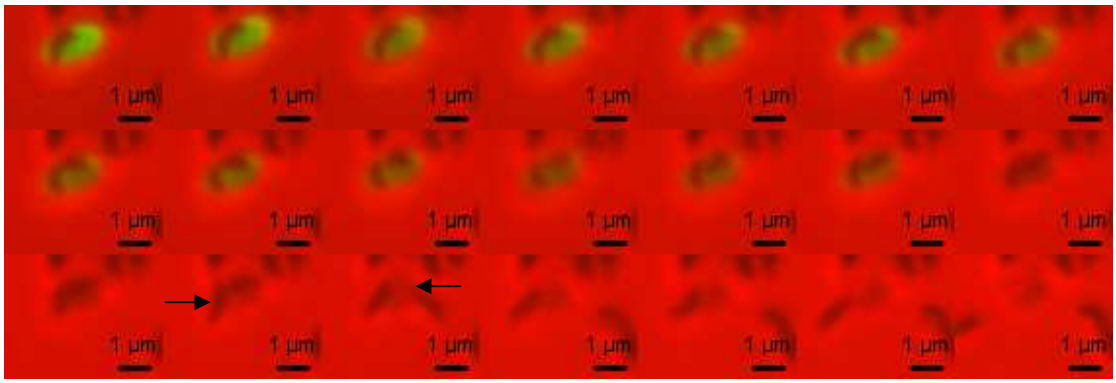

Appendix 4.2I Occasionally mature *B. bacteriovorus* progeny escape the bdelloplast via two holes **(also shown as supplementary Movie 9)**. Montage of images displaying every third frame of time-lapse Movie 9, overlaid brightfield (red) and fluorescence (green) images, images show a bdelloplast of an infected fluorescent prey cell with a dark elongated *B. bacteriovorus* cell within. The elongated growth-phase cell septates into 2 progeny, which lyse the bdelloplast resulting in loss of fluorescence activity; progeny cells are then seen leaving the now exhausted prey cell through two holes in the left and right hand side of the bdelloplast (arrows). This pattern was seen in 12% of observed bdelloplasts (n=67). Images were captured every 2.5 min, thus each frame represents 7.5 min, scale bar = 1 μm.

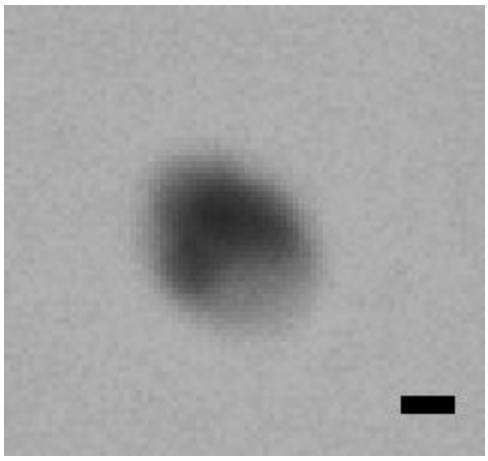

Appendix 4.2J First frame of a time-lapse brightfield Movie showing motile *Bdellovibrio* progeny cells within a bdelloplast, at maturation, after septation **(shown in supplementary Movie 10).** Three *Bdellovibrio* progeny cells appear to scramble over one another and collide with the inner wall of the bdelloplast which is immobilised on a glass surface in Ca/HEPES buffer. Internal collisions occasionally distort the shape of the bdelloplast. Images were captured at 25 frames per second using the IPLab software (version 3.64) and are shown at the same rate, scale bar = 1 μm.

Mascot Search Results

Protein View

Match to: Q6MGM1_BDEBA Score: 124
Hypothetical protein.- Bdellovibrio bacteriovorus.
Found in search of X:\QTOF DATA ARCHIVE\2008\December\A Fenton\0812012 AF BAND.raw\0812012 AF BAND.pkl

Nominal mass (M_r): 12953; Calculated pI value: 5.06
NCBI BLAST search of Q6MGM1_BDEBA against nr
Unformatted sequence string for pasting into other applications

Taxonomy: Bdellovibrio bacteriovorus
Links to retrieve other entries containing this sequence from NCBI Entrez:
CAE81258 from Bdellovibrio bacteriovorus HD100

Variable modifications: Carbamidomethyl (C),Oxidation (M)
Cleavage by Trypsin: cuts C-term side of KR unless next residue is P
Sequence Coverage: 26%

Matched peptides shown in Bold Red

```
     1 MAVNLSPALQ EDLLTGHVTA ILDQGTHFEG KLSFEGTVQI GGDFKGEIFT
    51 KDTIVINEGA SVTAQIEADT IVISGRVEGN LFARRRVIMH PPAIFKGTVT
   101 SPSLRIDEGV VFEGASYMPK S
```

Show predicted peptides also

Sort Peptides By ◉ Residue Number ○ Increasing Mass ○ Decreasing Mass

Start - End	Observed	Mr(expt)	Mr(calc)	Delta	Miss	Sequence
77 - 84	453.2465	904.4784	904.4767	0.0018	0	R.VEGNLFAR.R (Ions score 38)
97 - 105	459.2601	916.5056	916.4978	0.0078	0	R.GTVTSPSLR.I (Ions score 37)
106 - 120	829.3935	1656.7724	1656.7705	0.0019	0	R.IDEGVVFEGASYMPK.S Oxidation (M) (Ions score 49)

Appendix 4.3. MALDI-TOF MS output file of highlighted protein band shown in Fig. 4.3. MALDI-TOF MS analysis carried out by Dr Kevin Bailey of the University of Nottingham Biopolymer Analysis unit.

Appendix 4.4

A

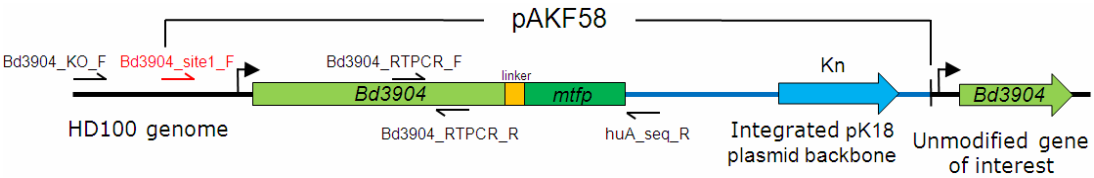

B

```
pAKF58 in HD100   TGCTGTAGAATCCTCAAACAAGAAAAAAGGTCTGGGCCGCGGCCTGGGCTCCCTGCTCGG
Bd3904_KO_F       -------------------------AAAAGGTCTGGGCCGCGGCCTGGGCTCCCTGCTCGG
Bd3904_RTPCR_R    ------------------------------------------------------------
huA_seq_R         ------------------------------------------------------------
Bd3904_RTPCR_F    ------------------------------------------------------------

pAKF58 in HD100   TGGCCCGGCTCCGGAGCAAACTCCGGCGGCTCCCAAGGCTGCTGCTGCTGCCCCATCTAT
Bd3904_KO_F       TGGCCCGGCTCCGGAGCAAACTCCGGCGGCTCCCAAGGCTGCTGCTGCTGCCCCATCTAT
Bd3904_RTPCR_R    ------------------------------------------------------------
huA_seq_R         ------------------------------------------------------------
Bd3904_RTPCR_F    ------------------------------------------------------------

pAKF58 in HD100   TAATAATACTGTAGCTTCAACTCCCGCTCCAGCGGCTGCTCCTCAAGTAGCGACACCCGT
Bd3904_KO_F       TAATAATACTGTAGCTTCAACTCCCGCTCCAGCGGCTGCTCCTCAAGTAGCGACACCCGT
Bd3904_RTPCR_R    ------------------------------------------------------------
huA_seq_R         ------------------------------------------------------------
Bd3904_RTPCR_F    ------------------------------------------------------------

pAKF58 in HD100   CGCCCCTCCCGTAGATCCTGAGAGCAAAATCTGGAAAGTGGGAATTGACAAGCTTTCACC
Bd3904_KO_F       CGCCCCTCCCGTAGATCCTGAGAGCAAAATCTGGAAAGTGGGAATTGACAAGCTTTCACC
Bd3904_RTPCR_R    ------------------------------------------------------------
huA_seq_R         ------------------------------------------------------------
Bd3904_RTPCR_F    ------------------------------------------------------------

pAKF58 in HD100   TGGTCAATACCAGCCTCGTAGAACATTTGAGAAAGAGCCGCTTCAGGAACTTGCTCAGTC
Bd3904_KO_F       TGGTCAATACCAGCCTCGTAGAACATTTGAGAAAGAGCCGCTTCAGGAACTTGCTCAGTC
Bd3904_RTPCR_R    ------------------------------GAAGAGCCGCTTCAGGAACTTGCTCAGTC
huA_seq_R         ------------------------------------------------------------
Bd3904_RTPCR_F    ------------------------------------------------------------

pAKF58 in HD100   TATTAAAGAGAACGGTATTCTTCAGCCCATCGTGGCTCGTCGTACGGCTTCCGGGAAACT
Bd3904_KO_F       TATTAAAGAGAACGGTATTCTTCAGCCCATCGTGGCTCGTCGTACGGCTTCCGGGAAACT
Bd3904_RTPCR_R    TATTAAAGAGAACGGTATTCTTCAGCCCATCGTGGCTCGTCGTACGGCTTCCGGGAAACT
huA_seq_R         ------------------------------------------------------------
Bd3904_RTPCR_F    ------------------------------------------------------------

pAKF58 in HD100   GGAAATCGTGGCCGGTGAACGCCGCTGGCGTGCATCCCAACTGGCGGGATTGCATGAAGT
Bd3904_KO_F       GGAAATCGTGGCCGGTGAACGCCGCTGGCGTGCATCCCAACTGGCGGGATTGCATGAAGT
Bd3904_RTPCR_R    GGAAATCGTGGCCGGTGAACGCCGCTGGCGTGCATCCCAACTGGCGGGATTGCATGAAGT
huA_seq_R         ------------------------------------------------------------
Bd3904_RTPCR_F    ------------------------------------------------------------

pAKF58 in HD100   TCCAGTTATCCTTAAGAATTACGACGACAAACAAGCGCTGGAACTGGCGATTGTTGAGAA
Bd3904_KO_F       TCCAGTTATCCTTAAGAATTACGACGACAAACAAGCGCTGGAACTGGCGATTGTTGAGAA
Bd3904_RTPCR_R    TCCAGTTATCCTTAAGAATTACGACGACAAACAAGCGCTGGAACTGGCGATTGTTGAGAA
huA_seq_R         ------------------------------------------------------------
Bd3904_RTPCR_F    ------------------------------------------------------------

pAKF58 in HD100   CATTCAGCGTGAAGATCTGAATCCGATCGAGGAAGCTGAAGGTTATTCCCGTCTGATTTC
Bd3904_KO_F       CATTCAGCGTGAAGATCTGAATCCGATCGAGGAAGCTGAAGGTTATTCCCGTCTGATTTC
Bd3904_RTPCR_R    CATTCAGCGTGAAGATCTGAATCCGATCGAGGAAGCTGAAGGTTATTCCCGTCTGATTTC
huA_seq_R         ------------------------------------------------------------
Bd3904_RTPCR_F    ------------------------------------------------------------
```

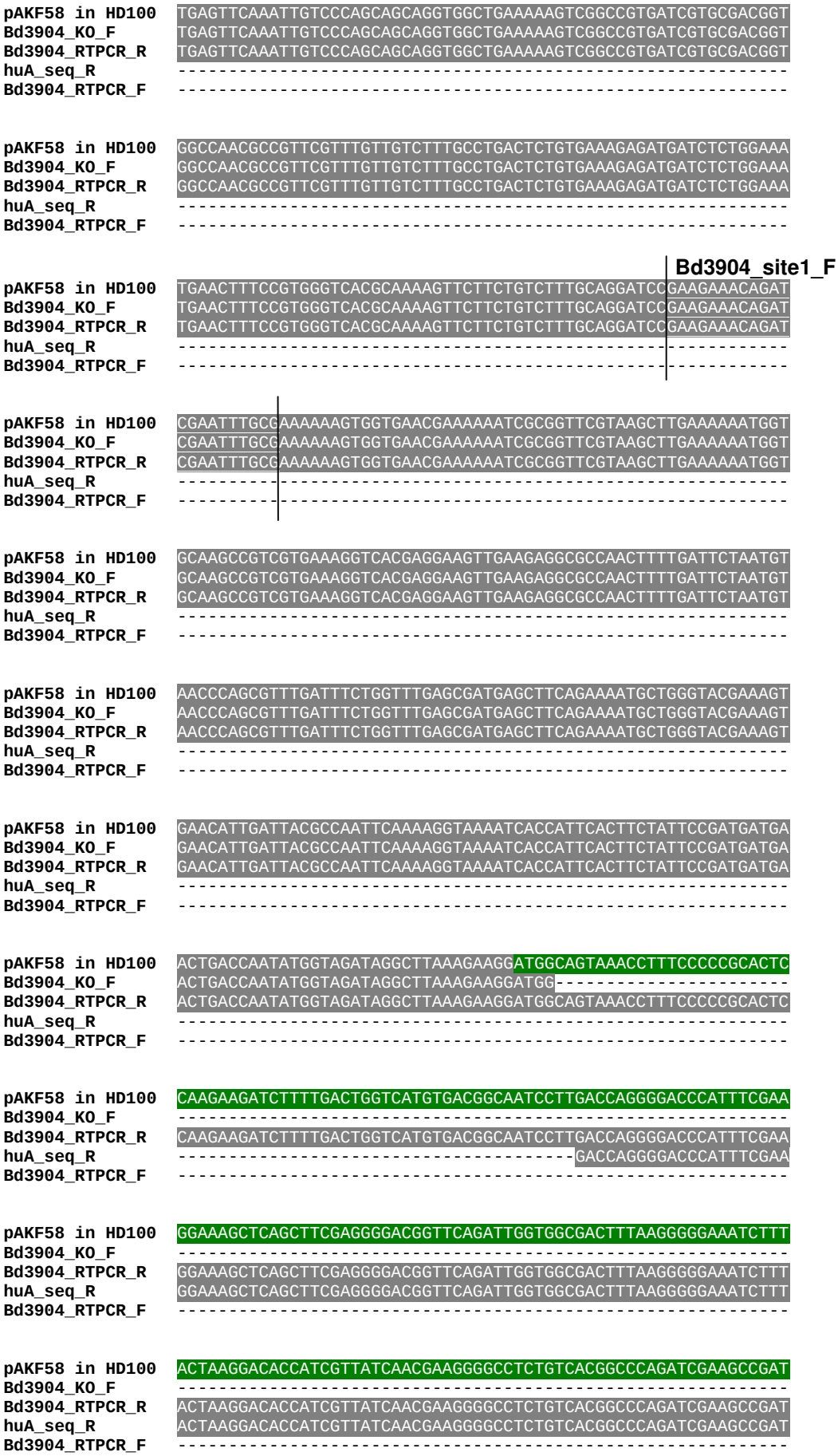
pAKF58 in HD100 TGAGTTCAAATTGTCCCAGCAGCAGGTGGCTGAAAAAGTCGGCCGTGATCGTGCGACGGT
Bd3904_KO_F TGAGTTCAAATTGTCCCAGCAGCAGGTGGCTGAAAAAGTCGGCCGTGATCGTGCGACGGT
Bd3904_RTPCR_R TGAGTTCAAATTGTCCCAGCAGCAGGTGGCTGAAAAAGTCGGCCGTGATCGTGCGACGGT
huA_seq_R ----------
Bd3904_RTPCR_F ----------
pAKF58 in HD100 GGCCAACGCCGTTCGTTTGTTGTCTTTGCCTGACTCTGTGAAAGAGATGATCTCTGGAAA
Bd3904_KO_F GGCCAACGCCGTTCGTTTGTTGTCTTTGCCTGACTCTGTGAAAGAGATGATCTCTGGAAA
Bd3904_RTPCR_R GGCCAACGCCGTTCGTTTGTTGTCTTTGCCTGACTCTGTGAAAGAGATGATCTCTGGAAA
huA_seq_R ----------
Bd3904_RTPCR_F ----------
Bd3904_site1_F
pAKF58 in HD100 TGAACTTTCCGTGGGTCACGCAAAAGTTCTTCTGTCTTTGCAGGATCCGAAGAAACAGAT
Bd3904_KO_F TGAACTTTCCGTGGGTCACGCAAAAGTTCTTCTGTCTTTGCAGGATCCGAAGAAACAGAT
Bd3904_RTPCR_R TGAACTTTCCGTGGGTCACGCAAAAGTTCTTCTGTCTTTGCAGGATCCGAAGAAACAGAT
huA_seq_R ----------
Bd3904_RTPCR_F ----------
pAKF58 in HD100 CGAATTTGCGAAAAAAGTGGTGAACGAAAAAATCGCGGTTCGTAAGCTTGAAAAAATGGT
Bd3904_KO_F CGAATTTGCGAAAAAAGTGGTGAACGAAAAAATCGCGGTTCGTAAGCTTGAAAAAATGGT
Bd3904_RTPCR_R CGAATTTGCGAAAAAAGTGGTGAACGAAAAAATCGCGGTTCGTAAGCTTGAAAAAATGGT
huA_seq_R ----------
Bd3904_RTPCR_F ----------
pAKF58 in HD100 GCAAGCCGTCGTGAAAGGTCACGAGGAAGTTGAAGAGGCGCCAACTTTTGATTCTAATGT
Bd3904_KO_F GCAAGCCGTCGTGAAAGGTCACGAGGAAGTTGAAGAGGCGCCAACTTTTGATTCTAATGT
Bd3904_RTPCR_R GCAAGCCGTCGTGAAAGGTCACGAGGAAGTTGAAGAGGCGCCAACTTTTGATTCTAATGT
huA_seq_R ----------
Bd3904_RTPCR_F ----------
pAKF58 in HD100 AACCCAGCGTTTGATTTCTGGTTTGAGCGATGAGCTTCAGAAAATGCTGGGTACGAAAGT
Bd3904_KO_F AACCCAGCGTTTGATTTCTGGTTTGAGCGATGAGCTTCAGAAAATGCTGGGTACGAAAGT
Bd3904_RTPCR_R AACCCAGCGTTTGATTTCTGGTTTGAGCGATGAGCTTCAGAAAATGCTGGGTACGAAAGT
huA_seq_R ----------
Bd3904_RTPCR_F ----------
pAKF58 in HD100 GAACATTGATTACGCCAATTCAAAAGGTAAAATCACCATTCACTTCTATTCCGATGATGA
Bd3904_KO_F GAACATTGATTACGCCAATTCAAAAGGTAAAATCACCATTCACTTCTATTCCGATGATGA
Bd3904_RTPCR_R GAACATTGATTACGCCAATTCAAAAGGTAAAATCACCATTCACTTCTATTCCGATGATGA
huA_seq_R ----------
Bd3904_RTPCR_F ----------
pAKF58 in HD100 ACTGACCAATATGGTAGATAGGCTTAAAGAAGGATGGCAGTAAACCTTTCCCCCGCACTC
Bd3904_KO_F ACTGACCAATATGGTAGATAGGCTTAAAGAAGGATGG----------
Bd3904_RTPCR_R ACTGACCAATATGGTAGATAGGCTTAAAGAAGGATGGCAGTAAACCTTTCCCCCGCACTC
huA_seq_R ----------
Bd3904_RTPCR_F ----------
pAKF58 in HD100 CAAGAAGATCTTTTGACTGGTCATGTGACGGCAATCCTTGACCAGGGGACCCATTTCGAA
Bd3904_KO_F ----------
Bd3904_RTPCR_R CAAGAAGATCTTTTGACTGGTCATGTGACGGCAATCCTTGACCAGGGGACCCATTTCGAA
huA_seq_R ----------GACCAGGGGACCCATTTCGAA
Bd3904_RTPCR_F ----------
pAKF58 in HD100 GGAAAGCTCAGCTTCGAGGGGACGGTTCAGATTGGTGGCGACTTTAAGGGGGAAATCTTT
Bd3904_KO_F ----------
Bd3904_RTPCR_R GGAAAGCTCAGCTTCGAGGGGACGGTTCAGATTGGTGGCGACTTTAAGGGGGAAATCTTT
huA_seq_R GGAAAGCTCAGCTTCGAGGGGACGGTTCAGATTGGTGGCGACTTTAAGGGGGAAATCTTT
Bd3904_RTPCR_F ----------
pAKF58 in HD100 ACTAAGGACACCATCGTTATCAACGAAGGGGCCTCTGTCACGGCCCAGATCGAAGCCGAT
Bd3904_KO_F ----------
Bd3904_RTPCR_R ACTAAGGACACCATCGTTATCAACGAAGGGGCCTCTGTCACGGCCCAGATCGAAGCCGAT
huA_seq_R ACTAAGGACACCATCGTTATCAACGAAGGGGCCTCTGTCACGGCCCAGATCGAAGCCGAT
Bd3904_RTPCR_F ----------

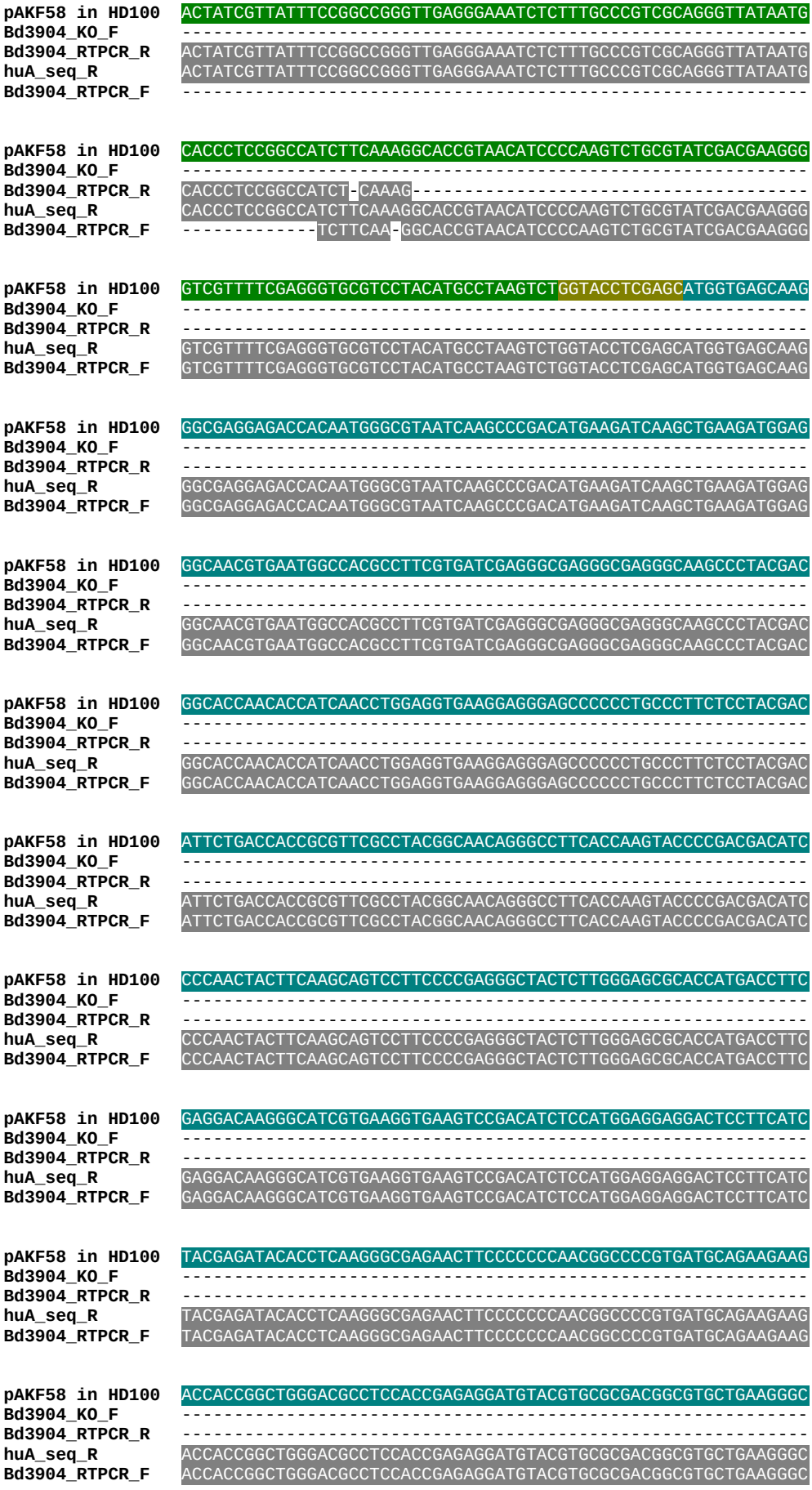
pAKF58 in HD100 ACTATCGTTATTTCCGGCCGGGTTGAGGGAAATCTCTTTGCCCGTCGCAGGGTTATAATG
Bd3904_KO_F ----------
Bd3904_RTPCR_R ACTATCGTTATTTCCGGCCGGGTTGAGGGAAATCTCTTTGCCCGTCGCAGGGTTATAATG
huA_seq_R ACTATCGTTATTTCCGGCCGGGTTGAGGGAAATCTCTTTGCCCGTCGCAGGGTTATAATG
Bd3904_RTPCR_F ----------
pAKF58 in HD100 CACCCTCCGGCCATCTTCAAAGGCACCGTAACATCCCCAAGTCTGCGTATCGACGAAGGG
Bd3904_KO_F ----------
Bd3904_RTPCR_R CACCCTCCGGCCATCT-CAAAG----------
huA_seq_R CACCCTCCGGCCATCTTCAAAGGCACCGTAACATCCCCAAGTCTGCGTATCGACGAAGGG
Bd3904_RTPCR_F ----------TCTTCAA-GGCACCGTAACATCCCCAAGTCTGCGTATCGACGAAGGG
pAKF58 in HD100 GTCGTTTTCGAGGGTGCGTCCTACATGCCTAAGTCTGGTACCTCGAGCATGGTGAGCAAG
Bd3904_KO_F ----------
Bd3904_RTPCR_R ----------
huA_seq_R GTCGTTTTCGAGGGTGCGTCCTACATGCCTAAGTCTGGTACCTCGAGCATGGTGAGCAAG
Bd3904_RTPCR_F GTCGTTTTCGAGGGTGCGTCCTACATGCCTAAGTCTGGTACCTCGAGCATGGTGAGCAAG
pAKF58 in HD100 GGCGAGGAGACCACAATGGGCGTAATCAAGCCCGACATGAAGATCAAGCTGAAGATGGAG
Bd3904_KO_F ----------
Bd3904_RTPCR_R ----------
huA_seq_R GGCGAGGAGACCACAATGGGCGTAATCAAGCCCGACATGAAGATCAAGCTGAAGATGGAG
Bd3904_RTPCR_F GGCGAGGAGACCACAATGGGCGTAATCAAGCCCGACATGAAGATCAAGCTGAAGATGGAG
pAKF58 in HD100 GGCAACGTGAATGGCCACGCCTTCGTGATCGAGGGCGAGGGCGAGGGCAAGCCCTACGAC
Bd3904_KO_F ----------
Bd3904_RTPCR_R ----------
huA_seq_R GGCAACGTGAATGGCCACGCCTTCGTGATCGAGGGCGAGGGCGAGGGCAAGCCCTACGAC
Bd3904_RTPCR_F GGCAACGTGAATGGCCACGCCTTCGTGATCGAGGGCGAGGGCGAGGGCAAGCCCTACGAC
pAKF58 in HD100 GGCACCAACACCATCAACCTGGAGGTGAAGGAGGGAGCCCCCCTGCCCTTCTCCTACGAC
Bd3904_KO_F ----------
Bd3904_RTPCR_R ----------
huA_seq_R GGCACCAACACCATCAACCTGGAGGTGAAGGAGGGAGCCCCCCTGCCCTTCTCCTACGAC
Bd3904_RTPCR_F GGCACCAACACCATCAACCTGGAGGTGAAGGAGGGAGCCCCCCTGCCCTTCTCCTACGAC
pAKF58 in HD100 ATTCTGACCACCGCGTTCGCCTACGGCAACAGGGCCTTCACCAAGTACCCCGACGACATC
Bd3904_KO_F ----------
Bd3904_RTPCR_R ----------
huA_seq_R ATTCTGACCACCGCGTTCGCCTACGGCAACAGGGCCTTCACCAAGTACCCCGACGACATC
Bd3904_RTPCR_F ATTCTGACCACCGCGTTCGCCTACGGCAACAGGGCCTTCACCAAGTACCCCGACGACATC
pAKF58 in HD100 CCCAACTACTTCAAGCAGTCCTTCCCCGAGGGCTACTCTTGGGAGCGCACCATGACCTTC
Bd3904_KO_F ----------
Bd3904_RTPCR_R ----------
huA_seq_R CCCAACTACTTCAAGCAGTCCTTCCCCGAGGGCTACTCTTGGGAGCGCACCATGACCTTC
Bd3904_RTPCR_F CCCAACTACTTCAAGCAGTCCTTCCCCGAGGGCTACTCTTGGGAGCGCACCATGACCTTC
pAKF58 in HD100 GAGGACAAGGGCATCGTGAAGGTGAAGTCCGACATCTCCATGGAGGAGGACTCCTTCATC
Bd3904_KO_F ----------
Bd3904_RTPCR_R ----------
huA_seq_R GAGGACAAGGGCATCGTGAAGGTGAAGTCCGACATCTCCATGGAGGAGGACTCCTTCATC
Bd3904_RTPCR_F GAGGACAAGGGCATCGTGAAGGTGAAGTCCGACATCTCCATGGAGGAGGACTCCTTCATC
pAKF58 in HD100 TACGAGATACACCTCAAGGGCGAGAACTTCCCCCCCAACGGCCCCGTGATGCAGAAGAAG
Bd3904_KO_F ----------
Bd3904_RTPCR_R ----------
huA_seq_R TACGAGATACACCTCAAGGGCGAGAACTTCCCCCCCAACGGCCCCGTGATGCAGAAGAAG
Bd3904_RTPCR_F TACGAGATACACCTCAAGGGCGAGAACTTCCCCCCCAACGGCCCCGTGATGCAGAAGAAG
pAKF58 in HD100 ACCACCGGCTGGGACGCCTCCACCGAGAGGATGTACGTGCGCGACGGCGTGCTGAAGGGC
Bd3904_KO_F ----------
Bd3904_RTPCR_R ----------
huA_seq_R ACCACCGGCTGGGACGCCTCCACCGAGAGGATGTACGTGCGCGACGGCGTGCTGAAGGGC
Bd3904_RTPCR_F ACCACCGGCTGGGACGCCTCCACCGAGAGGATGTACGTGCGCGACGGCGTGCTGAAGGGC

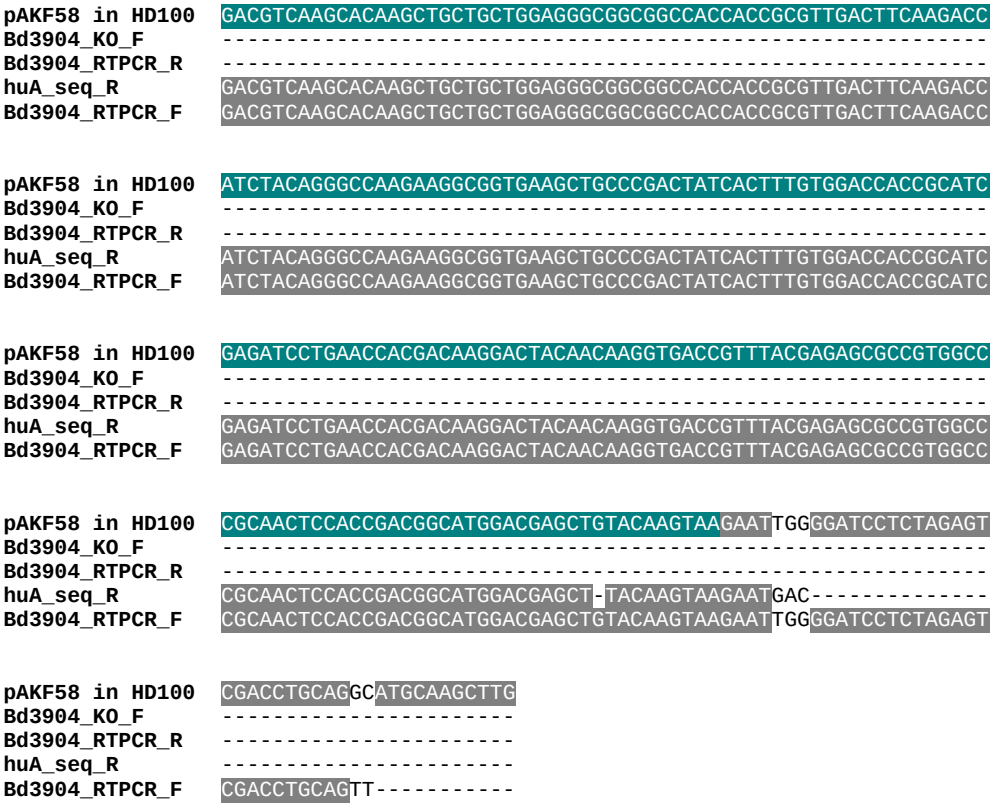

Appendix 4.4 Confirmatory sequencing data for the *bd3904-mtfp* HD100 strain. This strain contains the pAKF58 integrated plasmid which has a pK18 backbone used to confer kanamycin (Kn) resistance to exconjugants (For general recombination diagram see Fig. 2.1B). Direct sequencing confirms the *bd3904-mtfp* full ORF sequence and verifies the genomic context of the integrated pAKF58 plasmid using primers that bind outside of the construct (which begins at the highlighted Bd3904_site1_F primer binding site). All sequencing reactions were conducted directly on genome amplified PCR products using the primers: Bd3904_KO_F and huA_seq_R. (**A**) Diagrammatic representation of the expected pAKF58 HD100 excongugant genome and all primers used for both amplification and direct sequencing, Bd3904_site1_F primer is highlighted in red. (**B**) Multiply aligned sequencing data *bd3904*, *linker* and *mtfp* regions are highlighted in the same colours as (A), primers used for each reaction are shown. Bd3904_site1_F primer binding site is highlighted and underlined.

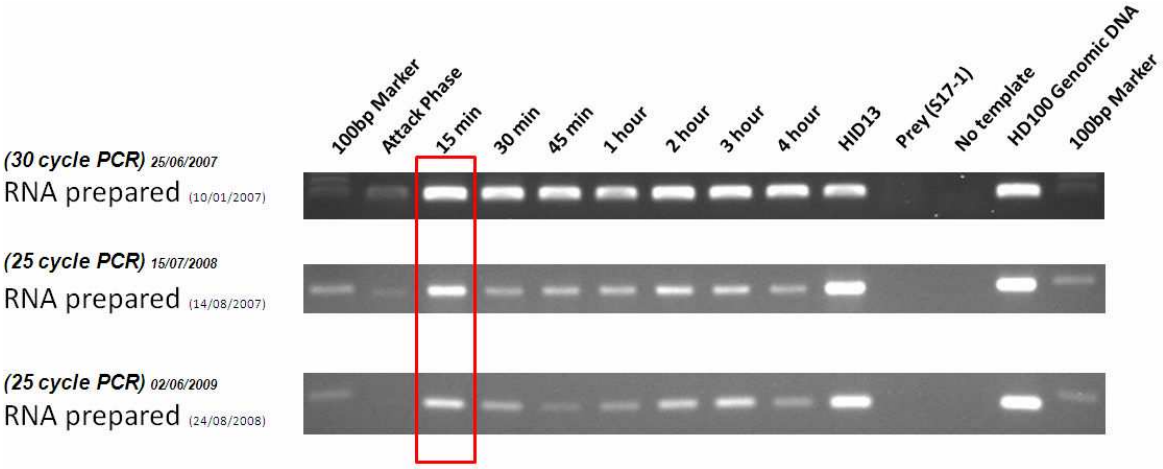

Appendix 5.1 Multiple RT-PCR reactions were carried out on three independent RNA preparations all show 15min peak in *mreB1* expression in a *B. bacteriovorus-E. coli* predation time course (See Materials and Methods section 2.14). The number of cycles used for each PCR, the dates of RNA preparation and the date that the RT-PCR reactions were carried out are shown (left).

Appendix 5.2

A

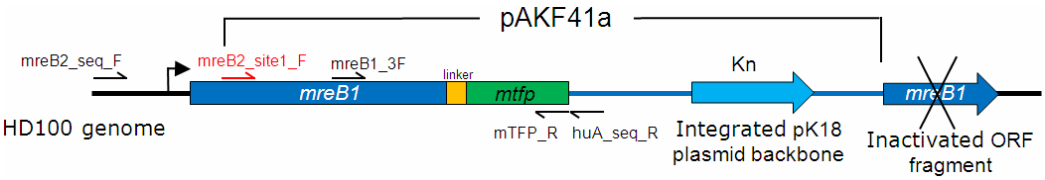

B

```
pAKF41a in HD100  ATTACACTGAAGTGAGATTCAGCATGAGTTTTTTTGACAAAGTTCAAGATTATTTTTCTA
mreB2_seq_F       ----------------------------------------------------ATTATTTTTCTA
mreB13F           ------------------------------------------------------------
mreB13F           ------------------------------------------------------------
mTFP_R            ------------------------------------------------------------
huA_seq_R         ------------------------------------------------------------

pAKF41a in HD100  ACGACATCGCCATTGACCTTGGCACCGCCAACACACTTGTTTACGTAAAAGGCCGCGGAA
mreB2_seq_F       ACGACATCGCCATTGACCTTGGCACCGCCAACACACTTGTTTACGTAAAAGGCCGCGGAA
mreB13F           ------------------------------------------------------------
mreB13F           ------------------------------------------------------------
mTFP_R            ------------------------------------------------------------
huA_seq_R         ------------------------------------------------------------

                  mreB2_site1_F
pAKF41a in HD100  TCATCCTTGATGAACCTTCCGTGGTTGCGGTCCAAAAGAATTATCGTGGGATGCAAAACC
mreB2_seq_F       TCATCCTTGATGAACCTTCCGTGGTTGCGGTCCAAAAGAATTATCGTGGGATGCAAAACC
mreB13F           --------------------------------------------------------
mreB13F           --------------------------------------------------------
mTFP_R            --------------------------------------------------------
huA_seq_R         --------------------------------------------------------

pAKF41a in HD100  GCGTTCTTGCCGTAGGTAAAGAAGCCAAAGACATGTTGGGACGTACACCTGGCAGCATCG
mreB2_seq_F       GCGTTCTTGCCGTAGGTAAAGAAGCCAAAGACATGTTGGGACGTACACCTGGCAGCATCG
mreB13F           ------------------------------------------------------------
mreB13F           ------------------------------------------------------------
mTFP_R            ------------------------------------------------------------
huA_seq_R         ------------------------------------------------------------

pAKF41a in HD100  TGGCGATCCGCCCGATCAAAGATGGTGTTATCGCTGACTTCGAAGTCACCCAGTCCATGC
mreB2_seq_F       TGGCGATCCGCCCGATCAAAGATGGTGTTATCGCTGACTTCGAAGTCACCCAGTCCATGC
mreB13F           ------------CGATCAA-GATGGTGTTATCGCTGACTTCGAAGTCACCCAGTCCATGC
mreB13F           ----------------------GGTGTTATCGCTGACTTCGAAGTCACCCAGTCCATGC
mreB13F           ------------------------------------------------------------
mTFP_R            ------------------------------------------------------------
huA_seq_R         ------------------------------------------------------------

pAKF41a in HD100  TGAAGTACTTCATCGGCAAATCCCTTGGCGAGAAAAAATCCTTCATCCGTCCTCGTATCA
mreB2_seq_F       TGACTCTTT-----------------------------------------------------
mreB13F           TGAAGTACTTCATCGGCAAATCCCTTGGCGAGAAAAAATCCTTCATCCGTCCTCGTATCA
mreB13F           TGAAGTACTTCATCGGCAAATCCCTTGGCGAGAAAAAATCCTTCATCCGTCCTCGTATCA
mTFP_R            ------------------------------------------------------------
huA_seq_R         ------------------------------------------------------------

pAKF41a in HD100  TCATCTGCGTTCCTTACGGAATCACTCAGGTTGAAAAACGTGCGGTGAAAGAGGCGGCTC
mreB2_seq_F       ------------------------------------------------------------
mreB13F           TCATCTGCGTTCCTTACGGAATCACTCAGGTTGAAAAACGTGCGGTGAAAGAGGCGGCTC
mreB13F           TCATCTGCGTTCCTTACGGAATCACTCAGGTTGAAAAACGTGCGGTGAAAGAGGCGGCTC
mTFP_R            ------------------------------------------------------------
huA_seq_R         ------------------------------------------------------------
```

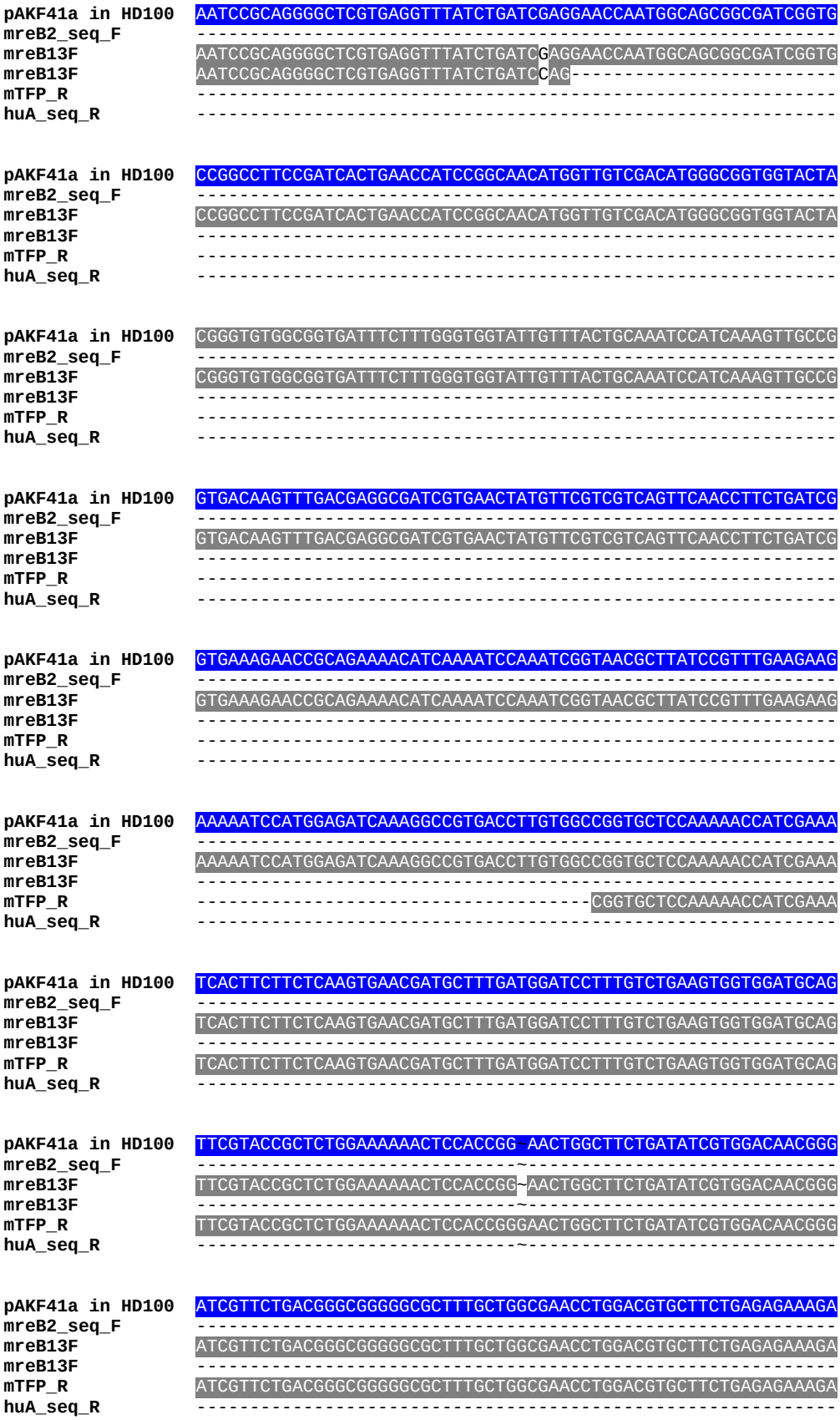
pAKF41a in HD100 AATCCGCAGGGGCTCGTGAGGTTTATCTGATCGAGGAACCAATGGCAGCGGCGATCGGTG
mreB2_seq_F
mreB13F AATCCGCAGGGGCTCGTGAGGTTTATCTGATCGAGGAACCAATGGCAGCGGCGATCGGTG
mreB13F AATCCGCAGGGGCTCGTGAGGTTTATCTGATCCAG
mTFP_R
huA_seq_R
pAKF41a in HD100 CCGGCCTTCCGATCACTGAACCATCCGGCAACATGGTTGTCGACATGGGCGGTGGTACTA
mreB2_seq_F
mreB13F CCGGCCTTCCGATCACTGAACCATCCGGCAACATGGTTGTCGACATGGGCGGTGGTACTA
mreB13F
mTFP_R
huA_seq_R
pAKF41a in HD100 CGGGTGTGGCGGTGATTTCTTTGGGTGGTATTGTTTACTGCAAATCCATCAAAGTTGCCG
mreB2_seq_F
mreB13F CGGGTGTGGCGGTGATTTCTTTGGGTGGTATTGTTTACTGCAAATCCATCAAAGTTGCCG
mreB13F
mTFP_R
huA_seq_R
pAKF41a in HD100 GTGACAAGTTTGACGAGGCGATCGTGAACTATGTTCGTCGTCAGTTCAACCTTCTGATCG
mreB2_seq_F
mreB13F GTGACAAGTTTGACGAGGCGATCGTGAACTATGTTCGTCGTCAGTTCAACCTTCTGATCG
mreB13F
mTFP_R
huA_seq_R
pAKF41a in HD100 GTGAAAGAACCGCAGAAAACATCAAAATCCAAATCGGTAACGCTTATCCGTTTGAAGAAG
mreB2_seq_F
mreB13F GTGAAAGAACCGCAGAAAACATCAAAATCCAAATCGGTAACGCTTATCCGTTTGAAGAAG
mreB13F
mTFP_R
huA_seq_R
pAKF41a in HD100 AAAAATCCATGGAGATCAAAGGCCGTGACCTTGTGGCCGGTGCTCCAAAAACCATCGAAA
mreB2_seq_F
mreB13F AAAAATCCATGGAGATCAAAGGCCGTGACCTTGTGGCCGGTGCTCCAAAAACCATCGAAA
mreB13F
mTFP_R CGGTGCTCCAAAAACCATCGAAA
huA_seq_R
pAKF41a in HD100 TCACTTCTTCTCAAGTGAACGATGCTTTGATGGATCCTTTGTCTGAAGTGGTGGATGCAG
mreB2_seq_F
mreB13F TCACTTCTTCTCAAGTGAACGATGCTTTGATGGATCCTTTGTCTGAAGTGGTGGATGCAG
mreB13F
mTFP_R TCACTTCTTCTCAAGTGAACGATGCTTTGATGGATCCTTTGTCTGAAGTGGTGGATGCAG
huA_seq_R
pAKF41a in HD100 TTCGTACCGCTCTGGAAAAAACTCCACCGG AACTGGCTTCTGATATCGTGGACAACGGG
mreB2_seq_F
mreB13F TTCGTACCGCTCTGGAAAAAACTCCACCGG AACTGGCTTCTGATATCGTGGACAACGGG
mreB13F
mTFP_R TTCGTACCGCTCTGGAAAAAACTCCACCGGGAACTGGCTTCTGATATCGTGGACAACGGG
huA_seq_R
pAKF41a in HD100 ATCGTTCTGACGGGCGGGGGCGCTTTGCTGGCGAACCTGGACGTGCTTCTGAGAGAAAGA
mreB2_seq_F
mreB13F ATCGTTCTGACGGGCGGGGGCGCTTTGCTGGCGAACCTGGACGTGCTTCTGAGAGAAAGA
mreB13F
mTFP_R ATCGTTCTGACGGGCGGGGGCGCTTTGCTGGCGAACCTGGACGTGCTTCTGAGAGAAAGA
huA_seq_R

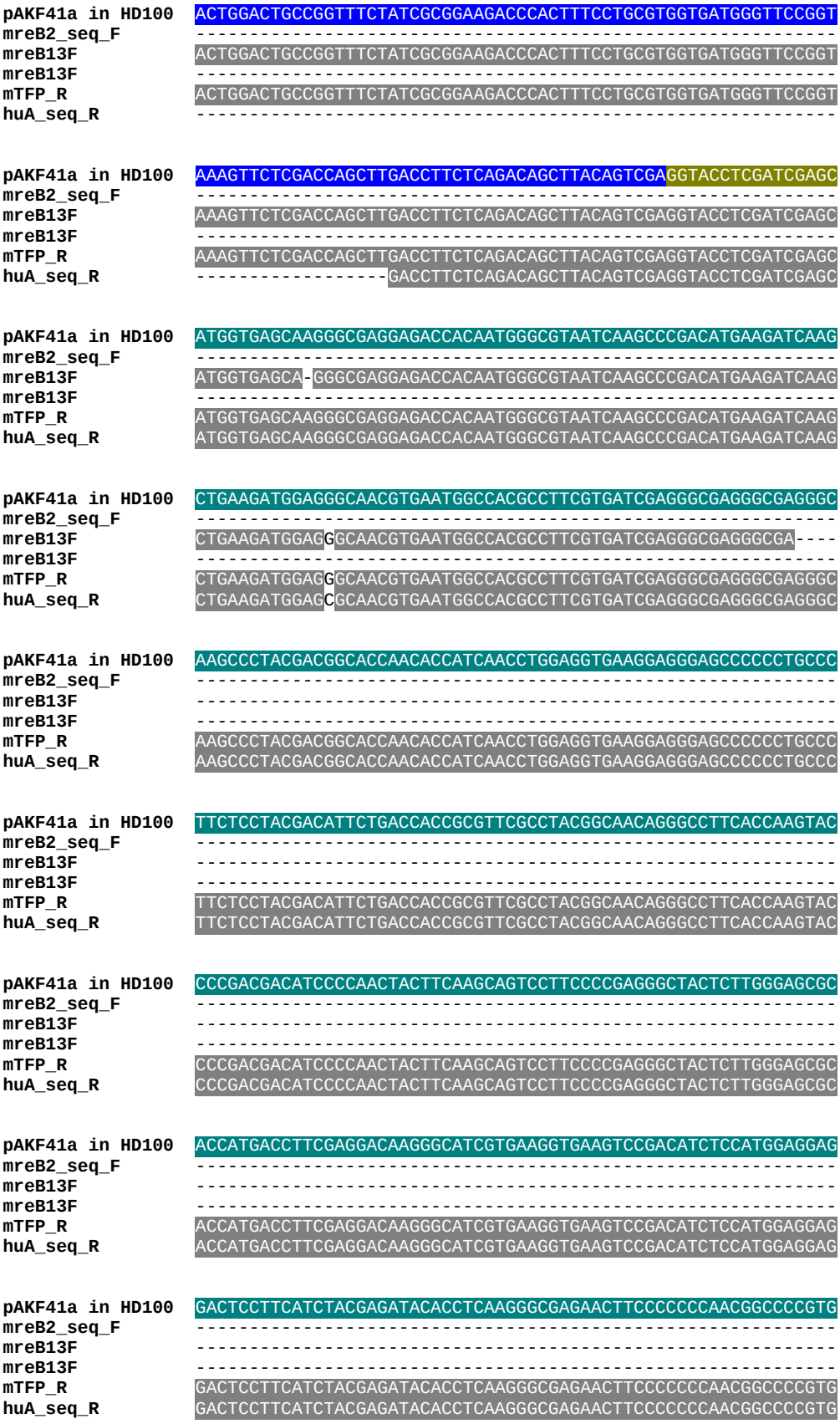
pAKF41a in HD100 ACTGGACTGCCGGTTTCTATCGCGGAAGACCCACTTTCCTGCGTGGTGATGGGTTCCGGT
mreB2_seq_F ----------
mreB13F ACTGGACTGCCGGTTTCTATCGCGGAAGACCCACTTTCCTGCGTGGTGATGGGTTCCGGT
mreB13F ----------
mTFP_R ACTGGACTGCCGGTTTCTATCGCGGAAGACCCACTTTCCTGCGTGGTGATGGGTTCCGGT
huA_seq_R ----------
pAKF41a in HD100 AAAGTTCTCGACCAGCTTGACCTTCTCAGACAGCTTACAGTCGAGGTACCTCGATCGAGC
mreB2_seq_F ----------
mreB13F AAAGTTCTCGACCAGCTTGACCTTCTCAGACAGCTTACAGTCGAGGTACCTCGATCGAGC
mreB13F ----------
mTFP_R AAAGTTCTCGACCAGCTTGACCTTCTCAGACAGCTTACAGTCGAGGTACCTCGATCGAGC
huA_seq_R ----------GACCTTCTCAGACAGCTTACAGTCGAGGTACCTCGATCGAGC
pAKF41a in HD100 ATGGTGAGCAAGGGCGAGGAGACCACAATGGGCGTAATCAAGCCCGACATGAAGATCAAG
mreB2_seq_F ----------
mreB13F ATGGTGAGCA-GGGCGAGGAGACCACAATGGGCGTAATCAAGCCCGACATGAAGATCAAG
mreB13F ----------
mTFP_R ATGGTGAGCAAGGGCGAGGAGACCACAATGGGCGTAATCAAGCCCGACATGAAGATCAAG
huA_seq_R ATGGTGAGCAAGGGCGAGGAGACCACAATGGGCGTAATCAAGCCCGACATGAAGATCAAG
pAKF41a in HD100 CTGAAGATGGAGGGCAACGTGAATGGCCACGCCTTCGTGATCGAGGGCGAGGGCGAGGGC
mreB2_seq_F ----------
mreB13F CTGAAGATGGAGGGCAACGTGAATGGCCACGCCTTCGTGATCGAGGGCGAGGGCGA----
mreB13F ----------
mTFP_R CTGAAGATGGAGGGCAACGTGAATGGCCACGCCTTCGTGATCGAGGGCGAGGGCGAGGGC
huA_seq_R CTGAAGATGGAGCGCAACGTGAATGGCCACGCCTTCGTGATCGAGGGCGAGGGCGAGGGC
pAKF41a in HD100 AAGCCCTACGACGGCACCAACACCATCAACCTGGAGGTGAAGGAGGGAGCCCCCCTGCCC
mreB2_seq_F ----------
mreB13F ----------
mreB13F ----------
mTFP_R AAGCCCTACGACGGCACCAACACCATCAACCTGGAGGTGAAGGAGGGAGCCCCCCTGCCC
huA_seq_R AAGCCCTACGACGGCACCAACACCATCAACCTGGAGGTGAAGGAGGGAGCCCCCCTGCCC
pAKF41a in HD100 TTCTCCTACGACATTCTGACCACCGCGTTCGCCTACGGCAACAGGGCCTTCACCAAGTAC
mreB2_seq_F ----------
mreB13F ----------
mreB13F ----------
mTFP_R TTCTCCTACGACATTCTGACCACCGCGTTCGCCTACGGCAACAGGGCCTTCACCAAGTAC
huA_seq_R TTCTCCTACGACATTCTGACCACCGCGTTCGCCTACGGCAACAGGGCCTTCACCAAGTAC
pAKF41a in HD100 CCCGACGACATCCCCAACTACTTCAAGCAGTCCTTCCCCGAGGGCTACTCTTGGGAGCGC
mreB2_seq_F ----------
mreB13F ----------
mreB13F ----------
mTFP_R CCCGACGACATCCCCAACTACTTCAAGCAGTCCTTCCCCGAGGGCTACTCTTGGGAGCGC
huA_seq_R CCCGACGACATCCCCAACTACTTCAAGCAGTCCTTCCCCGAGGGCTACTCTTGGGAGCGC
pAKF41a in HD100 ACCATGACCTTCGAGGACAAGGGCATCGTGAAGGTGAAGTCCGACATCTCCATGGAGGAG
mreB2_seq_F ----------
mreB13F ----------
mreB13F ----------
mTFP_R ACCATGACCTTCGAGGACAAGGGCATCGTGAAGGTGAAGTCCGACATCTCCATGGAGGAG
huA_seq_R ACCATGACCTTCGAGGACAAGGGCATCGTGAAGGTGAAGTCCGACATCTCCATGGAGGAG
pAKF41a in HD100 GACTCCTTCATCTACGAGATACACCTCAAGGGCGAGAACTTCCCCCCCAACGGCCCCGTG
mreB2_seq_F ----------
mreB13F ----------
mreB13F ----------
mTFP_R GACTCCTTCATCTACGAGATACACCTCAAGGGCGAGAACTTCCCCCCCAACGGCCCCGTG
huA_seq_R GACTCCTTCATCTACGAGATACACCTCAAGGGCGAGAACTTCCCCCCCAACGGCCCCGTG

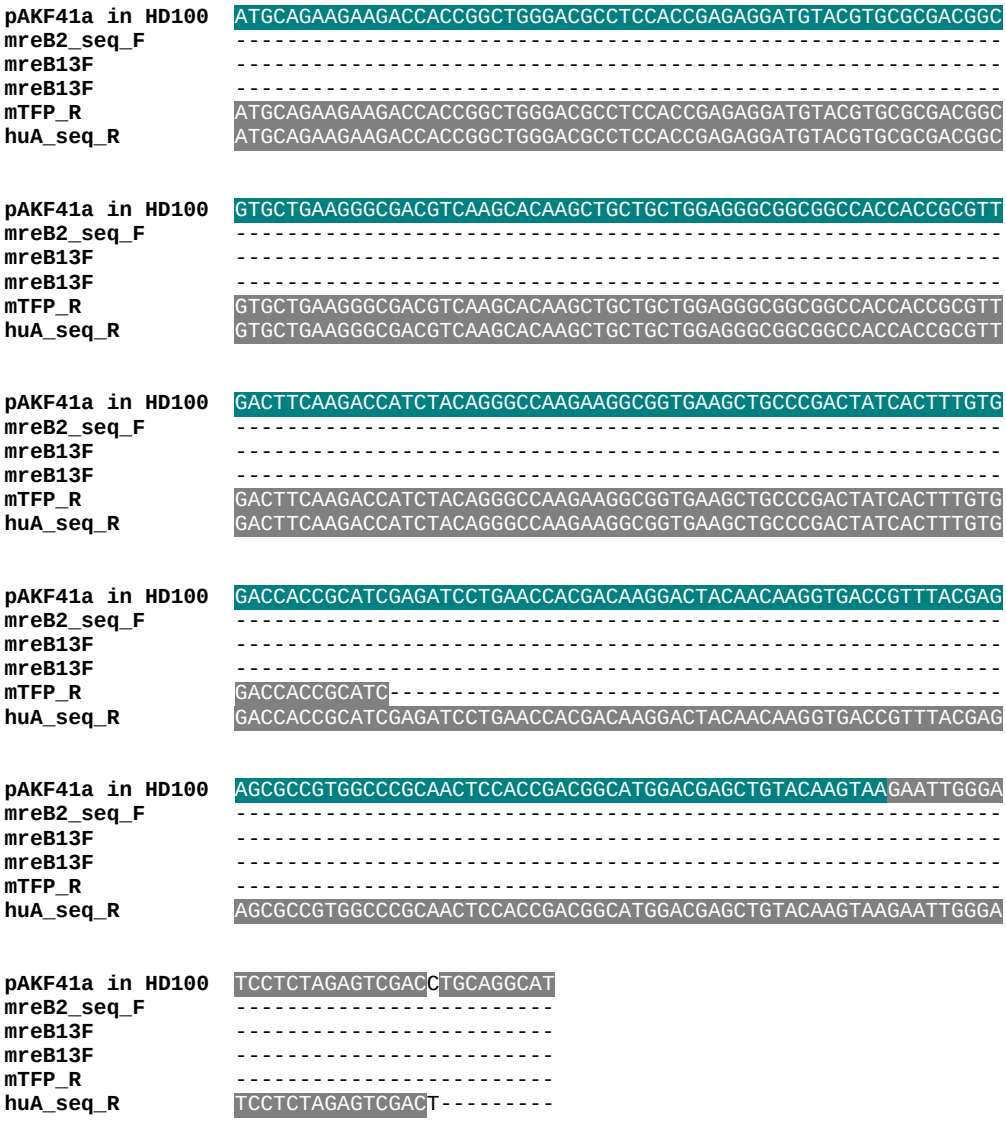

Appendix 5.2 Confirmatory sequencing data for the *mreB1-mtfp* HD100 strain. This strain contains the pAKF41a integrated plasmid which has a pK18 backbone used to confer kanamycin (Kn) resistance to exconjugants (For general recombination diagram see Fig. 2.1A). Direct sequencing confirms the *bd3904-mtfp* full ORF sequence and verifies the genomic context of the integrated pAKF58 plasmid using primers that bind outside of the construct (which begins at the highlighted Bd3904_site1_F primer binding site). All sequencing reactions were conducted directly on genome amplified PCR products using the primers: Bd3904_KO_F and huA_seq_R. (**A**) Diagrammatic representation of the expected pAKF58 HD100 excongugant genome and all primers used for both amplification and direct sequencing, Bd3904_site1_F primer is highlighted in red. (**B**) Multiply aligned sequencing data *bd3904*, *linker* and *mtfp* regions are highlighted in the same colours as (A), primers used for each reaction are shown. Bd3904_site1_F primer binding site is highlighted and underlined.

Appendix 5.3

A

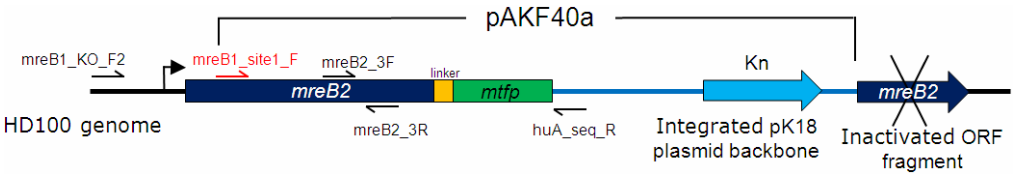

B

```
pAKF40a in HD100   TTTTGACCAACAAAGGTAATGGTGCCAACTTCAACGTGTTCTTTGATACGGCCCTGAGCG
primer mreB2_3R    ----------------------------------------------TACGGCCCTGAGCG
primer mreB2_3F    ~----------------------------------------------------------
primer huA_seq_R   ~~~----------------------------------------------------------

pAKF40a in HD100   ATTCTTCCAGCGCACGCATCAGCATGGGCGCAGGAGCTGTGGATTTTAACACTTTTGCCA
primer mreB2_3R    ATTCTTCCAGCGCACGCATCAGCATGGGCGCAGGAGCTGTGGATTTTAACACTTTTGCCA
primer mreB2_3F    ----------------------------------------------------------
primer huA_seq_R   ----------------------------------------------------------

pAKF40a in HD100   GCGTTAAATGGATCCCGATCCCTGACGTGGACAACCAGCCTGCGATGGGCCTTCGTGCTG
primer mreB2_3R    GCGTTAAATGGATCCCGATCCCTGACGTGGACAACCAGC-TGCGATGGGCCTTCGTGCTG
primer mreB2_3F    ----------------------------------------------------------
primer huA_seq_R   ----------------------------------------------------------

pAKF40a in HD100   GCGCCGGGATTGCCCGCGATGAGGACGAAAACCTGATCCAATTCCAGTTTGCCCCCCTGG
primer mreB2_3R    GCGCCGGGATTGCCCGCGATGAGGACGAAAACCTGATCCAATTCCAGTTTGCCCCCCTGG
primer mreB2_3F    ----------------------------------------------------------
primer huA_seq_R   ----------------------------------------------------------

pAKF40a in HD100   TCAGCAAACGCTTTGACACAGAATACGGATTGACCGTGCCTTACCTGGCGGTGCCGTTTA
primer mreB2_3R    TCAGCAAACGCTTTGACACAGAATACGGATTGACCGTGCCTTACCTGGCGGTGCCGTTTA
primer mreB2_3F    ----------------------------------------------------------
primer huA_seq_R   ----------------------------------------------------------

pAKF40a in HD100   CATTCCTGAACACCAAAGACGAAAACTTCGTTGCTTCCAACCTGGCGTTGGGAAGCGAAT
primer mreB2_3R    CATTCCTGAACACCAAAGACGAAAACTTCGTTGCTTCCAACCTGGCGTTGGGAAGCGAAT
primer mreB2_3F    ----------------------------------------------------------
primer huA_seq_R   ----------------------------------------------------------

pAKF40a in HD100   TCCACTATGTTGACTGGAAAGAAGTAAATATGGGCGCGGAAGTGGGTATTGACTTGAACA
primer mreB2_3R    TCCACTATGTTGACTGGAAAGAAGTAAATATGGGCGCGGAAGTGGGTATTGACTTGAACA
primer mreB2_3F    ----------------------------------------------------------
primer huA_seq_R   ----------------------------------------------------------

pAKF40a in HD100   AGTCTTATTCCTACATCTCCCTTTATCTGACATTCCCATTTGAAAGCCACAAAGGATTCG
primer mreB2_3R    AGTCTTATTCCTACATCTCCCTTTATCTGACATTCCCATTTGAAAGCCACAAAGGATTCG
primer mreB2_3F    ----------------------------------------------------------
primer huA_seq_R   ----------------------------------------------------------

                                                        MreB1_site1_F
pAKF40a in HD100   GGAAGTAATATGTTTTCATGGTTCTTTAAGGACGAAACCGGAACAGCTGCAGATCTATAC
primer mreB2_3R    GGAAGTAATATGTTTTCATGGTTCTTTAAGGACGAAACCGGAACAGCTGCAGATCTATAC
primer mreB2_3F    ----------------------------------------|-----------------
primer huA_seq_R   ----------------------------------------|-----------------

pAKF40a in HD100   GTAGATTTGGGGACTGCCAATACACTCATCGCAGCTCGTGGCAAAGGGATCATCCTGAAT
primer mreB2_3R    GTAGATTTGGGGACTGCCAATACACTCATCGCAGCTCGTGGCAAAGGGATCATCCTGAAT
primer mreB2_3F    -|--------------------------------------------------------
primer huA_seq_R   -|--------------------------------------------------------
```

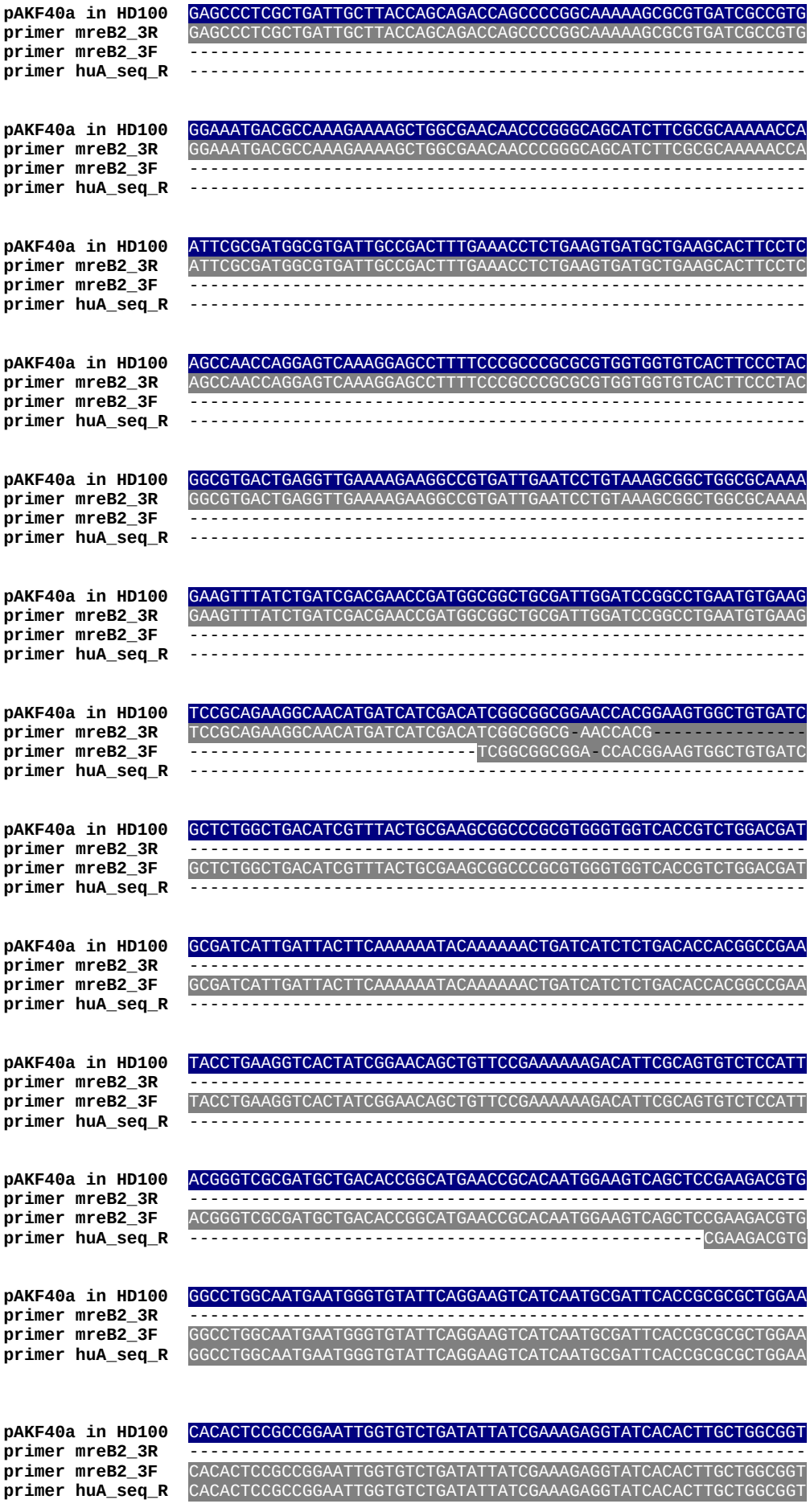
pAKF40a in HD100 GAGCCCTCGCTGATTGCTTACCAGCAGACCAGCCCCGGCAAAAAGCGCGTGATCGCCGTG
primer mreB2_3R GAGCCCTCGCTGATTGCTTACCAGCAGACCAGCCCCGGCAAAAAGCGCGTGATCGCCGTG
primer mreB2_3F
primer huA_seq_R
pAKF40a in HD100 GGAAATGACGCCAAAGAAAAGCTGGCGAACAACCCGGGCAGCATCTTCGCGCAAAAACCA
primer mreB2_3R GGAAATGACGCCAAAGAAAAGCTGGCGAACAACCCGGGCAGCATCTTCGCGCAAAAACCA
primer mreB2_3F
primer huA_seq_R
pAKF40a in HD100 ATTCGCGATGGCGTGATTGCCGACTTTGAAACCTCTGAAGTGATGCTGAAGCACTTCCTC
primer mreB2_3R ATTCGCGATGGCGTGATTGCCGACTTTGAAACCTCTGAAGTGATGCTGAAGCACTTCCTC
primer mreB2_3F
primer huA_seq_R
pAKF40a in HD100 AGCCAACCAGGAGTCAAAGGAGCCTTTTCCCGCCCGCGCGTGGTGGTGTCACTTCCCTAC
primer mreB2_3R AGCCAACCAGGAGTCAAAGGAGCCTTTTCCCGCCCGCGCGTGGTGGTGTCACTTCCCTAC
primer mreB2_3F
primer huA_seq_R
pAKF40a in HD100 GGCGTGACTGAGGTTGAAAAGAAGGCCGTGATTGAATCCTGTAAAGCGGCTGGCGCAAAA
primer mreB2_3R GGCGTGACTGAGGTTGAAAAGAAGGCCGTGATTGAATCCTGTAAAGCGGCTGGCGCAAAA
primer mreB2_3F
primer huA_seq_R
pAKF40a in HD100 GAAGTTTATCTGATCGACGAACCGATGGCGGCTGCGATTGGATCCGGCCTGAATGTGAAG
primer mreB2_3R GAAGTTTATCTGATCGACGAACCGATGGCGGCTGCGATTGGATCCGGCCTGAATGTGAAG
primer mreB2_3F
primer huA_seq_R
pAKF40a in HD100 TCCGCAGAAGGCAACATGATCATCGACATCGGCGGCGGAACCACGGAAGTGGCTGTGATC
primer mreB2_3R TCCGCAGAAGGCAACATGATCATCGACATCGGCGGCG-AACCACG
primer mreB2_3F TCGGCGGCGGA-CCACGGAAGTGGCTGTGATC
primer huA_seq_R
pAKF40a in HD100 GCTCTGGCTGACATCGTTTACTGCGAAGCGGCCCGCGTGGGTGGTCACCGTCTGGACGAT
primer mreB2_3R
primer mreB2_3F GCTCTGGCTGACATCGTTTACTGCGAAGCGGCCCGCGTGGGTGGTCACCGTCTGGACGAT
primer huA_seq_R
pAKF40a in HD100 GCGATCATTGATTACTTCAAAAAATACAAAAAACTGATCATCTCTGACACCACGGCCGAA
primer mreB2_3R
primer mreB2_3F GCGATCATTGATTACTTCAAAAAATACAAAAAACTGATCATCTCTGACACCACGGCCGAA
primer huA_seq_R
pAKF40a in HD100 TACCTGAAGGTCACTATCGGAACAGCTGTTCCGAAAAAAGACATTCGCAGTGTCTCCATT
primer mreB2_3R
primer mreB2_3F TACCTGAAGGTCACTATCGGAACAGCTGTTCCGAAAAAAGACATTCGCAGTGTCTCCATT
primer huA_seq_R
pAKF40a in HD100 ACGGGTCGCGATGCTGACACCGGCATGAACCGCACAATGGAAGTCAGCTCCGAAGACGTG
primer mreB2_3R
primer mreB2_3F ACGGGTCGCGATGCTGACACCGGCATGAACCGCACAATGGAAGTCAGCTCCGAAGACGTG
primer huA_seq_R CGAAGACGTG
pAKF40a in HD100 GGCCTGGCAATGAATGGGTGTATTCAGGAAGTCATCAATGCGATTCACCGCGCGCTGGAA
primer mreB2_3R
primer mreB2_3F GGCCTGGCAATGAATGGGTGTATTCAGGAAGTCATCAATGCGATTCACCGCGCGCTGGAA
primer huA_seq_R GGCCTGGCAATGAATGGGTGTATTCAGGAAGTCATCAATGCGATTCACCGCGCGCTGGAA
pAKF40a in HD100 CACACTCCGCCGGAATTGGTGTCTGATATTATCGAAAGAGGTATCACACTTGCTGGCGGT
primer mreB2_3R
primer mreB2_3F CACACTCCGCCGGAATTGGTGTCTGATATTATCGAAAGAGGTATCACACTTGCTGGCGGT
primer huA_seq_R CACACTCCGCCGGAATTGGTGTCTGATATTATCGAAAGAGGTATCACACTTGCTGGCGGT

```
pAKF40a in HD100   GGCGCTTTGATTCGCGACTTTGACCTGCGCATTCAGAATGAGGTTCGCCTGCAGGTTCGC
primer mreB2_3R    ------------------------------------------------------------
primer mreB2_3F    GGCGCTTTGATTCGCGACTTTGACCTGCGCATTCAGAATGAGGTTCGCCTGCAGGTTCGC
primer huA_seq_R   GGCGCTTTGATTCGCGACTTTGAC-TGCGCATTCAGAATGAGGTTCGCCTGCAGGTTCGC

pAKF40a in HD100   ATCGCGGATGACCCGCTGACGGCGATCGCCAAGGGCGGCGAAGCAGTGCTGAGTGATCCA
primer mreB2_3R    ------------------------------------------------------------
primer mreB2_3F    ATCGCGGATGACCCGCTGACGGCGATCGCCAAGGGCGGCGAAGCAGTGCTGAGTGATCCA
primer huA_seq_R   ATCGCGGATGACCCGCTGACGGCGATCGCCAAGGGCGGCGAAGCAGTGCTGAGTGATCCA

pAKF40a in HD100   GAACTGCTCGATAAAATTCAGTTGGAAGTGGTACCTCGATCGAGCATGGTGAGCAAGGGC
primer mreB2_3R    ------------------------------------------------------------
primer mreB2_3F    GAACTGCTCGATAAAATTCAGTTGGAAGTGGTACCTCGATCGAGCATGGTGAGCAAGGGC
primer huA_seq_R   GAACTGCTCGATAAAATTCAGTTGGAAGTGGTACCTCGATCGAGCATGGTGAGCAAGGGC

pAKF40a in HD100   GAGGAGACCACAATGGGCGTAATCAAGCCCGACATGAAGATCAAGCTGAAGATGGAGGGC
primer mreB2_3R    ------------------------------------------------------------
primer mreB2_3F    GAGGAGACCACAATGGGCGTAATCAAGCCCGACATGAAGATCAAGCTGAAGATGGAGGGC
primer huA_seq_R   GAGGAGACCACAATGGGCGTAATCAAGCCCGACATGAAGATCAAGCTGAAGATGGAGGGC

pAKF40a in HD100   AACGTGAATGGCCACGCCTTCGTGATCGAGGGCGAGGGCGAGGGCAAGCCCTACGACGGC
primer mreB2_3R    ------------------------------------------------------------
primer mreB2_3F    AACGTGAATGGCCACGCCTTCGTGATCGAGGGCGAGGGCGAGGGCAAGCCCTACGACGGC
primer huA_seq_R   AACGTGAATGGCCACGCCTTCGTGATCGAGGGCGAGGGCGAGGGCAAGCCCTACGACGGC

pAKF40a in HD100   ACCAACACCATCAACCTGGAGGTGAAGGAGGGAGCCCCCCTGCCCTTCTCCTACGACATT
primer mreB2_3R    ------------------------------------------------------------
primer mreB2_3F    ACCAACACCATCAACCTGGAGGTGAAGGAGGGAGCCCCCCTGCCCTTCTCCTACGACATT
primer huA_seq_R   ACCAACACCATCAACCTGGAGGTGAAGGAGGGAGCCCCCCTGCCCTTCTCCTACGACATT

pAKF40a in HD100   CTGACCACCGCGTTCGCCTACGGCAACAGGGCCTTCACCAAGTACCCCGACGACATCCCC
primer mreB2_3R    ------------------------------------------------------------
primer mreB2_3F    CTGACCACCGCGTTCGCCTACGGCAACAGGGCCTTCACCAAGTACCCCGACGACATCCCC
primer huA_seq_R   CTGACCACCGCGTTCGCCTACGGCAACAGGGCCTTCACCAAGTACCCCGACGACATCCCC

pAKF40a in HD100   AACTACTTCAAGCAGTCCTTCCCCGAGGGCTACTCTTGGGAGCGCACCATGACCTTCGAG
primer mreB2_3R    ------------------------------------------------------------
primer mreB2_3F    AACTACTTCAAGCAGTCCTTCCCCGAGGGCTACTCTTGGGAGCGCACCATGACCTTCGAG
primer huA_seq_R   AACTACTTCAAGCAGTCCTTCCCCGAGGGCTACTCTTGGGAGCGCACCATGACCTTCGAG

pAKF40a in HD100   GACAAGGGCATCGTGAAGGTGAAGTCCGACATCTCCATGGAGGAGGACTCCTTCATCTAC
primer mreB2_3R    ------------------------------------------------------------
primer mreB2_3F    GACAAGGGCATCGTGAAGGTGAAGTCCGACATCTCCATGGAGGAGGACTCCTTCATCTAC
primer huA_seq_R   GACAAGGGCATCGTGAAGGTGAAGTCCGACATCTCCATGGAGGAGGACTCCTTCATCTAC

pAKF40a in HD100   GAGATACACCTCAAGGGCGAGAACTTCCCCCCCAACGGCCCCGTGATGCAGAAGAAGACC
primer mreB2_3R    ------------------------------------------------------------
primer mreB2_3F    GAGATACACCTCAAGGGCGAGAACTTCCCCCCCAACGGCT--------------------
primer huA_seq_R   GAGATACACCTCAAGGGCGAGAACTTCCCCCCCAACGGCCCCGTGATGCAGAAGAAGACC

pAKF40a in HD100   ACCGGCTGGGACGCCTCCACCGAGAGGATGTACGTGCGCGACGGCGTGCTGAAGGGCGAC
primer mreB2_3R    ------------------------------------------------------------
primer mreB2_3F    ------------------------------------------------------------
primer huA_seq_R   ACCGGCTGGGACGCCTCCACCGAGAGGATGTACGTGCGCGACGGCGTGCTGAAGGGCGAC

pAKF40a in HD100   GTCAAGCACAAGCTGCTGCTGGAGGGCGGCGGCCACCACCGCGTTGACTTCAAGACCATC
primer mreB2_3R    ------------------------------------------------------------
primer mreB2_3F    ------------------------------------------------------------
primer huA_seq_R   GTCAAGCACAAGCTGCTGCTGGAGGGCGGCGGCCACCACCGCGTTGACTTCAAGACCATC
```

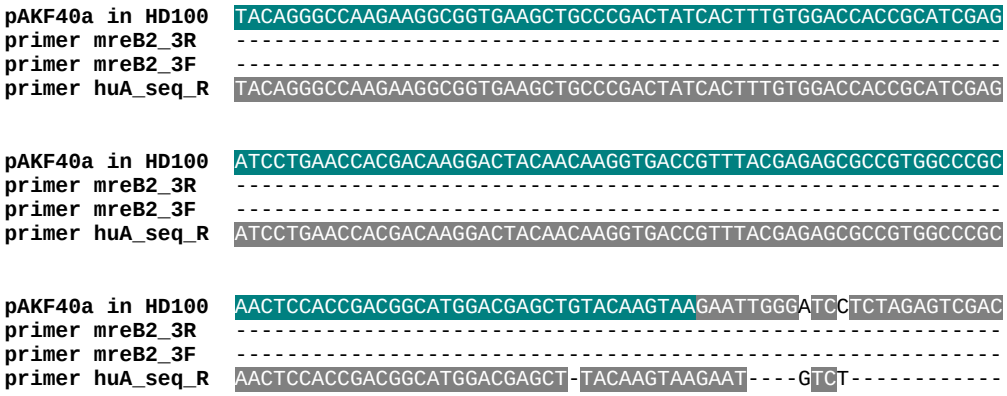

Appendix 5.3 Confirmatory sequencing data for the *mreB2mtfp* HD100 strain. This strain contains the pAKF40a integrated plasmid which has a pK18 backbone used to confer kanamycin (Kn) resistance to exconjugants (For general recombination diagram see Fig. 2.1A). Direct sequencing confirms almost the *mreB2-mtfp* full ORF sequence and verifies the genomic context of the integrated pAKF40a plasmid using primers that bind outside of the construct (which begins at the highlighted MreB1_site1_F primer binding site). All sequencing reactions were conducted directly on genome amplified PCR products using the primers: mreB1_KO_F2 and huA_seq_R. (**A**) Diagrammatic representation of the expected pAKF40a HD100 excongugant genome and all primers used for both amplification and direct sequencing, MreB1_site1_F primer is highlighted in red. (**B**) Multiply aligned sequencing data *mreB*, *linker* and *mtfp* regions are highlighted in the same colours as (A), primers used for each reaction are shown. MreB1_site1_F primer binding site is both highlighted and underlined.

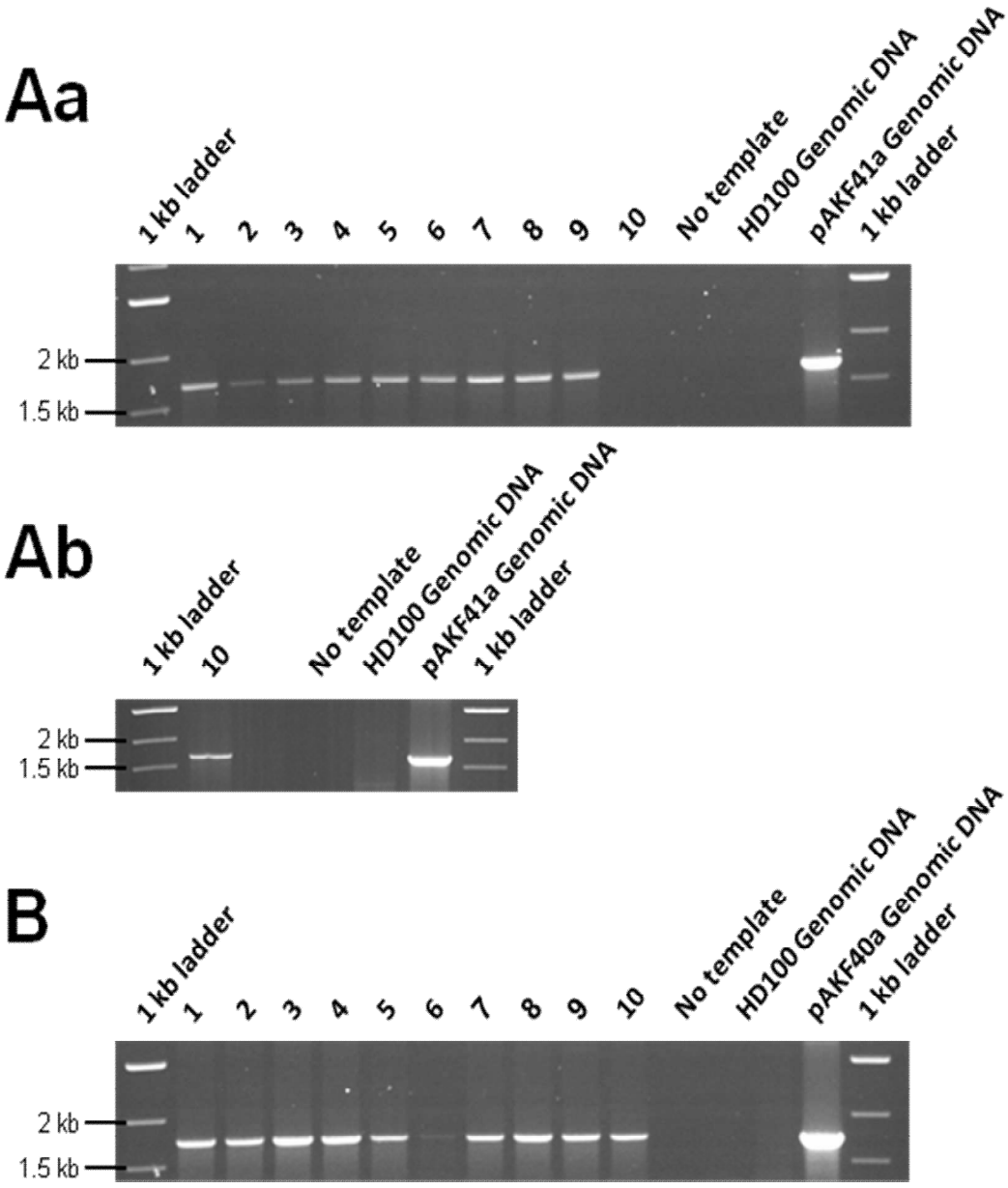

Appendix 5.4 Dagnostic *Taq* PCRs showing the presence of the *mreB-mtfp* constructs in ten HI derivative strains. (**Aa**) *Taq* PCR reactions using 2 µl of HI culture as template with primers: mreB2_site1_F and mTFP_F, which specifically amplify a 1,685 bp region of the genome integrated pAKF41a (*mreB1-mtfp*) construct, no template and HD100 genomic DNA were used as a negative controls, genomic DNA isolated from the *mreB1-mtfp* HD strain was used as a positive control. (**Ab**) As initially the PCR failed for *mreB2-mtfp* HI candidate 10 this was repeated. (**B**) *Taq* PCR reactions using 2 µl of HI culture as template with primers: mreB1_site1_F and mTFP_F, which specifically amplify a 1,747 bp region of the genome integrated pAKF40a (*mreB2-mtfp*) construct, no template and HD100 genomic DNA were used as a negative controls, genomic DNA isolated from the *mreB2-mtfp* HD strain was used as a positive control. 1 kb DNA ladder was used in each marker lane, appropriate bands have been highlighted.